New Mixed Anion Frameworks

A thesis presented for the degree of

Doctor of Philosophy

in the Faculty of Science of the University of St Andrews

by Zoe A.D. Lethbridge, BSc (Hons), AMRSC

February 2002

School of Chemistry

University of St Andrews

DECLARATIONS

I, Zoe Lethbridge, hereby certify that this thesis, which is approximately 27,000 words in length, has been written by me, that it is the record of work carried out by me and that it has not been submitted in any previous application for a higher degree.

Date 27/2/02 Signature of candidate

I was admitted as a research student in September 1998 and as a candidate for the degree of PhD in August 1999; the higher study for which this is a record was carried out in the University of St Andrews between 1998 and 2002.

Date 27/2/02 Signature of candidate

I hereby certify that the candidate has fulfilled the conditions of the Resolution and Regulations appropriate for the degree of PhD in the University of St Andrews and that the candidate is qualified to submit this thesis in application for that degree.

Date 27/2/02 Signature of supervisor

In submitting this thesis to the University of St Andrews I understand that I am giving permission for it to be made available for use in accordance with the regulations of the University Library for the time being in force, subject to any copyright vested in the work not being affected thereby. I also understand that the title and abstract will be published, and that a copy of the work may be made and supplied to any *bona fide* library or research worker.

Date 27/2/02 Signature of candidate

ACKNOWLEDGEMENTS

Firstly I would like to thank Phil, for giving me the opportunity to work in his group, and for his guidance, enthusiasm, optimism and expertise.

Thanks to Dr Alex Slawin for single crystal data collection on several of the materials in this thesis. Thanks to the ESRF, Grenoble, and the SRS, Daresbury, for beam time, and to the staff for their expertise.

Magnetic measurements have been carried out by Prof. Bob Cywinski and Dr Adrian Hillier, and Prof. Andrew Harrison and Dr Satish Tiwary. Thanks especially to Satish for his chemist-friendly explanations.

I am also grateful to many of the technical and scientific staff of the University of St Andrews for assistance, and to the EPSRC for funding this work.

On a more personal note, I'd like to thank the other Lightfeet: Chris, David, Charles, Alan, and others who have joined us over the past few years. To all those who I've shared a lab, offices and hours in the pub with, cheers, it's been fun!

Thanks to my parents for their support and continued interest in what I'm doing.

Finally, thanks to Martin for being there, especially over the past few months.

ABSTRACT

New mixed anion frameworks have been produced by hydrothermal synthesis. The manganese phosphate oxalate materials, labelled MnPOX-*n*, fall into four distinct structure types. MnPOX-1, $Mn_4(PO_4)_2(C_2O_4)(H_2O)_2$, is a three-dimensional framework constructed from manganese phosphate layers pillared by oxalate anions. MnPOX-2, -3 and -4 share similar frameworks but include different structure directing amines, and are described by the formula $[Mn_2(HPO_4)_2(C_2O_4)(H_2O)_2](AH_2)$, where A = ethylenediamine (MnPOX-2), 1,3-diaminopropane (MnPOX-3) and *trans*-1,4-diaminocyclohexane (MnPOX-4). Although quite different in structure to MnPOX-1, their architecture can also be described as pillared layers, with protonated amines located in channels parallel to the layers. The choice of amine is reflected in subtle structural variations. MnPOX-5 and MnPOX-6 ($[Mn_4(HPO_4)_2(C_2O_4)_3(H_2O)_2](AH_2)(H_2O)_2$) again differ mainly in the extra framework amine cations which they contain (A = ethylenediamine and piperazine respectively). The three-dimensional frameworks are built from manganese phosphate chains, which are connected to each other in two different directions by oxalate anions. Water and protonated amines are located in channels in the structure. A water molecule is also found as a ligand in the manganese co-ordination sphere. Both types of water can be removed from MnPOX-5 to give a related material MnPOX-7. Investigations into hydrothermal synthesis with low water content led to the formation of $Mn_2(H_2PO_4)_2(C_2O_4)$, MnPOX-8. Again a pillared layered structure is seen, containing continuous edge-sharing chains of MnO_6 octahedra.

All of the phosphate oxalates available as pure samples showed antiferromagnetic ordering at low temperatures. A rounded susceptibility maximum in MnPOX-1 indicates two-dimensional ordering, whilst a more complex ordering behaviour is suggested by the behaviour of MnPOX-8.

In addition, three other framework materials are presented. MnOX-1 ($Mn_2(C_2O_4)_3(C_4H_8(NH_2)_2)$) and GdOX-1 ($[Gd(C_2O_4)_2(H_2O)](CH_3NH_2CH_3)(H_2O)_3$) are three-dimensional metal oxalate frameworks which contain amine cations. $K_3[Fe_4O(OH)(PO_4)_4](H_2O)_4$ (FePO4-1) is related to the mineral leucophosphite.

CONTENTS

CHAPTER 1 – INTRODUCTION

"We seek to control with fine resolution the architecture of these crystalline solids, and to tailor their chemistries for particularly desired properties. This is the true realm of solid state chemistry."

John M. Newsam in *Solid State Chemistry: Compounds*[1]

The work described in this thesis is in the field of crystalline framework materials and is largely concerned with their structure, elucidated by x-ray diffraction. The first family of such frameworks to be explored was the zeolites, which are described below. Further advances and investigations in the field are then discussed in order to put the work in this thesis in context.

1.1 Zeolites[1-3]

1.1.1 Structure

Zeolites are crystalline aluminosilicates, of general formula $M_{x/n}[Si_{1-x}Al_xO_2].mH_2O$, where M is a cation with charge n^+. They possess a rigid framework with a well defined system of channels and cavities which are of a size similar to small molecules. Zeolites were first described as a class of minerals in 1756.[4] Approximately 40 occur naturally, with over 100 synthetic structure types that have not been found outwith the laboratory.

Zeolites are constructed from AlO_4 and SiO_4 tetrahedra, which share corners throughout the structure. These form so called secondary building units (SBUs) which are described by the number of tetrahedral (T) atoms involved, *e.g.* six-rings, double four-rings. They are often drawn using lines to represent the T-O-T linkages, and nodes for the T atoms. The SBUs join together to form larger

units, such as the well known sodalite cage. These and other such units can be joined by SBUs and stacked in different sequences to produce the full 3D framework. The sodalite cage and some framework types containing it are illustrated in Figure 1.1.

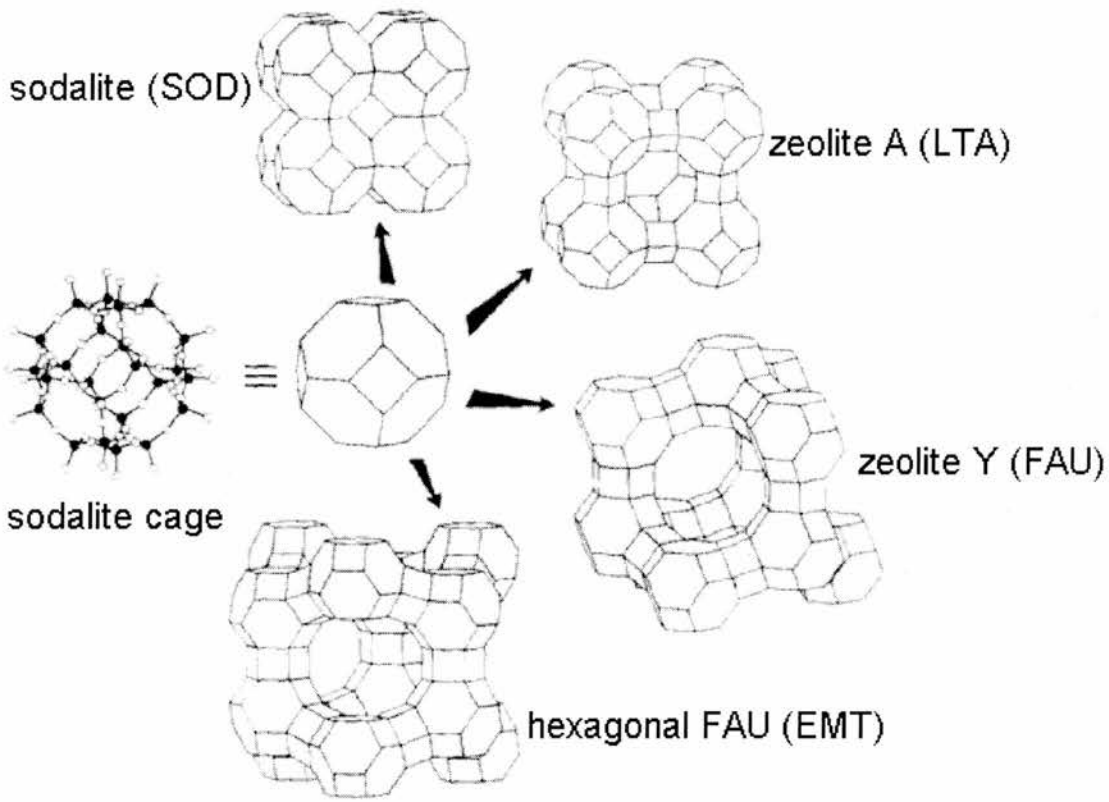

Figure 1.1 The sodalite cage and four zeolites that are constructed from it[1]

The construction of the framework produces different types of architectures, illustrated schematically in Figure 1.2.

Pure silica is neutral, but when Al^{3+} ions are substituted in place of Si^{4+} ions, the framework acquires a negative charge. This is balanced by an exchangeable extra-framework metal cation M, such as sodium. Zeolites may also contain other removable guests, usually water.

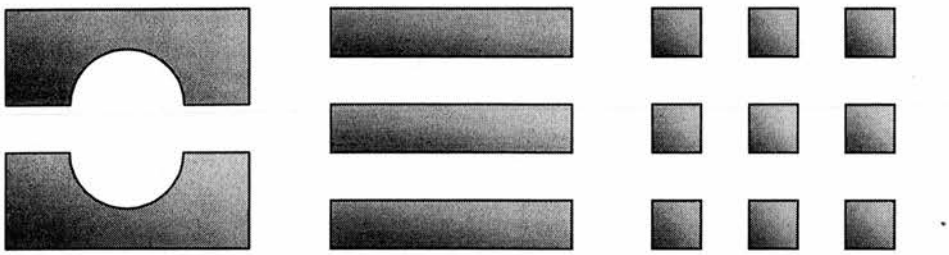

Figure 1.2 Structures found in zeolites. From left to right; a cage, 1D channels and 2D channels with intersection.

1.1.2 Synthesis

Early attempts to synthesise zeolites aimed to mimic the geological conditions under which they were thought to have formed, at high temperatures and pressures (T > 200 °C, P > 100 bar). In the late 1940s, milder hydrothermal synthesis was developed, and the first zeolite which was not naturally occurring was reported by Barrer in 1948.[5] The synthesis takes place at high pH, from sodium silicates and aluminates and alkali metal hydroxides. The silicate and aluminate species polymerise to form a gel, which is heated for around two days at temperatures between 60 - 100 °C. The high concentration of OH^- ions is required to solubilise the silicate and aluminate species. Hydroxide can be replaced by F^-, allowing the reactions to take place under neutral or acidic conditions.

Early synthetic zeolites often had high Al content, although it was observed by Loewenstein that the Si : Al ratio was always greater than one. He proposed that this is because Al-O-Al linkages are unfavourable, due to the higher stability of negative charge on the framework when it is spread out rather than in clusters.

The hydrated alkali metal cations direct the formation of the structure. This area was further developed when tetramethylammonium cations were used as structure directing agents.[6] As such cations are also present to balance the framework charge, they aid formation of materials with a high silica content due to their much higher size : charge ratio compared to alkali metal cations. Size and shape manipulation of these organic cations can be used in the development

of new structure types. Davis and Lobo discuss the function of these cations, proposing three roles of increasing specificity.[3] Firstly, they can act as **space filling species**, increasing the stability of the framework by occupying the void volume, effectively 'trapping' the metastable zeolite and preventing formation of a more thermodynamically stable product. Secondly, the cations can be **structure directing agents**, in which case a structure can only be synthesised using one particular cation. Lastly, they can have a **templating** effect, where enhanced host-guest interactions occur, for example free-rotation of the cation is restricted by the framework. These terms are, however, often used interchangeably.

1.1.3 Applications

The ordered systems of channels and cavities lead to a range of current applications for zeolites, discussed below.

1.1.3.1 Drying Agents

Water present in zeolites can be removed by heating under vacuum. Extra-framework cations tend to move on water loss, often to a position with a lower co-ordination number. These dehydrated zeolites will then act as drying agents, readily adsorbing water to allow the cations to move back to more favourable positions.

1.1.3.2 Ion Exchange

Zeolite A, containing Na^+ ions, is often used in detergents as a water softener. In hard water, the sodium ions will be exchanged for calcium and magnesium ions. Clinoptilite, a naturally occurring zeolite, can be used to extract the radioisotopes ^{137}Cs and ^{90}Sr from nuclear waste.

1.1.3.3 Adsorbents

With their large internal surface area, zeolites are capable of adsorbing large volumes of other substances. They are highly specific, the size of the adsorbed species depending on the size of the windows of the framework's cavities. The size of molecules a particular zeolite is capable of adsorbing can be tuned by manipulation of the cations in the material. The Ca^{2+} form of zeolite A adsorbs small straight chain alkanes, but not branched or cyclic molecules, for example.

1.1.3.4 Catalysis

The channels and cavities giving zeolites their large internal surface are well ordered so show good reproducibility in catalytic use compared to amorphous materials. They can also be shape selective, allowing control over reaction products.

Zeolites can be acid catalysts: if H^+ is used as the extra framework ion a Brønsted acid site is created. Heating can remove these protons as water, resulting in an aluminium site that is three co-ordinate which can then act as a Lewis acid. Small, highly charged hydrated cations such as La^{3+}, can also impart acidity to the structure by ionising the water ligands and releasing H^+. As the number of acid sites is related to the Al content of the material, the concentration can be modified as required.

Metals such as nickel, palladium and platinum can be exchanged into a zeolite and then reduced to give a supported metal catalyst. This results in very small clusters of metal atoms, and finds use in $DeNO_X$ materials.

Shape selectivity can be based on the reactants, products or transition state. The dehydration of butanol over Ca-zeolite A is a reactant selective process: only the straight chain 1-butanol has access to the internal surface. Methylation of toluene using methanol is carried out over the zeolite ZSM-5. This is product selective, as only the *para* isomer is able to diffuse out of the framework. An

example of transition state selectivity is seen in the reaction of two molecules of 1,3-dimethylbenzene to produce 1,2,4-trimethylbenzene. The transition state of the other possible product, 1,3,5-trimethylbenzene, requires more space than is available in the pores of mordenite, so the desired product is obtained.

Encapsulating homogeneous catalysts inside a zeolite framework (ship-in-a-bottle catalysis) aims to improve on the original homogeneous catalyst by allowing easier separation of the product from the catalyst and possibly increasing the stability of the active catalytic species. Use of a zeolite may also incorporate shape selectivity into the process.

1.1.3.5 Nanochemistry

Other areas of interest in zeolite applications include quantum confinement, for example using cadmium sulphide. Very small clusters of CdS can be contained within a framework allowing the band gap energies to be modified. Alignment of appropriate molecules within the channels of a zeolite or similar framework is of interest in non-linear optical applications.[7]

1.2 Aluminophosphates[1,3,8]

1.2.1 Structure

Closely related to the zeolites are the aluminophosphates, first synthesised by Flanigen and co-workers in 1982.[9] These have the general formula $[AlPO_4].yR.mH_2O$, where R is an extra-framework species, often an amine, and are denoted $AlPO_4$-*n*. $AlPO_4$ is neutral, however partial substitution of phosphorous by silicon can produce a charged framework requiring a counterion M^{n+}: $M_{x/n}[Si_xP_{1-x}AlO_4].yR.mH_2O$. Silicon substituted $AlPO_4$s are denoted SAPO-*n*. Many other elements can also be substituted into the framework, initially these were divalent metal cations, such as Mg, Mn, Fe, Co and Zn, to give

MAPO-*n*, where the metal substitutes for aluminium. Li, B, and Ga substitutions have also been reported.

Some MAPO structure types exist that have been impossible to synthesise without the metal substitution. The material DAF-1 requires magnesium, which substitutes for aluminium, and utilises decamethonium hydroxide as the template.[10]

Beryllo and zincophosphates have been reported, where the beryllium or zinc has totally replaced the aluminium (the corresponding arsenates also exist).[11] In addition, materials such as gallosilicates, aluminogermanates and gallogermanates exist. Metals have been incorporated into non-tetrahedral sites, for example in $NH_4[CoGa_2(PO_4)_3(H_2O)_2]$ the cobalt exists in octahedral co-ordination.[12]

1.2.2 Synthesis

$AlPO_4$s are, like zeolites, synthesised hydrothermally but under acidic or mildly basic conditions (pH ~ 5 - 8). A gel is formed from a reactive alumina, phosphoric acid, an organic structure directing agent or template (denoted R in the formula above) and water. Synthesis may take place between 100 and 300 °C, over periods of hours or weeks. Calcination in air between 500 - 600 °C removes the organic template. The development of new $AlPO_4$ frameworks is largely dependent on the organic template, and much research has been undertaken in this area.

1.2.3 Applications

Catalysis is the main area of interest for $AlPO_4$s. SAPOs and MAPOs, where charge balancing species are required, can be utilised as acid catalysts, *e.g.* MAPO-18 (where the substituted metal is Mg, Zn or Co) catalyses the

conversion of methanol to ethene and propene.[13] Cobalt and manganese have been substituted into $AlPO_4$-18 and -36 to produce oxidation catalysts which are capable of selectively oxidising linear alkanes at the terminal carbons with molecular oxygen.[14]

1.3 Non-tetrahedral Frameworks

Large growth occurred in the field of open frameworks in the 1990s; over 40 elements have been incorporated into these materials as major framework components.[15] The substitution of transition metals into $AlPO_4$ structures paved the way for new types of framework where the building blocks are no longer tetrahedral, but other metal co-ordination geometries such as octahedra, and rigid organic ligands are used. This permits incorporation of metals with different, possibly variable, oxidation states. Along with these developments has been a general decrease in the thermal stability of such structures, and problems with removal of extra-framework species. The robustness of zeolite frameworks is thought to be due to the strength of the Si-O bond (799.6 kJ mol^{-1}). The thermal stability of these new frameworks is lower, and the metal oxygen bonds are not as strong, *e.g.* Fe-O 390.4 kJ mol^{-1} and Mn-O 402.9 kJ mol^{-1}.[16]

1.3.1 Transition Metal Phosphates

Replacement of aluminium by transition metals is an obvious extension of $AlPO_4$ systems. Some transition metal phosphates are discussed below, beginning with the first family to be reported, the molybdenum phosphates.

1.3.1.1 Molybdenum Phosphates

Haushalter and co-workers synthesised molybdenum phosphates in an attempt to create a microporous framework capable of acting catalytically.[17] The ability of

Mo to exist in a variety of oxidation states made it suitable for such an aim. Initially this involved high temperature synthesis (> 750 °C) but this necessitated the use of an inorganic template, which did not permit the formation of suitably large channels. Milder, *i.e.* hydrothermal, conditions were used to enable organic templates to take part in the reaction. The first microporous 3D molybdenum phosphate, $[Mo_4O_8(PO_4)_2]((CH_3)_4N)_{1.3}(H_3O)_{0.7}(H_2O)_2$, was reported in 1989. The building unit for this material is the Mo_4O_8 cube. PO_4 groups connect these cubes to form the 3D structure. Cavities are formed which contain the tetramethylammonium cations as well as H_2O and H_3O^+, and have double Mo-O bonds pointing into them. The cavities are approximately 7 Å across between the Mo=O oxygen atoms, but are only accessible through a small window of 2.8 Å. The material shows reversible adsorption of water.

The framework $[Mo_2O_2(PO_4)_2(H_2PO_4)]^-$ can accommodate several different cations.[17] Mo and P atoms are arranged in a square grid, connected by O atoms. These layers are bridged by $H_2PO_4^-$ groups that can rotate to alter the relative positions of adjacent layers, allowing the framework to exist with H_3O^+, $CH_3NH_3^+$ or Cs^+ and H_3O^+ in the void space (in the last case the $H_2PO_4^-$ is replaced by HPO_4^{2-}). These materials also show reversible adsorption of water.

1.3.1.2 Vanadium Phosphates

Haushalter and co-workers have also reported a number of vanadium phosphates, again the choice of metal reflecting its catalytic interest. An example is $[V^{III}(H_2O)_2(V^{IV}O)_8(OH)_4(HPO_4)_4(PO_4)_4(H_2O)_2](H_3N(CH_2)_2NH_3)_2(H_3N(CH_2)_2NH_2)(H_2O)_2$.[18] The V^{III} is octahedral and the V^{IV} is square pyramidal. Layers of square pyramidal vanadium and phosphate groups are connected together by the octahedral vanadium. Elliptical channels are formed which are 18.4 Å across at their widest point, containing water and ethylenediammonium cations.

1.3.1.3 Iron Phosphates

Many iron phosphate minerals are known, cacoxenite being a particularly impressive example of a naturally occurring open framework. Its structure was finally elucidated by Moore in 1983, who reports he had been waiting 10 years for a suitable crystal.[19] Previous analysis had shown that the mineral contained an unusually high amount of water, now known to be mainly situated within large pores in the structure. Cacoxenite is a three dimensional aluminium containing iron phosphate, with proposed formula $[Al(Al,Fe)_3Fe_{21}O_6(OH)_{12}(PO_4)_{17}(H_2O)_{24}](H_2O)_{\sim 51}$. A projection of the structure down the *c* axis is shown in Figure 1.3.

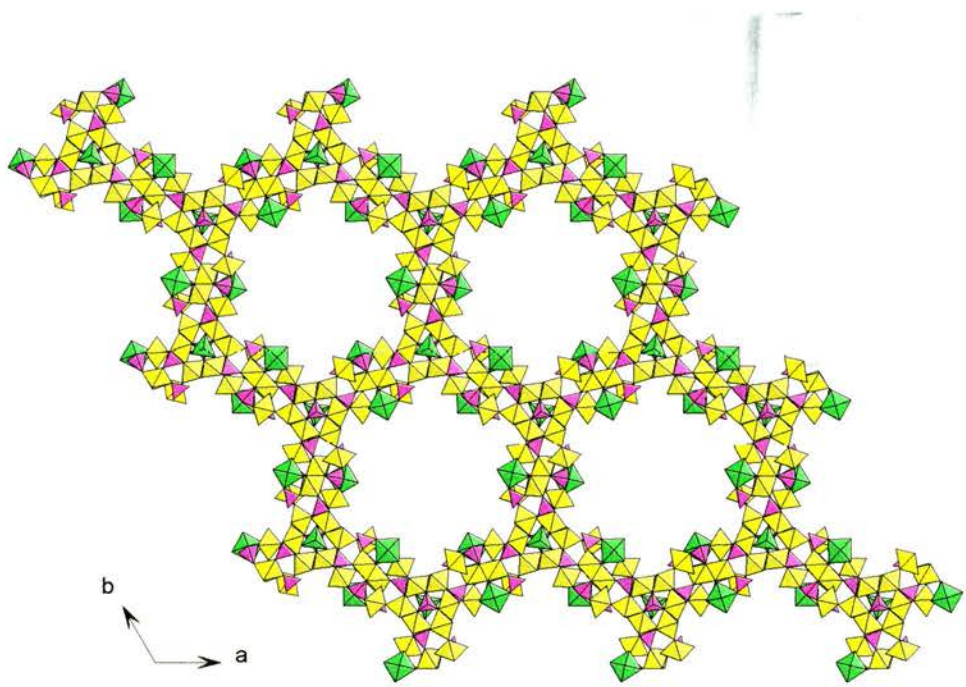

Figure 1.3 Cacoxenite in the ab plane.[19] Iron octahedra yellow, aluminium trigonal bipyramids green, phosphate tetrahedra purple. Water molecules in pores not shown.

Aluminium exists in trigonal bipyramidal co-ordination, while the iron is octahedral. The extra-framework water molecules were not located, but are believed to be distributed in the channels, which have a free pore diameter of

14.2 Å. Moore comments, "Is cacoxenite unique or does it represent just one of a family of phases based on octahedral-tetrahedral incompleted frameworks and large open channels, pores or cavities?"

The first synthetic open framework iron phosphates were two mineral analogues synthesised by Corbin *et al.* in 1986.[20] $Fe_5(PO_4)_2(HPO_4)_2(H_2O)_4$ is the pure iron version of the mineral hureaulite, which occurs naturally containing iron and manganese. This is a 3D structure with small channel systems in three different directions. The second, $NaFe_3(PO_4)_3$ is isostructural with alluaudite $(X_{4-8}(Y,Fe^{3+})_{12}(PO_4)_{12}$ where X = Na, Ca, K and/or Mn, and Y = Mn^{2+}, Fe^{2+}, Mg, Ca, Li and/or Na). Channels are also formed in this material, where sodium cations are found. The materials were synthesised hydrothermally in the presence of tetrapropylammonium or tetrabutylammonium hydroxide; the hureaulite structure was the major product, small amounts of alluaudite were obtained when tetrabutylammonium hydroxide and a low concentration of sodium ions were added. The alkylammonium hydroxides were deemed necessary to produce the open frameworks, the authors propose that the hydroxide neutralises the phosphoric acid used.

The majority of synthetic work on open framework iron phosphates has been carried out in the groups of Lii and Férey, both of who have recently reviewed the subject.[21,22]

The first synthetic open framework iron phosphates containing organic cations were the ULM-*n* phases, which were synthesised using fluoride, resulting in oxyfluorinated structures.[22] The first of these to be reported was $[Fe^{3+}Fe^{2+}F_2(HPO_4)_2(H_2O)_2](H_3N(CH_2)_2NH_2)$, ULM-10.[23] This is a layered material, with layers built up from FeO_4F_2, $FeO_2F_2(H_2O)_2$ and HPO_4 units. The organic cation is found between the layers with strong hydrogen bonding to the phosphate tetrahedra. The amine is unusually found half-protonated in this structure.

Many of these material are built up from secondary building units (SBUs), comparable to zeolites. ULM-3[24] and ULM-4[25] both contain an SBU made up

from two trigonal bipyramids, one octahedron and three tetrahedra. These SBUs share corners through O atoms to form the 3D framework.

Also of interest are ULM-12, $[Fe_4(PO_4)_4F_3(H_2O)_3](N_2C_6H_{14})$, and ULM-19, $[Fe_4(PO_4)_4F_3](N_2C_6H_{14})$.[26] ULM-12 is 3D, constructed from two types of SBU which share corners. Dehydration of ULM-12 forms ULM-19, which has a similar structure but due to the loss of water (which acts as a ligand) the co-ordination geometry and number changes around some of the iron centres. Both structures have channels parallel to the *c* direction, but the loss of water results in an extra set (in the same direction) appearing in ULM-19.

Lii and co-workers discuss several structural features seen in open framework iron phosphates: the "leucophosphite-type" cluster and Fe_4P_4 cubane-like clusters.[21] The first of these occurs in $[Fe_4(OH)_3(HPO_4)_2(PO_4)_3](H_3N(CH_2)_3NH_3)_2(H_2O)_x$[27] and consists of a tetramer of octahedral iron atoms which is also seen in the mineral leucophosphite, discussed further in section 6.4.2. At the centre of the tetramer two iron octahedra share an edge. Two additional octahedra share corners with the central irons through three co-ordinate oxygen atoms. The tetramers share corners to form columns, which are linked by phosphate tetrahedra to form channels along the *b* axis, containing water and ethylenediammonium cations. This structure has a very low framework density, with 10.5 M atoms per 1000 $Å^3$ (where M = Fe or P), compared to 12.1 for cacoxenite (discussed above). A similar iron tetrameric unit is reported in $[Fe_2O(PO_4)_2](H_3N(CH_2)_3NH_3)$, however the iron centres are trigonal bipyramids in this case.[28]

The Fe_4P_4 cubane-type clusters are seen in the mixed valence $[Fe_4O(PO_4)_4](H_3N(CH_2)_2NH_3)_2(H_2O)$.[29] There are two slightly different types of cluster in the material, one with four trigonal bipyramids and one with three trigonal bipyramids and one octahedron. Both have a tetrahedral arrangement of iron atoms with a four co-ordinate O atom at the centre. P atoms make up the remaining corners of the "cube". Fe-O-P linkages connect the clusters to form a 3D structure with two intersecting channel systems. A very similar material was also reported by DeBord *et al.*[30]

1.3.1.4 Cobalt Phosphates

J. M. Thomas and co-workers reported the first framework cobalt phosphate in 1994, DAF-2, in which cobalt is found exclusively in tetrahedral co-ordination.[31] $[CoPO_4](H_3N(CH_2)_2NH_3)_{0.5}$ is constructed from CoO_4 and PO_4 tetrahedra with ethylenediammonium cations to balance the framework charge. There are three channel systems, containing the amine cations at their intersections.

Two cobalt phosphates which share the zeolite framework type of a zeolite, ABW, were synthesised by Stucky and co-workers.[32] The two materials, $RbCoPO_4$ and NH_4CoPO_4, both contain relatively large cations (Rb^+ and NH_4^+; compared to K^+ or Na^+), the authors predict that the use of even larger cation will result in $CoPO_4$ frameworks with bigger pores. Stucky and co-workers have also reported many cobalt-rich aluminophosphates.[33]

1.3.1.5 Manganese Phosphates

A layered manganese (III) phosphate containing ammonium cations was reported in 1989.[34] $[Mn_2O(PO_4)(HPO_4)(H_2O)](NH_4)$ contains zigzag chains of edge-sharing distorted MnO_6 octahedra, which are linked by phosphate tetrahedra to form layers. Ammonium cations are found between these layers, hydrogen bonded to the framework. Zigzag chains are also present in the 3D structure of $LiMnPO_4(OH)$, which exhibits migration of the manganese octahedra on lithium exchange.[35]

Rajić *et al.* investigated ethylenediamine, piperidine and isopropylamine as potential templates for manganese phosphates.[36] The materials were obtained as powders (the structures were not determined), with piperidine and isopropylamine appearing to give the same structure, apparently not containing any organic material, whereas ethylenediamine gives a different product with amine in the structure.

Porous manganese oxides exist,[37] but there has not been much further development in open framework manganese phosphates.

1.3.1.6 Nickel Phosphates

As with manganese, few examples of open framework nickel phosphates exist. One material of particular interest is VSB-1, $Ni_{18}(HPO_4)_{14}(OH)_3F_9(H_3O,NH_4)_4(H_2O)_{12}$, which is constructed from a network of NiO_6 octahedra sharing edges and corners which form 1D channels.[38] The surface of these channels is decorated by the phosphate groups. Substitution of Mn, Fe, Co and Zn for Ni into the structures is possible. The structure can also form with K^+ in place of NH_4^+, when Li^+ or Na^+ can replace the K^+ by ion exchange. The material is stable to removal of extra framework species up to 550 °C, and has recently been shown to be catalytically active in the conversion of butadiene to ethylbenzene, showing an 82 % selectivity.[39] This reaction is of interest in styrene production.

1.3.1.7 Zinc Phosphates

The zinc phosphate $Na_6[ZnPO_4]_6(H_2O)_8$ with the sodalite structure has been prepared by Stucky and co-workers at relatively low temperatures (70 °C[11] and room temperature[40]). They also report zinc phosphates not analogous to zeolites prepared hydrothermally, which contain 1,4-diazabicyclo[2.2.2]octane (DABCO).[41] Both $[Zn_2(HPO_4)_3](H_2N_2C_6H_{12})$ and $[Zn_4(PO_4)_2(HPO_4)_2](H_2O)_3(H_2N_2C_6H_{12})$ have two different types of channels running in one direction.

An interesting zinc phosphate with large channels (10.5 Å at their narrowest point) was synthesised by Yang and Sevov in 1999.[42] Both the *cis* and *trans* forms of 1,2-diaminocyclohexane were used in the synthesis, but only the *trans* form was found to be incorporated in $[Zn_3(PO_4)_2(HPO_4)](C_6H_{10}(NH_3)_2)(H_2O)_2$, where it is found around the edges of the channels, resulting in free channels

space without removal of the cations. The material adsorbs benzene, toluene and cyclohexane without initial removal of the templating cations, but not *t*-butylbenzene, due to its size.

1.3.2 Co-ordination Polymers

The materials discussed so far are all constructed from various polyhedra. In order to create novel frameworks, especially with larger or more tailored internal spaces, the field has been extended by the use of rigid organic units. One way of achieving this is through organic modification of phosphate type materials, by incorporating phosphonate species into structures. Those that were first used were monophosphonates, which often formed layered materials.[8] The use of diphosphonates, *i.e.* $O_3P\text{-}R\text{-}PO_3$, where R is some organic based unit, led to the formation of 3D structures.

Co-ordination polymers, or metal-organic frameworks, are non-phosphate based, constructed from metal centres (octahedra, tetrahedra, etc) linked together by rigid organic units with several donor atoms available to co-ordinate to the metals. The aim of introducing new elements and building units is to enable materials to be constructed with cavities with designed size, shape and function, *e.g.* hydrophilic/hydrophobic character. It has been suggested that these materials should complement, rather than mimic, zeolite-type structures.[43]

With the introduction of new elements into framework materials, there has been a departure from oxide systems. Nitrides, sulphides, selenides and cyanides have all been incorporated into a variety of structures.[44] Further discussion here however, will concentrate mainly on oxygen based materials.

1.3.2.1 Main Group Elements

Several tin oxalate frameworks exist which contain amine cations. The materials are layered, with the amines occupying the space between the layers. In $[Sn_2(C_2O_4)_3]((CH_3)_2NH(CH_2)_2NH(CH_3)_2)(H_2O)$[45] and $[Sn_2(C_2O_4)_3]$ $((CH_3)_2NH(CH_2)_4NH(CH_3)_2)$[46] SnO_6 units are pentagonal bipyramidal, with a lone pair on one of the axial positions. Layers in both structures contain 12-membered rings. $[Sn_4(C_2O_4)_5](C(NH_2)_3)_2(H_2O)_2$ consists of SnO_4 and SnO_6 units, with 20-membered rings in the layers.[45]

1.3.2.2 Lanthanide and Actinide Elements

Frameworks containing lanthanide and actinide elements have been reported constructed from oxalate,[47-51] succinate,[52] glutarate,[52,53] adipate,[54] and terephthalate[55].

$[Tb(C_6H_4(COO)_2)(NO_3)](DMF)_2$ shows loss of the solvent molecules on heating with loss of long range order, but the structure reforms on readsorption of DMF or dichloromethane.[55] The material also shows solution adsorption of methanol, ethanol and isopropylalcohol in toluene, but is unstable in water.

The 3D lanthanum adipate $[La_2(C_4H_8(COO)_2)_3(H_2O)_4](H_2O)_6$ shows reversible dehydration to $[La_2(C_4H_8(COO)_2)_3(H_2O)_2]$, losing six free and two ligand water molecules.[54] Reversible water loss has also been reported in some of the glutaric acid structures $[Ln_2(O_2C(CH_2)_3CO_2)_3(H_2O)_2](H_2O)_4$ with Ln = Pr, Nd, Sm, Eu, Gd, Dy, Ho and Y.

Using two different metals introduces the possibility of interesting magnetic interactions. $[Gd_2Cu_3(C_2O_4)(pba)_3](Cu(H_2O)_5)(H_2O)_{20}$, where pba = 1,3-propylenebis(oxamato), is constructed from Gd-pba-Cu-pba-Gd and Gd-C_2O_4-Gd linkages (see Figure 1.4) which form ladder type chains.[49] These chains form layers with a honeycomb pattern, with $Cu(H_2O)_5$ and H_2O species in the interlayer space.

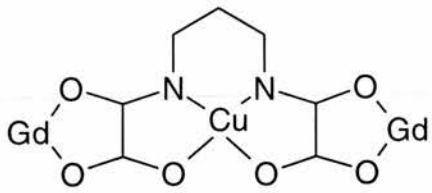

Figure 1.4 1,3-propylenebis(oxamato) linkage in $[Gd_2Cu_3(C_2O_4)(pba)_3](Cu(H_2O)_5)(H_2O)_{20}$[49]

A ferromagnetic interaction is observed between the Gd and Cu through the oxamato bridge, and a weak antiferromagnetic Gd-Gd interaction exists through the oxalate linkage.

$[LnCr(C_2O_4)_3(H_2O)_4]_2(H_2O)_n$ where Ln = La, Ce, Pr or Nd and n = 7 - 12 is also a ladder structure.[50] There are two sets of orthogonal ladders which are almost identical, with alternating Ln and Cr. Antiferromagnetic interaction between neighbouring metal centres result in overall ferrimagnetic behaviour.

$K_2[MnU(C_2O_4)_4](H_2O)_9$ is a 3D framework, with nine co-ordinate uranium and, unusually, eight co-ordinate manganese (surrounded by four oxalate anions).[56] The framework has channels running along the *b* axis. The magnetic properties are described by the authors as being a sum of the U(IV) and Mn(II) contributions. Magnetic coupling was found to be too weak to be observed in the experiment. The authors propose a change of metal or ligand may increase the size of the interactions.

1.3.2.3 Transition Metal Elements

The majority of the metal-organic frameworks that have been reported contain transition elements, especially those of the first row. As interest in open framework materials centres on their internal structure, access to the pores is essential. This is often prevented however, by non-removable guest species or self-interpenetration of two or more frameworks.

Frameworks do exist with void space despite interpenetration. $[Cu(C_{10}H_8N_2)_{1.5}]NO_3(H_2O)_{1.25}$, a 4,4'-bipyridine containing framework, is constructed from six interpenetrating networks which each contain a 3D channel system.[57] After interpenetration there remain two rectangular channels which contain water and nitrate ions. The water can be removed by heating to 120 °C, and the dehydrated material can undergo ion exchange, with SO_4^{2-} or BF_4^- ions replacing the NO_3^-.

Yaghi and co-workers have been successful in synthesising several metal-organic materials which show reversible exchange of guest species. 1,3,5-benzenetricarboxylic acid and pyridine form the layered cobalt material $[CoC_6H_3(COOH_{1/3})_3(NC_5H_5)_2](NC_5H_5)_{2/3}$.[58] As well as a ligand, pyridine is also a guest in this structure, lying between the layers in rectangular channels. This guest pyridine can be thermal removed leaving the framework intact. Absorption of aromatic molecules such as benzene, nitrobenzene, cyanobenzene and chlorobenzene is then possible, however non-aromatics such as acetonitrile, nitromethane and dichloroethane are not taken up by the structure. This selectivity is thought to be due to π-stacking interactions between the benzenetricarboxylic acid in the framework and the aromatic guests.

Benzenetricarboxylic acid has also been incorporated into the zigzag chain materials $[M_3(C_6H_3(COO)_3)_2](H_2O)_{12}$ with M = Co^{2+}, Ni^{2+} or Zn^{2+}.[59] The zinc containing material was the most robust, able to be dehydrated on heating but regaining its structure on exposure to water. Reversible absorption of ammonia was also reported, although an impurity appeared to form as well as the original framework. Similar sized molecules with no reactive lone pairs were not adsorbed by the material again suggesting an interaction with the framework is important in the inclusion process, in this case possibly with co-ordinatively unsaturated metal sites.

Similarly, a zinc nitrate benzenetricarboxylate shows absorption of alcohols up to the size of *t*-butyl alcohol, but larger alcohols and non-alcoholic molecules such as chloroform were not adsorbed, with the exception of DMF.[60] Again this is

thought to be due to co-ordination of zinc by the hydroxyl groups or the capacity for hydrogen bonding.

Recent work suggests that in some circumstances such guest exchange would be more accurately considered as solid state transformation of the framework as guest species are removed and replaced.[61] Experiments with zinc benzenedicarboxylates showed a number of absorption and removal steps with various guest species which were accompanied by structural changes in the host.

One of the simplest organic ligands suitable for construction of co-ordination polymers is the oxalate anion. Metal oxalate frameworks can exist as 2D or 3D structures. Decurtins and co-workers discuss this in terms of the chirality of an octahedral centre with three bidentate ligands.[62] The two enantiomers of the octahedra are denoted Δ and Λ (see Figure 1.5).

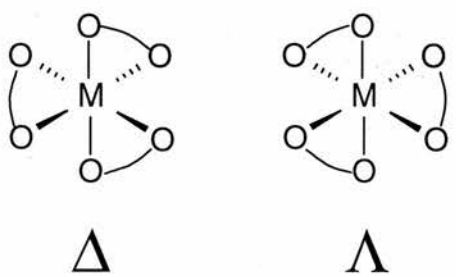

Figure 1.5 The two enantiomers, Δ and Λ, of an ML_3 octahedron, where L is a bidentate ligand, shown here with oxygen donor atoms.

The layered structure consists of alternating Δ and Λ $M(C_2O_4)_3$ octahedra, whilst all Δ or all Λ octahedra are found in the 3D framework. The 2D structure consists of honeycomb metal oxalate layers, illustrated in Figure 1.6.

Such structures have been reported with one metal, one metal in two different oxidation states or two metals, including Cr, Mn, Fe, Co, Ni, Cu and Zn.[62-67] A variety of counterions have also been included, which are situated between the layers. These include quaternary ammonium, phosphonium and arsonium species[62-65] and metal complexes (decamethylferrocenium and cobaltocenium)[66].

It has been proposed that the nature of the counterion may determine whether a 2D or 3D structure forms.[63]

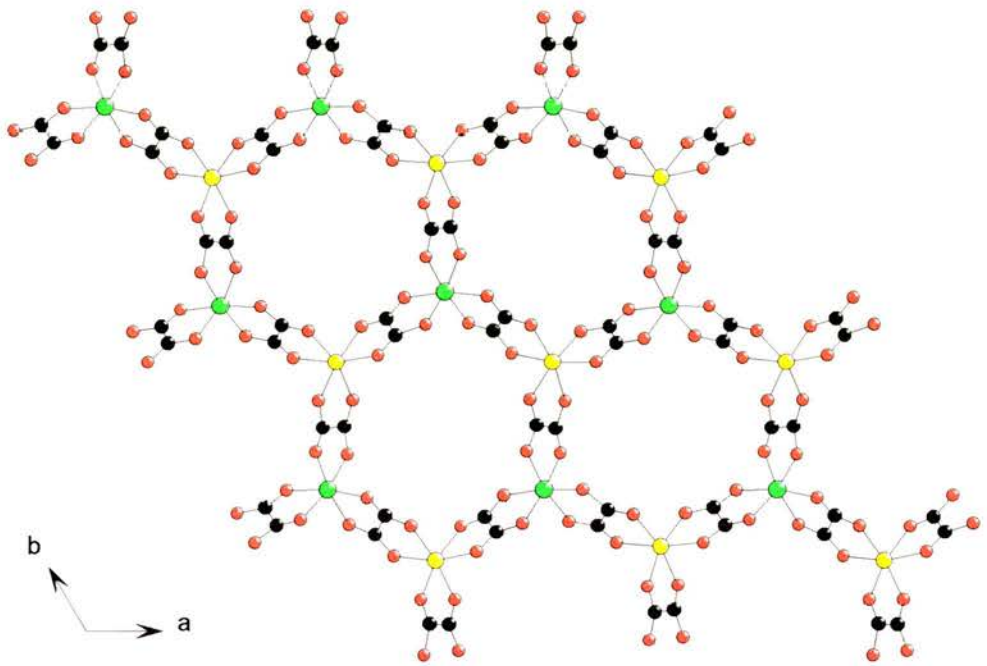

Figure 1.6 A honeycomb layer in a 2D metal oxalate.[62] Metal (manganese and chromium in this example) yellow and green, oxygen red, carbon black.

The 3D structure is illustrated in Figure 1.7. Identical helical metal oxalate strands run throughout the cubic structure in all three directions, appearing as small squares shapes running down the *a* axis in Figure 1.7.

Iron and nickel 2,2'-bipyridyl complexes have been used in these materials to balance the framework charge, these are located in the void space in the structure.[68,69] Iron and manganese based frameworks exist, as well as several mixed-metal materials, including some incorporating alkali metals.[69]

The majority of these metal oxalates have been synthesised as a result of interest in molecular based magnets. The oxalate anion is an ideal candidate as its co-

ordination modes allow for extended frameworks to be constructed, and it permits magnetic exchange interactions between the metal centres. The counterion in the layered materials can be used to tailor the interlayer spacing, and consequently the magnetic properties.

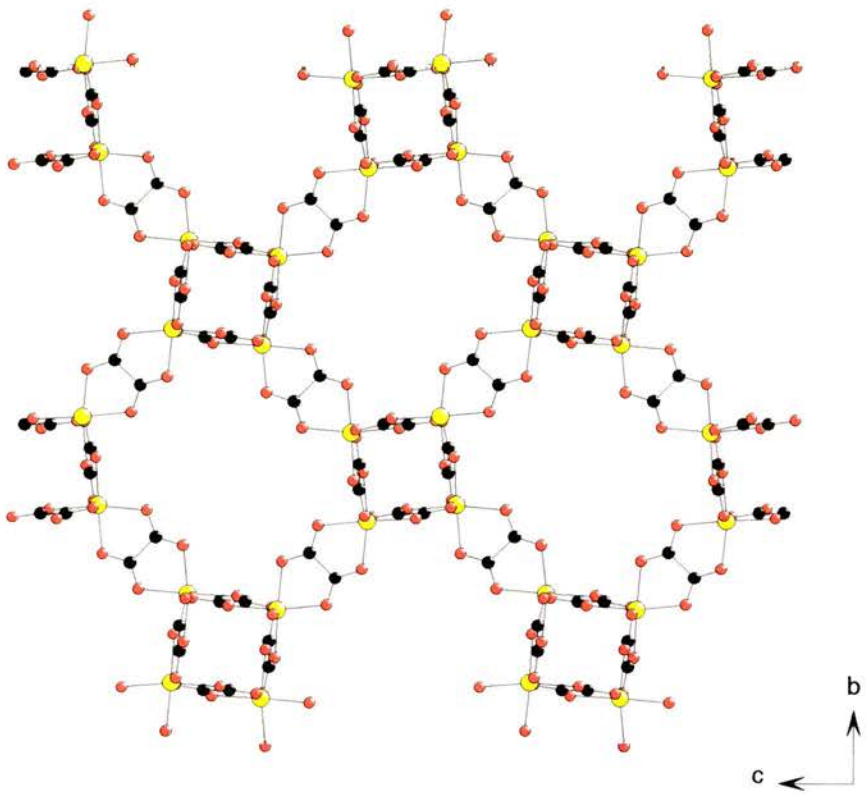

Figure 1.7 A *bc* plot of the 3D metal oxalate framework.[68] Metal (iron in this example) yellow, oxygen red, carbon black. Counterions not shown.

A series of layered materials with general formula $A[M^{II}Fe^{III}(C_2O_4)_3]$, where M^{II} = Mn, Fe and A = $N(n\text{-}C_mH_{2m+1})_4$ for m = 3 - 5, $N(n\text{-}C_4H_9)_3(C_6H_5CH_2)$, $P(n\text{-}C_4H_9)_4$, $P(C_6H_5)_4$, $(C_6H_5)_3PNP(C_6H_5)_3$ and $As(C_6H_5)_4$ has been reported.[63] All structures showed antiferromagnetic interactions between M^{II} and Fe^{III}, resulting in ferrimagnetic (M^{II} = Fe) and antiferromagnetic (M^{II} = Mn) ordering. In the M^{II} = Fe series with A = $N(n\text{-}C_mH_{2m+1})_4$, the ordering temperature was found to increase with increasing interlayer separation (*i.e.* increasing m) in contrast to the normal situation where increasing the layer spacing decreases the ordering temperature. The substances with M^{II} = Mn show a broad susceptibility maxima

characteristic of 2D antiferromagnetism. Some of the samples showed evidence of spin canting at low temperatures.

The series $A[M^{II}M^{III}(C_2O_4)_3]$ with M^{II} = Mn, Fe, Co, Ni, Cu and A = N(n-C_4H_9), decamethylferrocenium and decamethylcobaltocenium has been investigated using $M^{III} = Fe^{III}_{x}Cr^{III}_{(1-x)}$.[65] This is of interest as the M^{II}-Cr^{III} interactions are antiferromagnetic while those of M^{II}-Fe^{III} are ferromagnetic, so the two will be competing in the structure. As x increases, the θ values go from positive to negative, reflecting the predominant interaction. The hysteresis traces for these $Fe_xCr_{(1-x)}$ materials showed much larger coercive fields than for the pure iron and chromium forms.

In the 3D structure, a series of materials with iron and nickel 2,2'-bipyridyl cations has been synthesised.[69] As well as Mn^{II} and Fe^{II} containing frameworks, $NaFe^{III}$, $LiCr^{III}$ and $LiFe^{III}$ forms were also reported. Negative values of θ were observed for the divalent manganese and iron materials, whilst the lithium-iron structure had a small positive θ.

Other ligands have been used in place of oxalate, of which some other oxygen donors are discussed below, with the ligands illustrated in Figure 1.8.

Formic acid, with only two donor oxygen atoms compared to oxalate's four, forms a 3D framework with manganese (III).[70] $[Mn(HCOO)_3](CO_2)_{1/2}(HCOOH)_{1/4}(H_2O)_{2/3}$ consists of alternating MnO_6-HCOO chains in all three directions which forms two different types of cage, which contain carbon dioxide and formic acid guests (disordered water is also thought to be located here). From infra-red spectroscopy the rotation of the carbon dioxide appeared to be hindered, due to framework-guest interactions. Although displaying the same connectivity in all three dimensions, the symmetry of the structure is not cubic due to Jahn-Teller distortion in the manganese. This results in ferromagnetic layers, with weaker antiferromagnetic interactions between the layers.

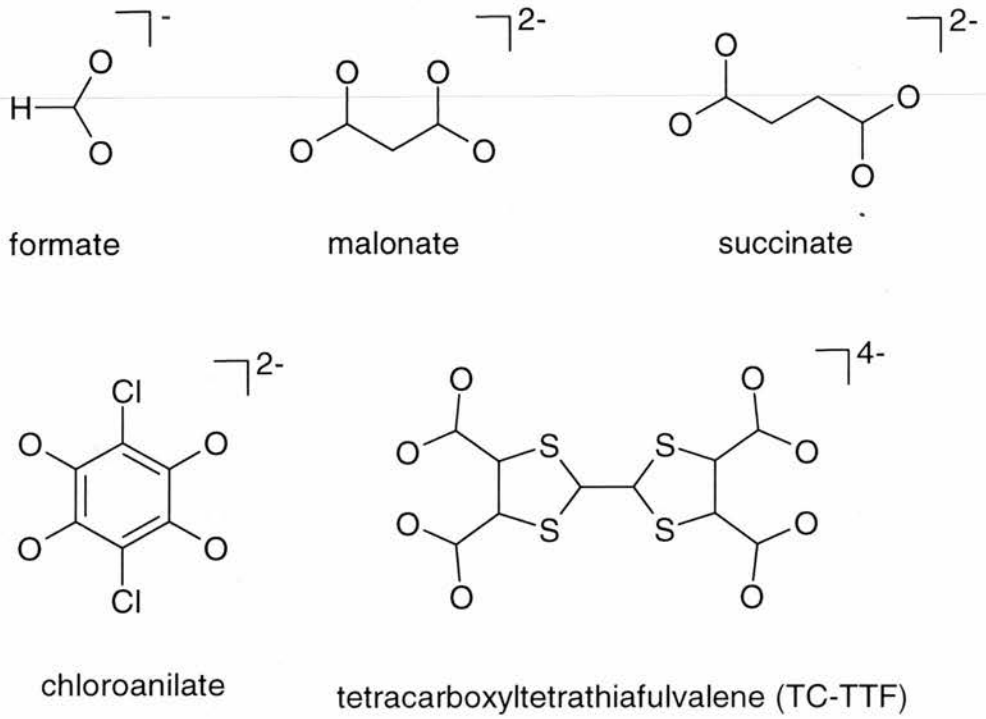

Figure 1.8 Examples of oxygen donor ligands which have been used in the construction of co-ordination polymers (references in text).

Malonic acid forms mixed metal materials $[MM'(C_3H_2O_2)_2(H_2O)_4]$ with M = Ba, Sr and M' = Cu, Mn.[71] The structure is constructed from copper malonate layers, with M atoms in-between. The materials can be used as precursors to mixed oxides.

Two cobalt succinates have been reported, $[Co_5(OH)_2(C_4H_4O_4)]$[72] and $[Co_4(OH)_2(H_2O)_2(C_4H_4O_4)_3](H_2O)_2$[73] both with similar 3D structures. Layers are formed from CoO_6 octahedra and succinate, which are pillared by further succinate ligands.

Materials with a high degree of hydrogen bonding have been synthesised incorporating more complex oxygen donor ligands. $[M(C_6Cl_2O_4)(H_2O)_2](H_2O)$ and $[M(C_6C_{l2}O_4)(H_2O)_2](C_{12}H_8N_2)$ where M = Fe, Co, Mn are similar structures built up from chloroanilic acid, containing water or phenazine guests.[74] Both consist of chains which are hydrogen bonded to each other to form layers. Variation of the guests, which are found between these layers, alters the shape of the chains: they are zigzag for H_2O but straight for phenazine.

Hydrogen bonds are also essential in $[Co(H_2O)_6](H_2TC\text{-}TTF)(H_2O)_2$, where TC-TTF = tetracarboxyltetrathiafulvalene.[75] This is a hydrogen bonded network of $Co(H_2O)_6$, H_2TC-TTF and water. The H_2TC-TTF units also display π-stacking interactions. At 50 °C the material dehydrates to form $[Co(H_2O)_6](H_2TC\text{-}TTF)$ which retains monocrystallinity despite structural changes. A change from triclinic to monoclinic is seen, with rotation of the cations and anions to form new hydrogen bonds. The tilt of the H_2TC-TTF anions also changes. The structure converts back to its original form on exposure to water. The dehydrated material shows uptake of methanol vapour, but not ethanol, carbon disulphide or acetonitrile, suggesting that the framework favours small polar molecules. A further dehydration to $[Co(H_2O)_2](H_2TC\text{-}TTF)$ occurs at 80 °C; the authors propose this material has direct co-ordination between cobalt and tetracarboxyltetrathiafulvalene.

1.4 Mixed Anion Frameworks

In an attempt to further increase the diversity of open framework structures a variety of anions can be included in the same material. These mixed anion frameworks offer the possibility of combining properties from inorganic anions such as thermal stability on guest removal (*e.g.* in zeolites and $AlPO_4$s) with the greater variety and chemical flexibility of organic units, which may enable the internal surface of the material to be furnished with desired chemical properties. With new topologies and components being introduced there is also an interest in functional materials where the guests or space filling species are central to the properties of the material. This has been illustrated in the metal oxalates discussed above (section 1.3.2.3), where variation of cations altered the magnetic properties of the materials.

A variety of structures have been synthesised containing both phosphate and oxalate anions. Prior to this work we had synthesised $[Al_4H(HPO_4)_4(H_2PO_4)_2(C_2O_4)_4](NH_3(CH_2)_2NH_3)$[76] and $Fe_4(PO_4)_2(C_2O_4)(H_2O)_2$[77]

Those reported by others have contained a variety of metals: Al,[78] Ga,[79-81] In,[82] Sn,[83] V,[84-86] Fe,[87-93] Co,[92] Zn[94] and Mo[95]. Many of these materials contain space filling or structure directing amines which balance the charge of the framework.

The majority of the structures are three dimensionally connected. A common structural architecture in these materials is that of metal phosphate layers with oxalate anions acting as pillars to give the 3D framework. Structures of this type are described in this work and will be discussed further on. Another common architecture is a ladder-like chain which is found in 1-, 2- and 3D structures.[76,82,84-86,90] A section of the chain is illustrated in Figure 1.9.

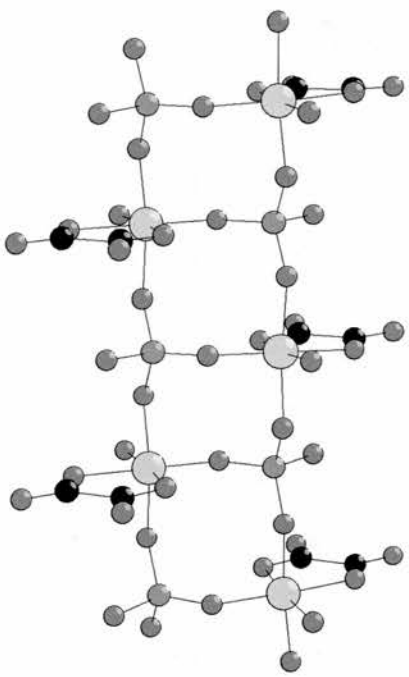

Figure 1.9 A chain found in several phosphate oxalate structures.[76] In this example, aluminium yellow, phosphorous purple, carbon black, oxygen red.

In the 1D example,[84] these chains are found hydrogen bonded to each other, with piperazine cations between the chains. To form a 2D structure, the chains can either join by bisbidentate oxalate co-ordination,[85,86] or *via* a corner sharing phosphate tetrahedron, located on the vacant aluminium co-ordination site in Figure 1.9[76]. This forms layers, between which amine cations reside. Both

modes of chain connectivity, *via* oxalate and phosphate simultaneously, result in a 3D framework.[82,90]

Also of interest in the phosphate oxalate series of structures is $[Fe_3PO_4(HPO_4)_3(C_2O_4)_{1.5}](NH_3(CH_2)_2NH_3)_{1.5}(H_2O)_x$, with x = 1.5 - 2.[89] The framework is built up from iron phosphate layers, which contain 12 membered rings (*i.e.* 12 Fe or P atoms). Oxalate anions pillar these layers to give a 3D structure, creating a 1D channel system throughout the structure. Water molecules are found in the centre of these channels, with the protonated amines towards the edges. The framework reversibly loses water at 110 °C. The dehydrated material can also take up methanol (one molecule per unit cell). Magnetic measurements show antiferromagnetic interactions and the presence of high spin Fe^{III}.

A wide variety of co-ordination geometries are displayed in zinc and gallium containing structures. In $[Ga_5(OH)_2(C_{10}H_9N_2)(C_2O_4)(PO_4)_4](H_2O)_2$ the 4,4'-bipyridine is directly co-ordinated to a gallium centre, rather than hydrogen bonded to the framework as is usually the case.[79] The structure contains GaO_4 tetrahedra, GaO_6 octahedra and GaO_4N square pyramids. The square pyramidal units link sheet made from the GaO_4 tetrahedra, GaO_6 octahedra, PO_4 tetrahedra and C_2O_4 units to form the 3D network. In $[Zn_6(PO_4)_4(C_2O_4)](NH_3(CH_2)_3NH_3)$ zinc exists in tetrahedral, trigonal bipyramidal and square pyramidal co-ordination.[94] Again, oxalate units pillar zinc phosphate layers, although the layers are constructed from double six rings, analogous to zeolite frameworks.

Another unique co-ordination environment in the phosphate oxalates is seen in the molybdenum compound $[(MoO_2)_4(H_2PO_4)_2(C_2O_4)_4](C_6H_{14}N_2)_3(H_2O)_{8.5}$.[95] Mo_2O_{10} dimeric units are formed from edge sharing MoO_6 octahedra, which also exhibits an Mo-Mo bond, confirmed by the diamagnetic nature of the material. The dimers share corners with phosphate tetrahedra to form chains with 'hanging' (*i.e.* bidentate) oxalate groups which are hydrogen bonded to diprotonated DABCO molecules between the chains.

Attempts have been made to synthesise a chiral phosphate oxalate framework. $[Ga_4(PO_4)_4(H_2PO_4)_2(C_2O_4)](R\text{-}C_5H_{14}N_2)_2(H_2O)_2$ is layered, with *R*-2-methylpiperazinium cation between the layers.[81] It appears however that the chirality of the amine is not reflected in the structure, as the authors note that framework atoms are nearly *n*-glide related, and propose that if ion exchange of a non-chiral cation were possible the structure may become centrosymmetric. The same cation has been incorporated into two very similar 3D frameworks $[Fe_4(C_2O_4)_3(HPO_4)_2(H_2O)_2](S\text{-}C_5H_{14}N_2)$ and $[Fe_4(C_2O_4)_3(HPO_4)_2](S\text{-}C_5H_{14}N_2)$, the two structures differing only in a water ligand on iron.[93] A racemic mixture of 2-methylpiperazine produced $[Fe_4(C_2O_4)_3(HPO_4)_2(H_2O)_2](S\text{-}C_5H_{14}N_2)$ as the minor product, along with $[Fe_4(C_2O_4)_3(HPO_4)_2](C_5H_{14}N_2)$, the material with no water ligand, but containing both *R* and *S* enantiomers. No pure *R* form of the hydrated version was formed. The use of *S*-2-methylpiperazine in the synthesis mixture formed $[Fe_4(C_2O_4)_3(HPO_4)_2(H_2O)_2](S\text{-}C_5H_{14}N_2)$ with a small quantity of $[Fe_4(C_2O_4)_3(HPO_4)_2](S\text{-}C_5H_{14}N_2)$. The fact that the hydrated structure only forms using the *S* enantiomer from a racemic mixture suggests that the chirality of the amine is in this case transferred to the framework, although isomorphous frameworks have been synthesised in this work with achiral amines (see section 4.4).

A cobalt selenate oxalate exits, $[Co_3(SeO_3)_2(C_2O_4)]$, with edge-sharing CoO_6 octahedra forming dimers.[96] The dimers are linked by further CoO_6 octahedra which share all six corners with four adjacent dimers. Selenium exists in the structure as SeO_3 species, in which all four atoms are almost planar. The three oxygens are also connected to two cobalts, making them three co-ordinate. Interestingly, of the four crystallographically distinct oxygen atoms only one is two co-ordinate, the remaining three are three co-ordinate, connected to two cobalt atoms and either a selenium or a carbon atom. The cobalt and selenium units form layers, which are bridged by bisbidentate oxalate units as is common in these materials.

A nickel nitrate 4,4'-bipyridyl structure has been synthesised which incorporates ethanol molecules.[97] Interlocking bilayers in $[Ni_2(NO_3)_4(C_{10}H_8N_2)_3]$ form 1D channels of 6 x 3 Å where the ethanol resides. The ethanol is easily removed

from the framework. Comprehensive adsorption studies have been undertaken on this material using nitrogen, argon, carbon dioxide, nitrous oxide, methanol and ethanol.[98] X-ray diffraction studies on methanol adsorption show the structure to be flexible, able to accommodate two hydrogen bonded guests (per formula unit) and is capable of rearrangement in order to take in further guests.

1.5 Applications for New Open Frameworks

Applications for the wide variety of new open frameworks discussed above are largely theoretical at this point, in contrast to the zeolite, and to some extent aluminophosphate families, whose catalytic uses are well known. Few instances of comparable uses for new open frameworks have been reported. One example is the nickel phosphate VSB-1, $Ni_{18}(HPO_4)_{14}(OH)_3F_9(H_3O,NH_4)_4(H_2O)_{12}$, which has been shown to be active in the conversion of butadiene to ethylbenzene (see section 1.3.1.6).[39]

An example of catalytic activity has also been reported in a cadmium 4,4'-bipyridyl 2D co-ordination polymer.[99] $[Cd(C_{10}H_8N_2)_2](NO_3)_2$ consists of square grid layers, with cadmium at the corners of the squares and the bipyridine along the edges. The material shows specific incorporation of *o*-dibromobenzene over the *meta* and *para* isomers; a 1:1 *ortho*:*meta* (or *para*) mixture was separated by the framework with > 99 % purity. Catalytic activity was observed for the cyanosilylation of aldehydes. For the reaction of benzaldehyde and cyanotrimethylsilane in dichloromethane, the product was obtained in a 70 % yield (see Figure 1.10).

This reaction appears to be dependent on the shape or size of the reactants, as both 1- and 2-naphthaldehyde formed the desired products, whereas 9-anthraldehyde did not (see Figure 1.11).

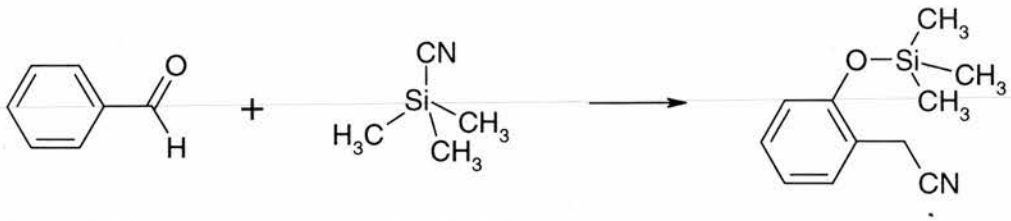

benzaldehyde cyanotrimethylsilane 2-(trimethylsiloxy)phenylacetonitrile

Figure 1.10 The cyanosilylation of benzaldehyde.

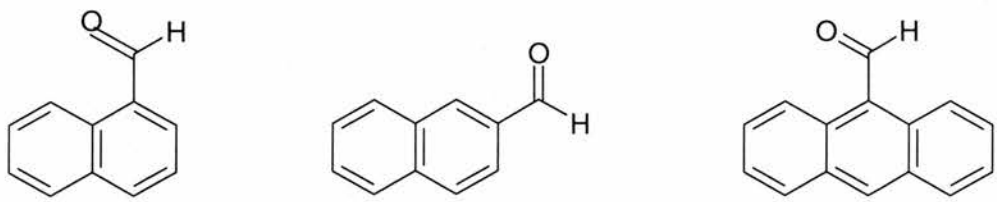

1-naphthaldehyde 2-naphthaldehyde 9-anthraldehyde

Figure 1.11 Aldehydes used in the cyanosilylation reaction.

It is hoped that future developments may result in materials combining porosity with properties such as ferromagnetism, ferroelectricity, ionic/electrical conductivity, metal-semiconductor transitions, superconductivity or optical properties such as second harmonic generation.[8]

Second harmonic generation has been observed in organic guests incorporated within zeolite,[100] aluminophosphate[7] and metal oxalate[101] hosts. Other 'multi-property' materials have been reported incorporating magnetism and non-linear optical properties[101,102] and magnetic and conducting properties[103].

A series of 2D metal oxalates were synthesised containing potentially NLO active species.[101] Some of these, for example DAMS[$MnCr(C_2O_4)_3$] show efficient second harmonic generation and strong magnetisation (DAMS = dimethylamino-N-methyl stilbazolium, illustrated in Figure 1.12). A study of any possible interaction between the two properties was not viable due to the low magnetic ordering temperatures.

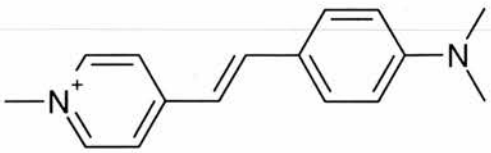

dimethylamino-N-methyl stilbazolium (DAMS+)

Figure 1.12 The DAMS cation which displays second harmonic generation when a guest in a 2D metal oxalate.[101]

1.6 Aims

The field of open frameworks is clearly a large and busy one. The aim of this work was to synthesise new open frameworks, specifically those containing two different types of anion: organic and inorganic. The choice of anions aimed to combine properties from these two families, such as thermal stability and robustness on guest removal from the phosphate type materials, and the structural variety and chemical flexibility of metal organic materials. It was envisaged that the combination of metals with unpaired spins and anions capable of multiple co-ordination in an extended network may produce materials with interesting magnetic interactions. The thermal stability and possibility of removing any guest molecules would also be investigated.

The techniques involved in this work are described in Chapter 2 and an overview of the experiments carried out in Chapter 3. Chapters 4, 5 and 6 detail the new frameworks which have been synthesised.

1.7 References

1. J. M. Newsam, in *Solid State Chemistry: Compounds*, eds. A. K. Cheetham and P. Day, Oxford University Press, Oxford, 1996, chpt. 7, 234.

2. *Solid State Chemistry: An Introduction*, L. Smart and E. Moore, Chapman and Hall, London, 1993, chpt 5, 183.

3. M. E. Davis and R. F. Lobo, *Chem. Mater.*, 1992, **4**, 756.

4. A. F. Cronstedt, *Koongl. Vetenskaps Acad. Handl Stockholm*, 1756, **17**, 120.

5. R. M. Barrer, *J. Chem. Soc.*, 1948, 127.

6. R. M. Barrer and P. J. Denny, *J. Chem. Soc.*, 1961, 971.

7. S. D. Cox, T. E. Gier and G. D. Stucky, *Chem. Mater.*, 1990, **2**, 609.

8. A. K. Cheetham, G. Férey and T. Loiseau, *Angew. Chem., Int. Ed.*, 1999, **38**, 3268.

9. S. T. Wilson, B. M. Lok, C. A. Messina, T. R. Cannan and E. M. Flanigen, *J. Am. Chem. Soc.*, 1982, **104**, 1146.

10. P. A. Wright, R. H. Jones, S. Natarajan, R. G. Bell, J. S. Chen, M. B. Hursthouse and J. M. Thomas, *J. Chem. Soc., Chem. Commun.*, 1993, 633.

11. T. E. Gier and G. D. Stucky, *Nature*, 1991, **349**, 508.

12. A. M. Chippindale, A. R. Cowley and R. I. Walton, *J. Mater. Chem.*, 1996, **6**, 611.

13. J. M. Thomas, *Angew. Chem., Int. Ed. Engl.*, 1994, **33**, 913.

14. J. M. Thomas, R. Raja, G. Sankar and R. G. Bell, *Nature*, 1999, **398**, 227.

15. G. Férey and A. K. Cheetham, *Science*, 1999, **283**, 1125.

16. *CRC Handbook of Chemistry and Physics*, ed. D. R. Lide, CRC Press, Florida, 80th Ed., 1999, chpt 9, 51.

17. R. C. Haushalter and L. A. Mundi, *Chem. Mater.*, 1992, **4**, 31.

18. V. Soghomonian, Q. Chen, R. C. Haushalter and J. Zubieta, *Angew. Chem., Int. Ed. Engl.*, 1993, **32**, 610.

19. P. B. Moore and J. Shen, *Nature*, 1983, **306**, 356.

20. D. R. Corbin, J. F. Whitney, W. C. Fultz, G. D. Stucky, M. M. Eddy and A. K. Cheetham, *Inorg. Chem.*, 1986, **25**, 2279.

21. K.-H. Lii, Y.-F. Huang, V. Zima, C.-Y. Huang, H.-M. Lin, Y.-C. Jiang, F.-L Liao and S.-L. Wang, *Chem. Mater.*, 1998, **10**, 2599.

22. M. Riou-Cavellec, D. Riou and G Férey, *Inorg. Chim. Acta*, 1999, **291**, 317.

23. M. Cavellec, D. Riou and G Férey, *J. Solid State Chem.*, 1994, **112**, 441.

24. M. Cavellec, D. Riou, J. M. Greneche and G Férey, *J. Magn. Magn. Mater.*, 1996, **163**, 173.

25. M. Cavellec, C. Egger, J. Linares, M. Nogues, F. Varret and G Férey, *J. Solid State Chem.*, 1997, **134**, 349.

26. M. Riou-Cavellec, J. M. Greneche, D. Riou and G Férey, *Chem. Mater.*, 1998, **10**, 2434.

27. K.-H. Lii and Y.-F. Huang, *Chem. Commun.*, 1997, 839.

28. K.-H. Lii and Y.-F. Huang, *Chem. Commun.*, 1997, 1311.

29. C.-Y. Huang, S.-L. Wang and K.-H. Lii, *J. Porous Mater.*, 1998, **5**, 147.

30. J. R. D. DeBord, W. M. Reiff, C. J. Warren, R. C. Haushalter and J. Zubieta, *Chem. Mater.*, 1997, **9**, 1994.

31. J. Chen, R. H. Jones, S. Natarajan, M. B. Hursthouse and J. M. Thomas, *Angew. Chem., Int. Ed. Engl.*, 1994, **33**, 629.

32. P. Feng. X. Bu, S. H. Tolbert and G. D. Stucky, *J. Am. Chem. Soc.*, 1997, **119**, 2497.

33. P. Feng, X. Bu and G. D. Stucky, *Nature*, 1997, **388**, 735.

34. P. Lightfoot and A. K. Cheetham, *J. Solid State Chem.*, 1989, **78**, 17.

35. M. A. G. Aranda, J. P. Attfield and S. Bruque, *Angew. Chem., Int. Ed. Engl.*, 1992, **31**, 1090.

36. N. Rajić, A. Ristić and V. Kaučič, *Zeolites*, 1996, **17**, 304.

37. S. L. Brock, N. G. Duan, Z. R. Tian, O. Giraldo, H. Zhou and S. L. Suib, *Chem. Mater.*, 1998, **10**, 2619.

38. N. Guillou, Q. Gao, M. Nogues, R. E. Morris, M. Hervieu, G. Férey and A. K. Cheetham, *C. R. Acad. Sci. Paris, 2, Series IIc, Solid chemistry and crystal chemistry*, 1999, 387.

39. J.-S. Chang, S.-E. Park, Q. Gao, G. Férey and A. K. Cheetham, *Chem. Commun.*, 2001, 859.

40. T. M. Nenoff, W. T. A. Harrison, T. E. Gier and G. D. Stucky, *J. Am. Chem. Soc.*, 1991, **113**, 378.

41. W. T. A. Harrison, T. E. Martin, T. E. Gier and G. D. Stucky, *J. Mater. Chem.*, 1992, **2**, 175.

42. G.-Y. Yang and S. C. Sevov, *J. Am. Chem. Soc.*, 1999, **121**, 8389.

43. C. Janiak, *Angew. Chem., Int. Ed. Engl.*, 1997, **36**, 1431.

44. C. L. Bowes and G. A. Ozin, *Adv. Mater.*, 1996, **8**, 13.

45. S. Natarajan, R Vaidhyanathan, C. N. R. Rao, S. Ayyappan and A. K. Cheetham, *Chem. Mater.*, 1999, **11**, 1633.

46. S. Ayyappan, A. K. Cheetham, S. Natarajan and C. N. R. Rao, *Chem. Mater.*, 1998, **10**, 3746.

47. S. Romero, A. Mosset and J. C. Trombe, *J. Solid State Chem.*, 1996, **127**, 256.

48. I. A. Kahwa, F. R. Fronczek and J. Selbin, *Inorg. Chim. Acta*, 1984, **82**, 161.

49. O. Guillou, P. Bergerat, O. Kahn, E. Bakalbassis, K. Boubekeur, P. Batail and M. Guillot, *Inorg. Chem.*, 1992, **31**, 110.

50. S. Decurtins, M. Gross, H. W. Schmalle and S. Ferlay, *Inorg. Chem.*, 1998, **37**, 2443.

51. T. Bataille, J.-P Auffrédic and D. Louër, *J. Mater. Chem.*, 2000, **10**, 1701.

52. F. Serpaggi, T. Luxbacher, A. K. Cheetham and G. Férey, *J. Solid State Chem.*, 1999, **145**, 580.

53. F. Serpaggi and G. Férey, *J. Mater. Chem.*, 1998, **8**, 2737.

54. V. Kiritsis, A. Michaelides, S. Skoulika, S. Golhen and L. Ouahab, *Inorg. Chem.*, 1998, **37**, 3407.

55. T. M. Reineke, M. Eddaoudi, M. O'Keeffe and O. M. Yaghi, *Angew. Chem., Int. Ed.*, 1999, **38**, 2590.

56. K. P. Mörtl, J.-P. Sutter, S. Golhen, L. Ouahab and O. Kahn, *Inorg. Chem.*, 2000, **39**, 1626.

57. O. M. Yaghi and H. Li, *J. Am. Chem. Soc.*, 1995, **117**, 10401.

58. O. M. Yaghi, G. Li and H. Li, *Nature*, 1995, **378**, 703.

59. O. M. Yaghi, H. Li, and T. L. Groy, *J. Am. Chem. Soc.*, 1996, **118**, 9096.

60. O. M. Yaghi, C. E. Davis, G. Li and H. Li, *J. Am. Chem. Soc.*, 1997, **119**, 2861.

61. M. Edgar, R. Mitchell, A. M. Z. Slawin, P. Lightfoot and P. A. Wright, *Chem. Eur. J.*, 2001, **7**, 5168.

62. S. Decurtins, H. W. Schmalle, H. R. Oswald, A. Linden, J. Ensling, P. Gütlich and A. Hauser, *Inorg. Chim. Acta*, 1994, **216**, 65.

63. C. Mathonière, C. J. Nuttall, S. G. Carling and P. Day, *Inorg. Chem.*, 1996, **35**, 1201.

64. R. Pellaux, H. W. Schmalle, R. Huber, P. Fischer, T. Hauss, B. Ouladdiaf and S. Decurtins, *Inorg. Chem.*, 1997, **36**, 2301.

65. C. J. Nuttall and P. Day, *Chem. Mater.*, 1998, **10**, 3050.

66. E. Coronado, J. R. Galán-Mascarós, C. J. Gómez-García and J. M. Martínez-Agudo, *Adv. Mater.*, 1999, **11**, 558.

67. R. Vaidhyanathan, S. Natarajan, A. K. Cheetham and C. N. R. Rao, *Chem. Mater.*, 1999, **11**, 3636.

68. S. Decurtins, H. W. Schmalle, P. Schneuwly and H. R. Oswald, *Inorg. Chem.*, 1993, **32**, 1888.

69. S. Decurtins, H. W. Schmalle, P. Schneuwly, J. Ensling and P. Gütlich, *J. Am. Chem. Soc.*, 1994, **116**, 9521.

70. A Cornia, A. Caneschi, P. Dapporto, A. C. Fabretti, D. Gatteschi, W. Malavasi, C. Sangregorio and R. Sessolo, *Angew. Chem., Int. Ed.*, 1999, **38**, 1780.

71. I. Gil de Muro, F. A. Mauther, M. Insansti, L. Lezama, M. I. Arriortua and R. Rojo, *Inorg. Chem.*, 1998, **37**, 3243.

72. C. Livage, C. Egger, M. Nogues and G. Férey, *J. Mater. Chem.*, 1998, **8**, 2743.

73. C. Livage, C. Egger, and G. Férey, *Chem. Mater.*, 1999, **11**, 1546.

74. S. Kawata, S. Kitagawa, H. Kumagai, T. Ishiyama, K. Honda, H. Tobita, K. Adachi and M. Katada, *Chem. Mater.*, 1998, **10**, 3902.

75. C. J. Kepert, D. Hesek, P. D. Beer and M. J. Rosseinsky, *Angew. Chem., Int. Ed.*, 1998, **37**, 3158.

76. P. Lightfoot, Z. A. D. Lethbridge, R. E. Morris, D. S. Wragg, P. A. Wright, Å Kvick and G. B. M. Vaughan, *J. Solid State Chem.*, 1999, **143**, 74.

77. Z. A. D. Lethbridge and P. Lightfoot, *J. Solid State Chem.*, 1999, **143**, 58.

78. K. Kedarnath, A. Choudhury and S. Natarajan, *J. Solid State Chem.*, 2000, **150**, 324.

79. C.-Y. Chen, P. P. Chu and K.-H. Lii, *Chem. Commun.*, 1999, 1473.

80. L.-C. Hung, H.-M. Kao and K.-H. Lii, *Chem. Mater.*, 2000, **12**, 2411.

81. K.-H. Lii and C.-Y. Chen, *Inorg. Chem.*, 2000, **39**, 3374.

82. Y.-F. Huang and K.-H. Lii, *J. Chem. Soc., Dalton Trans.*, 1998, **24**, 4085.

83. S. Natarajan, *J. Solid State Chem.*, 1998, **139**, 200.

84. Y.-M. Tsai, S.-L. Wang, C.-H. Huang and K.-H. Lii, *Inorg. Chem.*, 1999, **38**, 4183.

85. J. Do, R. P. Bontchev and A. J. Jacobson, *Inorg. Chem.*, 2000, **39**, 3230.

86. J. Do, R. P. Bontchev and A. J. Jacobson, *Chem. Mater.*, 2001, **13**, 2601.

87. P. Lightfoot, D.Phil. Thesis, University of Oxford, 1987.

88. A. Choudhury, S. Natarajan and C. N. R. Rao, *J. Solid State Chem.*, 1999, **146**, 538.

89. A. Choudhury, S. Natarajan and C. N. R. Rao, *Chem. Mater.*, 1999, **11**, 2316.

90. A. Choudhury and S. Natarajan, *J. Mater. Chem.*, 1999, **9**, 3113.

91. H.-M. Lin, K.-H. Lii, Y.-C. Jiang and S.-L. Wang, *Chem. Mater.*, 1999, **11**, 519.

92. A. Choudhury, S. Natarajan and C. N. R. Rao, *Chem. Eur. J.*, 2000, **6**, 1168.

93. W.-J. Chang, H.-M. Lin and K.-H. Lii, *J. Solid Sate. Chem.*, 2001, **157**, 233.

94. S. Neeraj, S. Natarajan and C. N. R. Rao, *J. Chem. Soc., Dalton Trans.*, 2001, 289.

95. M.-Y. Lee and S.-L. Wang, *Chem. Mater.*, 1999, **11**, 3588.

96. G. Giester, *Z. Kristallogr.*, 1997, **212**, 720.

97. C. J. Kepert and M. J. Rosseinsky, *Chem. Commun.*, 1999, 375.

98. A. J. Fletcher, E. J. Cussen, T. J. Prior, M. J. Rosseinsky, C. J. Kepert and K. M. Thomas, *J. Am. Chem. Soc.*, 2001, **123**, 10001.

99. M. Fujita, Y. J. Kwon, S. Washizu and K. Ogura, *J. Am. Chem. Soc.*, 1994, **116**, 1151.

100. I. Bull, L. A. Villaescusa, S. J. Teat, M. A. Camblor, P. A. Wright, P. Lightfoot and R. E. Morris, *J. Am. Chem. Soc.*, 2000, **122**, 7128.

101. S. Bénard, P. Yu, J. P. Audière, E. Rivière, R. Clément, J. Guilhem, L. Tchertanov and K. Nakatani, *J. Am. Chem. Soc.*, 2000, **122**, 9444.

102. R. Clément, P. G. Lacroix, D. O'Hare and J. Evans, *Adv. Mater.*, 1994, **6**, 794.

103. E Coronado, J. R. Galán-Mascarós, C. Giménez-Saiz and C. J. Gómez-Garcia, *Adv. Mater. Opt. Electron.*, 1998, **8**, 61.

CHAPTER 2 – TECHNIQUES

In common with many other open frameworks, materials in this work were synthesised under hydrothermal conditions. A brief description of hydrothermal synthesis is given below. This chapter also contains a discussion of x-ray diffraction, the main characterisation technique used, and a qualitative description of how magnetic measurements were obtained. Thermogravimetric and elemental (C, H and N) analysis have also been employed.

2.1 Hydrothermal Synthesis[1-4]

2.1.1 Background

Hydrothermal synthesis involves heating a mixture of reactants in water in a sealed container above water's normal boiling point. In 1851 de Sénarmont introduced the modern form of hydrothermal synthesis by heating glass ampoules in an autoclave consisting of a sealed gun barrel partly filled with water, and heated to a dull red glow. In this way he synthesised many oxide, carbonate, fluoride, sulphate and sulphide minerals.[1] The autoclaves used in this work are constructed from steel with a Teflon liner. Teflon has a limited temperature/ pressure range (~220 °C) and tends to be slightly porous, however its corrosion resistant properties make it ideal for use at these temperatures. In this work the reaction mixture typically consisted of a metal source, a phosphate source, an organic ligand and, in some reactions, an amine. Mixtures were heated for periods of one to two days at temperatures of 100 – 160 °C. Reactions at 100 °C were carried out in polypropylene bottles.

Hydrothermal synthesis is characterised by a large number of variables, such as time, temperature, pressure, pH, reactant source, template, ageing of mixture prior to heating and the percentage filling of the autoclave. Some of these variables are related and cannot be easily examined on their own.[4]

2.1.2 Mechanism in hydrothermal synthesis

In traditional high temperature solid state synthesis, the thermodynamic products of the system are formed.[3] Generally there is no mechanistic knowledge, and little control over any metastable (kinetically stable) intermediates. The rate-limiting step may be reactant diffusion. Hydrothermal synthesis has been compared mechanistically to organic synthesis, where reactants are dispersed in a solvent so diffusion is not a problem, and the reactions involve transformations of functional groups leaving most bonds intact. Similarly in hydrothermal reactions the increased solubilities of the reactants overcome diffusion aspects, and units of required geometry and composition may be used. Thus under hydrothermal conditions, as with organic reactions, metastable products may be obtained.

The mechanism of formation of materials under hydrothermal conditions begins with an initial dissolution and random distribution of the reactants. Ordering then occurs on a microscopic level, followed by growth at these nucleation sites to give long range order. Two mechanisms have been suggested: solution mediated transport and solid hydrogel transformation.[4] The former involves dissolution followed by diffusion of the reactants through the solution to the nucleation sites. In the solid hydrogel transformation, an amorphous solid phase reorganises to form the crystals of the product. Experimental evidence for both types of mechanism exists, and some phases have been shown to form by both methods. Nuclear magnetic resonance, infra-red and raman spectroscopies have been used to investigate the species which may be involved in the condensation process of zeolites, but some species have been observed which are not present in the final product. *In situ* methods, such as x-ray and neutron diffraction have also been used.

2.1.3 Water under hydrothermal conditions

Heated in a sealed container, water does not boil. As the temperature is increased, the vapour pressure increases until the density of the vapour and the liquid are equal and the interface between the phases disappears. At this critical temperature, T_C (see Figure 2.1), a single phase fills the container. T_C for water occurs at 374.1 °C and 218 atm. The term hydrothermal synthesis is generally used to cover all reactions above room temperature and pressure, *i.e.* no distinction is made above and below T_C, as there is virtually no discontinuity seen in the behaviour of the water above and below this temperature.[1] The value of T_C tends to increase with increasing concentration of reactants present, so often the critical temperature of a reacting system is unknown.

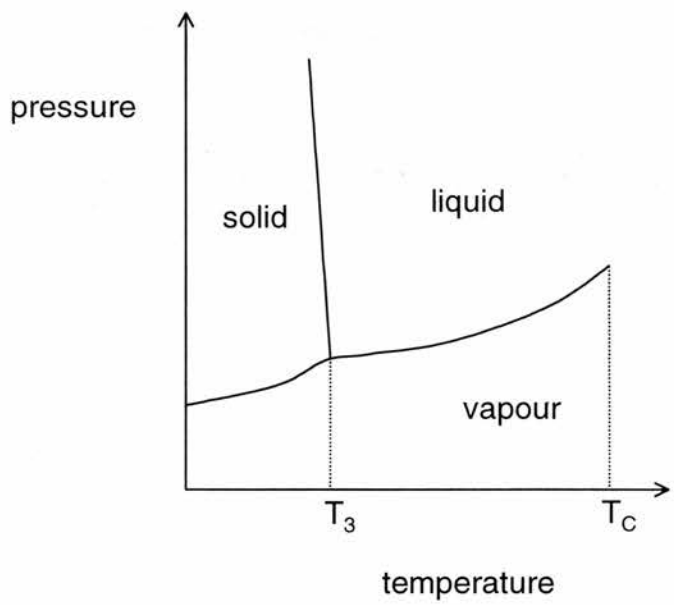

Figure 2.1 Phase diagram of water, showing the triple point (T_3) where ice, liquid and gaseous water can all exist; and the critical point (T_C) where the liquid/vapour interface disappears.

As the temperature is increased the viscosity of water decreases, allowing ions or atoms increased mobility. The dielectric constant also decreases with increasing temperature, however it is found to increase with increasing pressure. The temperature effect dominates, and some electrolytes, which are totally dissociated under normal conditions, can associate with rising temperature.

2.2 X-ray diffraction[2,5-7]

An object in the path of waves will cause diffraction if its size is comparable to the wavelength of the radiation. In 1912, Max von Laue realised that x-rays have wavelengths similar to the spacing between atoms in a crystal (~1Å) and proposed that they would be diffracted by a crystalline sample. The long-range order in a crystal results in interference between scattered x-rays, producing a diffraction pattern. When recorded on photographic film or using an electronic detector this gives a pattern of spots, each spot the result of constructive interference of scattered x-rays. The diffraction pattern has geometry related to the lattice and unit cell geometry of the crystal and symmetry related to the crystal system and space group.

W. L. Bragg described this diffraction as reflections from sets of parallel (*hkl*) planes of lattice points, as illustrated below (Figure 2.2), where incident and reflected rays make an angle θ with the *hkl* planes.

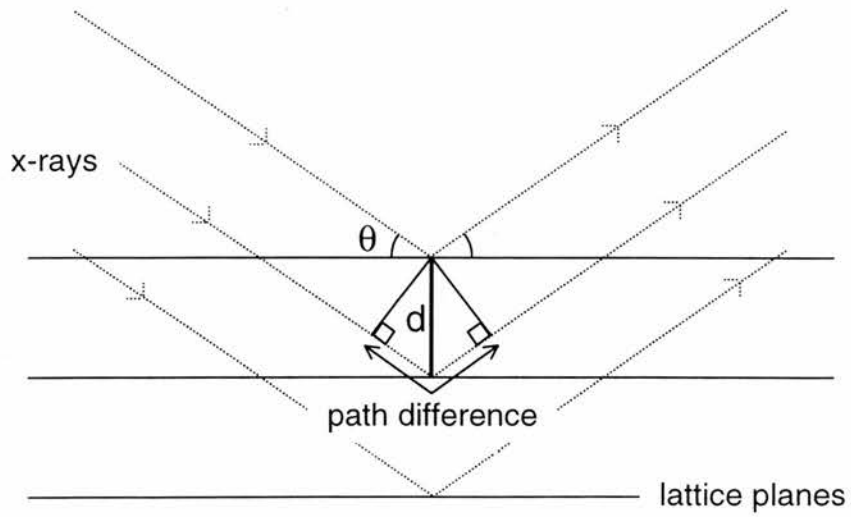

Figure 2.2 X-rays diffracting (reflecting) off lattice planes in a crystal at an angle θ.

For a diffraction spot to be observed the reflected x-rays must interfere constructively, *i.e.* the path difference between them (shown in Figure 2.2) must

be an integral number of wavelengths. This path difference expressed in terms of the *hkl* spacing, d_{hkl}, is the Bragg equation:

$$\text{path difference } n\lambda = 2d_{hkl} \sin\theta \qquad 2.1$$

Hence the geometry of the diffraction pattern ($\sin\theta$) is inversely related to the geometry of the crystal (d_{hkl}). Each diffraction spot can be labelled with the *hkl* values of the planes causing the reflection.

X-rays are scattered by the electrons of atoms, so the diffraction pattern is an indication of the location of electron density, *i.e.* atoms, within the crystal. Different elements scatter different intensities of radiation. This atomic scattering factor, or form factor (f), is also dependent on the angle of incidence of the radiation, as illustrated in Figure 2.3.

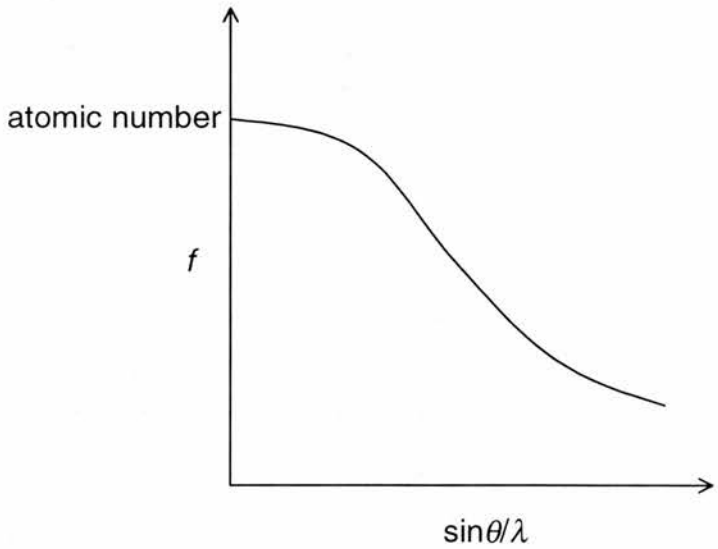

Figure 2.3 Variation of the form factor (f) with incident angle θ. When θ = 0 f is equal to the atomic number of the element.

Thermal vibrations also contribute to the decrease of scattering factor, *via* the isotropic displacement parameter U.

The structure factor, F_{hkl}, of each reflection consists of its amplitude and phase. This is related to the intensity, I_{hkl}, by

$$I_{hkl} \propto F_{hkl}^2 \qquad 2.2$$

Thus the measured intensities contain the amplitude information, but the phase information is lost as a consequence of the square root.

The diffraction pattern, *i.e.* the structure factor for each reflection, is the Fourier transform of the electron density ρ_{xyz}:

$$F_{hkl} = \int_{cell} \rho_{xyz} \exp\{2\pi i(hx+ky+lz)\}dV \qquad 2.3$$

Considering discrete atoms instead of continuous electron density, this formula becomes a summation and includes the scattering factor and a term involving thermal displacement:

$$F_{hkl} = \sum_n f_n \exp\{2\pi i(hx+ky+lz)\}\exp(-8\pi^2 U_n \sin^2\theta/\lambda^2) \qquad 2.4$$

for all n atoms in the unit cell.

The isotropic temperature factor assumes the atoms are free to vibrate equally in all directions, *i.e.* are represented by spheres. The thermal movement is described more accurately by an ellipsoid, which requires six parameters to define its shape and orientation. This can be expressed as the Debye-Waller factor $q(\mathbf{r}^*)$

$$q(\mathbf{r}^*) = \exp\{-2\pi^2(U_{11}^* x^{*2} + U_{22}^* y^{*2} + U_{33}^* z^{*2} + 2U_{12}^* x^* y^* + 2U_{13}^* x^* z^* + 2U_{23}^* y^* z^*)\} \qquad 2.5$$

which represents the thermal ellipsoid in reciprocal space.

The reverse Fourier transform relates electron density to structure factor:

$$\rho_{xyz} = 1/V \sum_{hkl} F_{hkl} \exp\{-2\pi i(hx+ky+lz)\} \qquad 2.6$$

2.2.1 Structure solution and refinement in single crystal diffraction

2.2.1.1 Determination of crystal system, lattice parameters and space group

Data may be collected using a four-circle diffractometer, or one equipped with an area detector. A four-circle diffractometer has three rotation axes for the crystal and one for the detector, which is usually a scintillation counter (see Figure 2.4). The detector and crystal are moved to the correct orientation for each reflection to be observed individually.

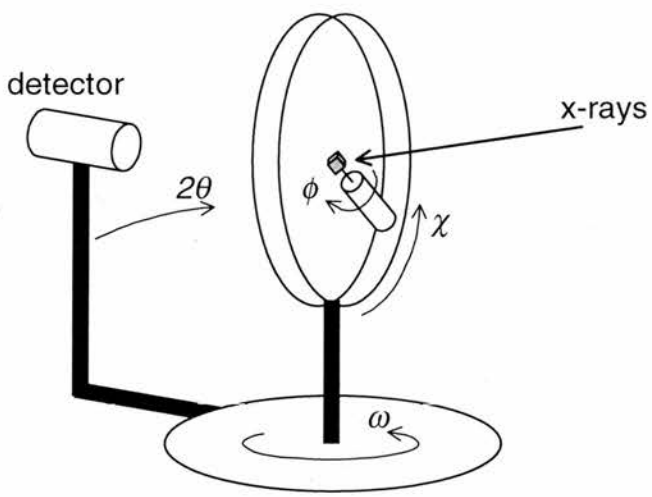

Figure 2.4 Schematic diagram of a four-circle diffractometer

Diffractometers equipped with area detectors can record many reflections at once, analogous to photographic film, and reduce the number of rotation axes, as well as time, required (see Figure 2.5).

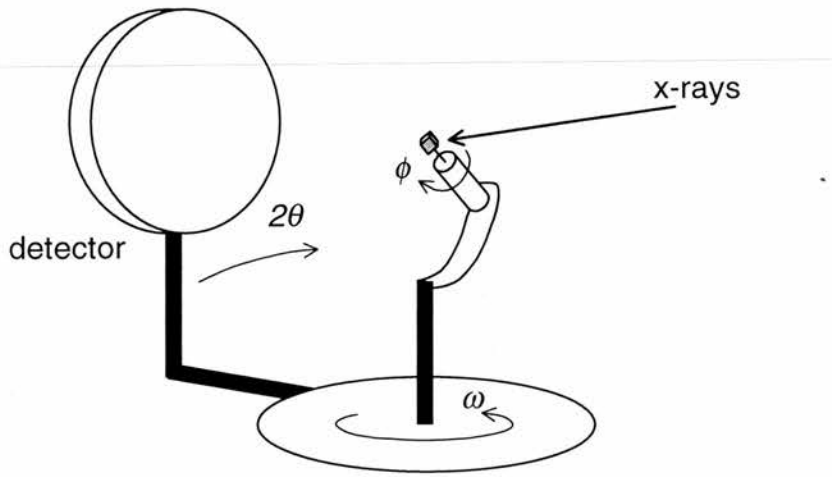

Figure 2.5 Schematic diagram of a diffractometer equipped with an area detector

A Rigaku AFC7S automated four-circle diffractometer and a Bruker SMART diffractometer with a CCD detector, both with MoK_α radiation, were used for data collection.

When using a four-circle machine, the initial stage in data collection is the measurement of around 20 reflections. When using an area detector, around 75 frames (analogous to photographs) are taken at different angular settings. These peaks are then indexed, *i.e.* assigned the correct *hkl* values, to give the crystal system and calculate unit cell parameters. This also allows the orientation of the crystal to the incident beam to be determined. Based on this information, the data are then collected, to give a list of *hkl*, intensity and error values for all the measured reflections. The space group can then be determined by examining systematic absences: reflections which are expected based on the unit cell and crystal system but which have zero intensity due to the presence of symmetry operators. Corrections to the data can be applied, such as an absorption correction, which accounts for x-rays losing intensity as they pass through the crystal. This is more important for needles or plates, which have a large relative difference between different crystal edges. In the case of a synchrotron experiment, corrections for beam decay are also applied.

In order to determine the type and location of atoms within the unit cell, the electron density needs to be calculated (equation 2.6). This is not straightforward due to the loss of phase information. There are two main methods to overcome this.

Direct Methods

Direct methods are those which obtain phase information from mathematical relationships between amplitudes. These are based on two conditions: that the electron density must be positive or zero everywhere (*i.e.* not negative), and that a structure is composed of discrete atoms, which are treated as being equal. Direct methods uses structure factors E_{hkl}, which are normalised for variation in scattering factor f with angle of incidence and element. E_{hkl} values are given by

$$|E_{hkl}|^2 = \frac{|F_{hkl}|^2}{\varepsilon \sum_n f_n{}^2} \qquad 2.7$$

for all n atoms in the unit cell. ε is normally equal to 1. The normalised structure factors have the same phases as F_{hkl}.

The Sayre probability equation is used to predict phase relationships:

$$S(hkl) \sim S(h'k'l') \cdot S(h-h', k-k', l-l') \qquad 2.8$$

where S means the sign of E_{hkl}. Thus the phase of a reflection can be predicted from others which are known. The probability P that this prediction is correct is given by

$$P = \frac{1}{2} + \frac{1}{2} \tanh\left(\frac{1}{N} \left| E_{hkl} \cdot E_{h'k'l'} \cdot E_{h-h',k-k',l-l'} \right| \right) \qquad 2.9$$

for N atoms in the unit cell.

A small set of reflections is selected with E_{hkl} values that are most likely to give a correct prediction. The possible phase combinations of these are then used to generate phases for other E_{hkl} values (approximately 10 per atom). A map of E_{hkl}s, analogous to an electron density map, is then calculated using the most self-consistent set of phases.

Patterson Methods

This method uses the amplitude of the structure factor squared, using equation 2.9.

$$P_{xyz} = 1/V \sum_{hkl} |F_{hkl}|^2 \exp\{-2\pi i(hx + ky + lz)\} \qquad 2.9$$

All waves are taken as being in phase. This gives a map similar in appearance to an electron density map, but indicates vectors between pairs of atoms in the structure, rather than the atoms themselves. This method is more suitable when a heavy atom is present, whereas direct methods treats all atoms as being equal.

2.2.1.3 Refinement

The model of the structure produced after the initial structure solution is then refined, by comparing the observed data with a diffraction pattern calculated for the model in a least squares process. The difference between these two sets of structure factors, F_o (observed) and F_c (calculated), expressed as the following sum, is minimised:

$$\sum w(|F_o| - |F_c|)^2 \qquad 2.10$$

This is a refinement on F, alternatively the data can be refined on F^2:

$$\sum w(F_o^2 - F_c^2)^2 \qquad 2.11$$

Here, w is a weighting factor, based on the reliability or uncertainty of each reflection. A measure of how well the model fits the data is given by the residual or R factor:

$$R = \frac{\sum \| F_o | - | F_c \|}{\sum | F_o |} \qquad 2.12$$

this can also be weighted, and may be calculated using F^2 values:

$$wR^2 = \sqrt{\frac{\sum w(F_o^2 - F_c^2)^2}{\sum w(F_o^2)^2}} \qquad 2.13$$

An R factor of around 3% indicates a good fit.

2.2.2 Powder diffraction

A powder sample contains crystallites in many different orientations, but some will be in the correct position to satisfy the Bragg equation for each set of hkl planes present. The same set of planes in different crystallites will lie at different angles around the incident beam, resulting in a cone of diffracted beams (see Figure 2.6). These cones are monitored electronically, and the data is obtained as a plot of intensity versus 2θ.

A powder pattern is characteristic of a particular structure and is used as a fingerprint for a substance. An unknown sample can be identified if its powder pattern can be matched to a known pattern. This is also used as a check on phase purity. If a powder pattern can be indexed, it is possible to calculate the

dimensions of the unit cell. Samples were analysed on a Philips diffractometer using CuK_α radiation (λ = 1.5418 Å).

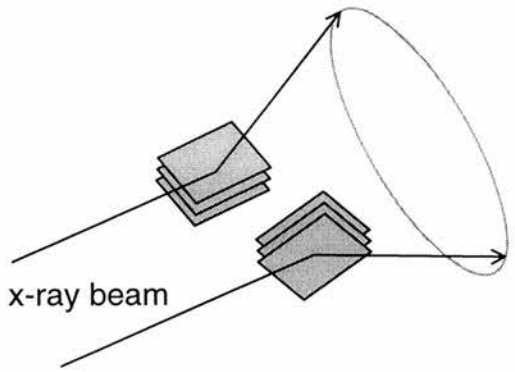

Figure 2.6 Diffraction from a powder sample showing the cone of x-rays. Different values of 2θ will give cones with different angles.

Structures can be refined from powder data provided a suitable starting model is available. The Rietveld method is a least squares refinement which minimises the difference between observed and calculated powder patterns, rather than individual structure factors, to take overlapping peaks into account. In addition to the atomic co-ordinates and temperature factors which are refined in single crystal experiments, lattice parameters, the detector zero-point, background and peak shape are also refined, using a suite of programs such as GSAS.[8]

2.2.3 Generation of x-rays

2.2.3.1 Laboratory sources

An x-ray tube is used in laboratory diffractometers. Electrons are generated by passing a current through a wire filament, and accelerated across a few millimetres by a high voltage. The electrons then collide with a metal target, the nature of which determines the x-ray's wavelength. Commonly used metals are copper (λ = 1.54184 Å) and molybdenum (λ = 0.71073 Å). Most of the electrons lose their kinetic energy as heat, but some collide with electrons in the inner shells of the metal atoms, expelling them from the core. An electron in a higher

level then drops down to fill the vacancy created, losing its excess energy as x-radiation (see Figure 2.7)

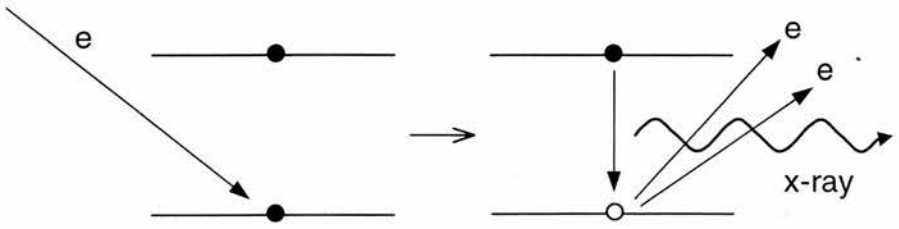

Figure 2.7 X-rays generated by ejecting core electrons.

The electron transitions produce characteristic lines, labelled *K*, *L* or *M* after the principle quantum number (n = 1, 2 or 3) of the orbital to which the electron falls. If the two orbitals involved in the transition are adjacent, the transition is denoted α, if there is another orbital between then it is denoted β (see Figure 2.8). As each n orbital has n different levels corresponding to the quantum number l (0 - (n-1)) the α and β lines are split further, however many of these transitions are forbidden. These lines are labelled 1, 2, etc.

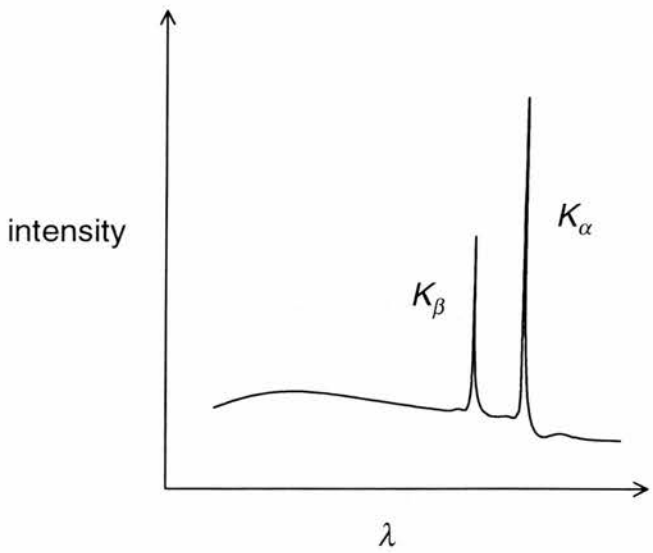

Figure 2.8 The spectrum of radiation produced by an x-ray tube.

A monochromator selects the required wavelength of radiation. A crystal may be used for this, oriented at an angle θ to the x-rays generated in the tube such that

only the desired wavelength is diffracted by the crystal (according to Bragg's Law) and all others are filtered out.

2.2.3.2 Synchrotron radiation

Very small crystals (around 100 μm^3) diffract too weakly to be measured on a laboratory diffractometer. A more intense beam of x-rays can be obtained from a synchrotron, which accelerates electrons at high speeds (close to the speed of light). Magnets are used to direct the electrons around a circular path. As these electrons are accelerating they emit a spectrum of radiation, from infra-red to gamma rays. The required wavelength of radiation (x-rays in this case) is selected using a monochromater and directed to experimental stations. Station 9.8 at the Synchrotron Radiation Source (SRS), Daresbury Laboratory and the materials beam line (ID11) at the European Synchrotron Radiation Facility (ESRF), Grenoble were used for single crystal diffraction for some of the structures reported here. A schematic diagram of the synchrotron a Daresbury is shown in Figure 2.9.

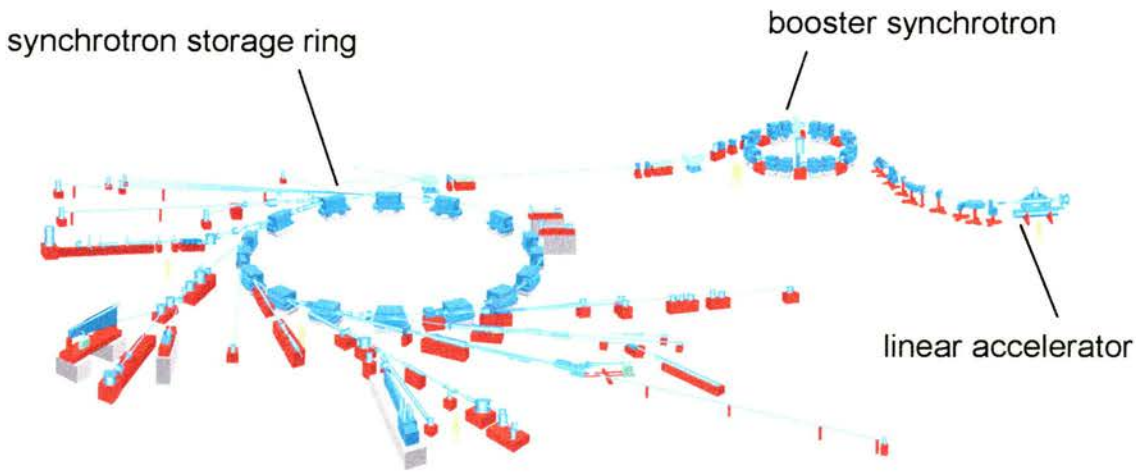

Figure 2.9 The Daresbury synchrotron[9]

The diffractometers are equipped with area detectors and receive radiation of around 0.693 Å (Daresbury) or 0.375 Å (Grenoble). Electrons are initially accelerated using the linear accelerator, then added to the booster synchrotron where they reach speeds near to that of light. They are then injected into the main storage ring, which has a circumference of 96 m (SRS).[10] The radiation is emitted tangentially from the synchrotron and the experimental stations are found all around the circumference.

2.3 Magnetism[11]

2.3.1 Origin of magnetism

All electrons, as a result of their spin and orbital motion possess a magnetic moment. Where electrons are paired the vector sum of the moments is cancelled, however if unpaired electrons exist the atom possesses a magnetic moment.

A sample with magnetisation M in a field H has a magnetic flux density B given by:

$$B = \mu_0 (H + M) \qquad 2.14$$

where μ_0 is the permeability of free space. The magnetic susceptibility of a sample, χ, is then defined as:

$$\chi = \frac{M}{H} \qquad 2.15$$

A material with no unpaired electrons, when placed in a magnetic field, acquires a small moment in the opposite direction to the field, resulting in a small negative susceptibility. All substances contain paired electrons and so all show this diamagnetic effect, but if unpaired electrons are present they will give a much larger contribution.

2.3.2 Classification of materials

Materials with unpaired electrons can be characterised by the arrangement of their atoms' magnetic moments and their behaviour in an applied field.

In a paramagnetic material, atoms have magnetic moments that are random in their orientation due to thermal energy. When a field is applied, the dipoles will tend to line up parallel to the field as this is the lowest energy state, resulting in a net moment in the sample in the same direction as the field. This is temperature dependent (see Figure 2.10)

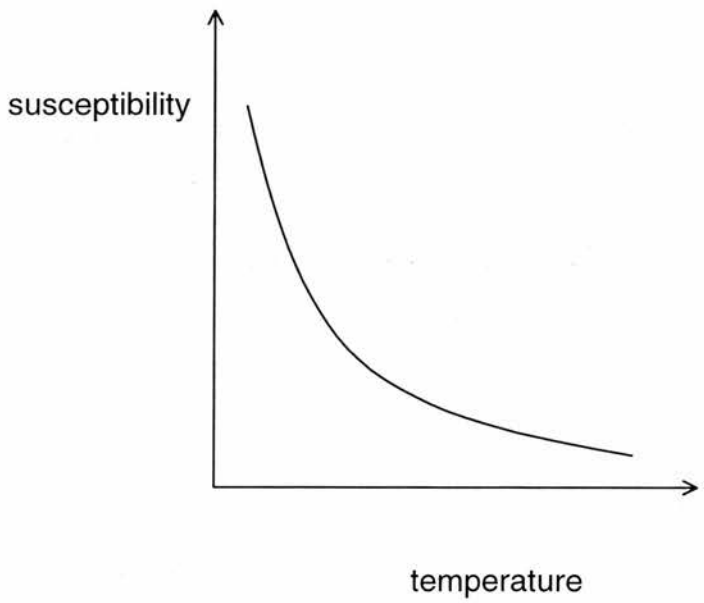

Figure 2.10 Variation of susceptibility with temperature in a paramagnetic material

This behaviour can be described by the Curie law:

$$\chi = \frac{C}{T} \qquad 2.16$$

where T is the Kelvin temperature and C is the Curie constant. C can be related to the magnetic moment of the sample, μ, by:

$$C = \frac{\mu^2 \mu_B^2 \mu_0 N}{3 k_B V} \qquad 2.17$$

where μ_B^2 is a Bohr magneton, k_B is the Boltzmann constant, N is the number of magnetic ions per unit cell and V is the volume of the unit cell.

Ferromagnetic materials exhibit a change in the susceptibility at a particular temperature, as illustrated in Figure 2.11.

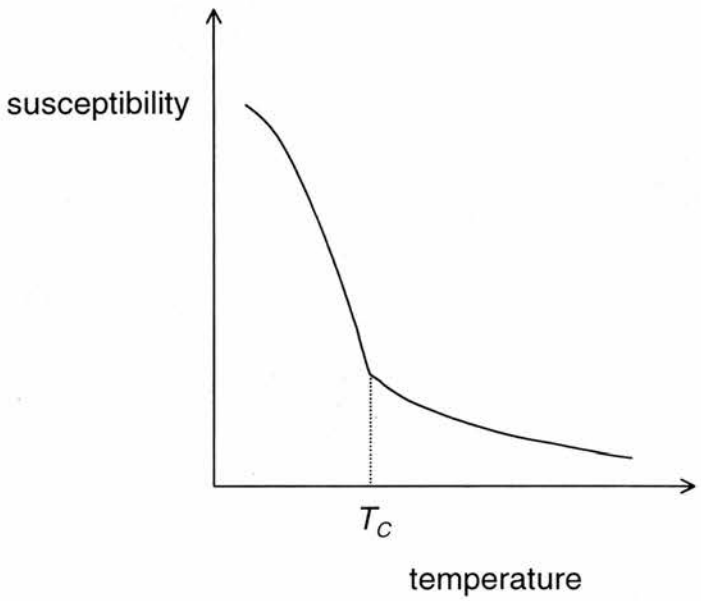

Figure 2.11 The variation of susceptibility with temperature in a ferromagnetic material, showing the Curie temperature, T_C, where parallel alignment of the dipoles occurs.

Above its Curie temperature, T_c, a ferromagnetic substance follows the Curie-Weiss law:

$$\chi = \frac{C}{T - \theta} \qquad 2.18$$

where θ is the Weiss constant, which is specific to a particular material and approximately equal to T_c. At this temperature, the susceptibility increases

dramatically, as all the magnetic moments line up in parallel. Ferromagnets show spontaneous magnetisation and hysteresis behaviour.

In an antiferromagnet, dipoles align in the opposite direction to their neighbours, and different behaviour under an applied field is seen (Figure 2.12).

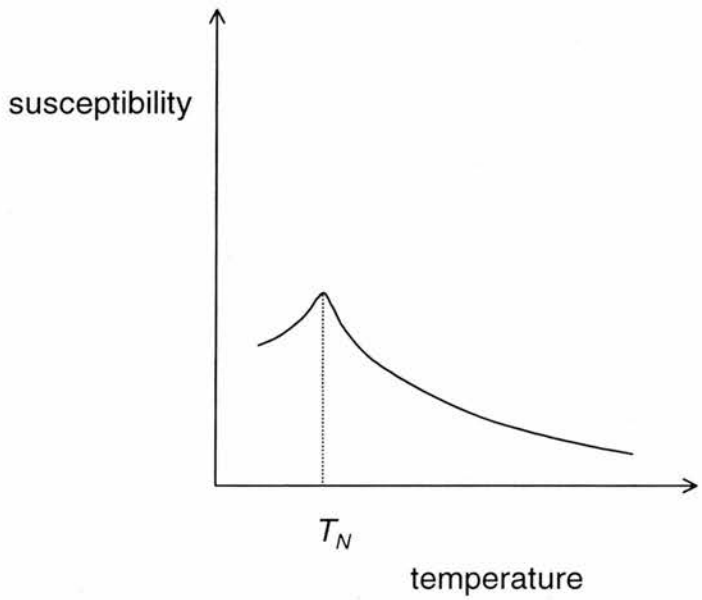

Figure 2.12 The variation of susceptibility with temperature in an antiferromagnet, showing the Néel temperature, T_N, where antiparallel alignment of dipoles occurs.

The ordering begins at a characteristic Néel temperature, T_N, below which the susceptibility decreases as the net moment becomes smaller. At higher temperatures the Curie-Weiss law is followed. In the case of antiferromagnetic ordering, θ is negative.

A ferrimagnet has ferromagnetic properties but the ordering of the dipoles is antiferromagnetic. This occurs either when there are unequal numbers of 'up' and 'down' dipoles, or the dipoles are unequal (see Figure 2.13).

Figure 2.13 Examples of ordering in ferrimagnetic materials.

This can occur if the same metal exists in different oxidation states in the material, *e.g.* $Fe^{2/3+}$, or if two different magnetically active species are present, *e.g.* Mn, Fe.

2.3.3 Exchange interactions

In ferro- and antiferromagnetic materials, dipoles on adjacent magnetic atoms interact in order to align parallel or antiparallel respectively.

Where orbitals of magnetic atoms overlap, direct exchange can occur. The energy difference between two parallel spins and two antiparallel spins gives the exchange energy. This is characterised by J_e, the exchange coefficient. If $J_e > 0$, parallel alignment (ferromagnetism) is energetically favoured. Where $J_e < 0$, antiparallel (antiferromagnetic) alignment is favoured. J_e is negative when atoms are closer together, as they move farther apart J_e becomes positive. This effect can be seen in first row transition metals, where manganese (antiferromagnetic) has a smaller interatomic distance than iron (ferromagnetic).

If orbitals on magnetic atoms are too far away to overlap, *e.g.* in insulators, indirect or superexchange can occur. Intermediate orbitals, such those on oxygen atoms, carry spin information between metal centres. This occurs in metal oxide materials, *e.g.* managnese oxide, illustrated in Figure 2.14.

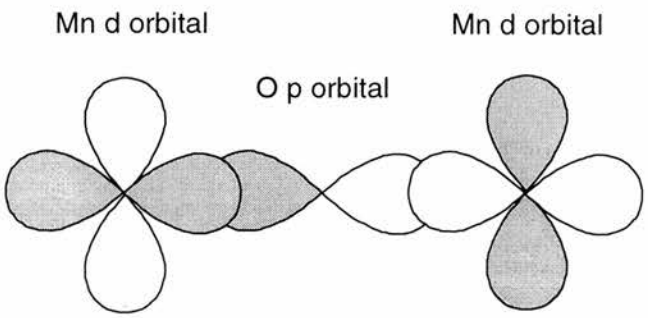

Figure 2.14 Superexchange *via* σ transfer in manganese oxide, where 180 º overlap occurs due to corner sharing octahedra.

The two O 2p electrons have opposite spin, forcing the adjacent Mn d orbitals to be aligned antiparallel.

In 4f elements, where the magnetic orbitals are buried within the atom and do not overlap at all, ordering occurs *via* the conduction electrons.

2.3.4 Magnetic measurements

In this work, magnetic measurements were obtained using a vibrating sample magnetometer (VSM) and a superconducting quantum interference device (SQUID). These are two quite different techniques, the former making use of the fact that a moving magnetic moment generates a current, the latter utilising a property of superconductors, the Josephson effect. These methods are outlined below.

2.3.4.1 Vibrating sample magnetometer (VSM)

A schematic representation of a VSM is shown in Figure 2.15. A sample is vibrated inside the coils and induces a current. The voltage, V, is related to the volume magnetisation of the sample, M_v

$$V \propto \frac{dM_V}{dt} \qquad 2.19$$

For a vibration frequency f

$$V = AM_S f \sin 2\pi ft \qquad 2.20$$

where A is a calibration constant and M_S is the sample magnetisation. In practice a calibration standard is often used, of magnetisation M_C at voltage V_C, so that

$$M_S = \frac{V_S}{V_C} M_C \qquad 2.21$$

Thus the magnetisation (and therefore the susceptibility) of the sample can be calculated. A VSM has a sensitivity of $\Delta M_S \approx 10^{-10}$ J T^{-1}.

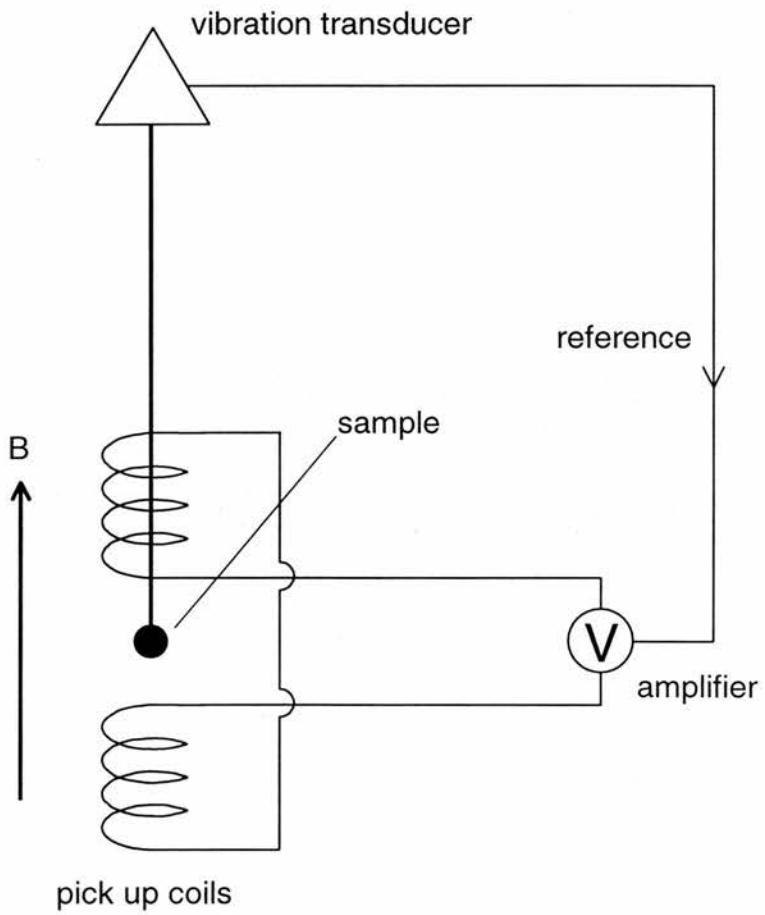

Figure 2.15 A schematic diagram of a vibrating sample magnetometer.

2.3.4.2 Superconducting quantum interference device (SQUID)[12,13]

A SQUID magnetometer uses a loop of superconducting material to measure magnetic flux. A SQUID generally has a slightly higher sensitivity than a VSM, with $\Delta M_S \approx 10^{-13} - 10^{-14}$ J T^{-1}.

Superconducting materials have zero resistance below a characteristic temperature, T_C, and so a current can flow indefinitely. Superconductors are also perfect diamagnets, *i.e.* in an applied field the internal flux density is zero (χ = -1, the so-called Meissner effect). This is due to currents flowing at the surface of the superconductor.

Different isotopes of the same element show different transition temperatures. Vibrational energy is a function of isotopic mass, so this suggests that that the superconducting effect is in some way related to lattice vibrations, *i.e.* deformations. One electron will cause a local disturbance of surrounding positive charges. This build-up of positive charge can attract another electron, hence a small attractive force occurs between the two electrons. Cooper showed that electrons can form pairs if they have opposite spins and wave vectors, and there is an attractive force between them.[11] Under conditions of low temperature the attraction can be enough to overcome the coulomb repulsion, and they exist as a Cooper pair. These pairs are the origin of superconductivity in the Bardeen-Cooper-Schrieffer (BCS) theory.

In a loop of superconductor, all Cooper pairs have the same momentum and the system can be expressed as a single wavefunction, so is quantised within the loop.

A Josephson junction consists of a superconducting ring broken by a thin insulating layer. If the insulator is very thin (~1 nm), Cooper pairs can tunnel through the insulator, *i.e.* a current will flow across it with no voltage. A phase difference occurs between either side of the junction. The junction is subjected to a magnetic field and the current through it is a function of the flux.

A schematic diagram of a SQUID is shown in Figure 2.16.

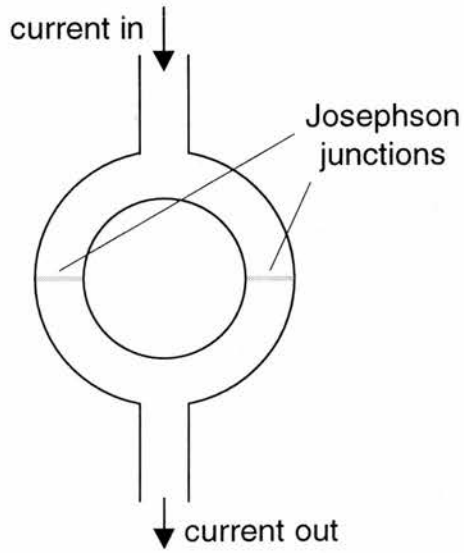

Figure 2.16 A schematic diagram of a SQUID

A current enters the ring and is divided along two paths, each of which contains a Josephson junction, before recombining. The recombined current experiences a phase shift relative to the original current due to the two junctions, analogous to light in an interferometer. This phase shift is also altered by the magnetic field in the area enclosed by the ring. The supercurrent shows a periodic variation with this magnetic field, thus measurement of the current in the presence of a magnetic sample allows the sample's magnetisation to be calculated.

2.4 Thermogravimetric analysis (TGA)

Some of the materials in this work were analysed using thermogravimetric analysis (TGA). A small amount of sample (~30 mg) is heated under an oxygen or nitrogen atmosphere with a reference sample of calcined alumina. Changes in mass of the sample are monitored as a function of temperature. Differential thermal analysis (DTA) is simultaneously performed, so exotherms or endotherms can be seen. Samples were analysed on a TA Instruments SDT 2960 Simultaneous DTA-TGA Furnace.

2.5 CHN microanalysis

Materials were analysed for carbon, hydrogen and nitrogen content as an indication of purity, using a Carlo Erba Model 1106 Elemental Analyser.

2.6 References

1. A. Rabenau, *Angew. Chem., Int. Ed. Engl.*, 1985, **24**, 1026.

2. P. W. Atkins, *Physical Chemistry*, Oxford University Press, Oxford, 5th Ed., 1995.

3. A. Stein, S. W. Keller and T. E. Mallouk, *Science*, 1993, **259**, 1558.

4. R. J. Francis and D. O'Hare, *J. Chem. Soc., Dalton Trans.*, 1998, 3133.

5. H. L. Monaco, in *Fundamentals of Crystallography*, ed. C. Giacovazzo, Oxford University Press, Oxford, 1992, chpt. 4, 229.

6. W. Clegg, *Crystal Structure Determination*, Oxford University Press, Oxford, 1998.

7. A. K. Cheetham, in *Solid State Chemistry: Techniques*, eds. A. K. Cheetham and P. Day, Oxford University Press, Oxford, 1995, chpt. 2, 39.

8. General Structure Analysis System (GSAS), A. C. Larson and R. B. Von Dreele, Los Alamos National Laboratory Report LAUR 86-748, 1987.

9. Figure from photorep@dl.ac.uk, reproduced with permission.

10. http://srs.dl.ac.uk/TOP/intro.htm

11. B. I. Bleaney and B. Bleaney, Electricity and Magnetism, Oxford University Press, London, 3rd Ed., 1976.

12. http://www.physics.carleton.ca/courses/75.364/mp-2html/node23.html

13. S. Elliot, *The Physics and Chemistry of Solids*, Wiley, Chichester, 1998.

CHAPTER 3 – OVERVIEW OF EXPERIMENTS

3.1 Synthetic strategy

During this work, a total of 482 hydrothermal reactions were carried out. In all experiments the reactants were mixed, added to a Teflon-lined stainless steel autoclave or a polypropylene bottle and heated in an oven for several days. After cooling, the contents of the autoclave were filtered and washed, then dried in air. Characterisation was by powder and single crystal x-ray diffraction. The synthesis mixtures contained some or all of the following: a metal source, a phosphate source, an organic ligand, a structure directing amine, a base to control pH and a solvent. Table 3.1 lists the metal sources used, Figure 3.1 the organic ligands and Figure 3.2 the amines. H_3PO_4(aq) was used most frequently as a source of phosphate, but $(NH_4)_2HPO_4$ was also used occasionally. KOH and NH_3(aq) were used in some reactions for pH control. Reactions took place at a wide range of pH values, between 1 and 11. The solvent was water in the majority of reactions, but a number of other solvents were used, on their own or in a 1:1 mix with water: ethanol, *iso*-propanol, *n*-butanol, ethylene glycol and pyridine. A few reactions were carried out at room temperature, however the majority were in the range 90 - 190 °C. Reactions at 90 and 100 °C were carried out in polypropylene bottles. Tables 3.2 and 3.3 list all the products that were formed in the reactions.

3.2 Discussion

Following earlier synthesis of an aluminium phosphate oxalate,[1] initial experiments aimed to form other aluminium frameworks, however this proved unsuccessful. For example, $Al(OH)_3$, H_3PO_4(aq) and phthalic, isophthalic or terephthalic acid mixed in a 1:1:1 ratio and heated at 160 °C for 48 hours gave $AlPO_4$ (JCPDS 15-265) and the appropriate dicarboxylic acid. Attention was turned to transition metal frameworks (an iron phosphate oxalate had also been

synthesised prior to this work[2]). Initially chlorides were used as a metal source, however this proved to be largely unsuccessful, producing a variety of phosphates (see Tables 3.2 and 3.3). A common product in both manganese and iron systems was the mineral hureaulite, $M_5(PO_4)_2(PO_3OH)_2.4H_2O$, with M = Mn or Fe. This was synthesised under a variety of conditions of pH and temperature. Metal chlorides were then replaced by nitrates, which in addition to several phosphates also lead to the formation of metal oxalates.

Mn^{3+} was introduced in the form of Mn_2O_3, which generally formed products containing Mn^{2+}, probably due to oxidation of $C_2O_4^{2-}$ to CO_2. The phosphate oxalates MnPOX-1 and -3 were formed as minor phases in these reactions, however better syntheses of both these materials were found.

It was with the introduction of metal oxalates as starting materials that most success was achieved. Thus experiments concentrated on oxalate as the organic ligand, particularly in manganese systems where the phosphate oxalates described in this thesis were formed. MnPOX-1 (Chapter 4) was formed using manganese oxalate and ammonium phosphate. Manipulation of synthesis conditions and amine structure directing agents (and the use of phosphoric acid in place of ammonium phosphate) led to the formation of the manganese phosphate oxalates MnPOX-2, -3, -4, -5 and -6 (Chapter 4). Formation of the two different structure types MnPOX-2, -3 and -4, and MnPOX-5 and -6 was achieved only with diamines; where an amine containing only one nitrogen atom was used manganese oxalate ($MnC_2O_4.2H_2O$ 25-544) was obtained as the product. This is presumably due to the charge balance requirements of the two framework types. Investigations into hydrothermal synthesis under conditions of low water content produced MnPOX-8 (Chapter 5).

Further experiments aimed to form phosphate oxalate frameworks containing two different metals. Gadolinium was selected because of the difference between its size and co-ordination preference compared to that of first row transition metals, so that it would not simply substitute for them in an existing framework. 3d - 4f heterometallic complexes have been synthesised in order to study the magnetic coupling between the metal centres,[3,4] and it was envisaged

that magnetic properties of a bimetallic framework may be of similar interest. Manganese, iron and cobalt oxalates were all mixed with gadolinium oxalate in a number of reactions. A new material was formed as an impurity in these reactions, however on further investigation this was found to be a gadolinium oxalate, GdOX-1 (Chapter 6). Attempts to introduce chromium and manganese into the same framework using $K_3Cr(C_2O_4)_3$ appeared to produce only MnPOX-1.

In experiments which produced phosphate oxalate frameworks water was used as the solvent. The use of other solvents, both pure and mixed with water, attempted to encourage all species into solution during the course of the reaction. This was more of a concern in reactions containing the larger organic molecules (see Figures 3.1 and 3.2). Such reactions proved unsuccessful, in many cases the colour and consistency of the resulting product suggested that the solvent may have reacted with another material in the synthesis mixture.

In hydrothermal reactions the effects of the many variables can be difficult to differentiate. The pH, for example, is linked to reactant ratios, and addition of other species to control the pH adds an extra reactant to the system. Although a range of pH values were achieved, it is noted that formation of MnPOX-1 to -6 occurred between pH 4.5 and 6.

Table 3.1 Metal sources used in syntheses in this work.

Metal source						
$Al(OH)_3$	$Ti(OCH(CH_3)_2)_4$	Mn_2O_3	$FePO_4.2H_2O$	$MnCl_2.4H_2O$	$Mn(NO_3)_2.xH_2O$	$K_3Cr(C_2O_4)_3.3H_2O$
				$FeCl_2.4H_2O$	$Fe(NO_3)_2.9H_2O$	$MnC_2O_4.2H_2O$
				$FeCl_3.6H_2O$	$Co(NO_3)_2.6H_2O$	$FeC_2O_4.2H_2O$
				$CoCl_2.6H_2O$	$Cu(NO_3)_2.3H_2O$	$CoC_2O_4.2H_2O$
					$Zn(NO_3)_2.6H_2O$	$GdC_2O_4.xH_2O$

Figure 3.1 Organic ligands used in syntheses.

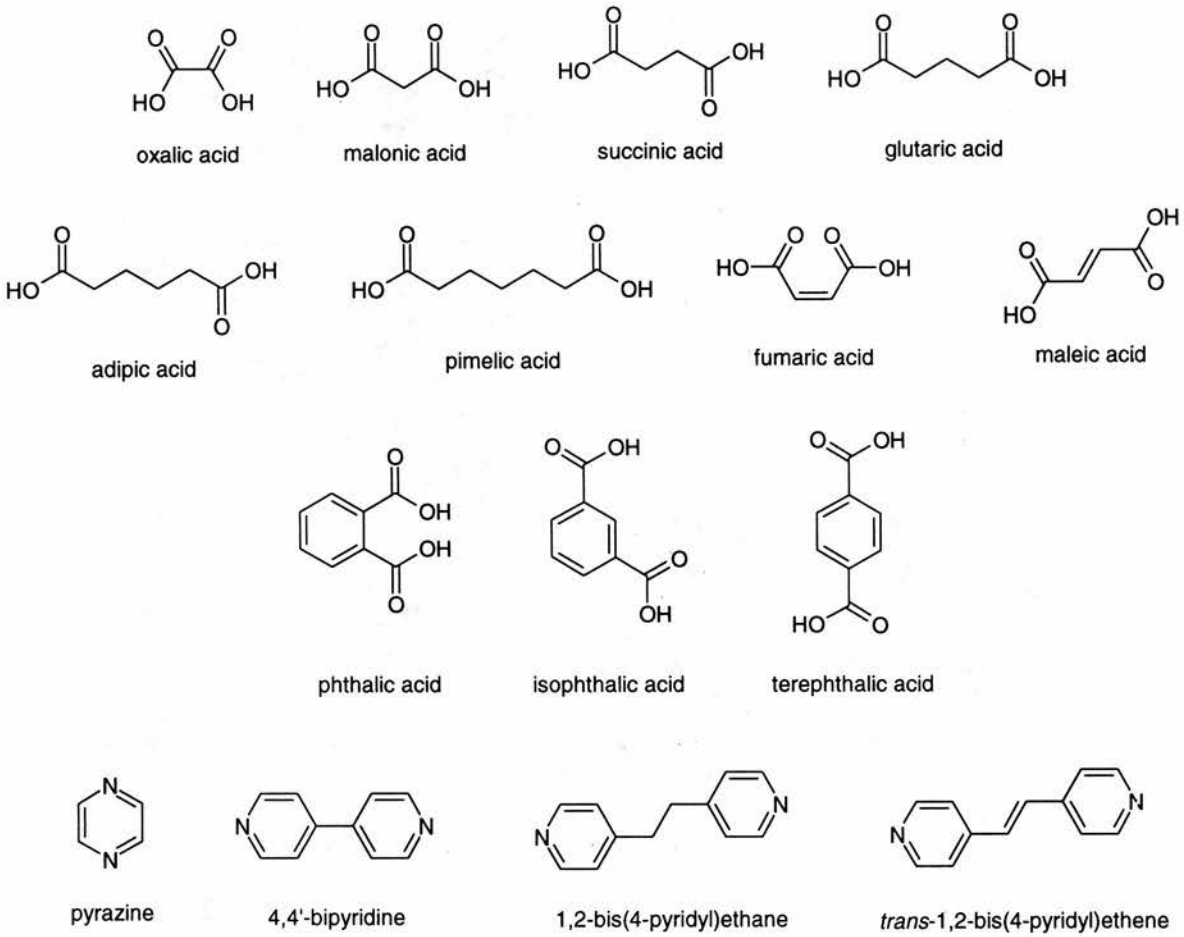

Figure 3.2 Amines used as structure directing agents.

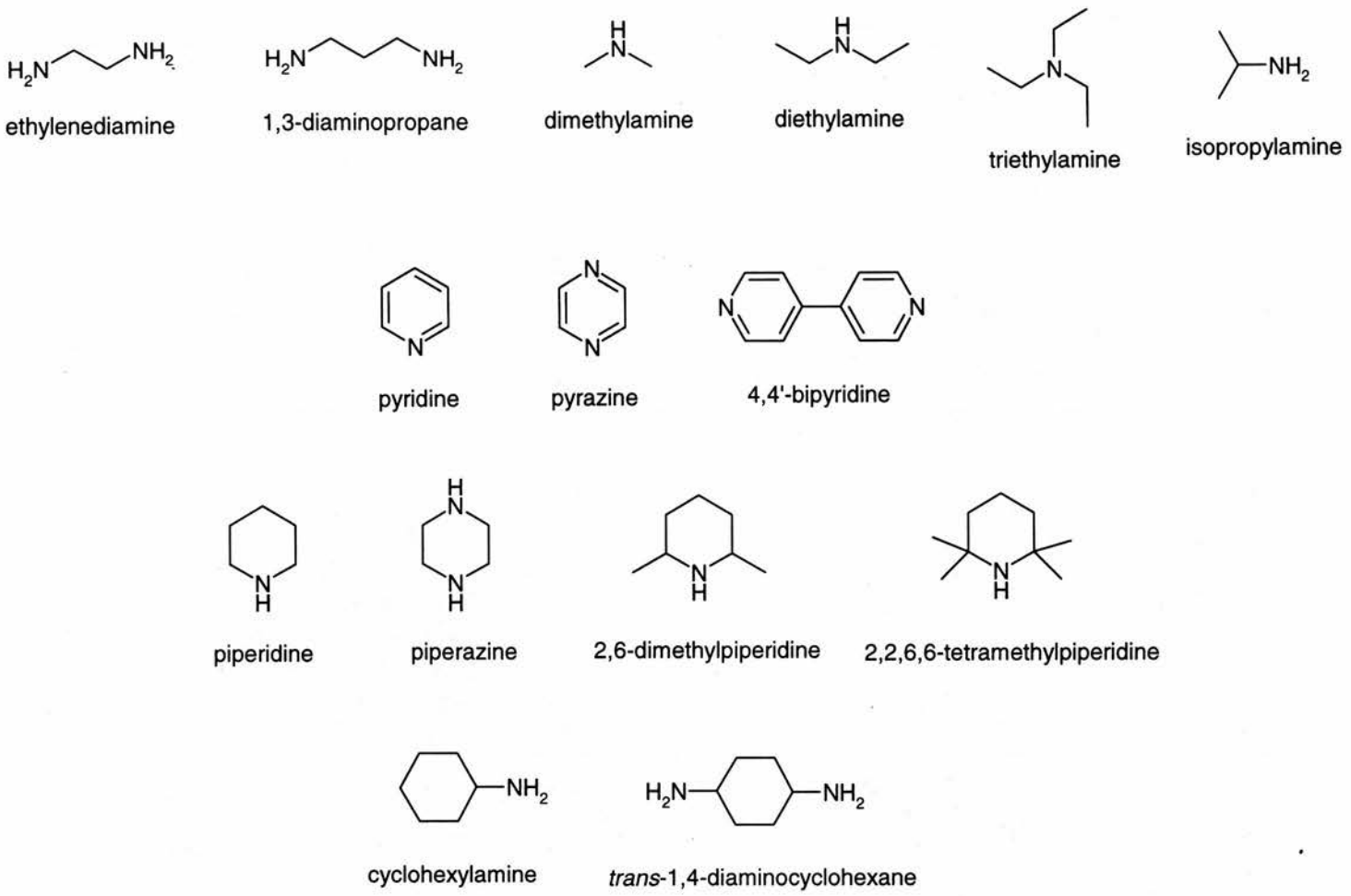

Table 3.2 Products formed in manganese and iron systems. JCPDS numbers are given where appropriate.

Products			
$Mn_4(PO_4)_2(C_2O_4)(H_2O)_2$ MnPOX-1	$Mn_7(PO_3OH)_4(PO_4)_2$ 38-224	$Fe_4(PO_4)_2(C_2O_4)(H_2O)_2$[2]	$Fe_5(PO_4)_2(PO_3OH)_2.4H_2O$ hureaulite[7]
$[Mn_2(HPO_4)_2(C_2O_4)(H_2O)_2](H_3N(CH_2)_2NH_3)$ MnPOX-2	$MnPO_4.H_2O$[5]	$Fe_4(PO_4)_2(C_2O_4)(H_2O)_2$[6]	$Fe^{2+}Fe^{3+}{}_2(HPO_4).H_2O$[8]
$[Mn_2(HPO_4)_2(C_2O_4)(H_2O)_2](H_3N(CH_2)_3NH_3)$ MnPOX-3	Mn_2O_3 24-508	$K_3[Fe_4O(OH)(PO_4)_4](H_2O)_4$ $FePO_4$-1	Fe_2O_3 21-290
$[Mn_2(HPO_4)_2(C_2O_4)(H_2O)_2](H_3NC_6H_{10}NH_3)$ MnPOX-4	$MnC_2O_4.2H_2O$ 25-544	$Fe^{2+}{}_xFe^{3+}{}_{3-x}(PO_4)_2(OH)_{3-x}$ 36-45	$FeC_2O_4.2H_2O$ 23-293
$[Mn_4(HPO_4)_2(C_2O_4)_3(H_2O)_2](H_3N(CH_2)_2NH_3)(H_2O)_2$ MnPOX-5	$MnC_2O_4.3H_2O$ 32-648	$FePO_4.2H_2O$ 33-666	
$[Mn_4(HPO_4)_2(C_2O_4)_3(H_2O)_2](C_4H_8(NH_2)_2)(H_2O)_2$ MnPOX-6		$FePO_4.2H_2O$ 33-667	
$Mn_2(H_2PO_4)_2(C_2O_4)$ MnPOX-8		$(NH_4)Fe_2(PO_4)_2(OH).2H_2O$ 41-593	
$Mn_5(PO_4)_2(PO_3OH)_2.4H_2O$ hureaulite 34-0146		$NH_4FePO_4.H_2$ 45-424	
$NH_4MnPO_4.H_2O$ 35-574		$Fe_5(PO_4)_4(OH)_3.2H_2O$ 45-1436	

Table 3.3 Products formed in aluminium, cobalt, copper, zinc and gadolinium systems. JCPDS numbers given where appropriate.

Products				
$AlPO_4$ 15-265	$NH_4CoPO_4.H_2O$ 21-793	Cu_2PO_4OH 36-404	$Zn_3(PO_4)_2.4H_2O$ 37-465	$[Gd(C_2O_4)_2(H_2O)](CH_3NH_2CH_3)(H_2O)_3$ GdOX-1
$(NH_2(CH_2)_2NH_2)Al_3(PO_4)_3.H_2O$ 45-179	$Co_3(PO_4)_2.4H_2O$ 34-544	$CuC_2O_4.xH_2O$ 21-297		$GdPO_4.3/2H_2$ 21-337
$AlPO_4$ berlinite 10-423	$Co_3(OH)_2(PO_3OH)_2$ 45-372	CuCl 6-344		
$AlPO_4$ 20-44	$CoC_2O_4.2H_2O$ 25-251	$CuClC_{10}H_8N_2$[9]		
$AlPO_4$ 11-500		$CuClC_4H_4N_2$[10]		
$C_{18}H_{12}N_2O_4$ adduct of phthalic acid and ethylenediamine				
$C_6H_4(CO_2H)_2$ phthalic acid 37-1919				
$C_6H_4(CO_2H)_2$ isophthalic acid 37-1920				
$C_6H_4(CO_2H)_2$ terephthalic acid 31-1916				

3.3 References

1. P. Lightfoot, Z. A. D. Lethbridge, R. E. Morris, D. S. Wragg, P. A. Wright, Å. Kvick and G. B. M. Vaughan, *J. Solid State Chem.*, 1999, **143**, 74.

2. Z. A. D. Lethbridge and P. Lightfoot, *J. Solid State Chem.*, 1999, **143**, 58.

3. R. E. P. Winpenny, *Chem. Soc. Rev.*, 1998, **27**, 447.

4. C. Benelli, M. Murrie, S. Parsons and R. E. P. Winpenny, *J. Chem. Soc., Dalton Trans.*, 1999, 4125.

5. P. Lightfoot, A. K. Cheetham and A. W. Sleight, *Inorg. Chem.*, 1987, **26**, 3544.

6. A. Choudhury, S. Natarajan and C. N. R. Rao, *J. Solid State Chem.*, 1999, **146**, 538.

7. D. R. Corbin, J. F. Whitney, W. C. Fultz, G. D. Stucky, M. M. Eddy and A. K. Cheetham, *Inorg. Chem.*, 1986, **25**, 2279.

8. I. Vencato, Y. P. Mascorenhas and E. Mattievich, *Am. Miner.*, 1986, **71**, 222.

9. O. M. Yaghi, G. Li and H. Li, *Nature*, 1995, **378**, 703.

10. J. M. Moreno, J. Suarezvarela, E. Colacio, J. C. Avilaroson, M. A. Hidalgo and D. Martinramos, *Can. J. Chem.*, 1995, **73**, 1591.

CHAPTER 4 – MANGANESE PHOSPHATE OXALATE MATERIALS

4.1 Introduction

Seven manganese phosphate oxalate materials, denoted MnPOX-*n*, are described in this chapter. They fall into three structure types: MnPOX-1; MnPOX-2, -3 and -4, which are all of similar connectivity but contain different amines; and MnPOX-5 and -6, which are isomorphous but also differ in their space filling species. MnPOX-7 is a dehydration product of, and structurally related to, MnPOX-5.

The synthesis and structures of these materials are discussed below. In addition, TGA and magnetic measurements have been carried out on those materials which are obtained as a single phase.

4.2 $Mn_4(PO_4)_2(C_2O_4)(H_2O)_2$ (MnPOX-1)

4.2.1 Experimental

4.2.1.1 Synthesis

$Mn_4(PO_4)_2(C_2O_4)(H_2O)_2$ (MnPOX-1) was formed by reacting $MnC_2O_4.2H_2O$, $(NH_4)_2HPO_4$ and H_2O in the ratio 2:1:555, followed by heating at 160 °C for 48 hours. The autoclave was then cooled in air, the mixture filtered and washed with distilled water and the product air-dried. In a typical reaction, $Mn_4(PO_4)_2(C_2O_4)(H_2O)_2$ (0.5272 g, 2.95 mmol) was added to water (10 ml) with stirring. $(NH_4)_2HPO_4$ (0.1976 g, 1.50 mmol) was added resulting in a pH of 6, and the mixture washed into a Teflon-lined stainless steel autoclave with a further 5 ml of water. The mixture retained its pH of 6 after heating. 0.3397 g of

pink diamond shaped crystals were obtained. (Found: C, 4.66; H, 0.76. $Mn_4(PO_4)_2(C_2O_4)(H_2O)_2$ requires C, 4.50; H, 0.76%).

4.2.1.2 Characterisation

X-ray data collection was carried out at room temperature on a Rigaku AFC7S four-circle diffractometer using graphite monochromated MoK_α radiation. Crystallographic details are given in Table 4.1. Structure solution and refinement were carried out using the SIR 92[1] and TEXSAN[2] suites.

Table 4.1 Crystal data and details of structure solution and refinement for MnPOX-1

	MnPOX-1
Formula	$Mn_4(PO_4)_2(C_2O_4)(H_2O)_2$
Formula weight	533.745
Crystal system	monoclinic
Space group	$P2_1/c$
a (Å)	10.263(3)
b (Å)	6.526(2)
c (Å)	10.082(3)
β (°)	116.84(2)
Volume (Å^3)	602.8(4)
Z	2
μ(MoK_α) (cm^{-1})	4.438
Total reflections	1496
Observed reflections ($I>3\sigma(I)$)	1240
R, R_w	0.0314, 0.0350

Magnetisation measurements were obtained on a 0.2119 g polycrystalline sample of MnPOX-1 using an Oxford Instruments Vibrating Sample Magnetometer in a field of 4 Tesla over the temperature range 4 - 170 K.

Thermogravimetric analysis (TGA) was carried out on at TA Instruments SDT 2960 simultaneous DTA-TGA furnace, from room temperature to 800 °C at a heating rate of 10 °C min^{-1} under both nitrogen and oxygen.

4.2.2 Discussion

4.2.1.2 Structure

MnPOX-1 is a three dimensional framework constructed from MnO_5, MnO_6 and PO_4 polyhedra and oxalate units. The building unit is shown in Figure 4.1, atomic co-ordinates, bond lengths and angles are in Appendix 1.

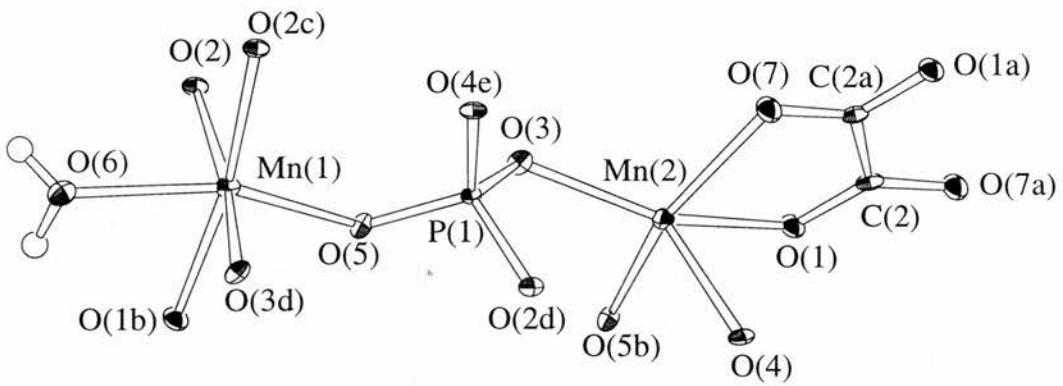

Figure 4.1 Building unit of MnPOX-1. Thermal ellipsoids are at 50% probability. Symmetry labels: a, 1-*x*, 2-*y*, 2-*z*; b, -*x*, 2-*y*, 1-*z*; c, -*x*, 2-*y*, -*z*; d, -*x*, *y*-1/2, 1/2-*z*; e, *x*, 3/2-*y*, *z*-1/2.

There are two different types of manganese in the structure, both in the 2+ oxidation state as indicated by bond valence calculations:[3] Mn(1) 2.050, Mn(2) 1.881. Mn(1) exists as a distorted octahedron, while Mn(2) is five co-ordinate. (The sixth oxygen, O(6), is at a distance of 2.555(3) Å from Mn(2)). Each Mn(1) is co-ordinated to one oxalate oxygen, four phosphate oxygens and a water molecule. Mn(2) is co-ordinated to both oxalate oxygens and three phosphate oxygens. The smallest O-Mn(2)-O angle (75.1°) is due to the bidentate oxalate co-ordination. Two $Mn(1)O_6$ and two $Mn(2)O_5$ polyhedra share edges to form a tetranuclear building unit, illustrated in Figure 4.2. These units are linked to each other *via* corner sharing of the manganese polyhedra, and also by corner sharing phosphate tetrahedra, to form manganese phosphate layers in the *bc* plane (see Figure 4.3).

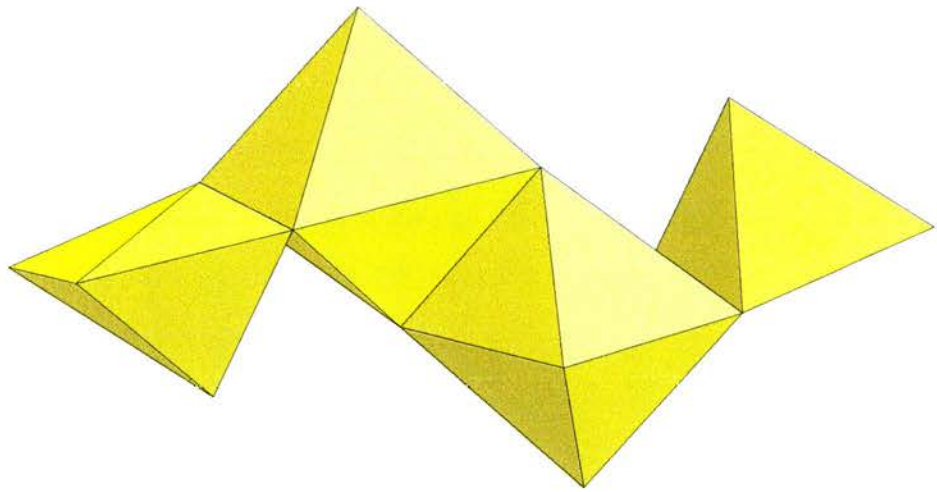

Figure 4.2 Tetranuclear unit in MnPOX-1 with edge sharing MnO_n polyhedra.

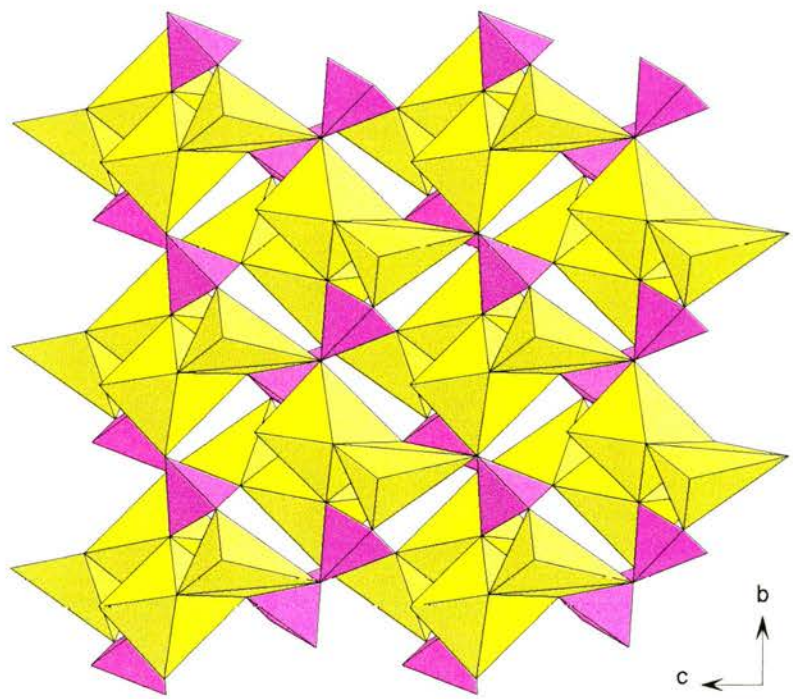

Figure 4.3 A layer of MnPOX-1 formed from tetrameric manganese units and PO_4 tetrahedra. Manganese polyhedra yellow, phosphate tetrahedra purple.

Oxalate units show bismonodentate co-ordination to Mn(1) and bisbidentate co-ordination to Mn(2), acting as pillars between adjacent manganese phosphate layers to produce the extended three dimensional network. The *ab* and *ac* projections of the structure (Figures 4.4 and 4.5) show a small amount of open space between the oxalate pillars.

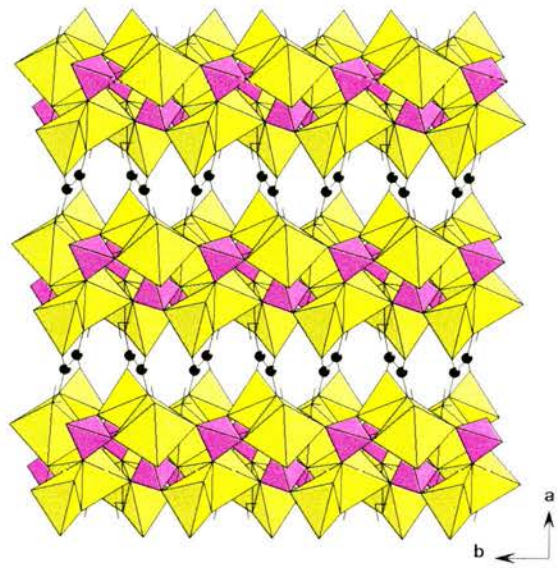

Figure 4.4 MnPOX-1 in the *ab* plane, showing the oxalate anions acting as pillars between the manganese phosphate layers. Colours as before; carbon black.

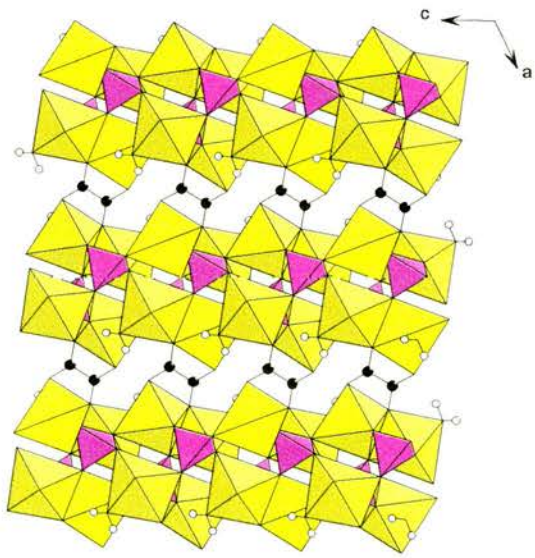

Figure 4.5 MnPOX-1 in the *ac* plane.

The Mn(1) co-ordination sphere is completed by a water molecule, indicated by the low bond valence of O(6) (0.2800). Hydrogen bonding occurs between the water and the framework oxygens (see Appendix 1).

4.2.2.2 Thermogravimetric Analysis

The TGA plot is shown in Figure 4.6.

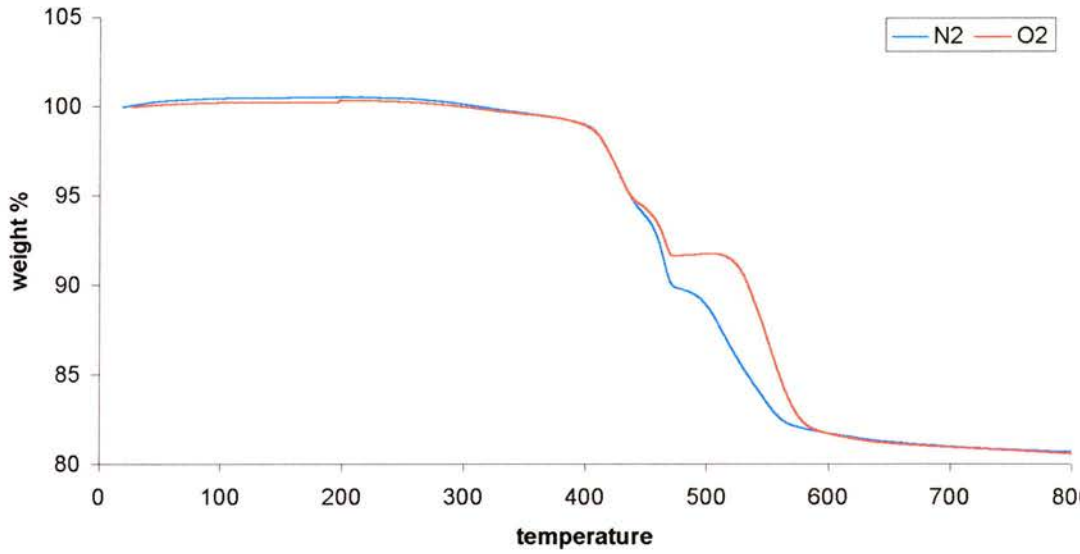

Figure 4.6 TGA plot of MnPOX-1

Under N_2, the weight loss can be split up into three steps, although these are not well separated. The first (240 °C - 448 °C), which is endothermic, can be attributed to loss of water (observed 6.41 %, $2H_2O$ calc. 6.75 %). Between 448 °C and 800 °C a further 13.4 % is lost in two exothermic steps, resulting in a brown powder containing $Mn_3(PO_4)_2$ (JCPDS 40-112) and Mn_3O_4 (JCPDS 18-803, 24-734) identified by powder x-ray diffraction. This may be accounted for by decomposition of the oxalate to a mixture of CO and CO_2. The mass lost of 13.4 %, compares to 10.5 % calc. for 2CO and 16.5 % calc. for $2CO_2$. A similar weight loss profile is obtained under O_2, however there is a plateau between the second and third steps. A sample heated to 485 °C, where the second step

finishes, gives a largely amorphous black material which shows some peaks in the x-ray powder pattern, thought to be $Mn_2P_2O_7$ (JCPDS 29-891, 35-1497). The weight loss begins at 242 °C; by 800 °C the total weight loss was 19.7 %, resulting in a black powder containing $Mn_3(PO_4)_2$ (JCPDS 40-112) as before. The first two steps in the process (5.77 %, 2.87 %) are exothermic, followed by a slight endotherm in the third (11.0 %). A similar water loss and oxalate decomposition is thought to occur in this case, possibly the extra O_2 forms Mn_2O_3, however it was not possible to identify this from the powder pattern, and the mechanism of the decomposition is not clear.

4.2.2.3 Magnetic Measurements

Figure 4.7 shows the susceptibility of MnPOX-1 with temperature.

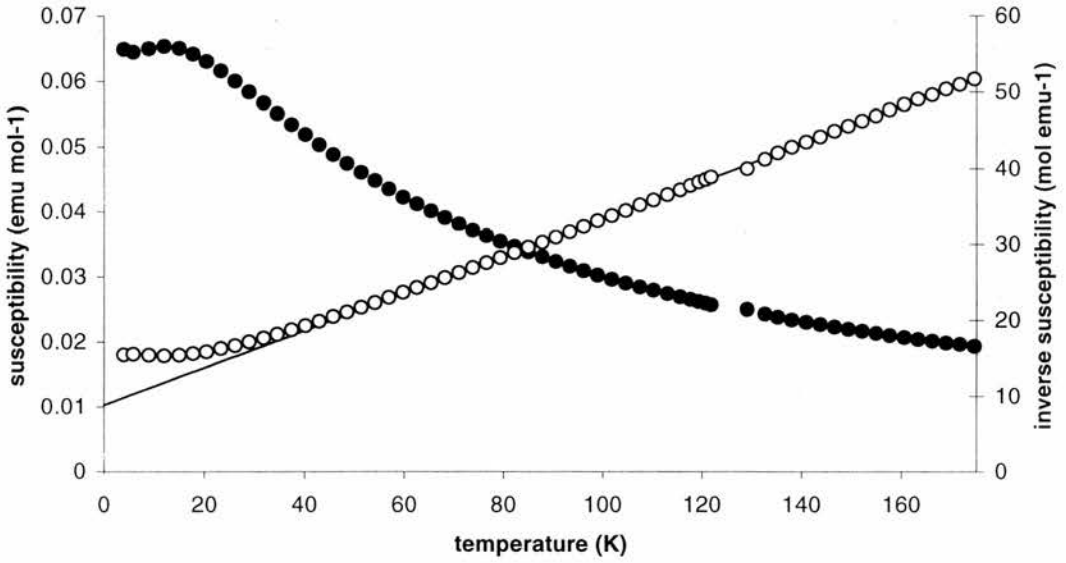

Figure 4.7 Magnetic susceptibility (closed circles) and inverse susceptibility (open circles) of MnPOX-1. The solid line shows the fit to the Curie-Weiss law above 50 K.

Above 50 K the sample shows Curie-Weiss behaviour with a θ value of -36.0 K and an effective moment per Mn ion μ_{eff} of 5.86 μ_B (spin only value for Mn^{2+} is 5.92 μ_B). The negative value of θ indicates antiferromagnetic interactions,

however the susceptibility maximum, around 15 K, is more rounded than would normally be expected. This is characteristic of 2D antiferromagnetism, as seen in the layered phosphonates $M^{II}(RPO_3)H2O$ (M = Mn, Co, Ni with R = CH_3, C_2H_5, C_6H_5 and M = Fe with R = C_2H_5, *n*-C_4H_9).[4] The Néel temperatures and susceptibility maxima did not vary greatly as the interlayer spacing changed, *i.e.* with different species of R. This behaviour was also observed in the metal oxalates $A[Mn^{II}Fe^{III}(C_2O_4)_3]$, where A is a variety of ammonium, phosphonium or arsonium species, previously discussed in section 1.3.2.3.[5]

4.3 $[Mn_2(HPO_4)_2(C_2O_4)(H_2O)_2](AH_2)$ (MnPOX-2, -3 and -4)

MnPOX-2, -3 and -4 all share the same general formula, with A = ethylenediamine (MnPOX-2), 1,3-diaminopropane (MnPOX-3) and *trans*-1,4-diaminocyclohexane (MnPOX-4)

4.3.1 Experimental

4.3.1.1 Synthesis

$[Mn_2(HPO_4)_2(C_2O_4)(H_2O)_2](H_3N(CH_2)_2NH_3)$ (MnPOX-2)

MnPOX-2 was prepared from $MnC_2O_4.2H_2O$, H_3PO_4(aq), $H_2N(CH_2)_2NH_2$ and H_2O in the approximate ratio 1:1:1:400, and heated in an autoclave at 120 °C for 24 hours. In a typical reaction, $MnC_2O_4.2H_2O$ (0.3637 g, 2.03 mmol) was added to H_2O (15 ml) with stirring, followed by H_3PO_4(aq) (85 %, 0.23 ml, 1.99 mmol) and $H_2N(CH_2)_2NH_2$ (0.13 ml, 1.94 mmol), giving a pH of 4.5. The resulting mixture (pH 3.5) was filtered, washed with distilled water and air-dried, giving 0.3018 g product. MnPOX-2 is formed along with MnPOX-5 (section 4.4), sonication can remove most of the larger MnPOX-5 crystals but the resulting MnPOX-2 still contains a small amount.

$[Mn_2(HPO_4)_2(C_2O_4)(H_2O)_2](H_3N(CH_2)_3NH_3)$ (MnPOX-3)

MnPOX-3 was synthesised using $MnC_2O_4.2H_2O$, H_3PO_4(aq), $H_2N(CH_2)_3NH_2$ and H_2O in the ratio 1:1:1:400, and heated in an autoclave at 120 °C for 48 hours. In a typical reaction, $MnC_2O_4.2H_2O$ (0.3601 g, 2.01 mmol) was added to H_2O (15 ml) with stirring, followed by H_3PO_4(aq) (85 %, 0.23 ml, 1.99 mmol) and $H_2N(CH_2)_3NH_2$ (0.17 ml, 2.04 mmol), giving a pH of 5. After heating the resulting pH was 3. The mixture was filtered, washed with distilled water and air-dried, giving 0.3477 g product. Preparations of MnPOX-3 sometimes showed a small amount of $MnC_2O_4.2H_2O$ (JCPDS 25-544) which may be removed by sonication.

$[Mn_2(HPO_4)_2(C_2O_4)(H_2O)_2](H_3NC_6H_{10}NH_3)$ (MnPOX-4)

MnPOX-4 is similarly prepared from $MnC_2O_4.2H_2O$, H_3PO_4(aq), $H_2NC_6H_{10}NH_2$, and H_2O in an approximate ratio of 1:1:1:400, and heated for 48 hours at 120 °C. Typically, $MnC_2O_4.2H_2O$ (0.3638 g, 2.03 mmol) was added to H_2O (15 ml) followed by addition of H_3PO_4(aq) (85 %, 0.23 ml, 1.99 mmol). *Trans*-1,4-$H_2NC_6H_{10}NH_2$ (0.2294 g, 2.01 mmol) was added and the mixture was heated, then cooled in air, filtered and washed with distilled water and air dried, giving 0.4255 g of a pink/grey material. Again, the product needed to be sonicated to give a pure sample (by x-ray diffraction).

4.3.1.2 Characterisation

X-ray data collection on MnPOX-3 was carried out at room temperature on a Rigaku AFC7S four-circle diffractometer using graphite monochromated MoK_α radiation. Single crystal X-ray data collection for MnPOX-2 and MnPOX-4 was carried out at room temperature on a Bruker SMART diffractometer with a CCD detector and MoK_α radiation. Structure solution and refinement were carried out

using the SIR 92[1] and TEXSAN[2] suites. Crystallographic details are given in Table 4.2.

Thermogravimetric analysis (TGA) was carried out on a TA Instruments SDT 2960 simultaneous DTA-TGA furnace, from room temperature to 600 or 800 °C at a heating rate of 10 °C min^{-1} under both nitrogen and oxygen.

Magnetisation measurements were carried out on polycrystalline samples of MnPOX-3 and -4, loaded into gelatine capsules using a Quantum Design $MPMS_2$ SQUID magnetometer. A field of 100 Oe was applied between 1.7 and 300 K. The data were corrected for the diamagnetic contribution of the sample holder and constituent elements.[6]

4.3.2 Discussion

4.3.2.1 Structure

$[Mn_2(HPO_4)_2(C_2O_4)(H_2O)_2](H_3N(CH_2)_2NH_3)$ (MnPOX-2)

MnPOX-2 is a three dimensional framework, constructed from MnO_6 octahedra, PO_4 tetrahedra and oxalate units, and contains diprotonated ethylenediamine in one dimensional channels in the *a* direction. The building unit is shown in Figure 4.8; atomic co-ordinates, bond lengths and angles are given in Appendix 2. Manganese is confirmed as 2+ by bond valence calculations (sum = 2.07).[3] The presence of a water (O(4)) and a hydroxyl group (O(7)) are also indicated by bond valence sums of 0.27 and 1.04 respectively. Manganese exists as a distorted MnO_6 octahedron. The co-ordination sphere consists of one water molecule, two oxalate oxygens and three phosphate oxygens. The distortion is caused by the bidentate oxalate co-ordination, resulting in an O(1)-Mn-O(5) angle of 73.23(9) °. The PO_4 tetrahedra are connected to MnO_6 octahedra at three vertices and an OH^- group is found on the fourth.

Table 4.2 Crystal data and details of structure solution and refinement for MnPOX-2, -3 and -4.

	MnPOX-2	MnPOX-3	MnPOX-4
Formula	$[Mn_2(HPO_4)_2(C_2O_4)(H_2O)_2]$ $(H_3N(CH_2)_2NH_3)$	$[Mn_2(HPO_4)_2(C_2O_4)(H_2O)_2]$ $(H_3N(CH_2)_3NH_3)$	$[Mn_2(HPO_4)_2(C_2O_4)(H_2O)_2]$ $(H_3NC_6H_{10}NH_3)$
Formula weight	488.00	502.03	542.09
Crystal system	Monoclinic	Monoclinic	Monoclinic
Space group	$P2_1/n$	$P2_1/n$	$P2_1/n$
a (Å)	5.4573(4)	5.474(2)	5.9778(3)
b (Å)	8.9650(7)	15.737(2)	16.6747(8)
c (Å)	15.253(1)	9.056(2)	8.4660(4)
β (°)	98.924(1)	93.47(3)	90.384(1)
V (Å)	737.22(8)	778.7(3)	843.85(6)
Z	2	2	2
$\mu(MoK_\alpha)$ (cm^{-1})	2.010	1.906	1.767
Total reflections	1136	1439	1272
Observed reflections ($I>3\sigma(I)$)	808	1094	883
R, R_w	0.0239, 0.0270	0.0408, 0.0388	0.0299, 0.0333

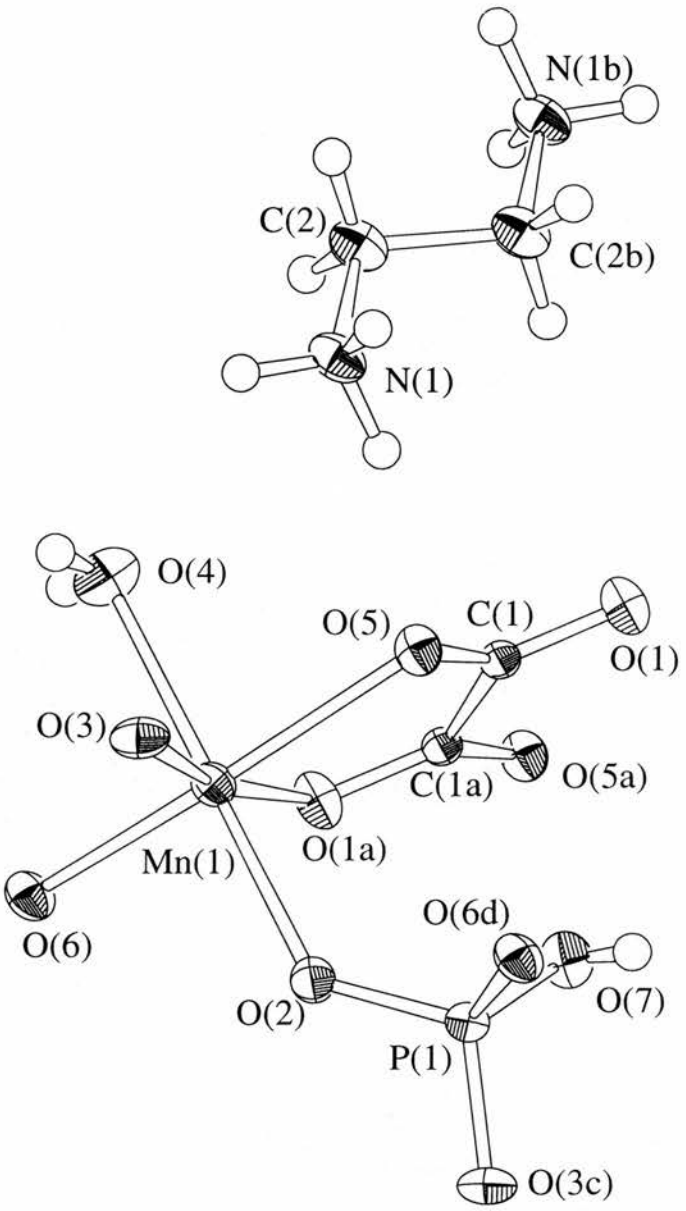

Figure 4.8 Building unit of MnPOX-2 with ellipsoids at 50 % probability. Symmetry labels: a, -*x*, -*y*+1, -*z*+2; b, -*x*, -*y*+2, -*z*+2; c, -*x*-1/2, *y*-1/2, -*z*+3/2; d, *x*-1, *y*, *z*.

Chains are formed in the *a* direction from alternating MnO_6 octahedra and PO_4 tetrahedra which share corners. The chains are connected to each other *via* a third corner on both the MnO_6 octahedra and PO_4 tetrahedra, forming sheets in the *ac* plane (Figure 4.9(a)). Thus each octahedron is connected to three tetrahedra and *vice versa*.

Bisbidentate oxalate anions co-ordinate to manganese centres in adjacent layers, producing the three-dimensional structure (Figure 4.10(a)). Each layer contains chains 'pointing' up and down, which alternate along the *b* direction. Oxalate anions co-ordinated to an 'up' chain connect one layer to the layer above, those co-ordinated to a 'down' chain to a layer below.

Channels are found in the *a* direction between these oxalate pillars, which contain diprotonated ethylenediamine. The cations are hydrogen bonded to the framework *via* N-H...O bonds, hydrogen bonding is also seen between the H_2O and OH groups and the oxalate oxygens (see Appendix 2).

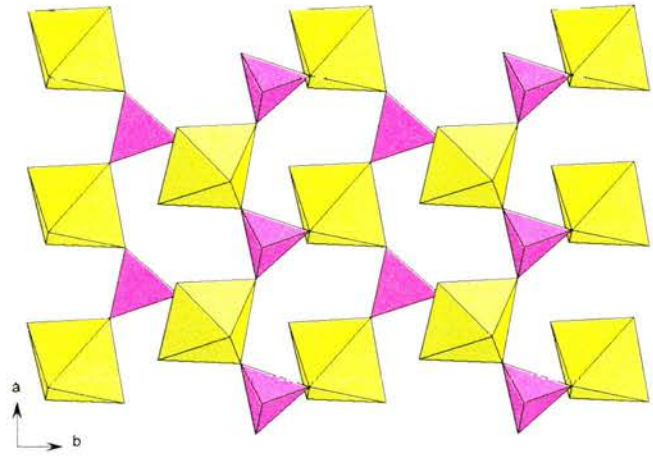

(a)

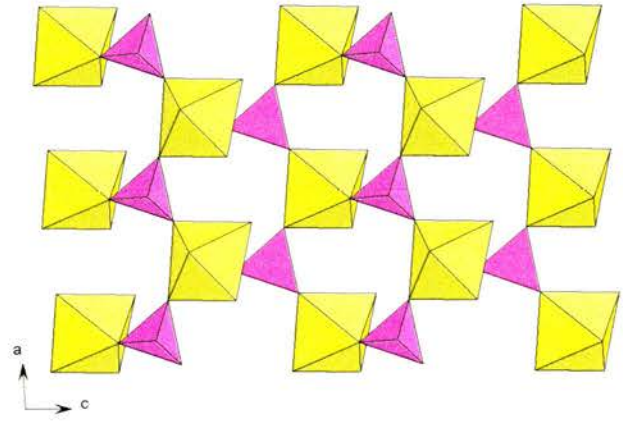

(b)

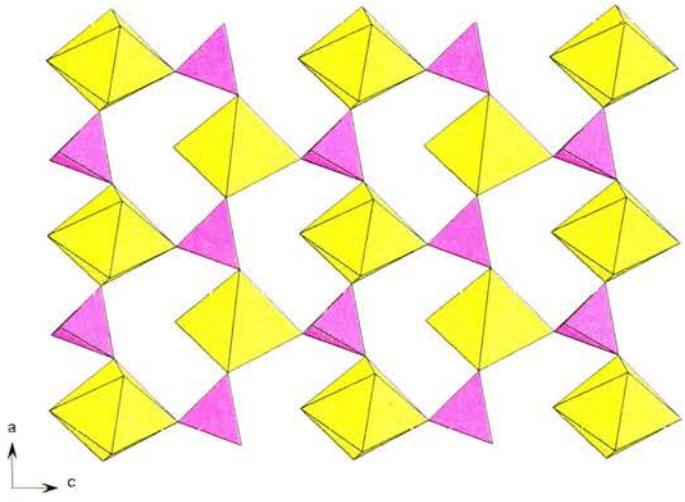

(c)

Figure 4.9 Manganese phosphate layers in (a) MnPOX-2, (b) MnPOX-3, and (c) MnPOX-4.

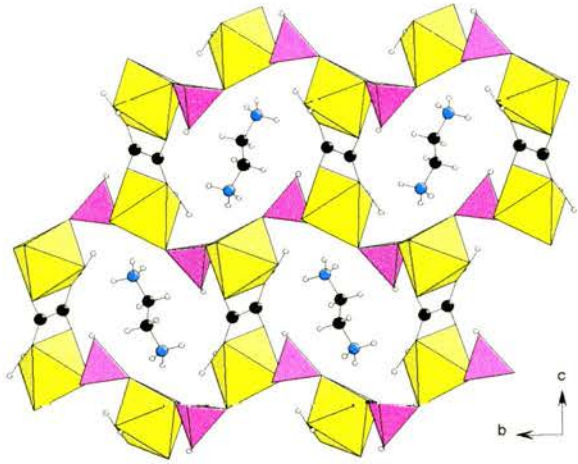

(a)

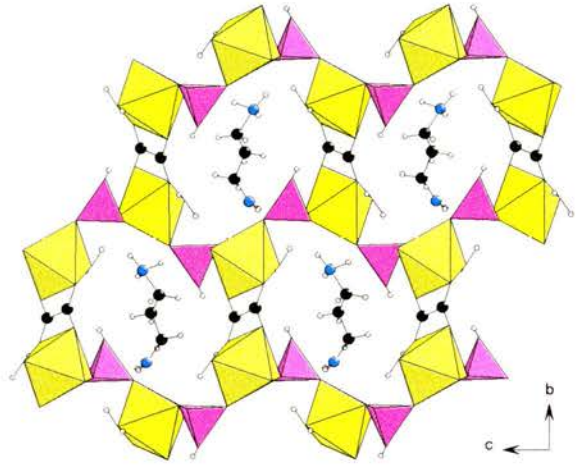

(b)

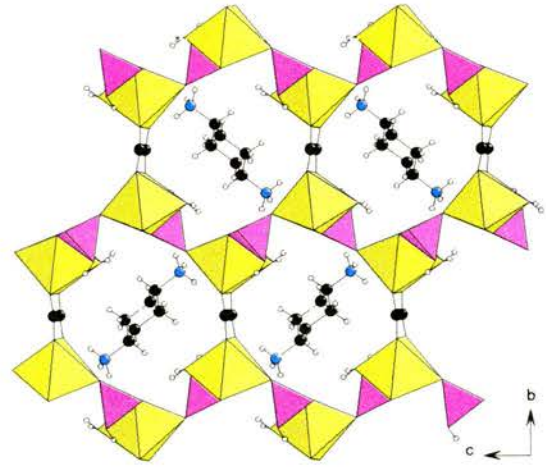

(c)

Figure 4.10 Oxalate anions acting as pillars to form channels in (a) MnPOX-2, (b) MnPOX-3, and (c) MnPOX-4. Colours as before; N blue, H white.

$[Mn_2(HPO_4)_2(C_2O_4)(H_2O)_2](H_3N(CH_2)_3NH_3)$ (MnPOX-3)

MnPOX-3 is isomorphous with MnPOX-2, but contains diprotonated 1,3-diaminopropane cations, which are found disordered over two positions.

The building unit is shown in Figure 4.11; atomic co-ordinates, bond lengths and angles are given in Appendix 3.

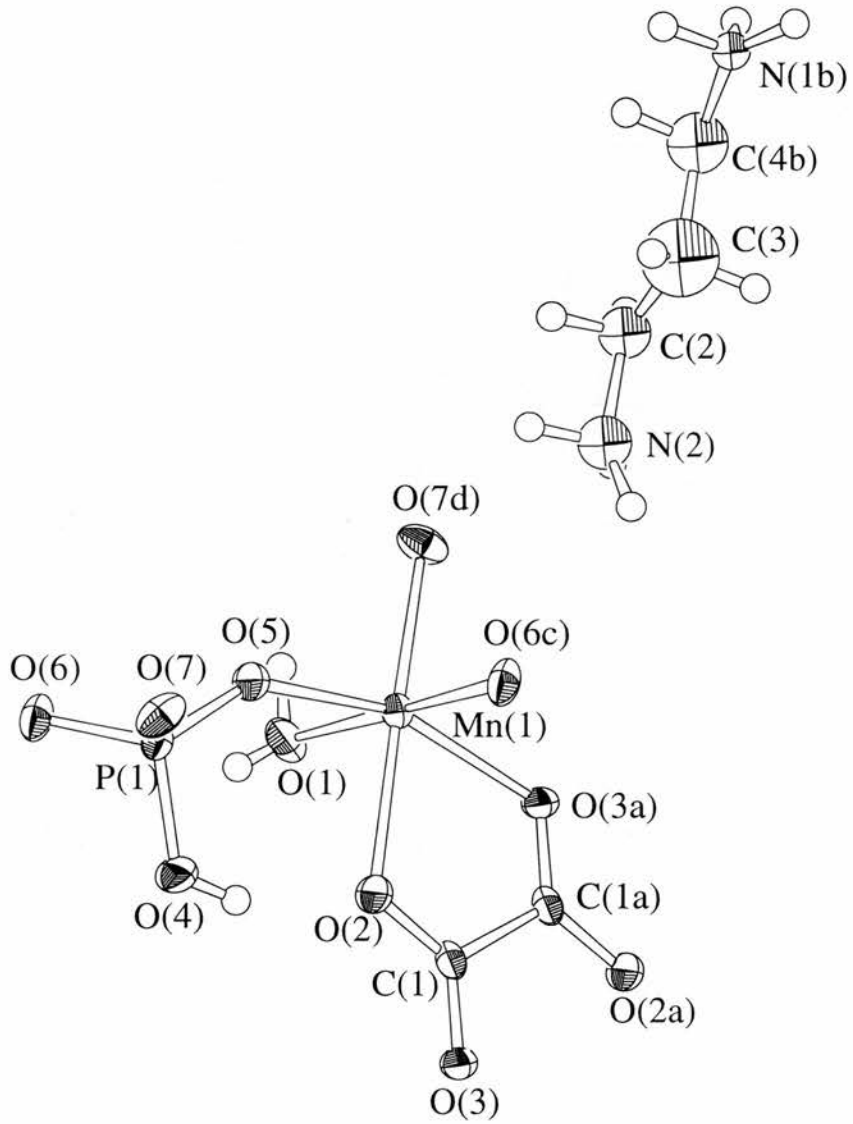

Figure 4.11 Building unit of MnPOX-3 with ellipsoids at 50 % probability; only one position of disordered 1,3-diaminopropane cation shown. Symmetry labels: a, 1-*x*, -*y*, 2-*z*; b, 2-*x*, 1-*y*, 2-*z*; c, 1+*x*, *y*, *z*; d, 1/2+*x*, 1/2-*y*, *z*-1/2.

Bond valence sums give 2.063 for Mn^{2+}, 0.27 for O(1) (*i.e.* OH_2) and 1.07 for O(4) (*i.e.* OH). The diprotonated 1,3-diaminopropane is disordered over two positions, with the central carbon atom C(3) lying on an inversion centre. The positions of the hydrogen atoms on the carbon and nitrogen of the amine were geometrically fixed. Figure 4.9(b) illustrates the *ac* layer, and Figure 4.10(b) shows the 3D structure.

$[Mn_2(HPO_4)_2(C_2O_4)(H_2O)_2](H_3NC_6H_{10}NH_3)$ (MnPOX-4)

MnPOX-4 is a three-dimensional manganese phosphate oxalate framework containing diprotonated *trans*-1,4-diaminocyclohexane cations. The framework is very similar in connectivity to MnPOX-2 and -3, though not isostructural. The basic building unit is shown in Figure 4.12; atomic co-ordinates, bond lengths and angles are in Appendix 4.

Again, bond valence sums confirm manganese as 2+ (Mn(1) 1.96).[3] The presence of the water molecule as a ligand on the manganese and also a hydroxyl group on the phosphate tetrahedron is indicated by the low bond valences of O(1) (0.28, H_2O) and O(5) (1.03, OH).

The framework is constructed from *cis* corner-sharing MnO_6–HPO_4 chains running along the *a* direction, which are linked to each other *via* corner sharing HPO_4 tetrahedra to form layers in the *ac* plane as before (Figure 4.9(c)).

A *bc* projection (Figure 4.10(c)) shows the full 3D structure, with diprotonated *trans*-1,4-diaminocyclohexane cations in the channels along the *a* direction. Hydrogen bonding occurs between the amine and the framework oxygens (see Appendix 4).

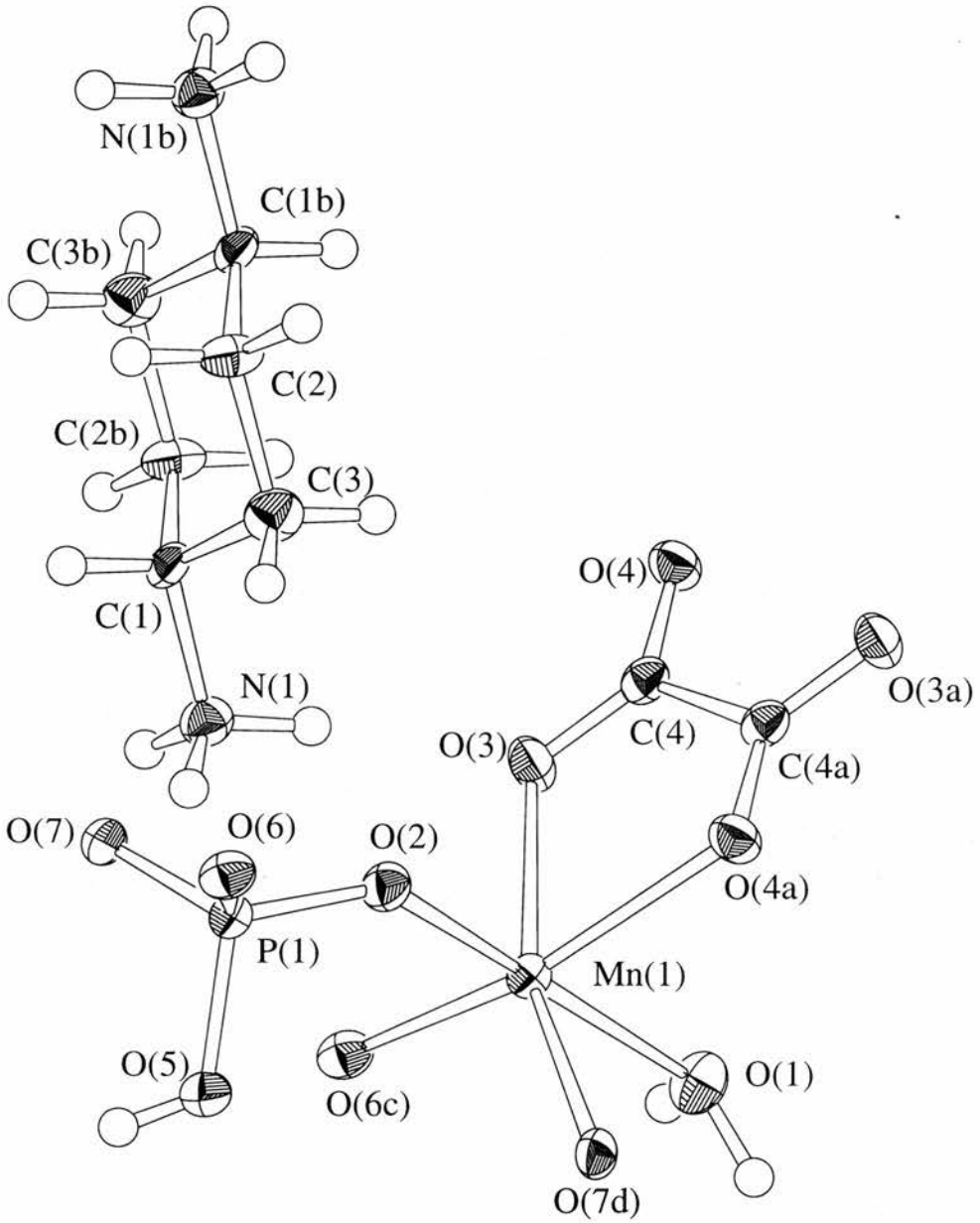

Figure 4.12 Building unit of MnPOX-4 with ellipsoids at 50 % probability. Symmetry labels: a, -*x*+1, -*y*, -*z*+1; b, -*x*+2, -*y*, -*z*; c, *x*-1, *y*, *z*; d, *x*-1/2, -*y*+1/2, *z*+1/2.

Comparison of MnPOX-2, -3 and -4

Figures 4.9 and 4.10, showing a comparison of the layers and 3D projections of MnPOX-2, -3 and -4, illustrate the similarity in appearance of MnPOX-2 and -3, and the different appearance of MnPOX-4. It can be seen in Figure 4.10 that the angles of the polyhedra are different in MnPOX-4 (c) compared to MnPOX-2

and -3 (a, b). The MnO_6 octahedra in MnPOX-4 almost lie in the *ac* plane, tilted up from it at approximately 9 °. The equivalent angles in MnPOX-2 and -3 are approximately 66 ° and 67 ° respectively. The oxalate anions also have a different appearance in MnPOX-4. In Figure 4.10(c) the appearance is of looking down the plane of the oxalate, reflected in the angle of the C-C bond to the *bc* plane, which is approximately 81 °. In MnPOX-2 the equivalent angle is 46 °, and in MnPOX-3 48 °. Although all structures have the same local co-ordination around the Mn site (three HPO_4 groups in a *fac-* configuration, a bidentate oxalate group and a terminal H_2O molecule), a difference in longer-range connectivity between the two can be seen. Although all phosphate tetrahedra are crystallographically equivalent, a distinction can be made between HPO_4 in one chain running along the *a* axis and HPO_4 in an adjacent one. The difference in connectivity of the chains is illustrated by the configuration of the MnO_6 octahedra in Figure 4.13, where the 'chain' HPO_4 ligands are either *cis-/trans-* or *trans-/trans-* to the oxalate group.

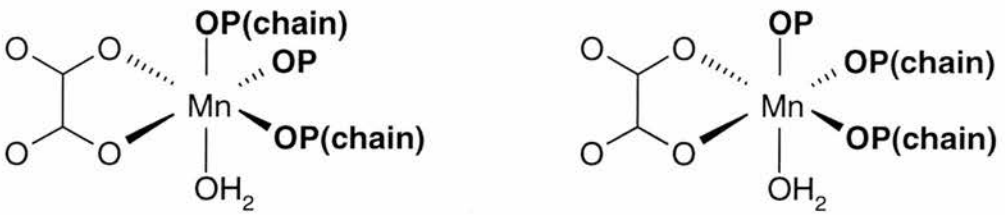

MnPOX-2 and -3 MnPOX-4

Figure 4.13 Co-ordination around the manganese centre showing the difference between MnPOX-2 and -3 and MnPOX-4.

A similar material exists in the iron phosphate oxalate system, $[Fe_2(HPO_4)_2(C_2O_4)(H_2O)_2]H_2O$, reported by Rao and co-workers.[7] Interestingly this material contains no amine despite the presence of cyclohexylamine in the synthesis mixture. As a consequence of the absence of a charge balancing species, the iron is found in the 3+ oxidation state. The channels in $[Fe_2(HPO_4)_2(C_2O_4)(H_2O)_2]H_2O$ contain water molecules only. The connectivity around the iron atom corresponds to that of MnPOX-2 and -3, rather than that of

MnPOX-4. A comparison of the channel sizes in MnPOX-2, -3 and -4 together with the Fe(III) phase is given in Table 4.3.

Table 4.3 Comparison of channel size in MnPOX-2, -3 and -4 and $[Fe_2(HPO_4)_2(C_2O_4)(H_2O)_2]H_2O$[7] (see Figure 4.14 for details)

Material	Oxalate – oxalate cross channel distance (Å)	Metal – metal cross channel distance (Å)
MnPOX-2	8.965	11.24
MnPOX-3	9.056	10.45
MnPOX-4	8.466	10.79
$[Fe_2(HPO_4)_2(C_2O_4)(H_2O)_2]H_2O$	7.342	13.34

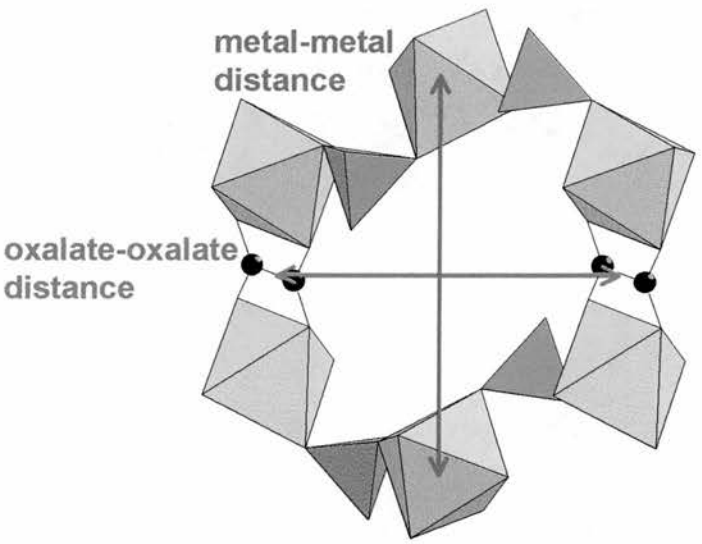

Figure 4.14 Channel dimensions measured in Table 4.3.

4.3.2.2 Thermogravimetric Analysis

$[Mn_2(HPO_4)_2(C_2O_4)(H_2O)_2](H_3N(CH_2)_3NH_3)$ (MnPOX-3)

The TGA plot of MnPOX-3 under O_2 and N_2 is shown in Figure 4.15.

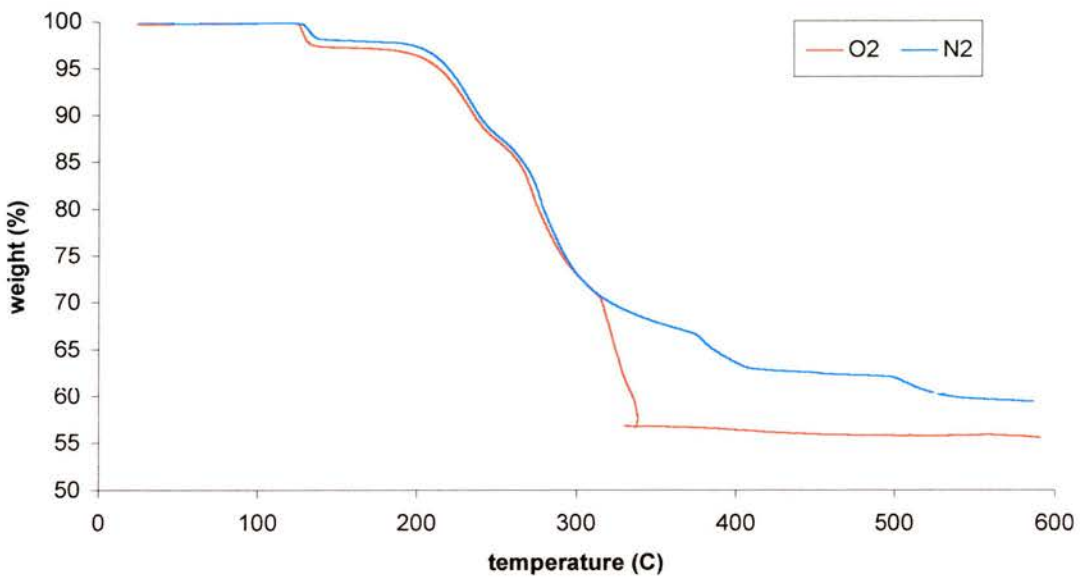

Figure 4.15 TGA of MnPOX-3

Under oxygen, MnPOX-3 loses 2.7 % weight between 119 and 157 °C (endothermic). A sample heated to 152 °C and then cooled and exposed to air showed the same powder diffraction pattern as MnPOX-3, so this loss is likely to be the loss of a small amount of water. After this small step, the material loses 40.5 % up to 341 °C, with a large sudden exotherm around 325 °C. The resulting product contains $Mn_2P_2O_7$ (JCPDS 29-891) with possibly a small amount of Mn_2O_3 (24-508). Loss of oxalate, amine and water from MnPOX-3 is 40.95 %.

A similar weight loss profile is seen under nitrogen, with an initial loss of 1.8 % up to 152 °C, followed by 38.8 % to 600 °C.

$[Mn_2(HPO_4)_2(C_2O_4)(H_2O)_2](H_3NC_6H_{10}NH_3)$ (MnPOX-4)

The TGA plot of MnPOX-4 is show in Figure 4.16. Two small weight losses occur when heating MnPOX-4 under O_2; 0.67 % starting at 36 °C, and a further 1.53 % to 180 °C. A sample heated to 180 °C and exposed to air when cooled, was identified as MnPOX-4. A large, relatively sudden weight loss of 49.15 % at 300 °C gives $Mn_2P_2O_7$ and Mn_2O_3 (JCPDS 29-891 and 24-508) which is highly exothermic.

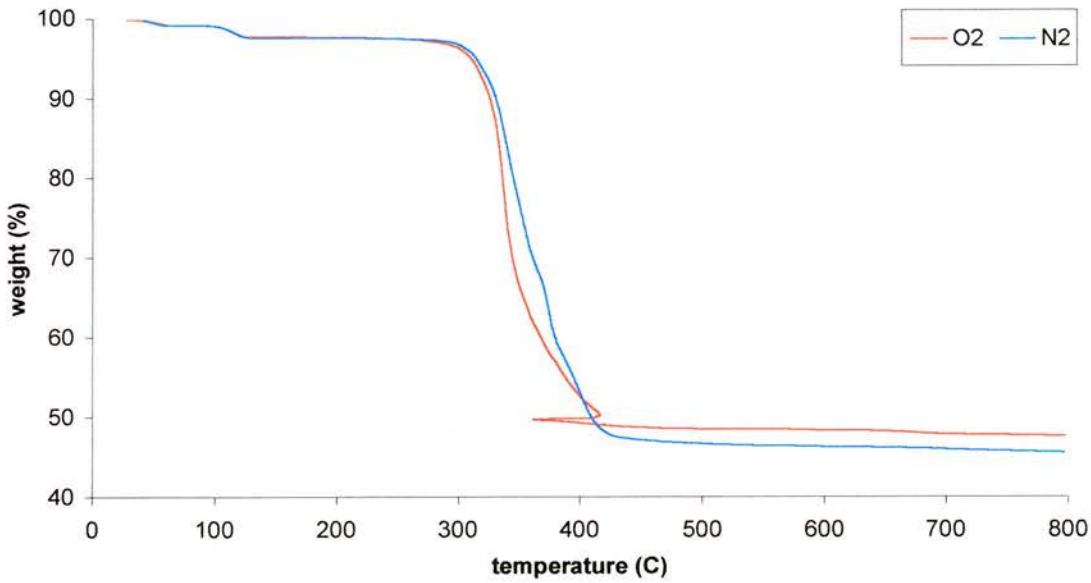

Figure 4.16 TGA of MnPOX-4

The N_2 trace follows a very similar path. The final losses at 800 °C are 54.36 % (N_2) and 52.34 % (O_2). Both losses are endothermic under N_2, the final product appears the same as under O_2 by powder x-ray diffraction. Loss of C_2O_4, $2H_2O$ and $H_2NC_6H_{10}NH_2$ from MnPOX-4 is 43.95 % weight.

4.3.2.3 Magnetic Measurements

$[Mn_2(HPO_4)_2(C_2O_4)(H_2O)_2](H_3N(CH_2)_3NH_3)$ (MnPOX-3)

A plot of magnetic susceptibility against temperature is shown in Figure 4.17, along with the fit to the Curie-Weiss law above 50 K, with C = 4.30 emu K mol^{-1}. The variation of magnetic moment with temperature is illustrated in Figure 4.18, with μ_{eff} rising to around 5.7 μ_B by 200 K, as expected from the spin only value.

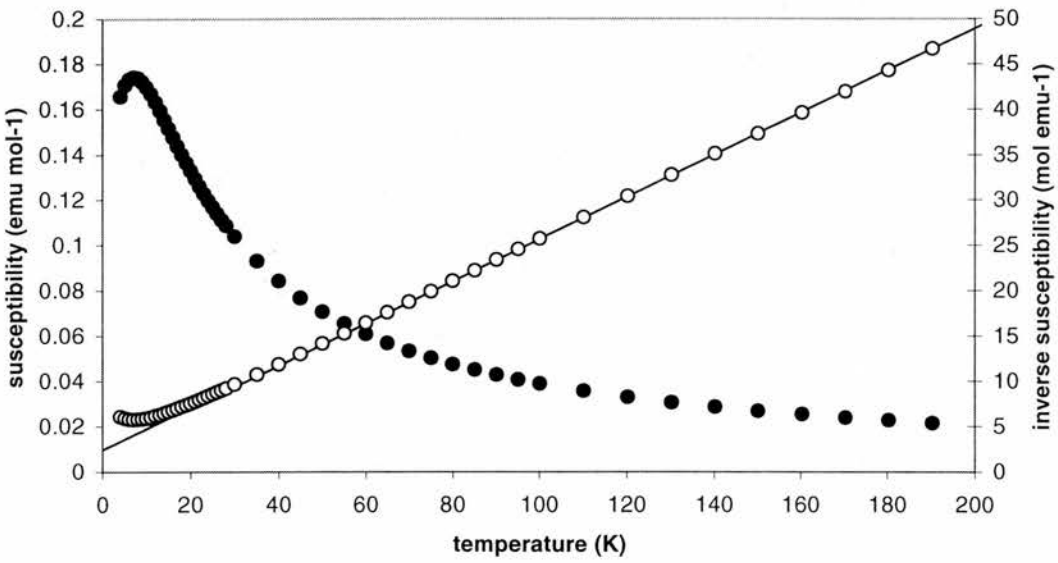

Figure 4.17 Magnetic susceptibility (closed circles) and inverse susceptibility (open circles) of MnPOX-3. The solid line shows the fit to the Curie-Weiss law above 50 K.

A maximum in the susceptibility (7.02 K at 0.174 emu mol^{-1}) and the value of θ (-10.4 K) indicate the presence of antiferromagnetic interactions.

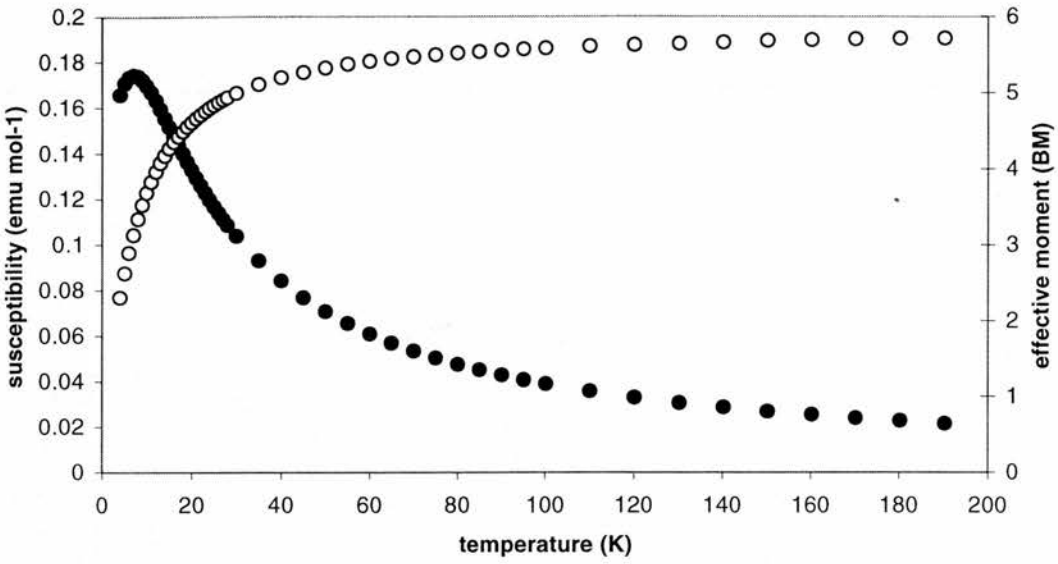

Figure 4.18 Magnetic susceptibility (closed circles) and effective moment (open circles) of MnPOX-3.

$[Mn_2(HPO_4)_2(C_2O_4)(H_2O)_2](H_3NC_6H_{10}NH_3)$ (MnPOX-4)

The susceptibility *versus* temperature curve for MnPOX-4 is very similar to MnPOX-3 (see Figure 4.19) and shows antiferromagnetic ordering as before, with a susceptibility maximum of 0.155 emu mol^{-1} at 7.00 K.

The Curie-Weiss fit above 50 K gives θ = -13.31 K, C = 4.128 emu K mol^{-1}. A plot illustrating the behaviour of effective moment with temperature is illustrated in Figure 4.20, showing similar behaviour to MnPOX-3 above.

The manganese octahedra in MnPOX-3 and -4 exhibit corner-sharing with PO_4 tetrahedra and bisbidentate co-ordination to oxalate anions, so no Mn-O-Mn linkages are present within the materials.

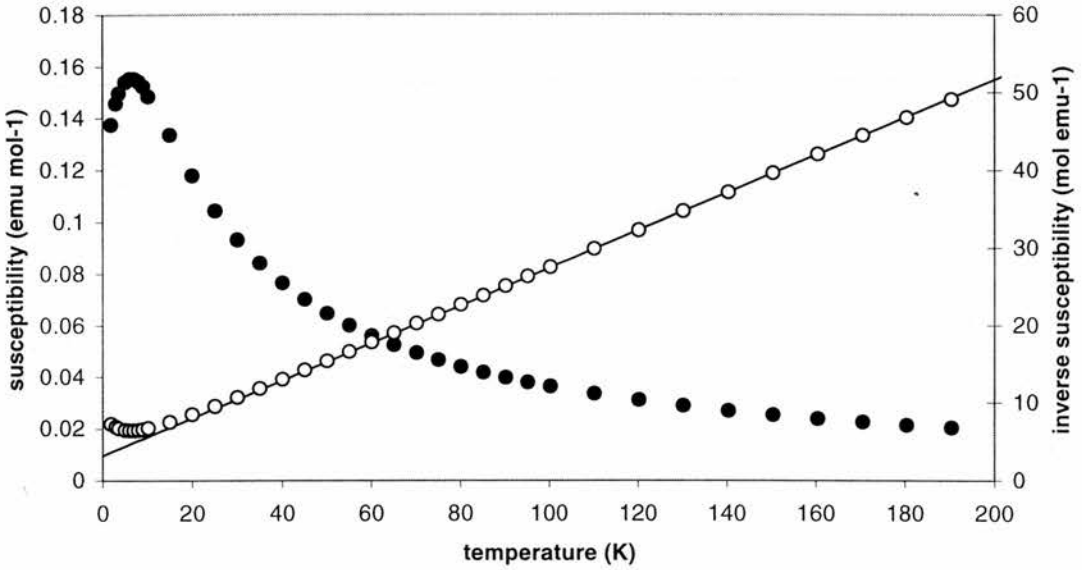

Figure 4.19 Magnetic susceptibility (closed circles) and inverse susceptibility (open circles) of MnPOX-4. The solid line shows the fit to the Curie-Weiss law above 50 K.

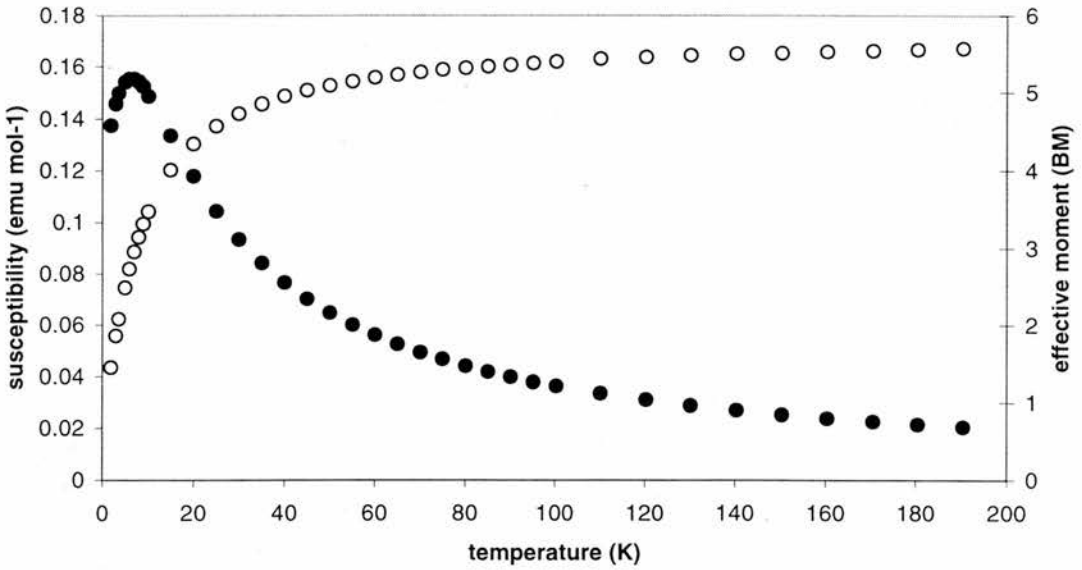

Figure 4.20 Magnetic susceptibility (closed circles) and effective moment (open circles) of MnPOX-4.

The isomorphous iron phosphate oxalate $[Fe_2(HPO_4)_2(C_2O_4)(H_2O)_2]H_2O$ is also antiferromagnetic, with Fe^{3+} in a high spin configuration, *i.e.* all three materials have a HS d^5 configuration.[7] A comparison of the magnetic parameters of

MnPOX-3, -4 and $[Fe_2(HPO_4)_2(C_2O_4)(H_2O)_2]H_2O$ is given in Table 4.4, the iron material showing higher θ and T_N values.

Table 4.4 Magnetic parameters of MnPOX-3, -4 and $[Fe_2(HPO_4)_2(C_2O_4)(H_2O)_2]H_2O$[7]

Material	θ (K)	T_N (K)
MnPOX-3	-10.4	7
MnPOX-4	-13.31	7
$[Fe_2(HPO_4)_2(C_2O_4)(H_2O)_2]H_2O$	-63.1	30

4.4 $[Mn_4(HPO_4)_2(C_2O_4)_3(H_2O)_2](H_2O)_2(AH_2)$ (MnPOX-5, -6 and -7)

MnPOX-5 and -6 are both of the same structure type, with different amines: A = ethylenediamine (MnPOX-5) and piperazine (MnPOX-6). MnPOX-5 can be dehydrated to form MnPOX-7.

4.4.1 Experimental

4.4.1.1 Synthesis

$[Mn_4(HPO_4)_2(C_2O_4)_3(H_2O)_2](H_2O)_2(H_3N(CH_2)_2NH_3)$ (MnPOX-5)

As with MnPOX-2, MnPOX-5 was prepared from $MnC_2O_4.2H_2O$, H_3PO_4(aq), $H_2N(CH_2)_2NH_2$ and H_2O in the approximate ratio 1:1:1:400 and heated at 120 °C. The ratio of MnPOX-5 to MnPOX-2 produced was generally higher after 48 hours (*cf.* 24 hours for MnPOX-2). The sample may be sonicated to give a pure sample of MnPOX-5. $MnC_2O_4.2H_2O$ (3.2399 g, 18.1 mmol) was added to water (135 ml), followed by addition of H_3PO_4(aq) (85 %, 2.07 ml, 17.9 mmol). A 15 ml portion of this mixture was placed in an autoclave with ethylenediamine (0.13

ml, 1.94 mmol), giving a pH of 4.5. After heating, the mixture (pH 3) was filtered and washed with distilled water, then air dried to give 0.3132 g product.

$[Mn_4(HPO_4)_2(C_2O_4)_3(H_2O)_2](H_2O)_2(C_4H_8(NH_2)_2)$ (MnPOX-6)

MnPOX-6 was similarly prepared from a 1:1:1:400 approximate ratio of $MnC_2O_4.2H_2O$, H_3PO_4(aq), $C_4H_8(NH)_2$ and H_2O, heated at 120 °C for 48 hours, then filtered and washed with distilled water and dried in air. $MnC_2O_4.2H_2O$ (3.2399 g, 18.1 mmol) was added to water (135 ml), followed by addition of H_3PO_4(aq) (85 %, 2.07 ml, 17.9 mmol). A 15 ml portion of this mixture was placed in an autoclave with piperazine (0.1761 g, 2.04 mmol), resulting in a pH of 6. After heating, the mixture (with a pH of 5.5) gave 0.1606 g product.

4.4.1.2 Characterisation

Single crystal X-ray data collection for MnPOX-5 was carried out on a Bruker SMART diffractometer with a CCD detector and MoK_α radiation. Data collection for MnPOX-6 was carried out at station 9.8 at the SRS, Daresbury. Structure solution and refinement were carried out using the SIR 92[1] and TEXSAN[2] suites. Crystallographic details are given in Table 4.5.

Powder diffraction data for MnPOX-7 was collected on station 9.1 at the SRS, Daresbury, with a wavelength of 1.000(1) Å in a 0.5 mm capillary for six hours.

Thermogravimetric analysis (TGA) was carried out on a TA Instruments SDT 2960 simultaneous DTA-TGA furnace, from room temperature to 600 or 800 °C at a heating rate of 10 °C min^{-1} under both nitrogen and oxygen.

Magnetisation measurements were carried out on polycrystalline samples loaded into gelatine capsules using a Quantum Design $MPMS_2$ SQUID magnetometer with an applied field of 100 Oe over the temperature range 1.7 to 300 K. The

data were corrected for the diamagnetic contribution of the sample holder, and the diamagnetic contribution of the constituent elements.[6]

Table 4.5 Details of structure solution and refinement

	MnPOX-5	MnPOX-6
Formula	$[Mn_4(HPO_4)_2(C_2O_4)_3(H_2O)_2]$ $(H_3N(CH_2)_2NH_3)(H_2O)_2$	$[Mn_4(HPO_4)_2(C_2O_4)_3(H_2O)_2]$ $(C_4H_8(NH_2)_2)(H_2O)_2$
Formula weight (g)	809.95	795.92
Crystal system	Triclinic	Triclinic
Space group	$P\bar{1}$	$P\bar{1}$
a (Å)	7.830(4)	7.7679(6)
b (Å)	8.041(4)	8.0674(6)
c (Å)	9.652(7)	9.6972(7)
α (°)	76.29(5)	76.075(2)
β (°)	78.47(6)	78.784(2)
γ (°)	86.36(6)	86.883(2)
V (Å)	578.4(6)	578.55(7)
Z	1	1
μ (cm^{-1})	2.389	2.381
Total reflections	1637	3135
Observed reflections ($I>3\sigma(I)$)	1343	2413
R, R_w	0.0305, 0.0390	0.0618, 0.0697

4.4.2 Discussion

4.4.2.1 Structure

$[Mn_4(HPO_4)_2(C_2O_4)_3(H_2O)_2](H_2O)_2(H_3N(CH_2)_2NH_3)$ (MnPOX-5)

MnPOX-5 is a 3D structure containing ethylenediamine cations and extra-framework water. The structure is built from edge-sharing MnO_6 octahedra and two crystallographically different types of oxalate anion. Two independent manganese cations are present, both adopting distorted octahedral co-ordination. The building unit is shown in Figure 4.20; atomic co-ordinates, bond lengths and angles are in Appendix 5.

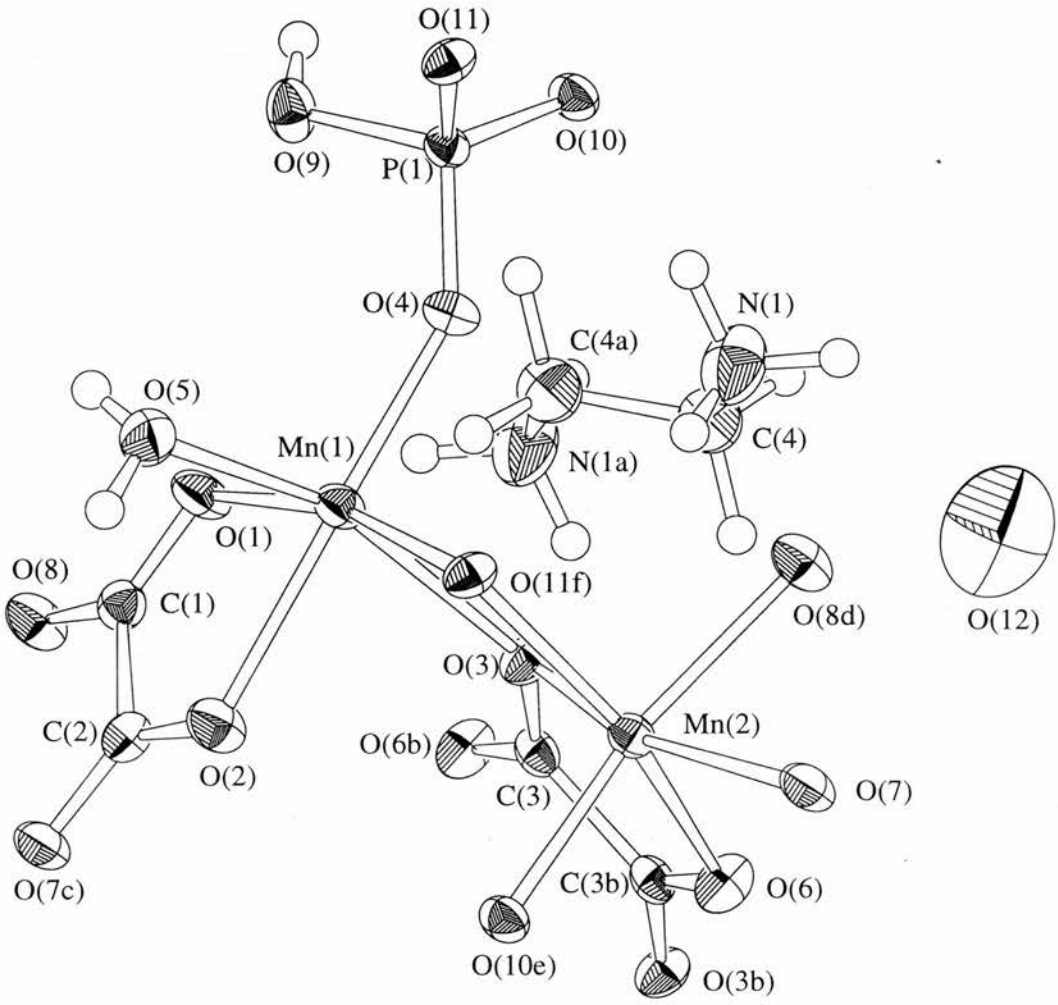

Figure 4.20 Building unit of MnPOX-5, with ellipsoids at 50 % probability. Symmetry labels: a, -*x*+2, -*y*-1, -*z*+2; b, -*x*+2, -*y*-2, -*z*+2; c, *x*+1, *y*, *z*; d, *x*-1, *y*, *z*; e, *x*, *y*-1, *z*; f, -*x*+2, -*y*-1, -*z*+1.

Bond valence sums give 2.03 for Mn(1) and 2.06 for Mn(2).[3] Calculations for O(5) (0.32) and O(9) (1.10) indicate the presence of H_2O on Mn(1) and OH on P(1) respectively.

$Mn(1)O_6$ and $Mn(2)O_6$ share an edge through a phosphate and an oxalate oxygen (O(11) and O(3), respectively); both O atoms therefore being three co-ordinate. These dimeric units share corners with HPO_4 tetrahedra, forming chains in the *b* direction containing eight-membered rings (see Figure 4.21(a)).

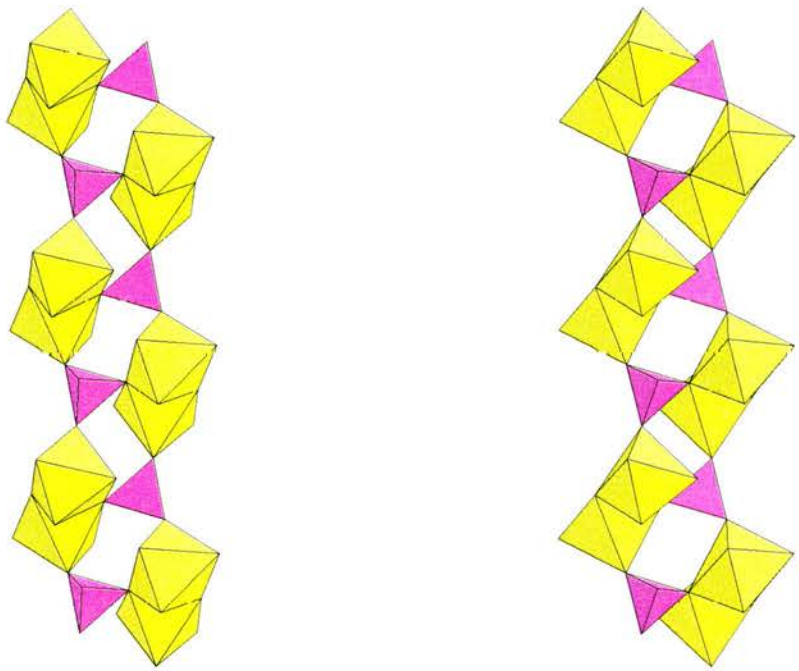

(a) (b)

Figure 4.21 Manganese phosphate chain in MnPOX-5 (a) and MnPOX-6 (b) constructed from edge-sharing MnO_6 octahedra, which share corners with PO_4 tetrahedra. Only one position of disordered oxygen O(5) shown in (b).

These chains are linked in both the *a* and *c* directions by oxalate anions to form a 3D network, illustrated in Figures 4.22(a) and 4.23(a). As seen in Figure 4.23, channels are created in the *a* direction, where diprotonated ethylenediamine cations and water molecules reside.

Interestingly this structure contains two different types of water; $H_2O(5)$ is a ligand on Mn(1), whilst $H_2O(12)$ is uncoordinated, residing in the channel space.

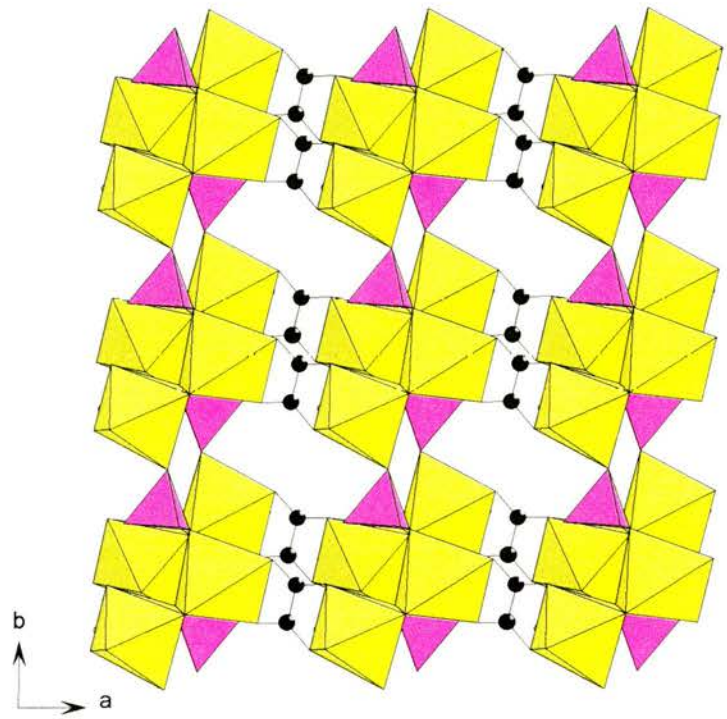

(a)

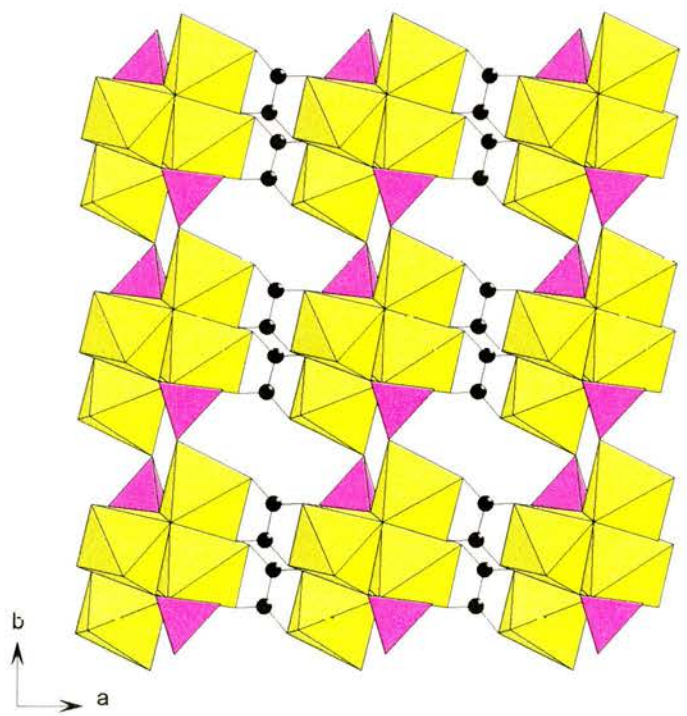

(b)

Figure 4.22 *ab* projections of MnPOX-5 (a) and MnPOX-6 (b) showing the oxalate anions linking chains in the *a* direction. Only one position of disordered oxygen shown in (b).

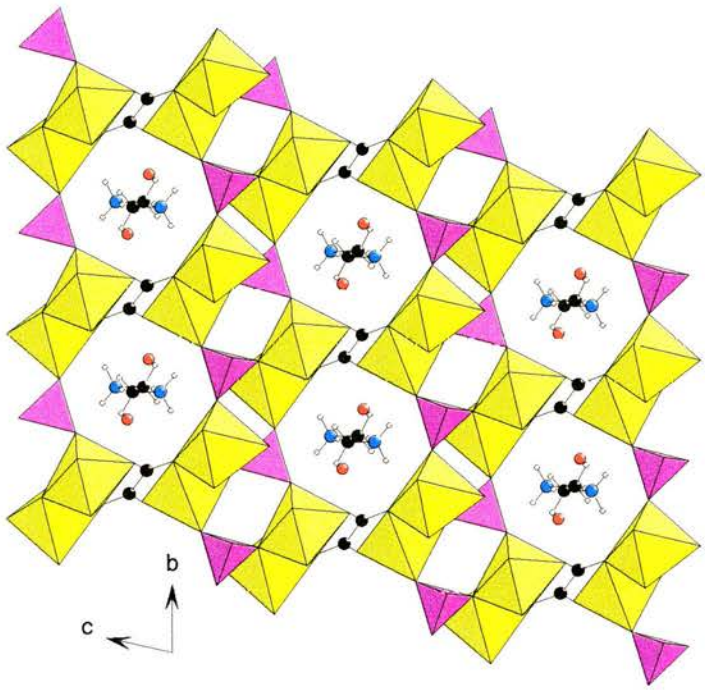

(a)

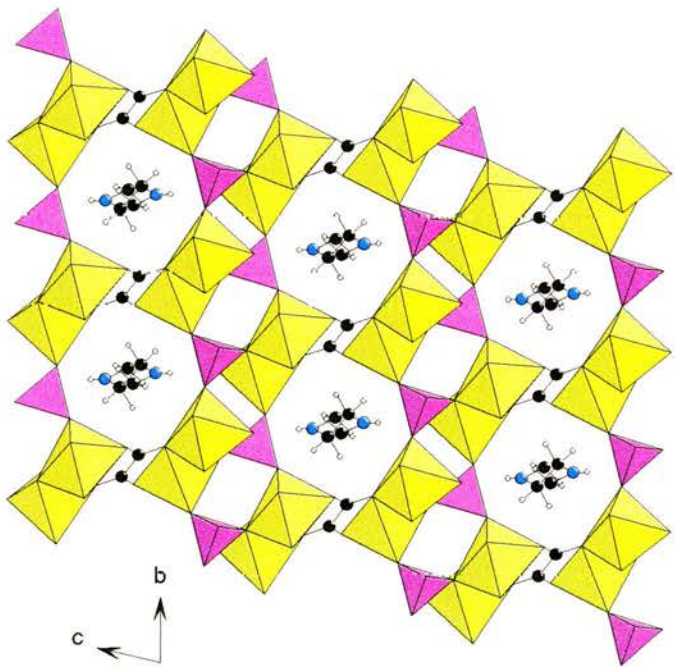

(b)

Figure 4.23 *bc* projection of MnPOX-5 (a) and MnPOX-6 (b), with oxalate linking chains in the *c* direction. Colours as before, O (water) red. Only one position of disordered oxygen and amine shown in (b).

$[Mn_4(HPO_4)_2(C_2O_4)_3(H_2O)_2](H_2O)_2(C_4H_8(NH_2)_2)$ (MnPOX-6)

MnPOX-6 is very similar to MnPOX-5, but contains piperazine cations in place of the ethylenediamine. The building unit is shown in Figure 4.24; atomic co-ordinates, bond lengths and angles are in Appendix 6.

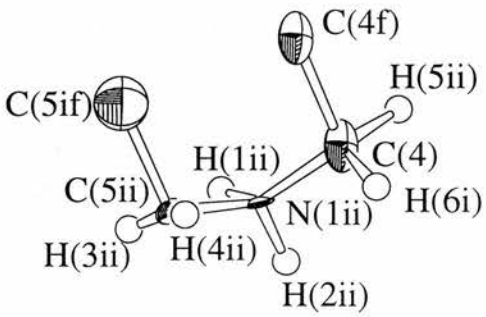

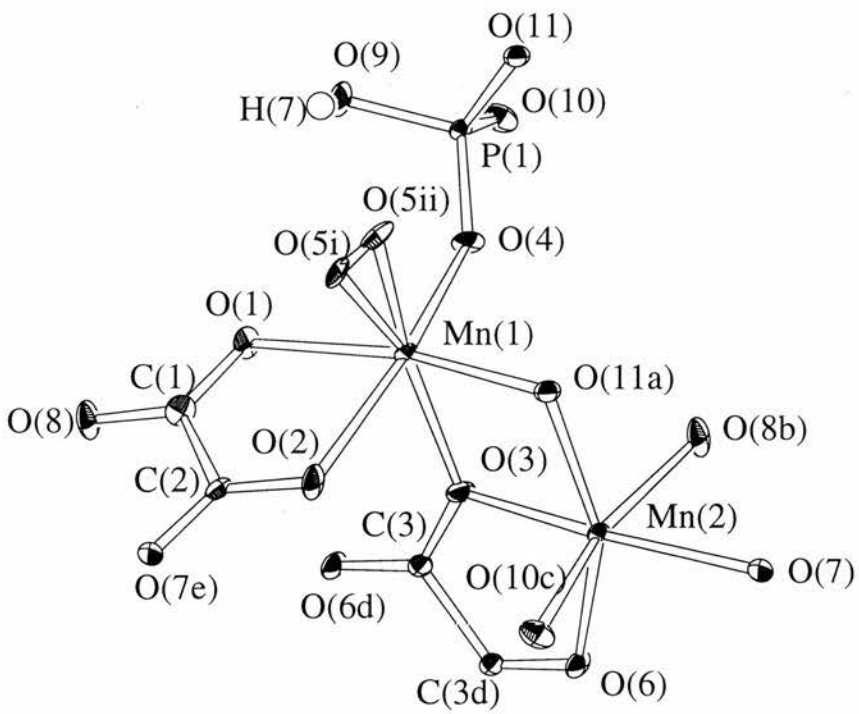

Figure 4.24 Building unit of MnPOX-6, with ellipsoids at 50 % probability. The piperazine template is disordered over two positions, only one position is illustrated here. Symmetry labels: a, 2-*x*, -*y*-1, 1-*z*; b, *x*-1, *y*, *z*; c, *x*, *y*-1, *z*; d, 2-*x*, -*y*-2, 2-*z*; e, *x*+1, *y*, *z*; f, 1-*x*, 1-*y*, -*z*.

Figures 4.22(b) and 4.23(b) show *ab* and *bc* projections, illustrating the similarity between MnPOX-5 and -6.

An iron-containing material, $[Fe_4(HPO_4)_2(C_2O_4)_3](N_2C_4H_{12})$, which is similar to MnPOX-5 and -6 was reported simultaneously by the groups of Rao[8] and Lii[9]. This contains piperazine, and no water molecules either in the channels or as ligands, resulting in a five co-ordinate Fe atom.

Recently Lii and co-workers have synthesised other iron materials with the same connectivity containing a chiral amine, *S*-2-methylpiperazine.[10] A racemic mix of 2-methylpiperazine produced $[Fe_4(HPO_4)_2(C_2O_4)_3(H_2O)_2](S\text{-}C_5H_{14}N_2)$ as a minor product, which is obtained as the major product if *S*-2-methylpiperazine is used, when a small amount of $[Fe_4(HPO_4)_2(C_2O_4)_3](S\text{-}C_5H_{14}N_2)$ is also produced. The two structures differ only in the water ligand on the iron centres, which is absent in the latter material as in $[Fe_4(HPO_4)_2(C_2O_4)_3](N_2C_4H_{12})$ above. $[Fe_4(HPO_4)_2(C_2O_4)_3](S\text{-}C_5H_{14}N_2)$ can also be formed containing disordered *R* and *S* enantiomers, however only the *S* enantiomer formed the hydrated material $[Fe_4(HPO_4)_2(C_2O_4)_3(H_2O)_2](S\text{-}C_5H_{14}N_2)$.

In addition an isomorphous cobalt phosphate oxalate, $[Co_4(HPO_4)_2(C_2O_4)_3](C_4N_2H_{12})$, has been synthesised.[11] Once again piperazine was used as the structure directing amine. In common with the iron structures discussed above, no water ligands are found in the structure, so cobalt exists in both five- and six-fold co-ordination. A comparison of structural parameters in these frameworks is given in Table 4.6.

The three structures with lower (triclinic) symmetry are those that have all metals in octahedral co-ordination, with water as a ligand on one of the metal centres. Those materials where a five co-ordinate metal is present are monoclinic. Given that the hydrothermal reactions used to synthesise these structures contain water far in excess of the other reagents it is not clear why the manganese structures reported here, and one iron structure, should contain more water than the other materials. Piperazine (and with a methyl substituent) is clearly an efficient structure directing agent for this type of structure. The exception is MnPOX-5,

which was formed from ethylenediamine, however the same synthesis conditions also formed MnPOX-2. MnPOX-2 appeared to be the favoured product for reactions of 24 hours, while after 48 hours more MnPOX-5 was formed, perhaps suggesting that MnPOX-5 is the more thermodynamically stable of the two.

Table 4.6 Comparison of structural and magnetic parameters in MnPOX-5, -6, -7 and related phases.

Material	Structure directing amine	Space group	Unit cell parameters						Magnetic parameters	
			a (Å)	b (Å)	c (Å)	α (°)	β (°)	γ (°)	θ (K)	T_N (K)
MnPOX-5	ethylenediamine	$P\bar{1}$	7.830(4)	8.041(4)	9.652(7)	76.2995)	78.47(6)	86.36(6)	-19.3	10
MnPOX-6	piperazine	$P\bar{1}$	7.7679(6)	8.0674(6)	9.6972(7)	76.075(2)	78.784(2)	86.883(2)	-	-
MnPOX-7*	ethylenediamine	mono	7.8934(9)	7.8730(8)	17.048(2)		94.63(1)		-21.8	11
$[Fe_4(HPO_4)_2(C_2O_4)_3](C_4H_{12}N_2)$[8]	piperazine	$P2_1/c$	7.569(2)	7.821(2)	18.033(4)		98.8(1)		-ve	~20
$[Fe_4(HPO_4)_2(C_2O_4)_3](C_4H_{12}N_2)$[9]	piperazine	$P2_1/c$	7.5573(4)	7.8188(4)	18.0421(9)		98.710(1)		-	-
$[Fe_4(HPO_4)_2(C_2O_4)_3(H_2O)_2](S\text{-}C_5H_{14}N_2)$[10]	*S*-2-methylpiperazine	$P1$	7.6999(4)	7.9542(4)	9.8262(5)	74.8444(7)	81.7716(8)	85.4075(8)	-	-
$[Fe_4(HPO_4)_2(C_2O_4)_3](S\text{-}C_5H_{14}N_2)$[10]	*S*-2-methylpiperazine	$P2_1$	7.5943	7.8172	18.318(2)		99.111(2)		-	-
$[Co_4(HPO_4)_2(C_2O_4)_3](C_4H_{12}N_2)$[11]	piperazine	$P2_1/c$	7.494(1)	7.726(1)	17.852(3)		97.7(1)		-35	25

*Cell parameters from Rietveld refinement.

4.4.2.2 Thermogravimetric Analysis and Dehydration

$[Mn_4(HPO_4)_2(C_2O_4)_3(H_2O)_2](H_2O)_2(H_3N(CH_2)_2NH_3)$ (MnPOX-5)

Heated under O_2, MnPOX-5 undergoes an endothermic loss between 150 °C and 200 °C of 7.74 % (see Figure 4.25). Above 300 °C, two further losses occur, of 27.66 and 2.35 %, both exothermic. The final product at 600 °C is largely amorphous, possibly containing Mn_2O_3 (JCPDS 24-508). The N_2 and O_2 plots again follow a similar path, the N_2 being a more simple two step process, both endothermic. The total losses at 600 °C are 42.68 % (O_2) and 40.25 % (N_2). The final product after heating with N_2 is thought to be $Mn_3(PO_4)_2$ (JCPDS 33-901). For MnPOX-5, loss of $3C_2O_4$, $4H_2O$ and $H_2N(CH_2)_2NH_2$ is 48.92 %.

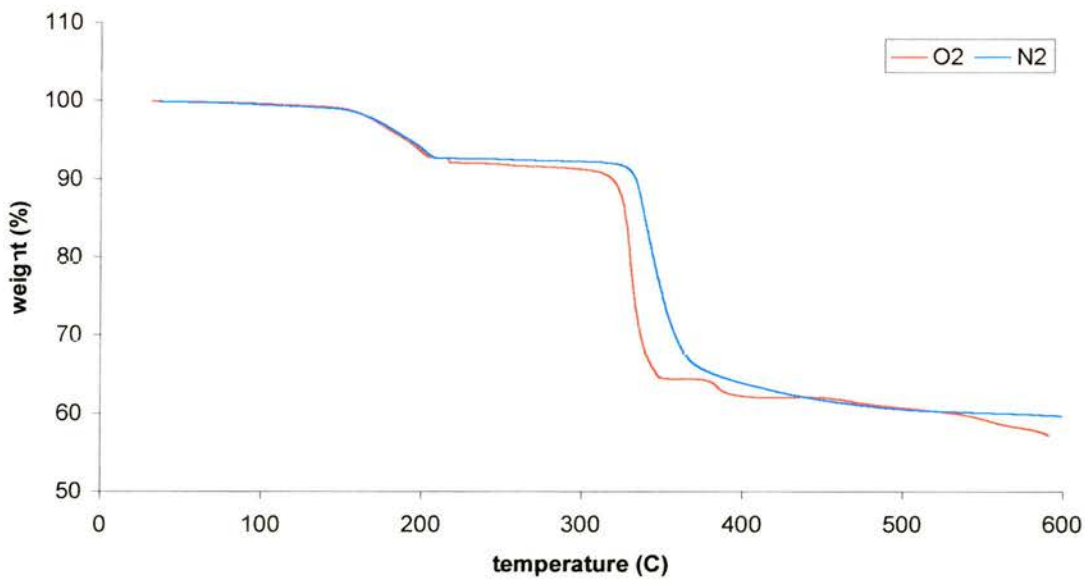

Figure 4.25 TGA of MnPOX-5

A sample heated to 225 °C (under O_2) and exposed to air when cool gave a new phase, MnPOX-7. This is believed to be a dehydration product involving the loss of the water ligand on one MnO_6 octahedron (calc. $2H_2O$ 4.45 %, $4H_2O$ 8.90 %, measured 7.74 %), resulting in a five co-ordinate manganese, as seen in similar phases discussed above. Indexing a powder pattern of MnPOX-7 using

the Visser algorithm gave a monoclinic cell of a = 7.906 Å, b = 7.881 Å, c = 17.071 Å and β = 94.52 °. This compares with values of 7.569(2) Å, 7.821(2) Å, 18.033(4) Å and 98.8(1) ° for $[Fe_4(HPO_4)_2(C_2O_4)_3](N_2C_4H_{12})$ in space group $P2_1/c$. Rietveld refinement of MnPOX-7 was attempted using $[Fe_4(HPO_4)_2(C_2O_4)_3](N_2C_4H_{12})$[8] as a starting model.[12] Refinement of lattice parameters, zero point and peak shape gave initially promising results. However when restrained refinement on P-O, C-O and Mn-O lengths and O-P-O and O-C-O angles were applied the results were unsatisfactory, illustrated by the bond lengths given in Table 4.7. Final values of *Rwp* and *Rp* were 0.1740 and 0.1389 respectively. No amine is included in the refinement, as MnPOX-7 contains ethylenediamine while $[Fe_4(HPO_4)_2(C_2O_4)_3](N_2C_4H_{12})$ is synthesised using piperazine. A Rietveld plot is shown in Figure 4.26.

Table 4.7 Selected bond lengths from Rietveld refinement of MnPOX-7

atom	atom	distance (Å)	atom	atom	distance (Å)
Mn(1)	O(4)	1.89(4)	P(3)	O(10)	1.44(4)
Mn(1)	O(5)	2.04(4)	P(3)	O(13)	1.80(4)
Mn(1)	O(7)	2.49(4)	C(14)	O(5)	1.31(5)
Mn(1)	O(8)	1.69(4)	C(14)	O(11)	1.05(5)
Mn(1)	O(9)	2.39(4)	C(14)	C(15)	1.86(5)
Mn(1)	C(16)	2.25(5)	C(15)	O(9)	1.44(5)
Mn(2)	O(9)	2.48(5)	C(15)	O(11)	2.14(5)
Mn(2)	O(11)	2.46(4)	C(15)	O(12)	1.46(5)
Mn(2)	O(12)	2.18(4)	C(15)	C(14)	1.86(5)
Mn(2)	O(13)	2.40(5)	C(16)	O(6)	1.29(5)
P(3)	O(4)	1.58(4)	C(16)	O(8)	1.43(5)
P(3)	O(7)	1.56(4)	C(16)	C(16)	1.63(6)

The problems encountered are thought to be due to preferred orientation. It is also possible that the preliminary model is incorrect, although this seems unlikely on the basis of the starting material (MnPOX-5) and the loss of water seen in the TGA experiment.

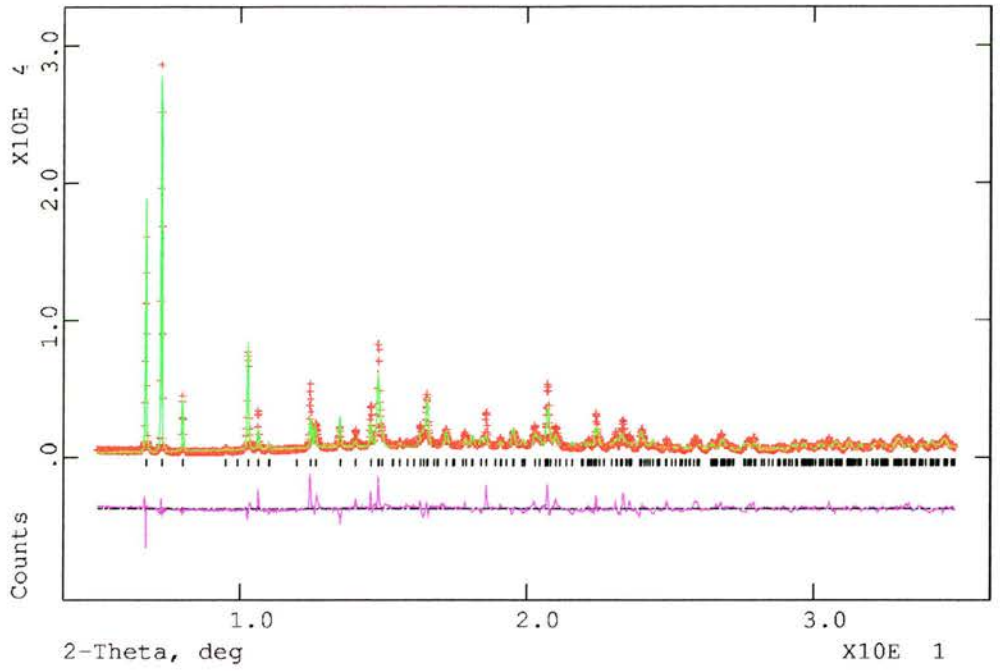

Figure 4.26 Rietveld plot of MnPOX-7. Observed data red, calculated profile green, difference profile purple.

4.4.2.3 Magnetic Measurements

$[Mn_4(HPO_4)_2(C_2O_4)_3(H_2O)_2](H_2O)_2(H_3N(CH_2)_2NH_3)$(MnPOX-5)

Susceptibility behaviour with temperature for MnPOX-5 is illustrated in Figure 4.27. Above 60 K the material shows Curie-Weiss behaviour with θ = -19.3 K and C = 4.28 emu K mol^{-1}, indicating antiferromagnetic ordering at lower temperatures. The susceptibility maximum of 0.121 emu mol^{-1} occurs at 9.96 K. A plot of effective moment with temperature is shown in Figure 4.28, again showing expected behaviour for a high spin d^5 species.

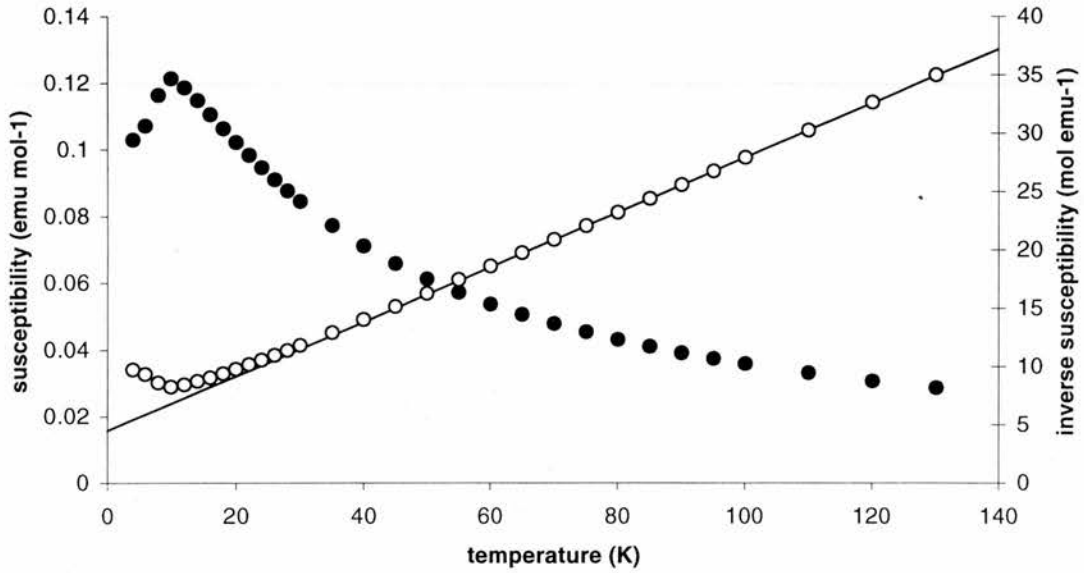

Figure 4.27 Magnetic susceptibility (closed circles) and inverse susceptibility (open circles) of MnPOX-5. The solid line shows the fit to the Curie-Weiss law above 60 K.

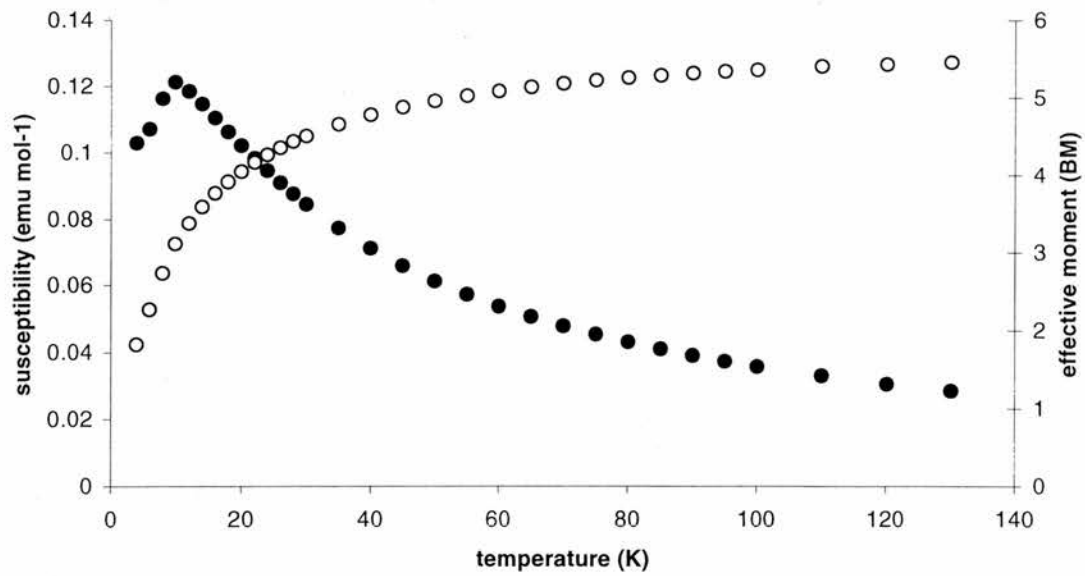

Figure 4.28 Susceptibility (open circles) and effective moment (closed circles) in MnPOX-5

MnPOX-7

Calculations were carried out on MnPOX-7 assuming the formula $[Mn_4(HPO_4)_2(C_2O_4)_3](H_3N(CH_2)_2NH_3)$, *i.e.* loss of both channel and ligand water from the structure. Variation of susceptibility with temperature is shown in Figure 4.29.

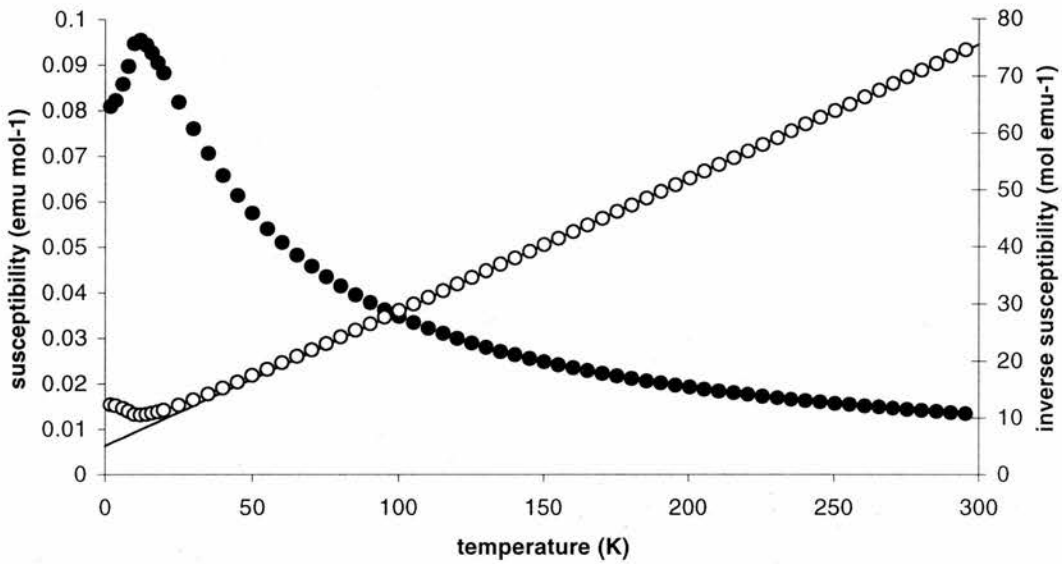

Figure 4.29 Magnetic susceptibility (closed circles) and inverse susceptibility (open circles) of MnPOX-7. The solid line shows the fit to the Curie-Weiss law above 100 K.

The maximum susceptibility (0.0954 emu mol^{-1}) occurs at 11 K. The sample shows Curie-Weiss behaviour at higher temperatures, with θ = -21.8 K and C = 4.26 emu K mol^{-1} obtained from a fit to the Curie-Weiss law with data above 100 K. Again, the plot of effective moment against temperature (Figure 4.30) shows expected behaviour for Mn^{2+}.

Although edge-sharing octahedra are present in MnPOX-5,-6 and -7, they are not directly linked to other manganese species, *i.e.* there is no continuous Mn-O-Mn bonding, so magnetic exchange must occur through phosphate and/or oxalate. Magnetic parameters that have been reported from related structures are given in Table 4.6. The iron and cobalt containing structures also demonstrate

antiferromagnetic ordering, with slightly higher ordering temperatures than for the manganese structures reported here. Measurements on $[Fe_4(HPO_4)_2(C_2O_4)_3](C_4H_{12}N_2)$ suggest that Fe^{2+} exists in an intermediate spin state $t_{2g}^5e_g^1$.[8]

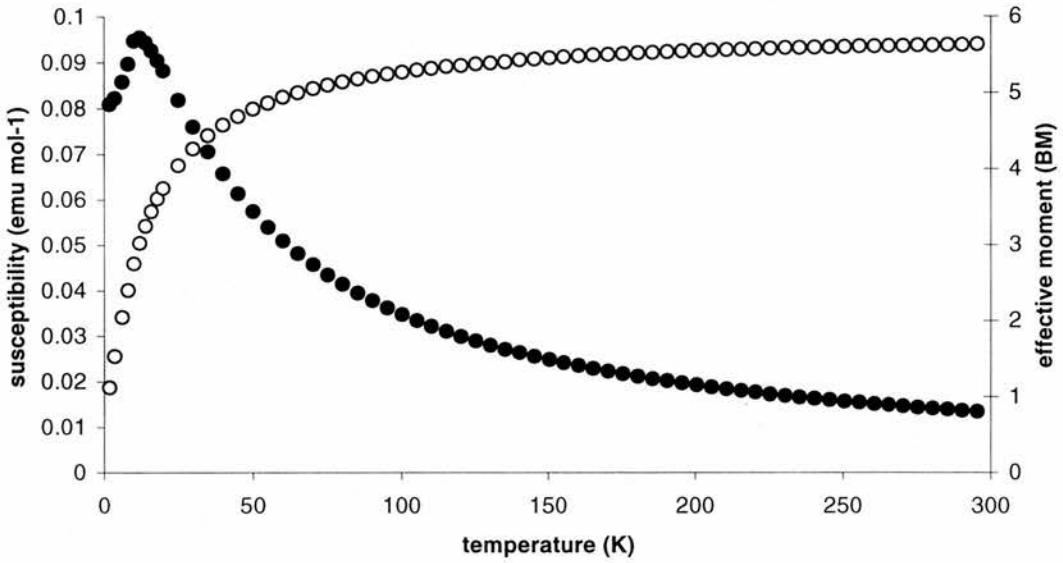

Figure 4.30 Magnetic susceptibility (closed circles) and effective moment (open circles) of MnPOX-7.

4.5 Conclusions

Two different anions, phosphate and oxalate, have been successfully incorporated into seven new materials, with three different framework topologies. MnPOX-1 is 3D, constructed from manganese phosphate layers with continuous Mn-O-Mn linkages, pillared by oxalate anions. The material shows antiferromagnetic ordering at around 15 K, with a broad susceptibility maximum that has been observed in 2D antiferromagnetic systems. MnPOX-2, -3 and -4 are also 3D phosphate oxalates, in addition they contain structure directing amines (ethylenediamine, 1,3-diaminopropane and *trans*-1,4-diaminocycloheaxne respectively). Again the structures can be described as metal phosphate layers with oxalate pillars. Although the overall connectivity of the three structures are the same, subtle differences were observed in co-

ordination geometries. Although variation of the structure directing amine resulted in these small structural differences, an isomorphous iron containing framework has been reported in the literature which contains extra-framework water molecules only.[7] MnPOX-3 and -4 both showed antiferromagnetic ordering at 7 K.

Using the same synthesis condition as MnPOX-2,-3 and -4, MnPOX-5 and -6 were formed. MnPOX-2 and -5 were both produced using the same amine (ethylenediamine), with MnPOX-2 the major phase after 24 hours and MnPOX-5 after 48 hours. Piperazine, which was incorporated into MnPOX-6, has also been used to synthesise similar frameworks containing iron[8,9,10] and cobalt[11]. Loss of water from MnPOX-5 after heating to 200 °C formed a new phase MnPOX-7. The removal of ligand water molecules gives MnPOX-7 a five co-ordinate manganese centre. Both MnPOX-5 and -7 show antiferromagnetic ordering at 10 and 11 K respectively, with very similar θ values (-19.3 and -21.8 K).

4.6 References

1. A. Altomare, M. C. Burla, M. Camalli, M. Cascarano, C. Giacovazzo, A. Gugliardi and G. Polidori, *J. Appl. Crystallogr.*, 1993, **26**, 343.

2. TEXSAN, Crystal Structure Analysis Package, Molecular Structure Corporation, Houston, TX, 1992.

3. I. D. Brown and D. Altermatt, *Acta Crystallogr., Sect. B: Struct. Sci.*, 1985, **41**, 244.

4. J. Le Bideau, C. Payen, B. Bujoli, P. Palvadeau and J. Rouxel, *J. Magn. Magn. Mater.*, 1995, **140**, 1719.

5. C. Mathonière, C. J. Nuttall, S. G. Carling and P. Day, *Inorg. Chem.*, 1996, **35**, 1201.

6. F. E. Mabbs and D. J. Machin, *Magnetism and Transition Metal Complexes*, Chapman and Hall, London, 1973, 5.

7. A. Choudhury, S. Natarajan and C. N. R. Rao, *Chem. Eur, J.*, 2000, **6**, 1168.

8. A. Choudhury, S. Natarajan and C. N. R. Rao, *J. Solid State Chem.*, 1999, **146**, 538.

9. H.-M. Lin, K.-H. Lii, Y.-C. Jiang and S.-L. Wang, *Chem. Mater.*, 1999, **11**, 519.

10. W.-J. Chang, H.-M. Lin and K.-H. Lii, *J. Solid State Chem.*, 2001, **157**, 233.

11. A. Choudhury and S. Natarajan, *Solid State Sciences*, 2000, **2**, 365.

12. General Structure Analysis System (GSAS), A. C. Larson and R. B. Von Dreele, Los Alamos National Laboratory Report LAUR 86-748, 2000.

CHAPTER 5 – LOW WATER CONTENT EXPERIMENTS

5.1 Introduction

The molar ratio of water to the other reactants in the majority of the experiments described here is of the order of 100:1. This chapter describes a series of experiments where the water was in reactant, rather than solvent quantities. As this adds another variable to the many already present in hydrothermal synthesis, a phase-composition diagram was used to provide a systematic approach to the reactions, in both iron and manganese systems. A new manganese phosphate oxalate, MnPOX-8, was synthesised in this way, which displays interesting magnetic properties.

5.2 Experimental

5.2.1 Synthesis

The phase-composition diagram illustrated in Figure 5.1 was used to formulate 12 experiments with water in reactant quantities, with M = Mn and Fe.

In all experiments, numbers x on the phase diagram were equivalent to $2x$ mmol in the reaction. The reactants were added directly to a Teflon-lined stainless steel autoclave, and heated in an oven at 160 °C for 48 hours. After cooling the autoclaves in air, the contents were filtered and washed with distilled water, then air-dried.

The following diagrams (Figure 5.2 and 5.3) show the identity of the materials synthesised at each experimental point. Three different materials were formed in the manganese system: $MnC_2O_4.2H_2O$, $MnC_2O_4.3H_2O$, and a new phosphate oxalate, $Mn_2(H_2PO_4)_2(C_2O_4)$ (MnPOX-8). As can be seen from the diagrams,

most experiments produced a mixture of two of these materials. The iron system also produced three substances: $FeC_2O_4.2H_2O$ (iron analogue of manganese dihydrate above), $Fe^{2+}Fe^{3+}{}_2(HPO_4)_4(H_2O)_4$[1] and an unknown material which was formed along with the iron oxalate. Identification of this substance has not proved possible. In both systems no solid product was formed in reactions 9 and 10, both of which had a high concentration of phosphoric acid.

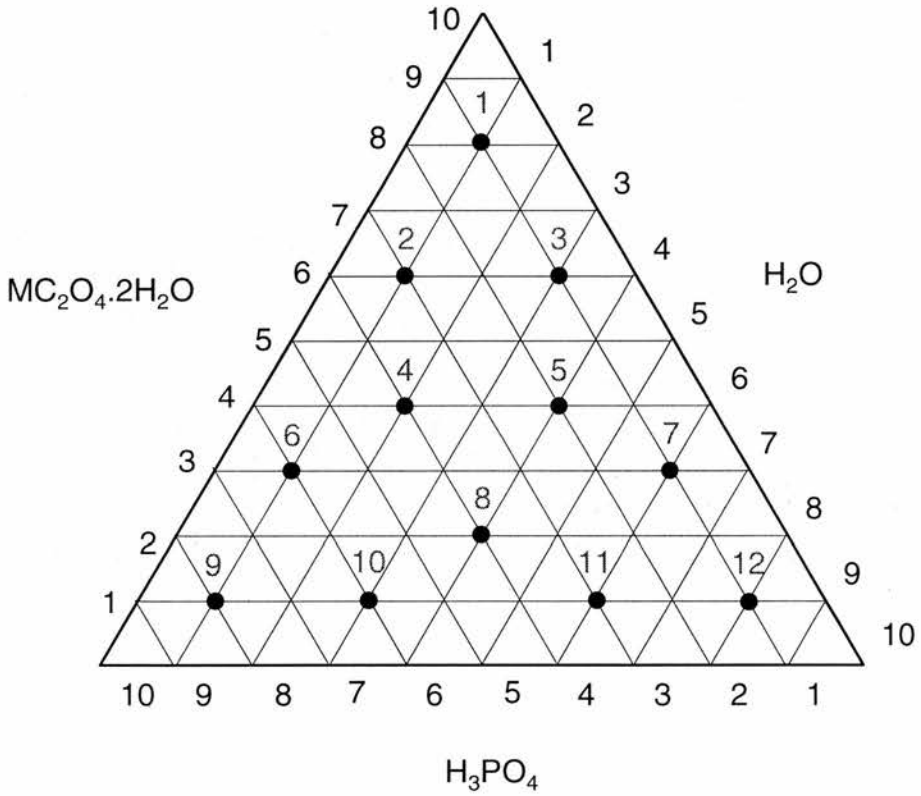

Figure 5.1 Phase-composition diagram showing positions of the 12 experiments

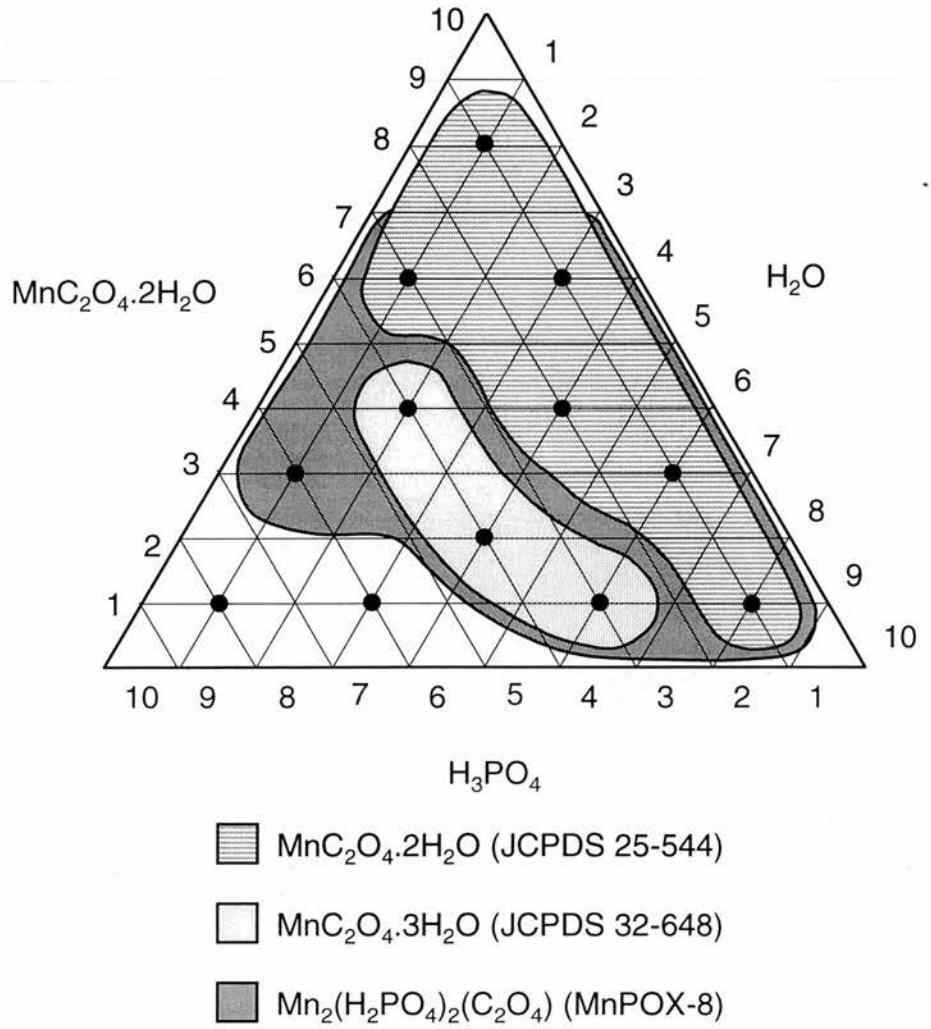

Figure 5.2 Results of manganese experiments, showing identity of the products formed.

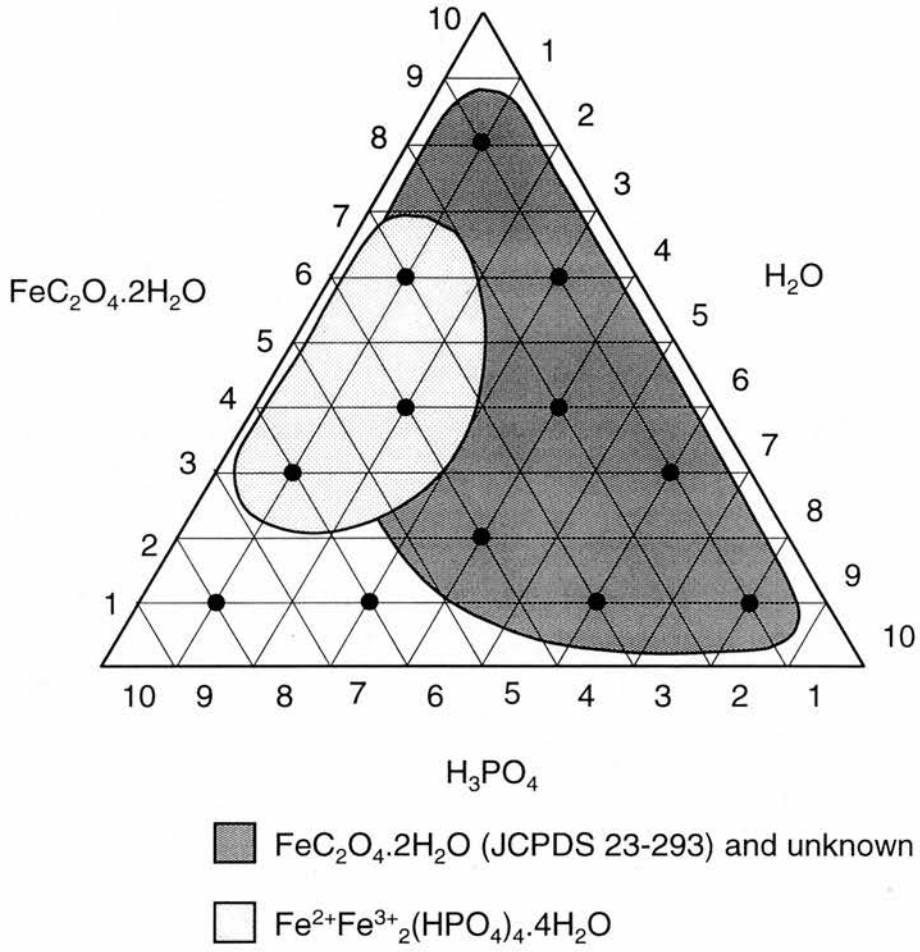

Figure 5.3 Diagram showing results of the iron experiments

5.2.2 Characterisation

X-ray powder diffraction data was collected on a Philips diffractometer with CuK_α radiation and was used to identify many of the samples. The iron sample $Fe^{2+}Fe^{3+}{}_2(HPO_4)_4.4H_2O$ was identified by single crystal diffraction at station 9.8, Daresbury laboratory. Single crystal diffraction data for MnPOX-8 was collected at room temperature on a Bruker SMART diffractometer with CCD detector and MoK_α radiation. Structure solution and refinement were carried out using SHELXS-86[2] and SHELXL-97[3]. Crystallographic details are given in Table 5.1.

Table 5.1 Crystal data and details of structure solution and refinement for MnPOX-8.

	MnPOX-8
Formula	$Mn_2(H_2PO_4)_2(C_2O_4)$
Formula weight	391.87
Crystal system	Monoclinic
Space group	C2/*m*
a (Å)	6.045(2)
b (Å)	15.064(4)
c (Å)	5.511(1)
β (°)	112.151(4)
Volume (Å^3)	464.9(2)
Z	2
μ(MoK_α) (cm^{-1})	3.130
Total reflections	348
Observed reflections ($I>2\sigma(I)$)	337
R_1, *wR2*	0.0232, 0.0606

Magnetisation measurements were obtained on a 0.1352 g polycrystalline sample of MnPOX-8 loaded into a gelatine capsule using a Quantum Design $MPMS_2$ SQUID magnetometer. A field of 100 Oe was applied between 1.7 and 300 K. The data were corrected for the diamagnetic contribution of the sample holder and constituent elements.[4]

5.3 Discussion

5.3.1 Manganese System: MnPOX-8

5.3.1.1 Structure

MnPOX-8 is a 3D framework constructed from MnO_6 octahedra, PO_4 tetrahedra and oxalate units. The building unit is shown in Figure 5.4; bond lengths, angles and co-ordinates are given in Appendix 7.

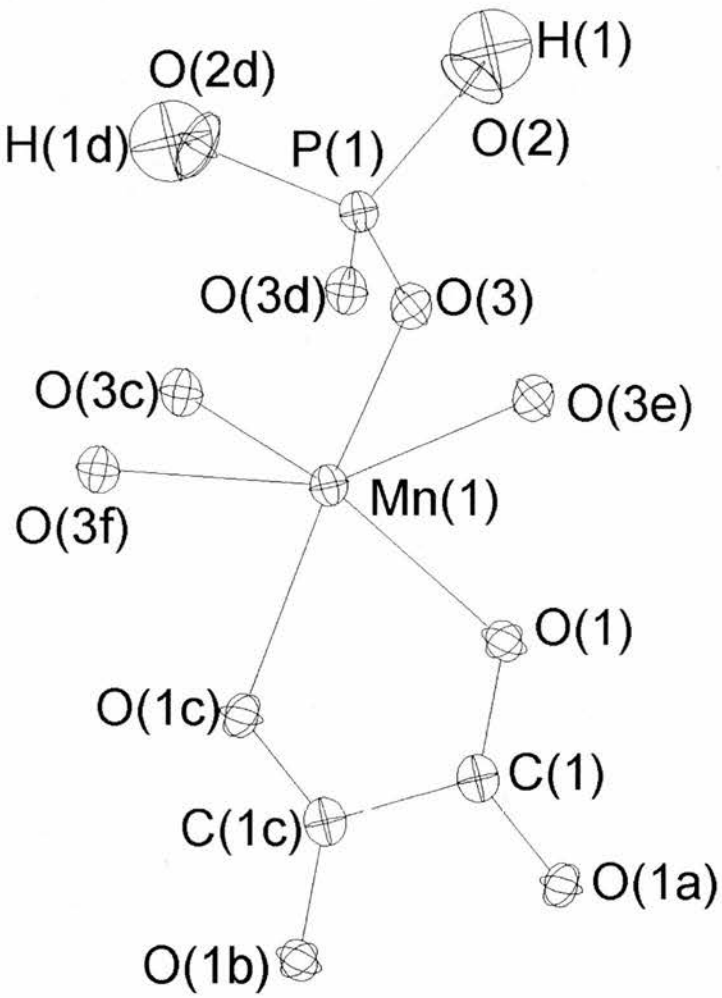

Figure 5.4 Building unit of MnPOX-8 showing the atom labelling scheme. Symmetry labels: a, *x*, -*y*, *z*; b, -*x*, -*y*, 1-*z*; c, -*x*, *y*, 1-*z*; d, -*x*, *y*, -*z*; e 1/2-*x*, 1/2-*y*, 1-*z*, f, *x*, -1/2+*x*, 1/2-*y*, *z*.

Manganese is confirmed as 2+ by bond valence calculations (sum = 1.91)[5] and exists in distorted octahedral co-ordination, as before the bisbidentate co-ordination mode of the oxalate anions results in a small O-Mn-O angle (73.98(9)°). The manganese octahedra share *cis*-edges, illustrated in Figure 5.5, to form zigzag shaped chains along the *a* axis.

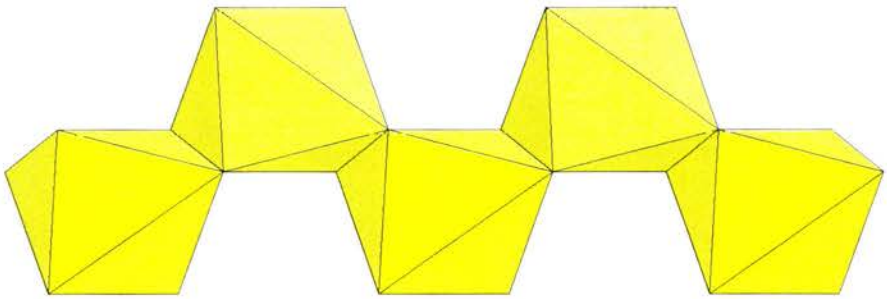

Figure 5.5 Chain of MnO_6 octahedra running along the *a* direction in MnPOX-8

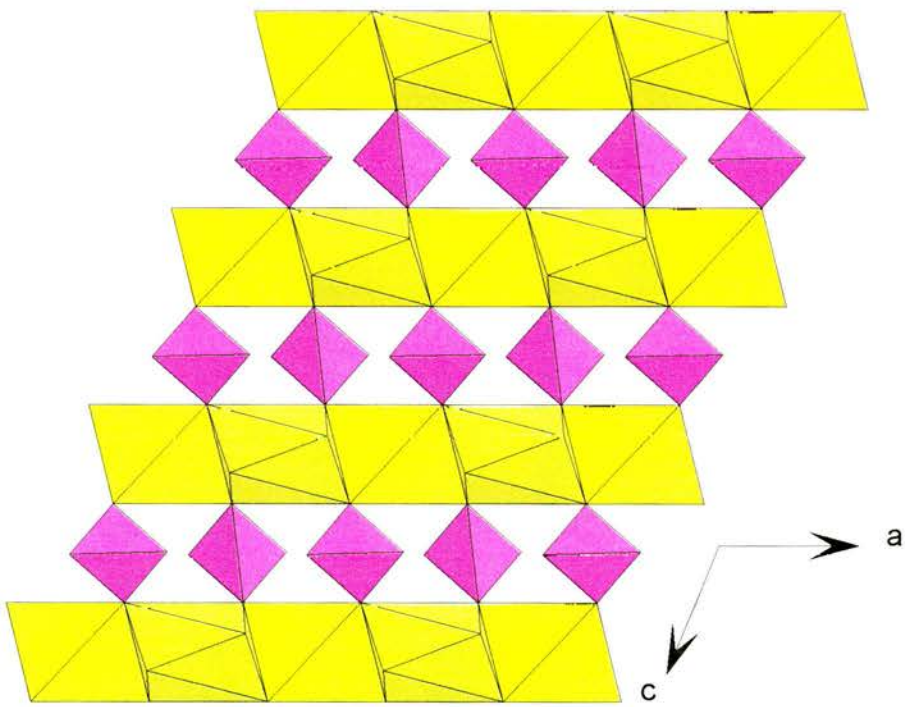

Figure 5.6 Manganese phosphate layer in MnPOX-8

The chains are linked to one another *via* corner sharing H_2PO_4 tetrahedra; the presence of hydrogen on O(2) is confirmed by its bond valence sum of 1.19. This leads to the formation of layers in the *ac* plane, with the tetrahedra pointing alternately up/down. (Figure 5.6).

The *bc* and *ab* plots (Figures 5.7 and 5.8) both show how the bisbidentate co-ordination of oxalate anions, once again acting as pillars, form the 3D structure.

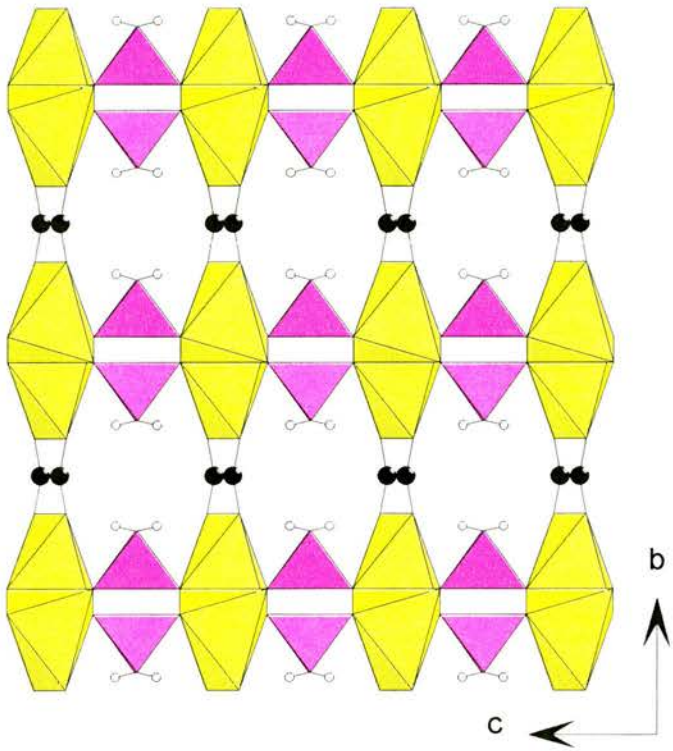

Figure 5.7 *bc* plot of MnPOX-8

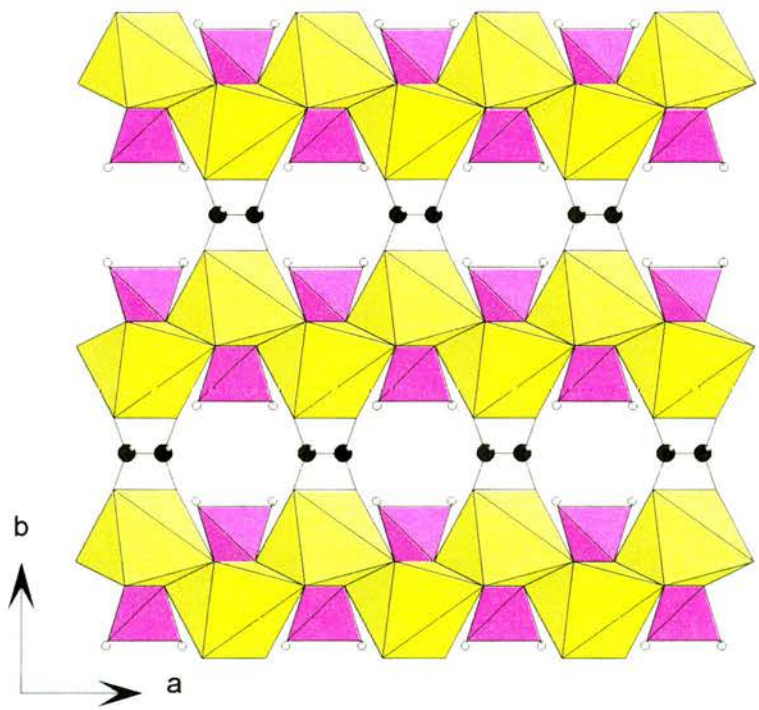

Figure 5.8 *ac* plot of MnPOX-8

5.3.1.2 Magnetism

The zero field-cooled and field-cooled data were identical for MnPOX-8. A plot of susceptibility and inverse susceptibility against temperature is shown in Figure 5.9.

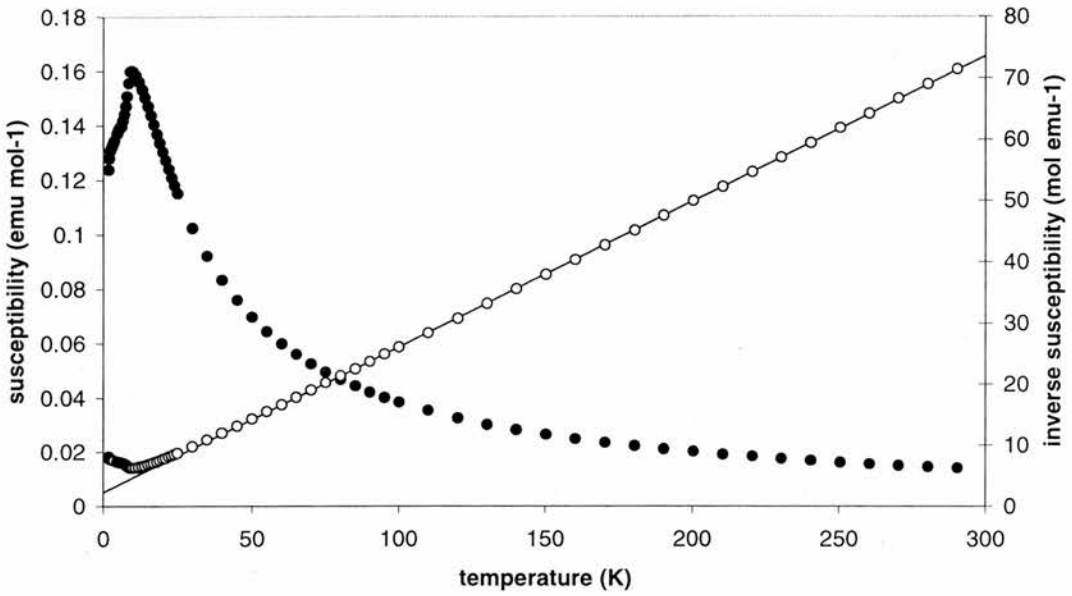

Figure 5.9 Magnetic susceptibility (closed circles) and inverse susceptibility (open circles) of MnPOX-8. The solid line shows the fit to the Curie-Weiss law above 50 K.

Curie-Weiss behaviour is seen above 50 K, with a θ value of -9.79 K indicating predominantly antiferromagnetic interactions. The susceptibility reaches a maximum of 0.16 emu mol^{-1} at 9.54 K. A plot of effective moment against temperature is shown in Figure 5.10, with the moment reaching around 5.7 μ_B (close to its expected spin only value) near room temperature.

MnPOX-8 shows interesting behaviour at temperatures below the susceptibility maximum, illustrated in Figure 5.11.

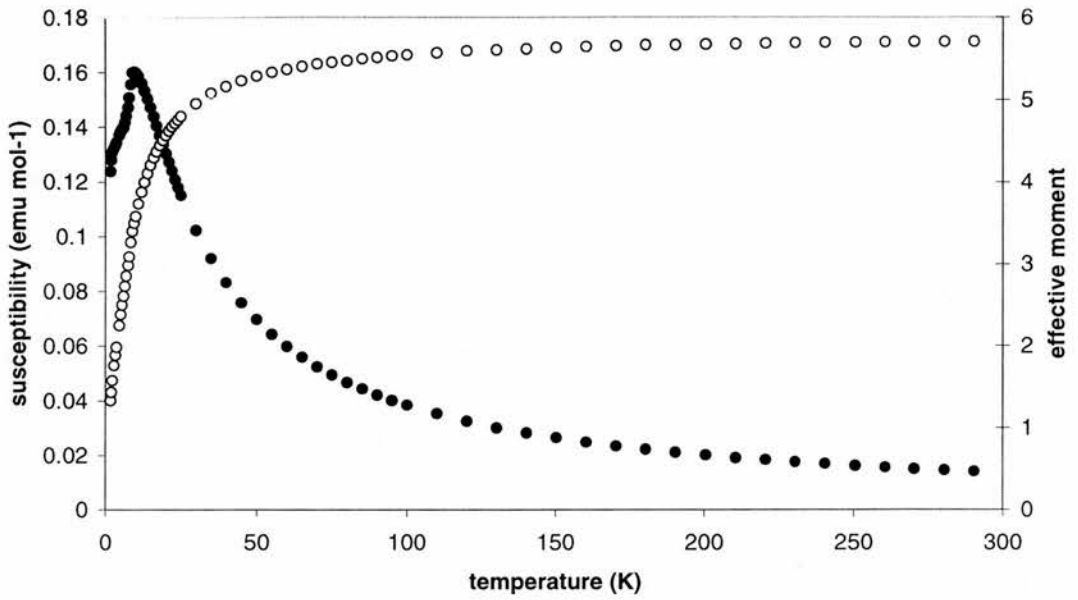

Figure 5.10 Magnetic susceptibility (closed circles) and effective moment (open circles) of MnPOX-8.

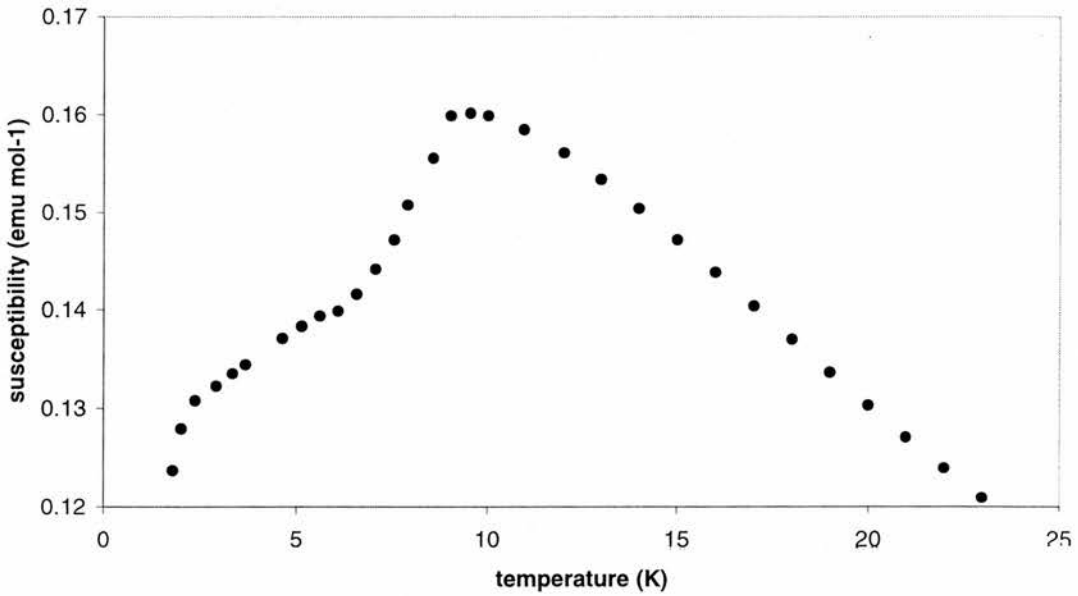

Figure 5.11 Magnetic susceptibility of MnPOX-8 in the range 1.8 – 25 K showing the shape of the curve below the susceptibility maximum.

This behaviour suggests that more than one type of ordering is taking place; possibly through the edge-sharing manganese octahedra, and also between manganese atoms connected by a phosphate or an oxalate group. Susceptibility

measurements on a single crystal of MnPOX-8 of sufficient size would enable the behaviour to be examined along the axes of the crystal and elucidate this ordering. It is also possible that the shape of the susceptibility peak is due to an impurity, however the sample appeared to be pure by x-ray powder diffraction. Single crystal measurements would also ensure a pure sample was under examination. To further investigate the ordering behaviour of MnPOX-8 it would be interesting to synthesise analogous structures with different anions. It can be envisaged that phosphate may be replaced by sulphate or arsenate, or oxalate by a larger ligand capable of the same co-ordination mode, but retaining the structure of the layers. In addition, replacing a small (5 - 10 %) amount of manganese by a diamagnetic cation, *e.g.* magnesium or zinc, but again retaining the structure, may reveal further details about the magnetic ordering.

MnPOX-8 is the only phosphate oxalate with a continuous array of edge-sharing metal-oxygen polyhedra. Edge-sharing dimers linked by corner sharing metal polyhedra through M-O-M linkages exist in MnPOX-1 and $[Fe_2(PO_4)(C_2O_4)_{0.5}(H_2O)]$[6]. MnPOX-1, which is antiferromagnetic with a θ value of -39.7 K, also showed interesting magnetic behaviour, with a rounded susceptibility maximum, indicative of 2D ordering (see section 4.2.2.3). $[Fe_2(PO_4)(C_2O_4)_{0.5}(H_2O)]$ displays Curie-Weiss behaviour, with a θ value of -35.4 K indicating antiferromagnetic interactions.

MnPOX-5 and -6, $[Fe_2(HPO_4)(C_2O_4)_{1.5}](N_2C_4H_{12})_{0.5}$,[6] and $[Co_2(HPO_4)(C_2O_4)_{1.5}](C_4N_2H_{12})_{0.5}$[7] all have edge-sharing dimers which are connected by corner-sharing phosphate tetrahedra. All order antiferromagnetically, with susceptibility maxima ranging between 9 and 40 K. Of these, $[Fe_2(HPO_4)(C_2O_4)_{1.5}](N_2C_4H_{12})_{0.5}$ shows the more interesting magnetic behaviour, with magnetic moment of $3.2\mu_B$ at temperatures above 150 K, consistent with intermediate spin Fe^{2+}, *i.e.* $t_{2g}^5 e_g^1$.

The *cis*-edge-sharing chain of octahedra present in this structure is discussed by Moore[8] and Hawthorne,[9] and is present in the mineral foggite, $Ca[CaAl_2(OH)_4(PO_4)_2](H_2O)_2$.[10] Foggite is constructed from *cis*-edge-sharing

AlO_6 octahedra which form a chain, bridged to other chains by PO_4 tetrahedra to form a $[Al(OH)_2(PO_4)]^{2-}$ layer. Distorted square antiprismatic CaO_8 units are also connected to the layers, and further $CaO_4(H_2O)_4$ polyhedra link the layers together.

Cis-edge-sharing octahedral chains are also found in the layered nickel phosphite $[Ni(HPO_3)]H_2O$.[11] The nickel octahedra also share corners with each other and with phosphite units to form the layers which have continuos Ni-O-Ni linkages throughout unlike MnPOX-8, where the *cis*-chains are linked only by phosphate. The layers are not connected to each other however, as they are (by oxalate) in MnPOX-8. A θ value of 4.22 K indicates predominantly ferromagnetic interactions, however antiferromagnetic ordering is seen at lower temperature (< 8 K). Cobalt can be substituted into the material to form $[Ni_xCo_{1-x}(HPO_3)]H_2O$. All the cobalt containing samples (and the pure cobalt form) are weak ferromagnets.

5.3.2 Iron System

It has not been possible to identify one of the three materials formed in the iron system. Although it always formed along with $FeC_2O_4.2H_2O$, the ratio of the two products varied. Positions 8 and 11 in Figure 5.1, corresponding to $FeC_2O_4.2H_2O$: H_3PO_4 : H_2O 2:4:4 and 1:3:6 respectively, gave the unknown material as the major product, with a small amount of $FeC_2O_4.2H_2O$. Figure 5.12 shows a comparison of its powder pattern (from position 8) with that of MnPOX-8, indicating that it is not simply an iron analogue of the manganese phosphate oxalate material.

A mixed valence iron phosphate was also formed in this system. $Fe^{2+}Fe^{3+}_2(HPO_4)_4(H_2O)_4$ is a 3D structure first reported by Vencato *et al.*[1] The same formula for this material was also found in this work through single crystal diffraction data, however Mössbauer measurements reported by Vencato and co-

workers suggested that the stoichiometry was not ideal, with a surplus of Fe^{3+} implying some disordered Fe^{2+} vacancies.

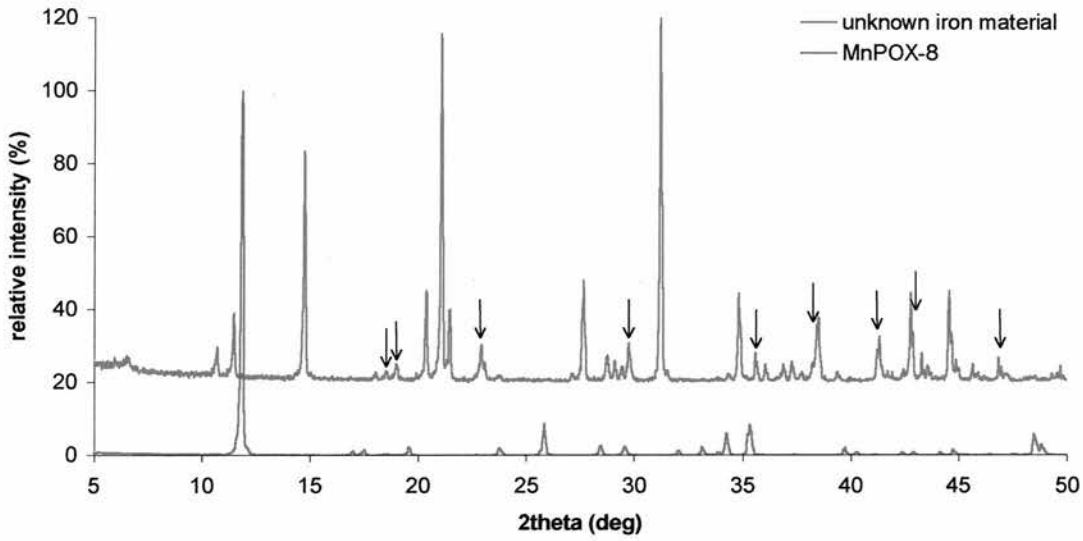

Figure 5.12 Powder x-ray diffraction pattern of the unknown material formed in the iron system, with the pattern obtained from a sample of MnPOX-8. Arrows indicate peaks from $FeC_2O_4.2H_2O$ (JCPDS 23-293) impurity.

Both Fe^{2+} and Fe^{3+} exist as FeO_6 octahedra. Fe^{2+} has two water ligands, the remaining four vertices are occupied by phosphate tetrahedra. Fe^{3+} has one water and five phosphates. The 3D structure is made up of continuous FeO_6-PO_4 corner sharing: there are no Fe-O-Fe linkages. The phosphate tetrahedra both contain an OH group. A *bc* view of the structure (Figure 5.13) shows channels which run along the *a* axis. These are constructed from 24 atom rings, however they are divided in two by the presence of hydrogen atoms on the HPO_4 groups which project into the channels.

Vencato *et al.* observed a two-stage water loss, thought to be loss of the ligand water on the iron at around 200 °C, followed by loss of water from the HPO_4 groups at 400 °C.

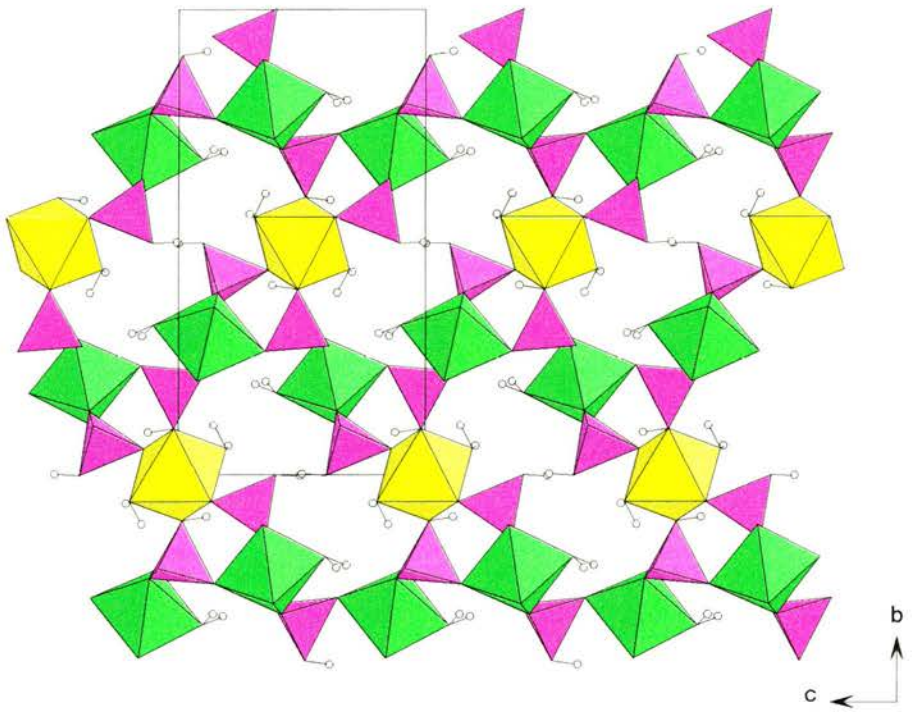

Figure 5.13 View down the *a* axis of $Fe^{2+}Fe^{3+}{}_2(HPO_4)_4(H_2O)_4{}^1$ showing the channels present in the structure. $Fe^{2+}O_6$ octahedra yellow, $Fe^{3+}O_6$ octahedra green, PO_4 tetrahedra purple, hydrogen white.

5.4 Conclusions

A systematic approach to a series of experiments with water at reactant concentrations was afforded using a phase-composition diagram, with the three variables metal oxalate, phosphoric acid and water. In the manganese system a new manganese phosphate oxalate framework was synthesised with magnetic properties worthy of further investigation. An unidentified material was formed in the iron system, which appears not to be isostructural with the manganese material. Incorporation of amines as potential structure directing agents in these low water content systems would be interesting, although an increase in the number of variables makes the use of phase diagrams more difficult. Preliminary work in this direction proved unsuccessful.

5.5 References

1. I. Vencato, Y. P. Mascarenhas and E. Mattievich, *Am. Miner.*, 1986, **71**, 222.

2. W. T. Robinson and G. M. Sheldrick, in *Crystallographic Computing 4. Techniques and New Technologies*, eds. N. W. Isaacs and M. R. Taylor, Oxford University Press, Oxford, 1988, 366.

3. SHELXL-97, A Program for Crystal Structure Refinement, G. M. Sheldrick, University of Göettingen, Germany, 1997, Release 97-2.

4. F. E. Mabbs and D. J. Machin, *Magnetism and Transition Metal Complexes*, Chapman and Hall, London, 1973, 5.

5. I. D. Brown and D. Altermatt, *Acta Crystallogr., Sect. B: Struct. Sci.*, 1985, **41**, 244.

6. A. Choudhury, S. Natarajan and C. N. R. Rao, *J. Solid State Chem.*, 1999, **146**, 538.

7. A. Choudhury, S. Natarajan and C. N. R. Rao, *Chem. Eur. J.*, 2000, **6**, 1168.

8. P. B. Moore, *Proceedings of the 2nd International Congress on Phosphorous Compounds*, 1980, 105.

9. F. C. Hawthorne, *Am. Miner.*, 1985, **70**, 455.

10. P. B. Moore, A. R. Kampf and T. Araki, *Am. Miner.*, 1975, **60**, 965.

11. M. D. Marcos, P. Amorós, F Sapiña, A. Beltrán-Porter, R. Martínez-Máñez and J. P. Attfield, *Inorg. Chem.*, 1993, **32**, 5044.

CHAPTER 6 – MISCELLANEOUS STRUCTURES

6.1 Introduction

In the course of this work many different, often known, materials have been synthesised. Several new phases have also been isolated. This chapter describes two new oxalates, one containing manganese and the other gadolinium, both of which are three-dimensional, containing protonated amines to balance the charge of the framework. A potassium iron phosphate is also discussed which is isotypic with the mineral leucophosphite but contains extra potassium ions.

6.2 $Mn_2(C_2O_4)_3(C_4H_8(NH_2)_2)$ (MnOX-1)

6.2.1 Experimental

6.2.1.1 Synthesis

A small crystal of $Mn_2(C_2O_4)_3(C_4H_8(NH_2)_2)$ (MnOX-1) was found in a sample of MnPOX-6, prepared as described previously (section 4.4.1.1).

6.2.1.2 Structural Characterisation

Single crystal diffraction was carried out at station 9.8, SRS, Daresbury. Structure solution and refinement were carried out using the SIR 92[1] and TEXSAN[2] suites. Crystallographic details are given in Table 6.1.

Table 6.1 Details of structure solution and refinement

	MnOX-1
Formula	$Mn_2(C_2O_4)_3(C_4H_8(NH_2)_2)$
Formula weight	462.09
Crystal system	Triclinic
Space group	$P\bar{1}$
a (Å)	5.9305(5)
b (Å)	7.7763(7)
c (Å)	8.1707(7)
α (°)	81.489(2)
β (°)	81.045(2)
γ (°)	86.076(2)
Volume (Å^3)	367.72(5)
Z	1
μ (cm^{-1})	1.792
Total reflections	1992
Observed reflections ($I>3\sigma(I)$)	1773
R, R_w	0.0467, 0.0596

6.2.2 Discussion

MnOX-1 is a 3D manganese oxalate framework which contains diprotonated piperazine cations. The building unit is shown in Figure 6.1; bond lengths, angles and atomic co-ordinates are in Appendix 8.

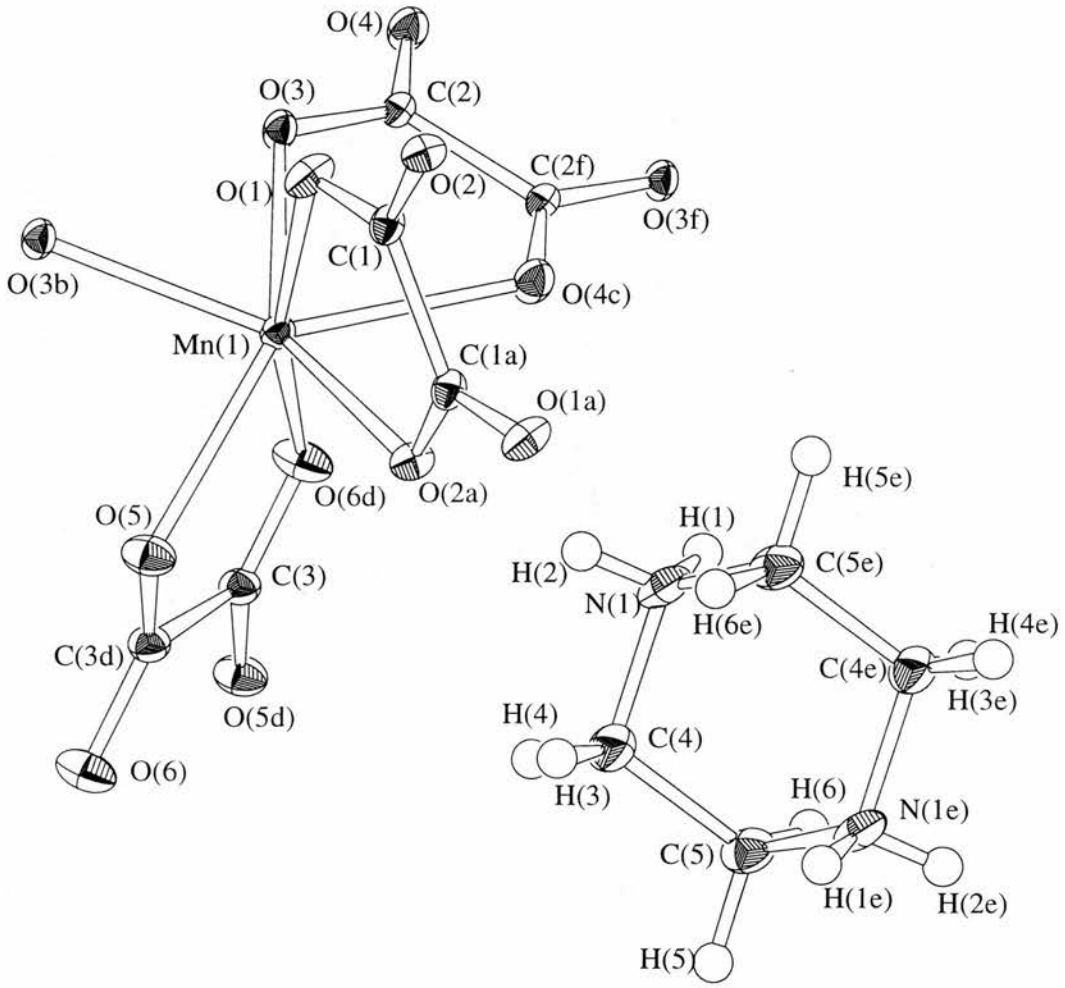

Figure 6.1 Building unit of MnOX-1 showing the atom labelling scheme, with thermal ellipsoids at 50 %. Symmetry labels: a, 1-*x*, 1-*y*, 1-*z*; b, 1-*x*, 1-*y*, 2-*z*; c, -*x*, 1-*y*, 1+*z*; d, 1-*x*, -*y*, 2-*z*; e, -*x*, -*y*, 1-*z*; f, -*x*, 1-*y*, 2-*z*.

The manganese atom is seven co-ordinate in this structure, with oxygen bond lengths ranging from 2.216(2) to 2.347(3) Å. Bond valence sums confirm the manganese as 2+, with a value of 2.03.[3] The basic structural unit is a dimer constructed from two MnO_7 polyhedra sharing an edge, as shown in Figure 6.2.

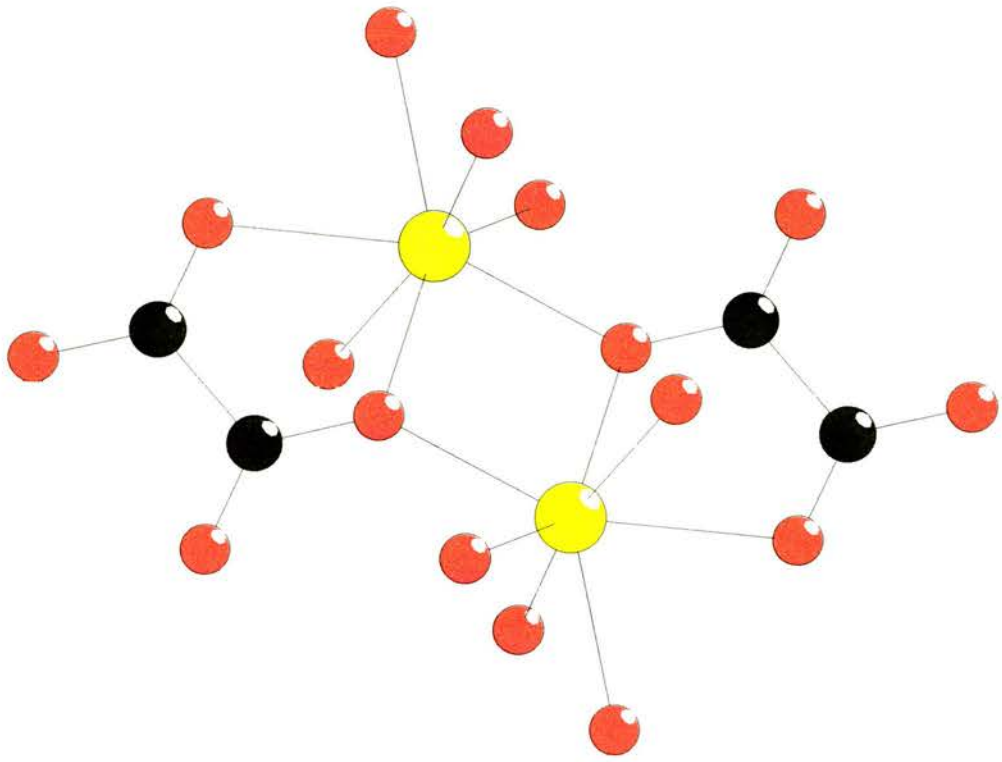

Figure 6.2 Edge-sharing seven co-ordinate manganese polyhedra in MnOX-1.

The oxygen atom through which the manganese polyhedra share an edge (O(3)) is three co-ordinate, bonded to an oxalate carbon and the two manganese atoms. O(3) has a bond valence sum of 1.99 as would be expected, *i.e.* this value has not been affected by the three-fold co-ordination. The O-Mn-O angles vary between 71.97(8) ° (O(3)-Mn(1)-O(4)) and 164.9(1) ° (O(1)-Mn(1)-O(6)), the smallest angles being due to bidentate oxalate co-ordination.

Each manganese atom is connected to two oxalate anions that have bisbidentate co-ordination (containing C(1) and C(3)). The third oxalate anion is connected to four manganese atoms, two through bidentate co-ordination (*via* O(4) and O(3)), and two through monodentate co-ordination (O(3)). Co-ordination modes of oxalate were discussed recently by Hernández-Molina *et al.*, who report that this co-ordination mode has been previously seen in materials containing iron, cobalt, nickel, zinc and cadmium, but not manganese.[4]

The manganese dimers are interconnected by oxalates in all three planes, leading to a three dimensional structure, shown in Figures 6.3 and 6.4. Channels exist in all three directions, forming cavities at their intersections where piperazine cations are found. One such cavity with an amine cation is illustrated in Figure 6.5.

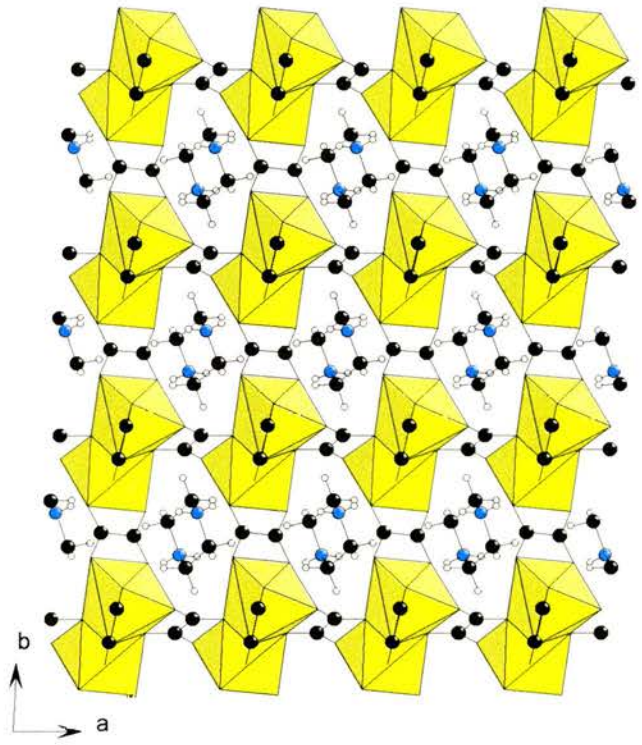

Figure 6.3 MnOX-1 in the *ab* plane showing the location of the piperazine cations

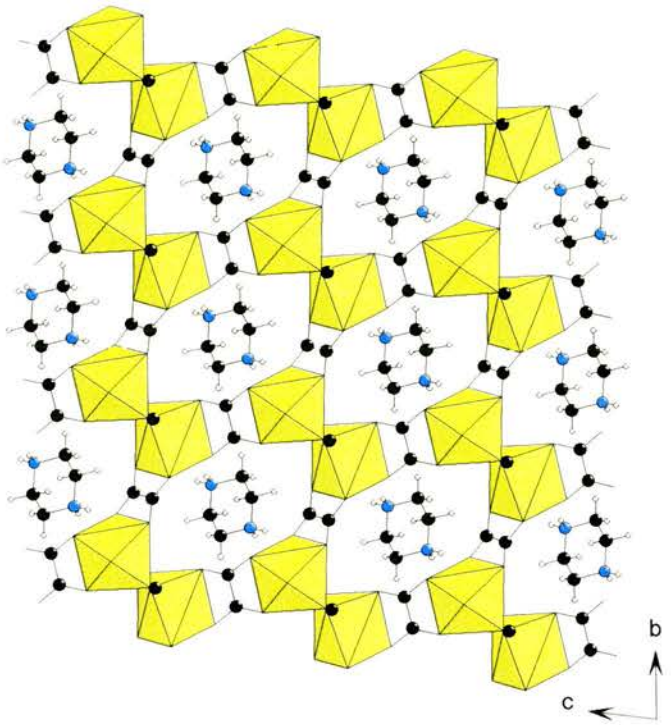

Figure 6.4 MnOX-1 in the *bc* plane

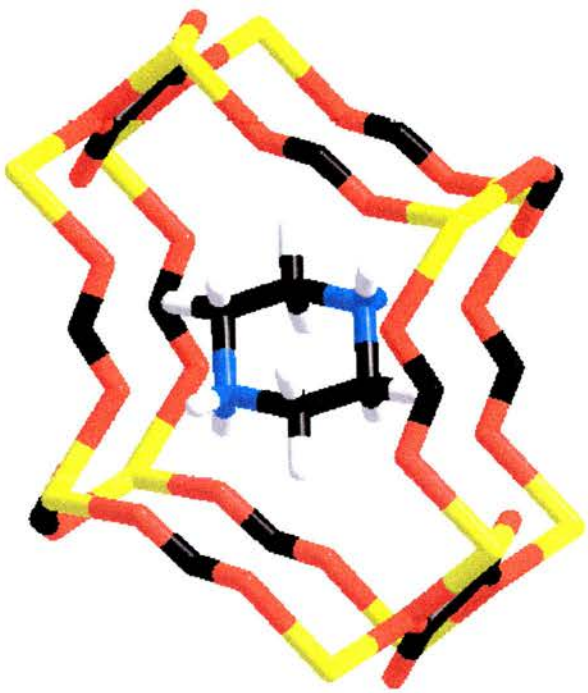

Figure 6.5 A cavity in MnOX-1 with a piperazine cation

Manganese oxalate dihydrate (JCPDS 25-544) consists of 1D chains, with each manganese co-ordinated to two bisbidentate oxalate and two water molecules.[5] Another dihydrate exists (JCPDS 32-647) which is constructed from different chains, where each oxalate shows bisbidentate co-ordination to one manganese and monodentate co-ordination to two others.[6] Hernández-Molina *et al.* report this co-ordination mode as being seen previously only with copper.[4]

No other amine-containing manganese oxalates have been reported in the literature, however two zinc oxalates containing amines have been synthesised by Rao and co-workers.[7] $[Zn_2(C_2O_4)_3](H_3N(CH_2)_3NH_3)(H_2O)_3$ is a layered honeycomb structure with amines found between the layers. Each zinc is octahedrally co-ordinated to three oxalate anions, and each oxalate is co-ordinated to two zinc centres. Changing the amine to *n*-propylamine results in $[Zn_2(C_2O_4)_3](C_3H_7NH_3)_2(H_2O)_3$ which shows similar co-ordination around the zinc, but in this case the honeycomb layers are 'interrupted' and form a 3D framework with two channel systems.

Iron and nickel bipyridyl complexes act as the counterion in manganese oxalate frameworks, $[Mn^{II}_2(C_2O_4)_3](M^{II}(bpy)_3)$ (M = Fe, Ni; bpy = 2,2'-bipyridine) synthesised by Decurtins *et al.* The manganese is co-ordinated to three bisbidentate oxalate anions to form a 3D structure with the bipyridyl complexes located in the void space.[8]

Many bimetallic oxalate structures have been reported containing manganese. The honeycomb layer structure mentioned above is often seen in these systems, for example $AMn^{II}Fe^{III}(C_2O_4)_3$ (where A is one of a variety of amines or phosphines),[9] discussed previously in section 1.3.2.3.

All these oxalates contain manganese in six-fold co-ordination, which is by far the most common co-ordination number, in contrast to the seven-fold co-ordination in MnOX-1. Oxalate materials exist with eight co-ordinate manganese: $K_2MnU(C_2O_4)_4.9H_2O$[10] and $[MnCr_2(bpy)_2(C_2O_4)_4]$[11]. A search of the Cambridge Structural Database (CSD) using the QUEST program[12,13] shows no structures with seven co-ordinate manganese where oxalate is one of the

ligands, however a seven co-ordinate manganese is seen in the 3D framework $Mn(O_2CCH_3)_2$.[14] This material is built up from trimers of acetate bridged manganese polyhedra, one of which is seven co-ordinate (the other two being six co-ordinate).

6.3 $[Gd(C_2O_4)_2(H_2O)](CH_3NH_2CH_3)(H_2O)_3$ GdOX-1

6.3.1 Experimental

6.3.1.1 Synthesis

$Gd_2(C_2O_4)_3$ (0.5812 g, 1.00 mmol) was added to water (10 ml, 555 mmol) with stirring. CH_3NHCH_3(aq) (40 %, 0.11 ml, 0.959 mmol) was then added to give a ratio of $Gd_2(C_2O_4)_3$: CH_3NHCH_3 : H_2O 1 : 1 : 555, and the mixture placed in an autoclave and heated at 160 °C for 48 hours. After cooling the mixture was filtered and washed with distilled water, then dried in air. 0.2828 g of a mixture of small colourless needles (possibly gadolinium oxalate, JCPDS 20-411) and blocks was obtained, and a block submitted for single crystal x-ray diffraction.

6.3.1.2 Structural Characterisation

Single crystal diffraction was carried out at room temperature on a Bruker SMART diffractometer with a CCD detector and MoK_α radiation. Structure solution and refinement were carried out using the SIR 92[1] and TEXSAN[2] suites. Atoms C(1) and O(6) are did not refine satisfactorily, both having a negative thermal parameter. These appear as spheres in the ORTEP plot (Figure 6.6). Crystallographic details are given in Table 6.2.

Table 6.2 Details of structure solution and refinement for GdOX-1

	GdOX-1
Formula	$[Gd(C_2O_4)_2(H_2O)](CH_3NH_2CH_3)(H_2O)_3$
Formula weight	445.39
Crystal system	monoclinic
Space group	$P2_1/n$
a (Å)	9.6416(9)
b (Å)	11.684(1)
c (Å)	12.271(1)
β (°)	99.232(2)
Volume (Å^3)	1364.5(2)
Z	4
μ MoK_α (cm^{-1})	4.933
Total reflections	2059
Observed reflections ($I>3\sigma(I)$)	1142
R, R_w	0.0461, 0.0460

6.3.2 Discussion

GdOX-1 is a 3D gadolinium oxalate containing extra-framework water and dimethylammonium cations. Tables of bond lengths and angles are given in Appendix 9; the building unit is illustrated in Figure 6.6.

The gadolinium is nine co-ordinate, with four bisbidentate oxalate groups and one water molecule, and can be approximately described as a capped square antiprism, illustrated in Figure 6.7. Four of the five smallest O-Gd-O angles (65.9(4) - 66.8(5) °) are due to the oxalate co-ordination mode.

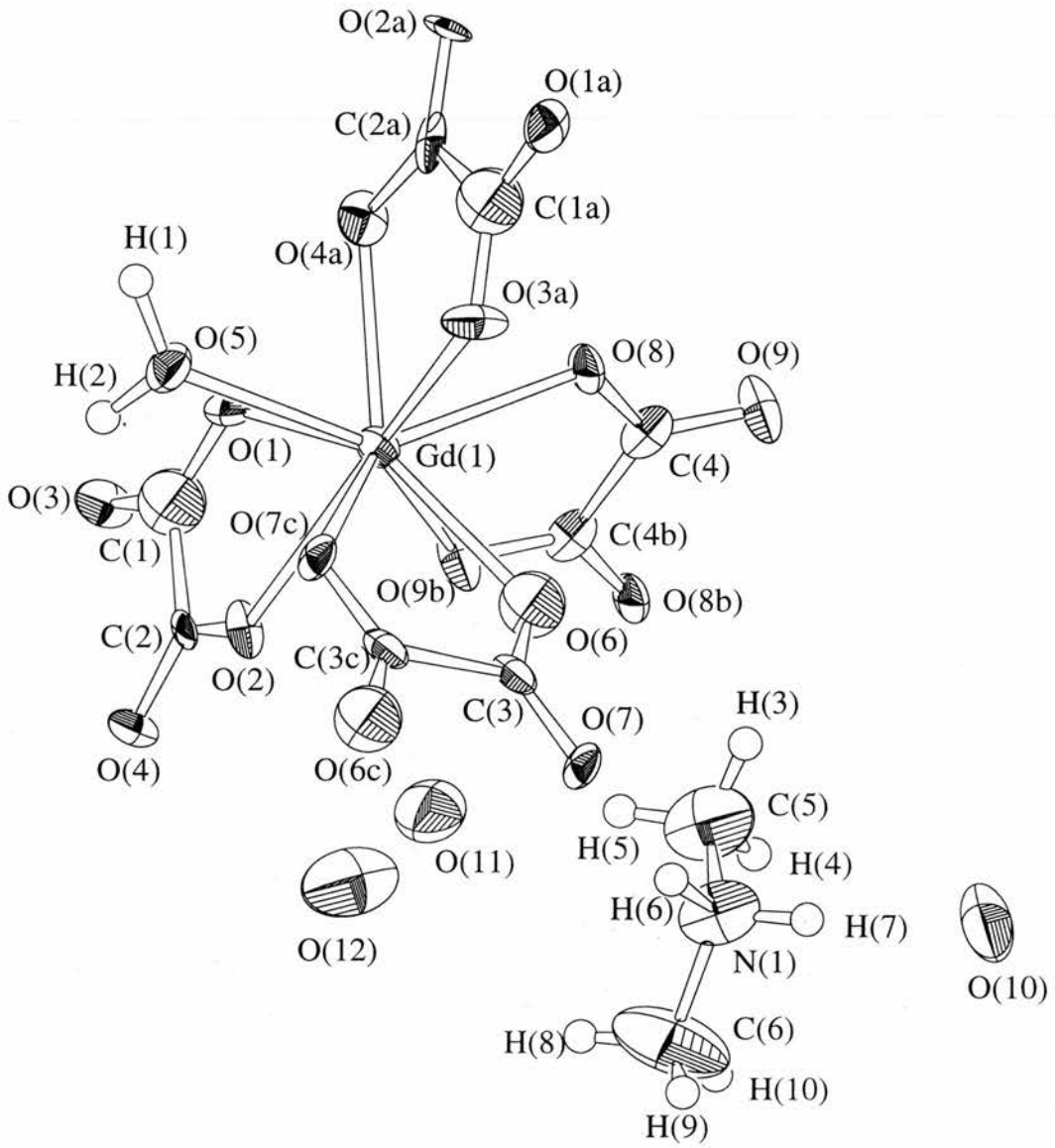

Figure 6.6 Building unit of GdOX-1 showing the atom labelling scheme, with thermal ellipsoids at 50 % probability. Symmetry labels: a, 1/2-*x*, 1/2+*y*, 1/2-*z*; b, -*x*, -*y*, -*z*; c, 1-*x*, -*y*, -*z*.

The hydrogen atoms on the dimethylamine could not be located and were placed in fixed positions. The amine is protonated to balance the framework charge. Three free oxygen atoms were located but their hydrogen atoms were not found.

The oxalate units link the gadolinium polyhedra in all three directions to form the 3D framework, shown in Figure 6.8.

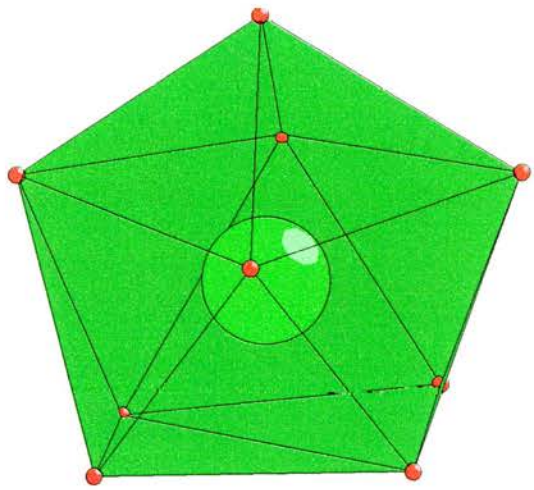

Figure 6.7 Gadolinium (large green central atom) surrounded by nine oxygen atoms (smaller red spheres) in a capped square antiprism arrangement.

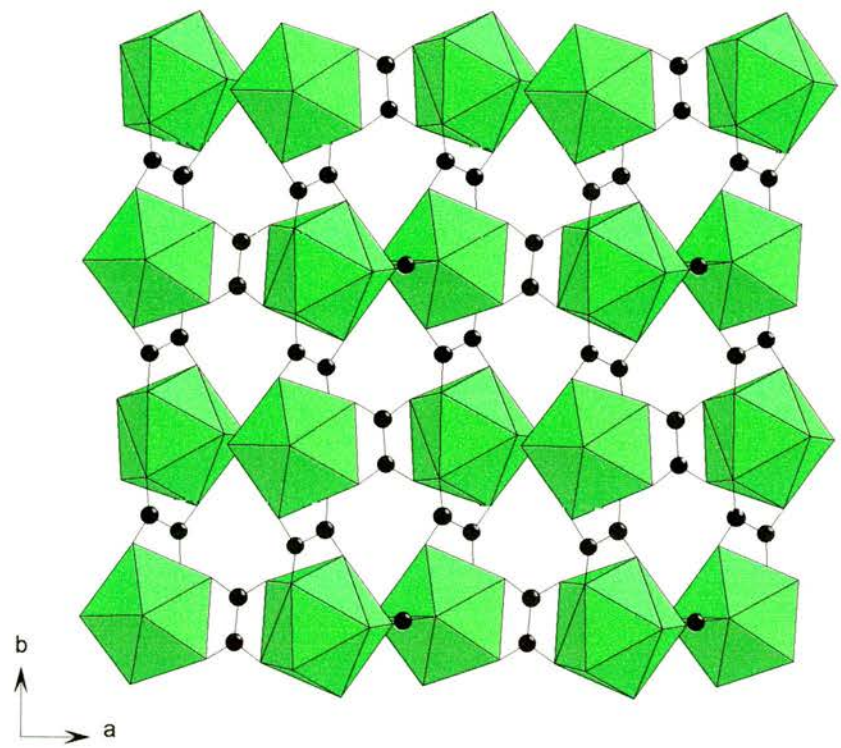

Figure 6.8 *ab* projection of GdOX-1 showing the gadolinium polyhedra (green) and the linking oxalate groups (C black).

Channels are found along both the *a* and *b* directions. Those along *a* are approximately 10 Å at their widest point and 3.7 Å at their narrowest (atom - atom centre distances) and contain the extra-framework water molecules, as seen in Figure 6.9.

The *b* channels contain the protonated dimethylamine cations (see Figure 6.10) and are approximately 8 x 10 Å in size.

The structures of $[Ln_2(C_2O_4)_3(H_2O)_6](H_2O)_4$ for Ln = La, Ce, Pr and Nd were reported by Ollendorff and Weigel, which are all isostructural with $[Gd_2(C_2O_4)_3(H_2O)_6](H_2O)_4$.[15,16] In this 3D structure the gadolinium is also nine co-ordinate, with three oxalate O atoms and three from water molecules. Gadolinium exists as a trigonal prism in $K_3[Gd(C_2O_4)_3(H_2O)](H_2O)_2$.[17] In this case the gadolinium is surrounded by eight oxalate oxygen atoms and one from water, and forms zigzag chains.

A capped square antiprism is seen in the erbium oxalate $[Er(C_2O_4)(HC_2O_4)](H_2O)_3$, where the erbium is co-ordinated to eight oxalate and one water O atoms as in GdOX-1.[18]

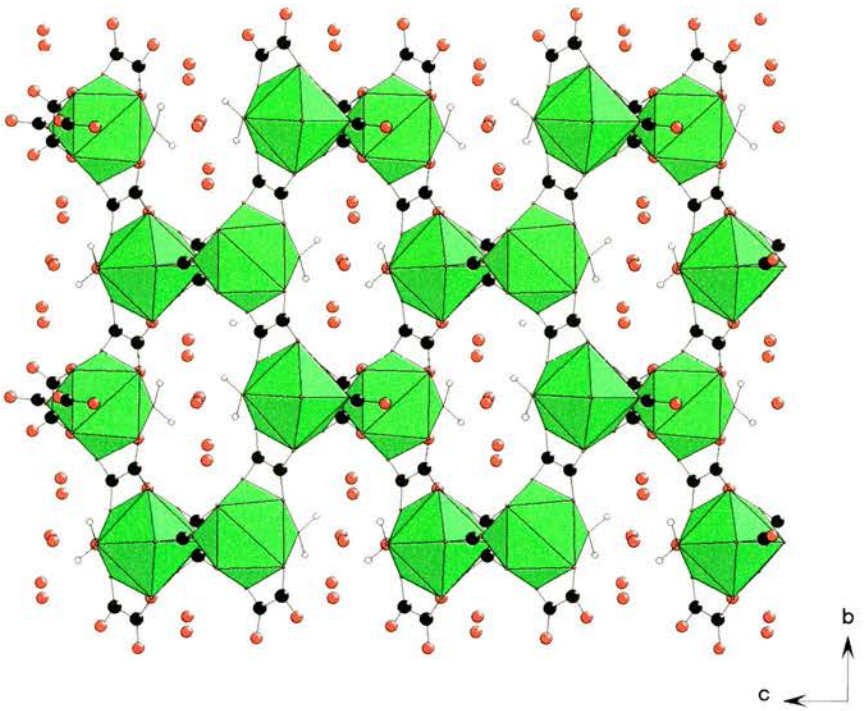

Figure 6.9 GdOX-1 in the *bc* plane showing the channels formed in the *a* direction which contain water (O red).

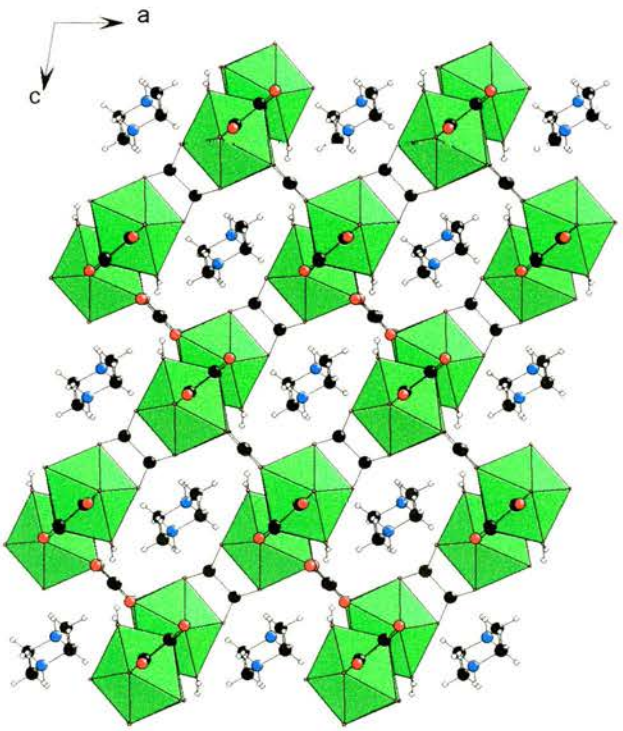

Figure 6.10 GdOX-1 in the *ac* plane showing the dimethylamine cations in the *b* channels (N blue)

6.4 $K_3[Fe_4O(OH)(PO_4)_4(H_2O)_2](H_2O)_2$ $FePO_4$-1

6.4.1 Experimental

6.4.1.1 Synthesis

$FeCl_2.4H_2O$ (0.6049 g, 3.04 mmol) was added to water (15 ml, 833 mmol) with stirring. H_3PO_4(aq) (85 %, 0.35 ml, 3.04 mmol), $HO_2CCH_2CO_2H$ (0.3075 g, 2.96 mmol) and KOH (1.0473 g, 18.7 mmol) were then added to give an approximate ratio of $FeCl_2.4H_2O$: H_3PO_4 : $HO_2CCH_2CO_2H$: KOH : H_2O 1:1:1:6:278. The mixture (with a pH of 6.5 - 7) was heated in an autoclave at 180 °C for 48 hours, then cooled, washed with distilled water and air dried to give 0.4381 g of product containing small needles of $K_3[Fe_4O(OH)(PO_4)_4(H_2O)_2](H_2O)_2$.

6.4.1.2 Structural Characterisation

Single crystal diffraction was carried out on beamline ID11 at the ESRF, Grenoble. Structure solution and refinement were carried out using the SIR 92[1] and TEXSAN[2] suites. Crystallographic details are given in Table 6.3.

Table 6.3 Details of structure solution and refinement

	$FePO_4$-1
Formula	$K_3[Fe_4O(OH)(PO_4)_4](H_2O)_4$
Formula weight	825.64
Crystal system	monoclinic
Space group	$P2_1/n$
a (Å)	9.551(2)
b (Å)	9.997(1)
c (Å)	9.836(2)
β (°)	100.022(8)
Volume (Å^3)	924.8(2)
Z	2
λ (Å)	0.375(4)
μ (cm^{-1})	1.458
Total reflections	10019
Observed reflections ($I>3\sigma(I)$)	8005
R, R_w	0.0441, 0.0623

6.4.2 Discussion

$FePO_4$-1 is a three dimensional iron(III) phosphate which contains extra-framework potassium and water. It is isotypic with the mineral Leucophosphite ($K_2[Fe_4(OH)_2(PO_4)_2(H_2O)_2](H_2O)_2$)[19] but contains an extra potassium ion instead of a hydrogen. The building unit is illustrated in Figure 6.11; bond lengths, angles and atomic co-ordinates are in Appendix 10.

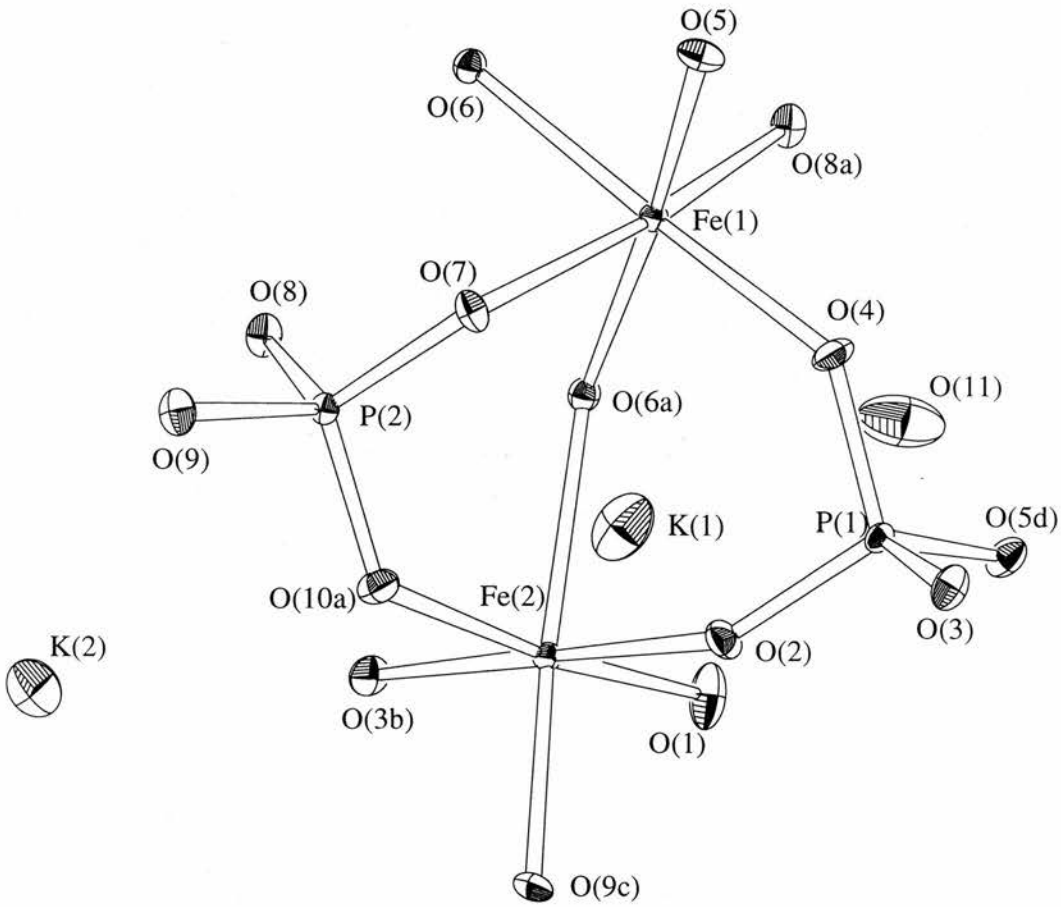

Figure 6.11 Building unit of $FePO_4$-1 showing the atom labelling scheme, with thermal ellipsoids at 50 % probability. Symmetry labels: a, 1-*x*, 1-*y*, -*z*; b, 1-*x*, 1/2-*y*, 1/2+*z*; c, 2*x*-1, *y*-1/2, -*z*-1/2; d, 1/2-*x*, 1-*y*, -1/2-*z*.

Both iron atoms are confirmed as 3+ by bond valence calculations, with a sum of 2.95 for Fe(1) and 2.93 for Fe(2), and exist in approximately octahedral co-ordination. The framework is built up from iron tetramers, illustrated in Figure 6.12. Two edge-sharing $Fe(1)O_6$ octahedra are at the centre of each unit, and both share a corner with two $Fe(2)O_6$ octahedra.

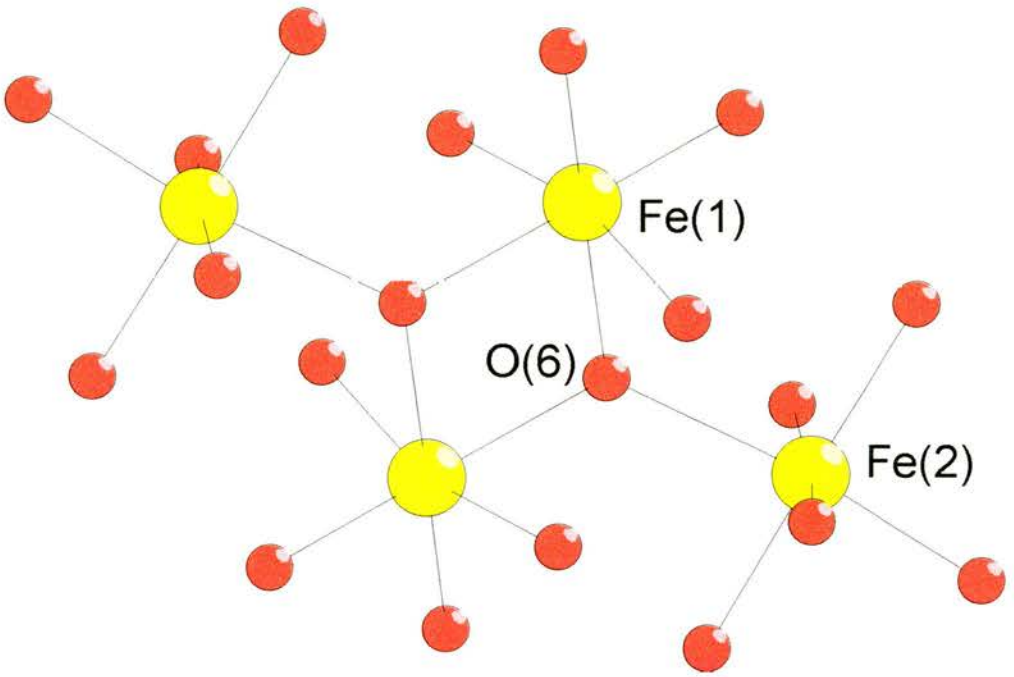

Figure 6.12 Iron tetramer in $FePO_4$-1 showing the two different iron atoms and the three co-ordinate oxygen

O(6) is involved in both edge- and corner-sharing and is therefore three co-ordinate. These tetramers are linked *via* PO_4 tetrahedra into the 3D framework, however there is no direct linkage between the iron octahedra in adjacent tetramers, *i.e.* no continuous Fe-O-Fe bonding. Bond valence sums (given in Table 6.4) for the bridging O(6) indicate that this is a hydroxyl group (sum 1.02), and that O(1) is a water co-ordinated to Fe(2) (sum 0.512).[3]

Small channels are formed in the framework in both the *a* and *b* directions, as shown in Figures 6.13 and 6.14. Potassium ions are located with these channels. An extra framework water molecule O(11) is also seen in the structure.

Table 6.4 Bond valence sums for the oxygen atoms in $FePO_4$-1

Atom	Sum	Nature
O(1)	0.5116	H_2O
O(2)	1.7632	
O(3)	1.7843	
O(4)	1.7633	
O(5)	1.8445	
O(6)	1.0190	OH
O(7)	1.6835	
O(8)	1.7306	
O(9)	1.8221	
O(10)	1.6900	

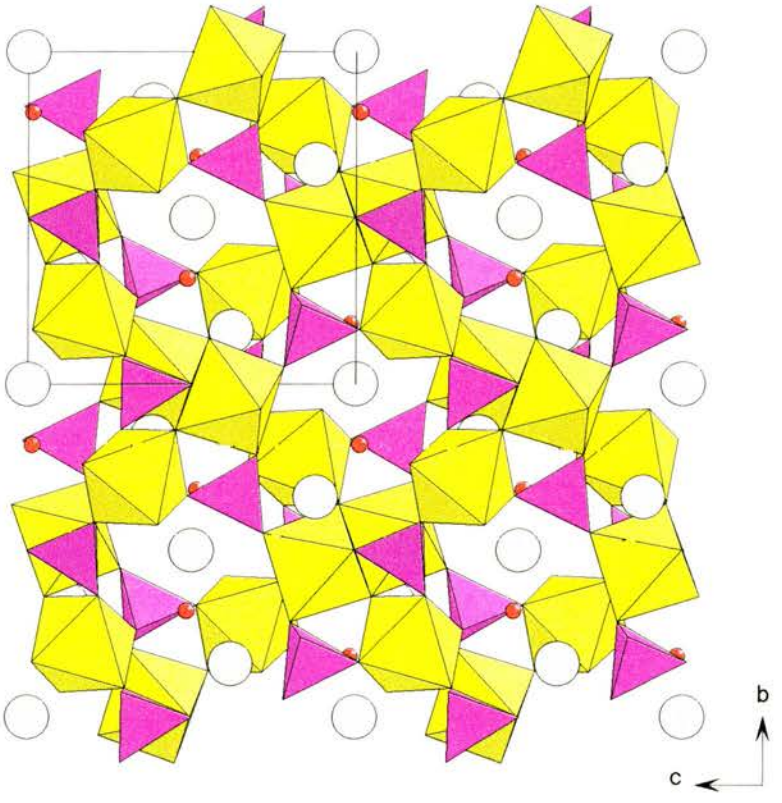

Figure 6.13 *bc* projection of $FePO_4$-1 showing the *a* channels and the location of potassium ions (grey) and free water (O red)

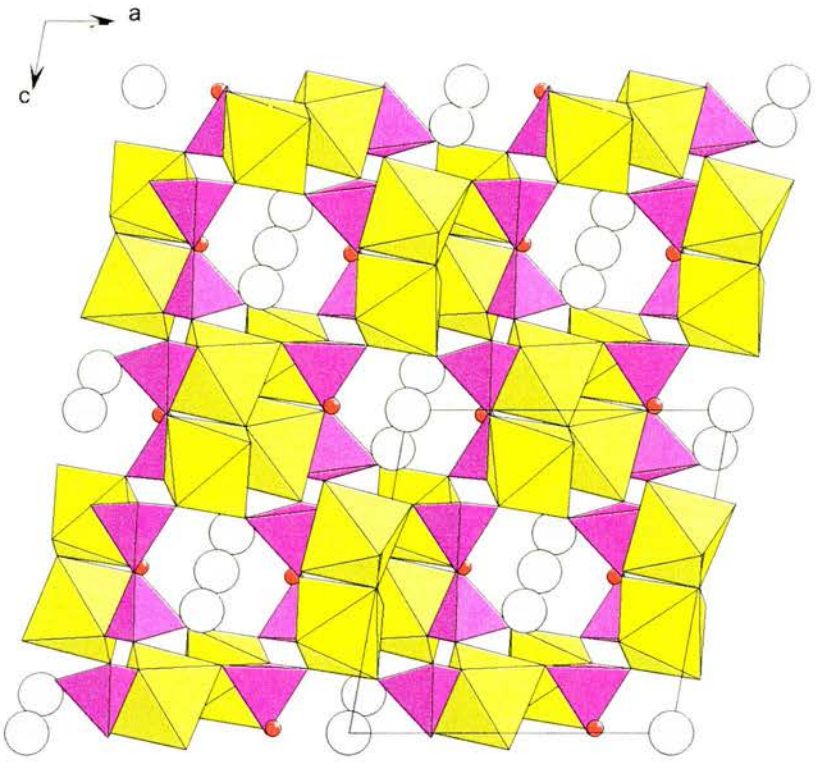

Figure 6.14 $FePO_4$-1 in the ac plane

The structure of leucophosphite was first determined by Moore in 1972,[19] but the location of the hydrogen atoms was the subject of a recent neutron diffraction study.[20] These H locations are in agreement with the values obtained here from bond valence sums, *i.e.* one free water, one ligand water and one bridging hydroxyl group. These three O atoms form six-rings with a distorted chair configuration *via* hydrogen bonding.

Due to the presence of an extra potassium ion in $FePO_4$-1, the formula $(K_3[Fe_4(PO_4)_4(OH)_2(H_2O)_2](H_2O)_2)$ would have an overall charge of 1+. The extra K^+ ion is located on the special position 1/2, 1/2, -1/2. As a potassium ion this is well behaved, with a thermal parameter B_{iso}/B_{eq} of 2.0392 and R = 0.044, R_w = 0.062. The possibility that this is in fact an oxygen atom (*i.e.* another extra-framework water molecule) was considered, however a full refinement with an oxygen in place of the potassium was unstable. A scale factor refinement gave R = 0.105, R_w = 0.136, suggesting that the atom is indeed potassium. To achieve charge balance, it is assumed that one of the hydrogen sites must be half-

occupied, most likely the bridging hydroxyl group (O(6)), reflected in the formula given. The other possibility is that this potassium is a chloride ion, as iron chloride was one of the reactants. As K^+ and Cl^- are isoelectronic, they are indistinguishable using x-rays. If this is the case, extra cations are required for charge balance, *e.g.* the bridging O(6) could be doubly protonated (this would then be five co-ordinate in total) or HPO_4 groups may be present. Bond valence sums for the remainder of the oxygen atoms (see Table 6.4) do not suggest a potential location for an H^+ ion.

Several structures isomorphous with leucophosphite have been reported, including those with partial and complete replacement of the potassium with ammonium, $K_{1-x}(NH_4)_x[Fe_{2-y}Al_y(PO_4)_2(OH)(H_2O)](H_2O)$ and $NH_4[Ga_2(PO_4)_2(OH)(H_2O)](H_2O)$.[20] Two leucophosphite-type structures containing mixed valence molybdenum exist, where a Mo-Mo double bond occurs between molybdenum(IV) atoms in the edge-sharing polyhedra and the bridging three co-ordinate O atom is unprotonated.[21,22] Of particular interest is $Rb[Mo_2O_2(PO_4)_2](H_2O)_{0.9}$.[22] The rubidium cation (replacing K^+ in leucophosphite) is found in three different sites in the framework's channels, in a ratio of 85:10:5. The 10 % occupied site is too close to the water's site for both to be occupied at once, hence the 0.9 figure in the formula above.

6.5 Conclusions

Two new amine-containing 3D metal oxalate frameworks have been synthesised, in manganese and gadolinium systems. A small crystal of the manganese framework MnOX-1 was found in a sample of MnPOX-6, whereas the gadolinium material GdOX-1 was synthesised from a mixture of gadolinium oxalate and dimethylamine. It was hoped that it would be possible to incorporate both manganese and gadolinium into a framework; such a structure may have ferrimagnetic interactions as it combines a d^5 (Mn^{2+}) and an f^7 (Gd^{3+}) metal. Unfortunately such a material was not successfully synthesised during the course of this work.

An analogue of the potassium iron phosphate mineral leucophosphite was also synthesised ($FePO_4$-1), which incorporates an extra potassium ion. $FePO_4$-1 formed as very small needles which required a synchrotron source for structure elucidation.

6.6 References

1. A. Altomare, M. C. Burla, M. Camalli, M. Cascarano, C. Giacovazzo, A. Gugliardi and G. Polidori, *J. Appl. Crystallogr.*, 1993, **26**, 343.

2. TEXSAN, Crystal Structure Analysis Package, Molecular Structure Corporation, Houston, TX, 1992.

3. I. D. Brown and D. Altermatt, *Acta Crystallogr., Sect. B: Struct. Sci.*, 1985, **41**, 244.

4. M. Hernández-Molina, P. A. Lorenzo-Luis and C. Ruiz-Pérez, *CrystEngComm.*, 2001, 16.

5. I. Sledzinska, A. Murasik and P. Fischer, *J. Phys. C: Solid State Phys.*, 1987, **20**, 2247.

6. P. Lightfoot and A. Congreve, unpublished results.

7. R. Vaidhyanathan, S. Natarajan, A. K. Cheetham and C. N. R. Rao, *Chem. Mater.*, 1999, **11**, 3636.

8. S. Decurtins, H. W. Schmalle, P. Schneuwly, J. Ensling and P. Gütlich, *J. Am. Chem. Soc.*, 1994, **116**, 9521.

9. C. Mathonière, C. J. Nuttall, S. G. Carling and P. Day, *Inorg. Chem.*, 1996, **35**, 1201.

10. K. P. Mörtl, J.-P. Sulter, S. Golhen, L. Ouahab and O. Kahn, *Inorg. Chem.*, 2000, **39**, 1626.

11. F. D. Rochon, R. Melanson and M. Andruh, *Inorg. Chem.*, 1996, **35**, 6085.

12. D. A. Fletcher, R. F. McMeeking and D. Parkin, *J. Chem. Inf. Comput. Sci.*, 1996, **36**, 746.

13. F. H. Allen and O. Kennard, *Chemical Design Automation News*, 1993, **8**, 1; 31.

14. J. D. Martin and R. F. Hess, *Chem. Commun.*, 1996, 2419.

15. W. Ollendorff and F. Weigel, *Inorg. Nucl. Chem. Lett.*, 1969, **5**, 263.

16. H. Chi, *Bull. Chem. Soc. Jpn.*, 1970, **43**, 1703.

17. I. A. Kahwa, F. R. Fronczek and J. Selbin, *Inorg. Chim. Acta*, 1984, **82**, 161.

18. H. Steinfink and G. D. Brunton, *Inorg. Chem.*, 1970, **9**, 2112.

19. P. B. Moore, *Am. Miner.*, 1972, **57**, 397.

20. S. Dick and T. Zeiske, *J. Solid State Chem.*, 1997, **133**, 508.

21. H. E. King, L. A. Mundi, K. G. Strohmaier and R. C. Haushalter, *J. Solid State Chem.*, 1991, **92**, 1.

22. A. Leclaire, M. M. Borel, A. Grandin and B. Raveau, *J. Solid State Chem.*, 1994, **108**, 177.

CHAPTER 7 – CONCLUDING REMARKS

7.1 Conclusions

The initial aim of this work, to construct frameworks containing two different types of anion, has been realised in the synthesis of several 3D manganese phosphate oxalates. Although many experiments were carried out with a variety of metallic elements and organic ligands, the manganese oxalate system proved by far the most fruitful. Manipulation of the structure directing amine and the water content has resulted in a variety of structure types.

MnPOX-1 ($Mn_4(PO_4)_2(C_2O_4)(H_2O)_2$), in common with other phosphate oxalate structures, is constructed from metal phosphate layers, which are pillared by oxalate anions. A similar construction is seen in the amine-containing MnPOX-2, -3 and -4 ($[Mn_2(HPO_4)_2(C_2O_4)(H_2O)_2](AH_2)$, where A = ethylenediamine, 1,3-diaminopropane and *trans*-1,4-diaminocyclohexane respectively). Variation of the structure directing amine has subtle structural effects. Amines have also been incorporated into MnPOX-5 ($[Mn_4(HPO_4)_2(C_2O_4)_3(H_2O)_2](H_2O)_2(AH_2)$, A = ethylenediamine) MnPOX-6 (A = piperazine). MnPOX-5 and -6 are of different construction, with metal phosphate chains connected in two directions by oxalate anions. The use of a phase-composition diagram was successful in synthesising MnPOX-8 ($Mn_2(H_2PO_4)_2(C_2O_4)$), also a 3D material, again with oxalate anions pillaring metal phosphate layers. This was achieved with water at a much lower concentration than in normal hydrothermal conditions.

Materials that were obtained as pure samples were examined using thermogravimetric analysis. Removal of structure directing amines with retention of the framework architecture was not achieved, however MnPOX-5 showed a dehydration (apparently irreversible) to MnPOX-7, believed to be a related structure with water absent from the channels and from one manganese co-ordination sphere.

Magnetic measurements on all pure manganese phosphate oxalate materials have shown that they order antiferromagnetically at low temperatures. Of the most interest is MnPOX-8, which displayed an unusual shape in the plot of susceptibility against temperature, possibly indicating a more complex ordering behaviour than in the other materials.

In addition to the manganese phosphate oxalate frameworks discussed above, two new amine containing oxalates were synthesised, as well as a potassium iron phosphate isostructural with the mineral leucophosphite.

7.2 Opportunities for Further Research

Of the materials synthesised in this work, MnPOX-8 shows the most potential for further exploration. Whilst it is possible that its unexpected magnetic properties are due to an impurity, it is more likely to be the result of two different ordering modes. The material could be investigated more fully by single crystal measurements if a crystal of suitable size could be obtained, perhaps through manipulation of the reaction conditions. Substitution of manganese with a small amount of a diamagnetic element, such as magnesium or zinc, may also reveal more about the magnetic ordering. Replacing the phosphate units with, *e.g.* sulphate, or the oxalate units with another organic group may give more information on the magnetic exchange between manganese centres. Experiments carried out in the course of this work with other organic ligands suggest the latter option to be the most difficult.

As removal of the structure directing amines appears to be a major obstacle in the production of open frameworks, the use of functional extra-framework molecules as an integral part of the material could be considered. It has been illustrated in the layered oxalates $A[M^{II}M^{III}(C_2O_4)_3]$[1,2] that variation of the cation A can be used to alter the magnetic properties of the material. Also of interest is the production of non-linear optical materials by incorporation of suitable species

into open frameworks.[3,4] The attraction of this idea is the ability of the framework to contain the molecules with the desired orientation.

7.3 References

1. C. Mathonière, C. J. Nuttall, S. G. Carling and P. Day, *Inorg. Chem.*, 1996, **35**, 1201.

2. C. J. Nuttall and P. Day, *Chem. Mater.*, 1998, **10**, 3050.

3. S. D. Cox, T. E. Gier and G. D. Stucky, *Chem. Mater.*, 1990, **2**, 609.

4. S. Bénard, P. Yu, J. P. Audière, E. Rivière, R. Clément, J. Guilhem, L. Tchertanov and K. Nakatani, *J. Am. Chem. Soc.*, 2000, **122**, 9444.

APPENDIX 1 - MnPOX-1

$(Mn_4(PO_4)_2(C_2O_4)(H_2O)_2)$

Atomic co-ordinates and temperature factors in MnPOX-1

atom	x	y	z	B(eq)
Mn(1)	0.02692(6)	0.35342(9)	0.38383(7)	0.65(1)
Mn(2)	0.73259(6)	0.47430(9)	0.73426(7)	0.77(1)
P(1)	0.3946(1)	0.3487(1)	0.6012(1)	0.48(2)
O(1)	0.9635(3)	0.5910(4)	0.8282(3)	0.91(6)
O(2)	0.0139(3)	0.6738(4)	0.4219(3)	0.68(5)
O(3)	0.5025(3)	0.5337(4)	0.6566(3)	0.75(5)
O(4)	0.8375(3)	0.2030(4)	0.7119(3)	0.69(5)
O(5)	0.2607(3)	0.4015(4)	0.4540(3)	0.83(6)
O(6)	-0.2167(3)	0.3572(4)	0.2221(3)	1.00(6)
O(7)	1.1804(3)	0.5688(5)	1.0309(3)	1.13(6)
C(2)	1.0426(4)	0.5468(6)	0.9598(4)	0.77(8)
H(1)	-0.222(6)	0.383(8)	0.132(6)	2(1)
H(2)	-0.283(7)	0.44(1)	0.222(7)	5(1)

Bond lengths in MnPOX-1

atom	atom	distance (Å)	atom	atom	distance (Å)
Mn(1)	O(1)	2.253(3)	Mn(2)	O(5)	2.126(3)
Mn(1)	O(2)	2.142(3)	Mn(2)	O(7)	2.181(3)
Mn(1)	O(2)	2.219(3)	P(1)	O(2)	1.552(3)
Mn(1)	O(3)	2.121(3)	P(1)	O(3)	1.551(3)
Mn(1)	O(5)	2.153(3)	P(1)	O(4)	1.526(3)
Mn(1)	O(6)	2.261(3)	P(1)	O(5)	1.544(3)
Mn(2)	O(1)	2.214(3)	O(1)	C(2)	1.254(5)
Mn(2)	O(3)	2.120(3)	O(7)	C(2)	1.252(5)
Mn(2)	O(4)	2.127(3)	C(2)	C(2)	1.560(7)

Bond angles in MnPOX-1

atom	atom	atom	angle (°)	atom	atom	atom	angle (°)
O(1)	Mn(1)	O(2)	93.0(1)	O(5)	Mn(2)	O(7)	153.3(1)
O(1)	Mn(1)	O(2)	171.3(1)	O(2)	P(1)	O(3)	105.1(1)
O(1)	Mn(1)	O(3)	91.9(1)	O(2)	P(1)	O(4)	113.7(2)
O(1)	Mn(1)	O(5)	77.4(1)	O(2)	P(1)	O(5)	109.4(2)
O(1)	Mn(1)	O(6)	78.1(1)	O(3)	P(1)	O(4)	109.7(2)
O(2)	Mn(1)	O(2)	82.1(1)	O(3)	P(1)	O(5)	110.1(2)
O(2)	Mn(1)	O(3)	168.8(1)	O(4)	P(1)	O(5)	108.8(1)
O(2)	Mn(1)	O(5)	86.8(1)	Mn(1)	O(1)	Mn(2)	97.4(1)
O(2)	Mn(1)	O(6)	89.3(1)	Mn(1)	O(1)	C(2)	142.7(2)
O(2)	Mn(1)	O(3)	91.8(1)	Mn(2)	O(1)	C(2)	115.0(2)
O(2)	Mn(1)	O(5)	109.3(1)	Mn(1)	O(2)	Mn(1)	97.9(1)
O(2)	Mn(1)	O(6)	94.6(1)	Mn(1)	O(2)	P(1)	126.9(1)
O(3)	Mn(1)	O(5)	104.1(1)	Mn(1)	O(2)	P(1)	124.1(2)
O(3)	Mn(1)	O(6)	81.8(1)	Mn(1)	O(3)	Mn(2)	106.6(1)
O(5)	Mn(1)	O(6)	155.0(1)	Mn(1)	O(3)	P(1)	132.9(2)
O(1)	Mn(2)	O(3)	149.0(1)	Mn(2)	O(3)	P(1)	117.6(1)
O(1)	Mn(2)	O(4)	81.8(1)	Mn(2)	O(4)	P(1)	129.6(2)
O(1)	Mn(2)	O(5)	78.8(1)	Mn(1)	O(5)	Mn(2)	103.3(1)
O(1)	Mn(2)	O(7)	75.1(1)	Mn(1)	O(5)	P(1)	129.5(2)
O(3)	Mn(2)	O(4)	128.6(1)	Mn(2)	O(5)	P(1)	127.1(1)
O(3)	Mn(2)	O(5)	93.8(1)	Mn(2)	O(7)	C(2)	114.6(2)
O(3)	Mn(2)	O(7)	105.4(1)	O(1)	C(2)	O(7)	126.9(4)
O(4)	Mn(2)	O(5)	89.8(1)	O(1)	C(2)	C(2)	115.3(4)
O(4)	Mn(2)	O(7)	92.4(1)	O(7)	C(2)	C(2)	117.8(4)

Hydrogen Bonds in MnPOX-1

A	H	B	A-H (Å)	H...B (Å)	A...B (Å)	A-H...B (°)
O(6)	H(1)	O(7)	0.92(5)	1.92(5)	2.825(4)	166(5)
O(6)	H(1)	O(1)	0.92(5)	2.45(5)	2.883(4)	106(4)
O(6)	H(2)	O(3)	0.83(6)	2.01(6)	2.870(4)	141(5)
O(6)	H(2)	O(5)	0.83(6)	2.12(6)	3.011(4)	120(5)

APPENDIX 2 - MnPOX-2

$[Mn_2(HPO_4)_2(C_2O_4)(H_2O)_2](H_3N(CH_2)_2NH_3)$

Atomic co-ordinates and temperature factors in MnPOX-2

atom	x	y	z	B(eq)
Mn(1)	0.1010(1)	0.48380(6)	0.81816(4)	1.36(1)
P(1)	-0.3903(2)	0.2596(1)	0.81943(7)	1.23(2)
O(1)	-0.2249(5)	0.6014(3)	1.0434(2)	1.83(6)
O(2)	-0.1476(5)	0.3016(3)	0.7899(2)	1.65(6)
O(3)	-0.0463(5)	0.5956(3)	0.6988(2)	1.72(6)
O(4)	0.3711(6)	0.6762(4)	0.8505(2)	2.30(8)
O(5)	-0.1248(5)	0.6057(3)	0.9073(2)	1.57(6)
O(6)	0.3975(5)	0.3602(3)	0.7795(2)	1.67(6)
O(7)	-0.3452(8)	0.2784(5)	0.9252(3)	1.90(7)
N(1)	-0.0578(8)	0.9267(4)	0.8829(2)	1.87(9)
C(1)	-0.1010(7)	0.5598(4)	0.9858(3)	1.25(8)
C(2)	0.0765(8)	1.0043(5)	0.9623(3)	2.0(1)
H(1)	0.37(1)	0.720(7)	0.810(4)	6(1)
H(2)	0.51(1)	0.646(7)	0.871(4)	5(1)
H(3)	0.032(8)	0.924(4)	0.837(3)	2.1(8)
H(4)	-0.10(1)	0.824(7)	0.898(4)	6(1)
H(5)	0.231(7)	0.955(4)	0.979(2)	1.1(7)
H(7)	0.082(8)	1.105(5)	0.947(3)	2.8(9)
H(8)	-0.195(9)	0.978(5)	0.859(3)	3(1)
H(9)	-0.46(2)	0.29(1)	0.933(6)	8(1)

Bond lengths in MnPOX-2

atom	atom	distance (Å)	atom	atom	distance (Å)
Mn(1)	O(1)	2.249(3)	O(4)	H(2)	0.80(6)
Mn(1)	O(2)	2.125(3)	O(5)	C(1)	1.254(4)
Mn(1)	O(3)	2.123(3)	O(7)	H(9)	0.68(9)
Mn(1)	O(4)	2.273(3)	N(1)	C(2)	1.487(5)
Mn(1)	O(5)	2.254(3)	N(1)	H(3)	0.92(5)
Mn(1)	O(6)	2.119(3)	N(1)	H(4)	0.99(6)
P(1)	O(2)	1.511(3)	N(1)	H(8)	0.90(5)
P(1)	O(3)	1.526(3)	C(1)	C(1)	1.551(7)
P(1)	O(6)	1.519(3)	C(2)	C(2)	1.525(8)
P(1)	O(7)	1.602(4)	C(2)	H(5)	0.95(4)
O(1)	C(1)	1.246(4)	C(2)	H(7)	0.94(4)
O(4)	H(1)	0.73(6)			

Bond angles in MnPOX-2

atom	atom	atom	angle (°)	atom	atom	atom	angle (°)
O(1)	Mn(1)	O(2)	91.1(1)	O(2)	P(1)	O(3)	111.7(2)
O(1)	Mn(1)	O(3)	169.7(1)	O(2)	P(1)	O(6)	112.4(2)
O(1)	Mn(1)	O(4)	87.9(1)	O(2)	P(1)	O(7)	105.6(2)
O(1)	Mn(1)	O(5)	73.23(9)	O(3)	P(1)	O(6)	111.2(2)
O(1)	Mn(1)	O(6)	87.2(1)	O(3)	P(1)	O(7)	106.3(2)
O(2)	Mn(1)	O(3)	92.5(1)	O(6)	P(1)	O(7)	109.2(2)
O(2)	Mn(1)	O(4)	178.9(1)	Mn(1)	O(1)	C(1)	116.3(2)
O(2)	Mn(1)	O(5)	95.9(1)	Mn(1)	O(2)	P(1)	133.9(2)
O(2)	Mn(1)	O(6)	91.9(1)	Mn(1)	O(3)	P(1)	131.0(2)
O(3)	Mn(1)	O(4)	88.5(1)	Mn(1)	O(5)	C(1)	115.6(2)
O(3)	Mn(1)	O(5)	96.8(1)	Mn(1)	O(6)	P(1)	140.1(2)
O(3)	Mn(1)	O(6)	102.3(1)	O(1)	C(1)	O(5)	126.1(3)
O(4)	Mn(1)	O(5)	84.1(1)	O(1)	C(1)	C(1)	116.8(4)
O(4)	Mn(1)	O(6)	87.7(1)	O(5)	C(1)	C(1)	117.2(4)
O(5)	Mn(1)	O(6)	159.0(1)	N(1)	C(2)	C(2)	109.4(5)

Hydrogen Bonds in MnPOX-2

A	H	B	A-H (Å)	H...B (Å)	A...B (Å)	A-H...B (°)
O(4)	H(1)	O(6)	0.73(6)	2.24(7)	2.811(5)	136(7)
O(4)	H(2)	O(5)	0.80(6)	2.04(6)	2.825(4)	168(6)
O(7)	H(9)	O(1)	0.68(9)	2.04(9)	2.691(5)	162(10)
N(1)	H(3)	O(6)	0.92(5)	1.96(5)	2.817(5)	155(4)
N(1)	H(4)	O(5)	0.99(6)	1.97(6)	2.932(5)	165(5)
N(1)	H(8)	O(3)	0.90(5)	1.87(5)	2.771(5)	173(4)
O(4)	H(1)	O(2)	0.73(6)	2.41(7)	3.022(4)	142(7)
N(1)	H(8)	O(2)	0.90(5)	2.79(5)	3.079(4)	100(3)

APPENDIX 3 - MnPOX-3

$[Mn_2(HPO_4)_2(C_2O_4)(H_2O)_2](H_3N(CH_2)_3NH_3)$

Atomic co-ordinates and temperature factors in MnPOX-3

atom	x	y	z	B(eq)
Mn(1)	0.3216(1)	0.17405(5)	1.01095(8)	1.38(2)
P(1)	-0.1547(2)	0.17836(9)	1.2432(1)	1.37(3)
O(1)	0.0439(8)	0.1468(3)	0.8203(5)	2.2(1)
O(2)	0.2546(6)	0.0416(2)	1.0890(4)	1.94(8)
O(3)	0.4084(6)	-0.0899(2)	1.0954(4)	1.79(8)
O(4)	-0.1357(7)	0.0775(2)	1.2469(5)	2.13(9)
O(5)	0.0366(6)	0.2127(2)	1.1452(4)	2.23(9)
O(6)	-0.4144(6)	0.2004(2)	1.1871(4)	2.03(8)
O(7)	-0.1144(7)	0.2081(2)	1.4030(4)	2.19(9)
N(1)	0.851(2)	0.3455(6)	0.977(1)	1.6(2)
N(2)	0.815(2)	0.3674(7)	1.045(1)	3.3(2)
C(1)	0.4019(9)	-0.0145(3)	1.0539(6)	1.5(1)
C(2)	0.861(2)	0.4440(8)	0.960(1)	3.1(3)
C(3)	1	0.5	1	7.1(4)
C(4)	0.953(3)	0.4178(10)	1.055(2)	4.3(3)
H(1)	0.04(1)	0.198(5)	0.762(9)	7(1)
H(2)	-0.06(1)	0.131(5)	0.849(8)	4(1)
H(3)	-0.02(1)	0.053(5)	1.224(8)	6(1)
H(4)	0.8492	0.4535	0.8572	4
H(5)	0.7161	0.463	1.0027	4
H(6)	1.1548	0.4726	1.0017	4
H(7)	0.958	0.5109	1.0985	4
H(8)	0.8452	0.5274	0.9983	4
H(9)	1.0419	0.4891	0.9015	4
H(10)	1.0957	0.3894	1.0331	4
H(11)	0.9497	0.4295	1.1571	4
H(12)	0.9853	0.3205	0.9311	4
H(13)	0.7019	0.3254	0.9267	4
H(14)	0.8086	0.3448	0.9462	4
H(15)	0.6624	0.385	1.0701	4
H(16)	0.8722	0.3213	1.1104	4
H(17)	0.8532	0.3299	1.077	4

Bond lengths in MnPOX-3

atom	atom	distance (Å)	atom	atom	distance (Å)
Mn(1)	O(1)	2.271(4)	O(2)	C(1)	1.250(6)
Mn(1)	O(2)	2.238(4)	O(3)	C(1)	1.244(6)
Mn(1)	O(3)	2.245(3)	N(1)	N(2)	0.75(1)
Mn(1)	O(5)	2.124(3)	N(1')	C(2)	1.56(2)
Mn(1)	O(6)	2.128(4)	N(1)	C(4)	1.44(2)
Mn(1)	O(7)	2.135(4)	N(2)	C(2)	1.46(2)
P(1)	O(4)	1.591(4)	N(2)	C(4)	1.09(2)
P(1)	O(5)	1.513(4)	C(1)	C(1)	1.563(9)
P(1)	O(6)	1.521(4)	C(2)	C(3)	1.21(1)
P(1)	O(7)	1.524(4)	C(3)	C(4)	1.42(2)

Bond angles in MnPOX-3

atom	atom	atom	angle (°)	atom	atom	atom	angle (°)
O(1)	Mn(1)	O(2)	87.1(2)	N(2)	N(1)	C(2)	69(1)
O(1)	Mn(1)	O(3)	89.4(2)	N(2)	N(1)	C(4)	48(1)
O(1)	Mn(1)	O(5)	90.5(2)	C(2)	N(1)	C(4)	41.1(7)
O(1)	Mn(1)	O(6)	179.1(1)	N(1)	N(2)	C(2)	83(1)
O(1)	Mn(1)	O(7)	86.4(2)	N(1)	N(2)	C(4)	101(2)
O(2)	Mn(1)	O(3)	73.2(1)	C(2)	N(2)	C(4)	46(1)
O(2)	Mn(1)	O(5)	86.9(1)	O(2)	C(1)	O(3)	127.2(4)
O(2)	Mn(1)	O(6)	93.5(1)	O(2)	C(1)	C(1)	115.6(6)
O(2)	Mn(1)	O(7)	171.1(1)	O(3)	C(1)	C(1)	117.3(6)
O(3)	Mn(1)	O(5)	160.0(1)	N(1)	C(2)	N(2)	28.5(5)
O(3)	Mn(1)	O(6)	90.1(1)	N(1)	C(2)	C(3)	136(1)
O(3)	Mn(1)	O(7)	100.7(1)	N(1)	C(2)	C(4)	63(1)
O(5)	Mn(1)	O(6)	90.2(1)	N(2)	C(2)	C(3)	125(1)
O(5)	Mn(1)	O(7)	99.2(1)	N(2)	C(2)	C(4)	48(1)
O(6)	Mn(1)	O(7)	92.9(1)	C(3)	C(2)	C(4)	77(1)
O(4)	P(1)	O(5)	108.8(2)	C(2)	C(3)	C(2)	180
O(4)	P(1)	O(6)	107.1(2)	C(2)	C(3)	C(4)	46.7(8)
O(4)	P(1)	O(7)	106.3(2)	C(2)	C(3)	C(4)	133.3(8)
O(5)	P(1)	O(6)	112.9(2)	C(2)	C(3)	C(4)	133.3(8)
O(5)	P(1)	O(7)	112.4(2)	C(2)	C(3)	C(4)	46.7(8)
O(6)	P(1)	O(7)	109.0(2)	C(4)	C(3)	C(4)	180
Mn(1)	O(2)	C(1)	117.2(3)	N(1)	C(4)	N(2)	30.8(8)
Mn(1)	O(3)	C(1)	116.2(3)	N(1)	C(4)	C(2)	76(1)
Mn(1)	O(5)	P(1)	142.4(2)	N(1)	C(4)	C(3)	128(1)
Mn(1)	O(6)	P(1)	141.7(2)	N(2)	C(4)	C(2)	86(2)
Mn(1)	O(7)	P(1)	133.1(2)	N(2)	C(4)	C(3)	141(2)
C(2)	C(4)	C(3)	56(1)				

Hydrogen Bonds in MnPOX-3

A	H	B	A-H (Å)	H...B (Å)	A...B (Å)	A-H...B (°)
O(1)	H(2)	O(3)	0.68(6)	2.11(6)	2.783(5)	170(8)
N(1)	H(16)	O(5)	1.27	1.95	2.747	116
N(2)	H(15)	O(1)	0.92	2.45	2.98	117
N(1)	H(12)	O(6)	0.95	2.33	3.075	135
N(2)	H(15)	O(7)	0.92	2.54	2.87	102

APPENDIX 4 - MnPOX-4

$[Mn_2(HPO_4)_2(C_2O_4)(H_2O)_2](H_3NC_6H_{10}NH_3)$

Atomic co-ordinates and temperature factors in MnPOX-4

atom	x	y	z	B(eq)
Mn(1)	0.5153(1)	0.17646(4)	0.50446(10)	1.35(2)
P(1)	1.0071(2)	0.24515(8)	0.3775(2)	1.26(3)
O(1)	0.5287(7)	0.1610(3)	0.2400(5)	2.30(9)
O(2)	0.7237(6)	0.0649(2)	0.5382(4)	1.87(8)
O(3)	0.7193(6)	-0.0691(2)	0.5150(4)	1.84(8)
O(4)	1.0048(6)	0.1605(2)	0.2874(5)	1.89(9)
O(5)	0.8234(6)	0.2440(2)	0.5008(4)	1.71(8)
O(6)	1.2373(5)	0.2557(2)	0.4507(4)	1.64(8)
O(7)	0.9585(6)	0.3068(2)	0.2502(4)	1.65(8)
N(1)	1.0100(8)	0.1310(3)	-0.2194(5)	1.7(1)
C(1)	0.6288(8)	-0.0010(4)	0.5160(5)	1.5(1)
C(2)	1.0223(8)	0.0769(3)	-0.0788(6)	1.4(1)
C(3)	0.7947(9)	0.0414(4)	-0.0456(7)	2.0(1)
C(4)	0.8028(9)	-0.0124(3)	0.1009(6)	1.9(1)
H(1)	0.44(1)	0.187(3)	0.175(7)	3(1)
H(2)	0.65(1)	0.167(4)	0.203(7)	2(1)
H(3)	1.04(1)	0.127(4)	0.333(7)	2(1)
H(4)	0.89(1)	0.180(4)	-0.194(7)	4(1)
H(5)	1.149(8)	0.152(3)	-0.242(5)	0.6(9)
H(6)	0.95(1)	0.100(4)	-0.301(7)	3(1)
H(7)	1.076(7)	0.111(3)	0.015(5)	0.7(9)
H(8)	0.689(8)	0.084(3)	-0.035(5)	1.2(9)
H(9)	0.744(9)	0.013(3)	-0.133(7)	2(1)
H(10)	0.848(9)	0.019(3)	0.193(6)	1(1)
H(11)	0.663(9)	-0.035(3)	0.128(6)	2(1)

Bond lengths in MnPOX-4

atom	atom	distance (Å)	atom	atom	distance (Å)
Mn(1)	O(1)	2.256(4)	P(2)	O(7)	1.516(4)
Mn(1)	O(2)	2.159(3)	O(3)	C(4)	1.251(7)
Mn(1)	O(3)	2.256(4)	O(4)	C(4)	1.258(7)
Mn(1)	O(4)	2.279(4)	N(1)	C(1)	1.495(7)
Mn(1)	O(6)	2.169(3)	C(1)	C(2)	1.512(7)
Mn(1)	O(7)	2.128(3)	C(1)	C(3)	1.511(7)
P(2)	O(2)	1.520(4)	C(2)	C(3)	1.532(8)
P(2)	O(5)	1.605(4)	C(4)	C(4)	1.562(9)
P(2)	O(6)	1.516(3)			

Bond angles in MnPOX-4

atom	atom	atom	angle (°)	atom	atom	atom	angle (°)
O(1)	Mn(1)	O(2)	90.5(1)	O(2)	P(2)	O(7)	111.2(2)
O(1)	Mn(1)	O(3)	90.5(1)	O(5)	P(2)	O(6)	107.5(2)
O(1)	Mn(1)	O(4)	82.2(1)	O(5)	P(2)	O(7)	104.9(2)
O(1)	Mn(1)	O(6)	83.9(1)	O(6)	P(2)	O(7)	112.4(2)
O(1)	Mn(1)	O(7)	172.8(1)	Mn(1)	O(2)	P(2)	129.5(2)
O(2)	Mn(1)	O(3)	87.8(1)	Mn(1)	O(3)	C(4)	117.1(3)
O(2)	Mn(1)	O(4)	158.9(1)	Mn(1)	O(4)	C(4)	116.4(3)
O(2)	Mn(1)	O(6)	109.4(1)	Mn(1)	O(6)	P(2)	135.1(2)
O(2)	Mn(1)	O(7)	95.0(1)	Mn(1)	O(7)	P(2)	138.8(2)
O(3)	Mn(1)	O(4)	72.6(1)	N(1)	C(1)	C(2)	111.2(4)
O(3)	Mn(1)	O(6)	161.9(1)	N(1)	C(1)	C(3)	110.2(4)
O(3)	Mn(1)	O(7)	94.3(1)	C(2)	C(1)	C(3)	111.7(4)
O(4)	Mn(1)	O(6)	89.6(1)	C(1)	C(2)	C(3)	109.6(4)
O(4)	Mn(1)	O(7)	94.1(1)	C(1)	C(3)	C(2)	110.9(4)
O(6)	Mn(1)	O(7)	89.9(1)	O(3)	C(4)	O(4)	126.9(4)
O(2)	P(2)	O(5)	108.2(2)	O(3)	C(4)	C(4)	117.0(6)
O(2)	P(2)	O(6)	112.3(2)	O(4)	C(4)	C(4)	116.2(6)

Hydrogen Bonds in MnPOX-4

A	H	B	A-H (Å)	H...B (Å)	A...B (Å)	A-H...B (°)
O(1)	H(1)	O(2)	0.89(6)	1.99(6)	2.843(5)	161(6)
O(5)	H(3)	O(4)	0.72(6)	2.14(6)	2.793(5)	152(7)
N(1)	H(4)	O(7)	0.92(5)	1.98(5)	2.888(6)	170(4)
N(1)	H(5)	O(3)	0.93(6)	2.00(6)	2.882(6)	157(5)
N(1)	H(6)	O(6)	1.09(6)	1.88(6)	2.887(6)	151(5)
O(1)	H(1)	O(6)	0.89(6)	2.80(6)	3.087(5)	101(4)

APPENDIX 5 - MnPOX-5

$[Mn_4(HPO_4)_2(C_2O_4)_3(H_2O)_2](H_3N(CH_2)_2NH_3)(H_2O)_2$

Atomic co-ordinates and temperature factors in MnPOX-5

atom	x	y	z	B(eq)
Mn(1)	1.19076(9)	-0.68967(9)	0.61460(8)	1.60(2)
Mn(2)	0.84283(9)	-0.96611(9)	0.74818(8)	1.37(2)
P(1)	1.0778(2)	-0.2671(2)	0.5903(1)	1.27(3)
O(1)	1.4157(4)	-0.6399(4)	0.7039(4)	2.09(8)
O(2)	1.3444(4)	-0.9384(4)	0.6493(4)	2.14(8)
O(3)	1.0311(4)	-0.8415(4)	0.8382(3)	1.70(7)
O(4)	1.0744(4)	-0.4595(4)	0.6350(4)	1.86(8)
O(5)	1.3454(5)	-0.6416(6)	0.3914(5)	2.42(9)
O(6)	0.8138(4)	-1.0985(4)	0.9836(4)	2.02(8)
O(7)	0.5904(4)	-1.0531(4)	0.7169(4)	1.93(8)
O(8)	1.6538(4)	-0.7610(4)	0.7830(4)	2.13(8)
O(9)	1.2748(4)	-0.2141(5)	0.5650(4)	2.14(9)
O(10)	0.9717(4)	-0.1893(4)	0.7099(3)	1.66(7)
O(11)	1.0166(4)	-0.1985(4)	0.4458(3)	1.61(7)
O(12)	0.5254(10)	-0.675(1)	1.0501(9)	10.2(3)
N(1)	0.8169(6)	-0.4842(7)	0.8976(5)	3.4(1)
C(1)	1.5196(6)	-0.7620(6)	0.7308(5)	1.6(1)
C(2)	1.4817(6)	-0.9330(6)	0.6951(5)	1.6(1)
C(3)	1.0639(6)	-0.9265(6)	0.9589(5)	1.5(1)
C(4)	0.9043(8)	-0.5198(8)	1.0242(6)	2.8(1)
H(1)	1.413(9)	-0.585(9)	0.367(8)	3(1)
H(2)	1.381(8)	-0.735(8)	0.364(7)	3(1)
H(3)	0.8585	-0.3806	0.8326	4.4
H(4)	0.6956	-0.4787	0.9275	4.4
H(5)	0.846	-0.5759	0.847	4.4
H(6)	0.845(6)	-0.460(6)	1.086(6)	1(1)
H(7)	0.888(7)	-0.647(7)	1.076(6)	2(1)
H(8)	1.284(7)	-0.126(7)	0.585(6)	1(1)

Bond lengths in MnPOX-5

atom	atom	distance (Å)	atom	atom	distance (Å)
Mn(1)	O(1)	2.205(3)	O(2)	C(2)	1.248(6)
Mn(1)	O(2)	2.258(3)	O(3)	C(3)	1.269(6)
Mn(1)	O(3)	2.362(3)	O(5)	H(1)	0.69(7)
Mn(1)	O(4)	2.045(3)	O(5)	H(2)	0.87(7)
Mn(1)	O(5)	2.208(4)	O(6)	C(3)	1.247(6)
Mn(1)	O(11)	2.144(3)	O(7)	C(2)	1.254(6)
Mn(2)	O(3)	2.246(3)	O(8)	C(1)	1.254(6)
Mn(2)	O(6)	2.242(3)	O(9)	H(8)	0.79(5)
Mn(2)	O(7)	2.237(4)	N(1)	C(4)	1.478(8)
Mn(2)	O(8)	2.186(3)	N(1)	H(3)	0.948
Mn(2)	O(10)	2.076(3)	N(1)	H(4)	0.937
Mn(2)	O(11)	2.158(3)	N(1)	H(5)	0.969
P(1)	O(4)	1.505(3)	C(1)	C(2)	1.554(7)
P(1)	O(9)	1.582(4)	C(3)	C(3)	1.55(1)
P(1)	O(10)	1.519(3)	C(4)	C(4)	1.51(1)
P(1)	O(11)	1.532(3)	C(4)	H(6)	0.89(5)
O(1)	C(1)	1.247(6)	C(4)	H(7)	1.03(6)

Bond angles in MnPOX-5

atom	atom	atom	angle (°)	atom	atom	atom	angle (°)
O(1)	Mn(1)	O(2)	74.1(1)	O(3)	C(3)	C(3)	115.6(5)
O(1)	Mn(1)	O(3)	95.5(1)	O(6)	C(3)	C(3)	118.2(5)
O(1)	Mn(1)	O(4)	92.6(1)	N(1)	C(4)	C(4)	110.4(6)
O(1)	Mn(1)	O(5)	92.0(2)	O(7)	Mn(2)	O(11)	112.7(1)
O(1)	Mn(1)	O(11)	166.0(1)	O(8)	Mn(2)	O(10)	166.5(1)
O(2)	Mn(1)	O(3)	78.7(1)	O(8)	Mn(2)	O(11)	91.0(1)
O(2)	Mn(1)	O(4)	163.9(1)	O(10)	Mn(2)	O(11)	95.0(1)
O(2)	Mn(1)	O(5)	84.8(1)	O(4)	P(1)	O(9)	106.8(2)
O(2)	Mn(1)	O(11)	93.0(1)	O(4)	P(1)	O(10)	110.6(2)
O(3)	Mn(1)	O(4)	93.8(1)	O(4)	P(1)	O(11)	112.0(2)
O(3)	Mn(1)	O(5)	159.3(1)	O(9)	P(1)	O(10)	108.9(2)
O(3)	Mn(1)	O(11)	76.0(1)	O(9)	P(1)	O(11)	106.8(2)
O(4)	Mn(1)	O(5)	105.1(2)	O(10)	P(1)	O(11)	111.4(2)
O(4)	Mn(1)	O(11)	99.1(1)	Mn(1)	O(1)	C(1)	116.6(3)
O(5)	Mn(1)	O(11)	92.5(1)	Mn(1)	O(2)	C(2)	115.1(3)
O(3)	Mn(2)	O(6)	73.7(1)	Mn(1)	O(3)	Mn(2)	97.6(1)
O(3)	Mn(2)	O(7)	159.9(1)	Mn(1)	O(3)	C(3)	137.1(3)
O(3)	Mn(2)	O(8)	89.0(1)	Mn(2)	O(3)	C(3)	114.5(3)
O(3)	Mn(2)	O(10)	104.0(1)	Mn(1)	O(4)	P(1)	148.7(2)
O(3)	Mn(2)	O(11)	78.3(1)	Mn(2)	O(6)	C(3)	114.1(3)
O(6)	Mn(2)	O(7)	96.1(1)	Mn(2)	O(7)	C(2)	112.8(3)
O(6)	Mn(2)	O(8)	95.4(1)	Mn(2)	O(8)	C(1)	114.7(3)
O(6)	Mn(2)	O(10)	85.0(1)	Mn(2)	O(10)	P(1)	142.6(2)
O(6)	Mn(2)	O(11)	151.2(1)	Mn(1)	O(11)	Mn(2)	107.5(1)
O(7)	Mn(2)	O(8)	74.4(1)	Mn(1)	O(11)	P(1)	123.1(2)
O(7)	Mn(2)	O(10)	92.1(1)	Mn(2)	O(11)	P(1)	127.3(2)
O(2)	C(2)	O(7)	126.2(5)	O(1)	C(1)	O(8)	126.6(5)
O(2)	C(2)	C(1)	116.7(4)	O(1)	C(1)	C(2)	117.4(4)
O(7)	C(2)	C(1)	117.1(4)	O(8)	C(1)	C(2)	116.0(4)
O(3)	C(3)	O(6)	126.2(4)				

Hydrogen Bonds in MnPOX-5

A	H	B	A-H (Å)	H...B (Å)	A...B (Å)	A-H...B (°)
O(5)	H(1)	O(1)	0.69(7)	2.21(7)	2.887(6)	167(8)
O(5)	H(2)	O(7)	0.87(7)	2.02(7)	2.868(5)	166(6)
N(1)	H(3)	O(10)	0.95	1.86	2.797	172
N(1)	H(4)	O(12)	0.94	2.07	2.901	147
N(1)	H(3)	O(4)	0.95	2.46	2.881	107

APPENDIX 6 - MnPOX-6

$[Mn_4(HPO_4)_2(C_2O_4)_3(H_2O)_2](C_4H_8(NH_2)_2)(H_2O)_2$

Atomic co-ordinates and temperature factors in MnPOX-6

atom	x	y	z	B(eq)
Mn(1)	1.1781(1)	-0.69160(10)	0.62824(9)	0.80(2)
Mn(2)	0.8411(1)	-0.9672(1)	0.74808(9)	0.73(2)
P(1)	1.0736(2)	-0.2703(2)	0.5960(2)	0.69(2)
O(1)	1.4122(5)	-0.6390(5)	0.7043(5)	1.26(8)
O(2)	1.3399(5)	-0.9360(5)	0.6463(5)	1.32(8)
O(3)	1.0339(5)	-0.8472(5)	0.8361(4)	0.99(7)
O(4)	1.0575(6)	-0.4621(5)	0.6464(5)	1.11(8)
O(5i)	1.357(1)	-0.653(1)	0.410(1)	1.1(2)
O(5ii)	1.290(1)	-0.584(1)	0.403(1)	1.3(2)
O(6)	0.8101(5)	-1.0970(5)	0.9856(4)	1.07(8)
O(7)	0.5907(5)	-1.0484(5)	0.7128(5)	1.30(8)
O(8)	1.6541(5)	-0.7582(6)	0.7792(5)	1.46(9)
O(9)	1.2737(6)	-0.2266(6)	0.5786(5)	1.34(9)
O(10)	0.9684(6)	-0.1859(5)	0.7097(5)	1.31(8)
O(11)	1.0238(5)	-0.2031(5)	0.4465(4)	0.95(7)
N(1i)	0.273(2)	0.451(1)	0.123(1)	1.3(2)
N(1ii)	0.559(2)	0.365(1)	0.156(1)	1.1(2)
C(1)	1.5191(8)	-0.7610(7)	0.7294(6)	1.1(1)
C(2)	1.4795(7)	-0.9299(7)	0.6930(6)	0.83(9)
C(3)	1.0669(7)	-0.9277(6)	0.9587(6)	0.78(9)
C(4)	0.4513(10)	0.424(1)	0.0510(7)	2.3(1)
C(5i)	0.169(2)	0.540(2)	0.014(1)	1.1(2)
C(5ii)	0.730(2)	0.304(2)	0.081(1)	1.0(2)
H(1i)	0.28(2)	0.55(2)	0.22(2)	1.4795
H(1ii)	0.61(2)	0.41(2)	0.22(2)	1.1529
H(2i)	0.28(2)	0.43(2)	0.19(2)	1.4795
H(2ii)	0.49(2)	0.29(2)	0.24(2)	1.1529
H(3i)	0.09(2)	0.54(2)	0.07(2)	1.4317
H(3ii)	0.78(2)	0.29(2)	0.11(2)	1.0607
H(4i)	0.18(2)	0.48(2)	-0.06(2)	1.4317
H(4ii)	0.72(2)	0.26(2)	0.00(2)	1.0607
H(5i)	0.55(3)	0.33(3)	0.12(3)	2.6651
H(5ii)	0.35(3)	0.51(3)	0.12(2)	4
H(6i)	0.49(2)	0.33(2)	-0.01(2)	2.6651
H(6ii)	0.53(3)	0.36(3)	0.10(3)	4
H(7)	1.322(10)	-0.257(10)	0.543(8)	0.5036

Bond lengths in MnPOX-6

atom	atom	distance (Å)	atom	atom	distance (Å)
Mn(1)	O(1)	2.188(4)	O(9)	H(7)	0.55(7)
Mn(1)	O(2)	2.269(4)	N(1i)	C(4)	1.46(1)
Mn(1)	O(3)	2.225(4)	N(1i)	C(5i)	1.47(2)
Mn(1)	O(4)	2.060(4)	N(1i)	H(2i)	0.7(2)
Mn(1)	O(5i)	2.258(9)	N(1i)	H(5ii)	0.7(2)
Mn(1)	O(5ii)	2.170(9)	N(1ii)	C(4)	1.42(1)
Mn(1)	O(11)	2.142(4)	N(1ii)	C(5ii)	1.50(2)
Mn(2)	O(3)	2.227(4)	N(1ii)	H(1ii)	0.9(2)
Mn(2)	O(6)	2.261(4)	N(1ii)	H(2ii)	1.0(2)
Mn(2)	O(7)	2.199(4)	N(1ii)	H(5i)	0.5(2)
Mn(2)	O(8)	2.203(4)	N(1ii)	H(6ii)	0.6(3)
Mn(2)	O(10)	2.052(4)	C(1)	C(2)	1.548(8)
Mn(2)	O(11)	2.165(4)	C(3)	C(3)	1.56(1)
P(1)	O(4)	1.510(4)	C(4)	C(4)	1.51(2)
P(1)	O(9)	1.581(5)	C(4)	H(5i)	1.3(2)
P(1)	O(10)	1.516(4)	C(4)	H(5ii)	1.2(2)
P(1)	O(11)	1.537(4)	C(4)	H(6i)	1.1(2)
O(1)	C(1)	1.262(7)	C(4)	H(6ii)	0.9(2)
O(2)	C(2)	1.262(7)	C(5i)	C(5ii)	1.52(2)
O(3)	C(3)	1.277(7)	C(5i)	H(3i)	0.7(1)
O(5i)	O(5ii)	0.74(1)	C(5i)	H(4i)	0.9(2)
O(6)	C(3)	1.232(7)	C(5ii)	H(3ii)	0.5(2)
O(7)	C(2)	1.258(7)	C(5ii)	H(4ii)	0.9(2)
O(8)	C(1)	1.240(7)			

Bond angles in MnPOX-6

atom	atom	atom	angle (°)	atom	atom	atom	angle (°)
O(1)	Mn(1)	O(2)	74.6(1)	O(4)	P(1)	O(9)	107.0(3)
O(1)	Mn(1)	O(3)	98.2(2)	O(4)	P(1)	O(10)	110.0(2)
O(1)	Mn(1)	O(4)	94.5(2)	O(4)	P(1)	O(11)	112.0(2)
O(1)	Mn(1)	O(5i)	84.8(3)	O(9)	P(1)	O(10)	108.2(3)
O(1)	Mn(1)	O(5ii)	93.3(3)	O(9)	P(1)	O(11)	106.7(2)
O(1)	Mn(1)	O(11)	167.3(2)	O(10)	P(1)	O(11)	112.7(2)
O(2)	Mn(1)	O(3)	79.7(2)	Mn(1)	O(1)	C(1)	116.9(4)
O(2)	Mn(1)	O(4)	167.7(2)	Mn(1)	O(2)	C(2)	114.0(4)
O(2)	Mn(1)	O(5i)	76.7(3)	Mn(1)	O(3)	Mn(2)	98.4(2)
O(2)	Mn(1)	O(5ii)	95.4(3)	Mn(1)	O(3)	C(3)	138.1(4)
O(2)	Mn(1)	O(11)	92.8(1)	Mn(2)	O(3)	C(3)	116.3(3)
O(3)	Mn(1)	O(4)	96.6(2)	Mn(1)	O(4)	P(1)	144.6(3)
O(3)	Mn(1)	O(5i)	154.5(3)	Mn(1)	O(5i)	O(5ii)	74(1)
O(3)	Mn(1)	O(5ii)	165.8(3)	Mn(1)	O(5ii)	O(5i)	87(1)
O(3)	Mn(1)	O(11)	79.5(1)	Mn(2)	O(6)	C(3)	113.8(3)
O(4)	Mn(1)	O(5i)	108.4(3)	Mn(2)	O(7)	C(2)	114.1(4)
O(4)	Mn(1)	O(5ii)	90.7(3)	Mn(2)	O(8)	C(1)	114.2(4)
O(4)	Mn(1)	O(11)	98.2(2)	Mn(2)	O(10)	P(1)	145.5(3)
O(5i)	Mn(1)	O(5ii)	19.1(3)	Mn(1)	O(11)	Mn(2)	102.9(2)
O(5i)	Mn(1)	O(11)	92.0(3)	Mn(1)	O(11)	P(1)	124.5(2)
O(5ii)	Mn(1)	O(11)	87.4(3)	Mn(2)	O(11)	P(1)	131.3(2)
O(3)	Mn(2)	O(6)	73.3(1)	C(4)	N(1i)	C(5i)	109.5(9)
O(3)	Mn(2)	O(7)	161.0(2)	C(4)	N(1ii)	C(5ii)	108.2(9)
O(3)	Mn(2)	O(8)	89.5(2)	O(1)	C(1)	O(8)	126.3(6)
O(3)	Mn(2)	O(10)	103.0(2)	O(1)	C(1)	C(2)	117.0(5)
O(3)	Mn(2)	O(11)	78.9(1)	O(8)	C(1)	C(2)	116.8(5)
O(6)	Mn(2)	O(7)	97.5(2)	O(2)	C(2)	O(7)	126.2(5)
O(6)	Mn(2)	O(8)	95.4(2)	O(2)	C(2)	C(1)	117.4(5)
O(6)	Mn(2)	O(10)	86.3(2)	O(7)	C(2)	C(1)	116.5(5)
O(6)	Mn(2)	O(11)	152.0(2)	O(3)	C(3)	O(6)	127.0(5)
O(7)	Mn(2)	O(8)	74.6(2)	O(3)	C(3)	C(3)	113.8(6)
O(7)	Mn(2)	O(10)	92.7(2)	O(6)	C(3)	C(3)	119.2(6)
O(7)	Mn(2)	O(11)	110.3(2)	N(1i)	C(4)	N(1ii)	109.7(8)
O(8)	Mn(2)	O(10)	167.3(2)	N(1i)	C(4)	C(4)	118(1)
O(8)	Mn(2)	O(11)	88.3(2)	N(1ii)	C(4)	C(4)	104.0(8)
O(10)	Mn(2)	O(11)	96.1(2)	N(1i)	C(5i)	C(5ii)	109(1)
				N(1ii)	C(5ii)	C(5i)	108(1)

Hydrogen Bonds in MnPOX-6

A	H	B	A-H (Å)	H...B (Å)	A...B (Å)	A-H...B (°)
O(9)	H(7)	O(5i)	0.55(7)	2.65(8)	2.99(1)	124(13)
N(1i)	H(2i)	O(5ii)	0.7(2)	2.0(2)	2.69(1)	171(19)
N(1ii)	H(1ii)	O(1)	0.9(2)	2.1(2)	2.90(1)	136(12)
N(1ii)	H(2ii)	O(5i)	1.0(2)	1.9(1)	2.63(1)	129(12)
N(1ii)	H(5i)	O(7)	0.5(2)	2.6(2)	2.77(1)	106(30)
N(1ii)	H(1ii)	O(9)	0.9(2)	2.4(2)	3.06(1)	123(11)
N(1i)	H(2i)	O(5i)	0.7(2)	2.2(2)	2.90(1)	165(17)
N(1i)	H(2i)	O(4)	0.7(2)	2.8(2)	3.07(1)	110(15)
N(1ii)	H(2ii)	O(5ii)	1.0(2)	2.4(1)	2.95(2)	119(10)
N(1i)	H(5ii)	O(8)	0.7(2)	2.5(2)	2.98(1)	127(22)

APPENDIX 7 - MnPOX-8

$Mn_2(H_2PO_4)_2(C_2O_4)$

Atomic co-ordinates and temperature factors in MnPOX-8

atom	x	y	z	B(eq)
Mn(1)	0	0.19222(4)	0.5	1.17(3)
P(1)	0	0.32914(7)	0	1.05(3)
O(1)	0.1748(3)	0.07444(13)	0.4072(4)	1.47(5)
O(2)	0.2048(4)	0.3902(2)	-0.0060(4)	2.00(6)
O(3)	0.1110(3)	0.27588(13)	0.2504(3)	1.35(5)
C(1)	0.1019(6)	0	0.4453(7)	1.22(9)
H(1)	0.2115(83)	0.4003(31)	-0.1185(97)	4.42(16)

Bond lengths in MnPOX-8

atom	atom	distance (Å)	atom	atom	distance (Å)
Mn(1)	O(3)	2.151(2)	P(1)	O(2)	1.553(2)
Mn(1)	O(3)	2.151(2)	P(1)	O(2)	1.553(2)
Mn(1)	O(1)	2.221(2)	O(1)	C(1)	1.251(3)
Mn(1)	O(1)	2.221(2)	C(1)	O(1)	1.251(3)
Mn(1)	O(3)	2.283(2)	C(1)	C(1)	1.563(7)
Mn(1)	O(3)	2.283(2)	O(2)	H(1)	0.65(5)
P(1)	O(3)	1.517(2)	O(3)	Mn(1)	2.283(2)
P(1)	O(3)	1.517(2)			

Bond angles in MnPOX-8

atom	atom	atom	angle (°)	atom	atom	atom	angle (°)
O(3)	Mn(1)	O(3)	108.3(1)	O(3)	P(1)	O(3)	116.1(2)
O(3)	Mn(1)	O(1)	91.75(7)	O(3)	P(1)	O(2)	104.5(1)
O(3)	Mn(1)	O(1)	154.89(7)	O(3)	P(1)	O(2)	112.1(1)
O(3)	Mn(1)	O(1)	154.89(7)	O(3)	P(1)	O(2)	112.1(1)
O(3)	Mn(1)	O(1)	91.75(7)	O(3)	P(1)	O(2)	104.5(1)
O(1)	Mn(1)	O(1)	73.98(9)	O(2)	P(1)	O(2)	107.4(2)
O(3)	Mn(1)	O(3)	89.45(6)	C(1)	O(1)	Mn(1)	116.7(2)
O(3)	Mn(1)	O(3)	76.29(7)	O(1)	C(1)	O(1)	127.3(3)
O(1)	Mn(1)	O(3)	120.06(7)	O(1)	C(1)	C(1)	116.3(2)
O(1)	Mn(1)	O(3)	80.52(7)	O(1)	C(1)	C(1)	116.3(2)
O(3)	Mn(1)	O(3)	76.29(7)	P(1)	O(2)	H(1)	120(4)
O(3)	Mn(1)	O(3)	89.45(6)	P(1)	O(3)	Mn(1)	138.9(1)
O(1)	Mn(1)	O(3)	80.52(7)	P(1)	O(3)	Mn(1)	116.0(1)
O(1)	Mn(1)	O(3)	120.06(7)	Mn(1)	O(3)	Mn(1)	103.71(7)
O(3)	Mn(1)	O(3)	155.7(1)				

APPENDIX 8 - MnOX-1

$Mn_2(C_2O_4)_3(C_4H_8(NH_2)_2)$

Atomic co-ordinates and temperature factors in MnOX-1

atom	x	y	z	B(eq)
Mn(1)	0.44784(8)	0.36712(6)	0.85331(6)	0.776(9)
O(1)	0.5218(5)	0.6054(3)	0.6703(3)	1.32(4)
O(2)	0.5513(4)	0.7109(3)	0.3981(3)	1.06(4)
O(3)	0.2754(4)	0.5382(3)	1.0335(3)	0.95(4)
O(4)	-0.0639(4)	0.5882(3)	1.1875(3)	1.26(4)
O(5)	0.6838(4)	0.1249(3)	0.8494(3)	1.35(4)
O(6)	0.7219(5)	-0.1543(3)	0.9616(3)	1.57(5)
N(1)	0.0550(6)	0.1139(4)	0.6095(4)	1.48(5)
C(1)	0.5214(5)	0.5908(4)	0.5221(4)	0.92(5)
C(2)	0.0579(5)	0.5381(4)	1.0654(4)	0.84(5)
C(3)	0.3819(5)	0.0099(4)	1.0541(4)	1.01(5)
C(4)	0.1514(6)	-0.0689(5)	0.6197(5)	1.70(7)
C(5)	-0.0096(6)	-0.1832(5)	0.5639(5)	1.62(6)
H(1)	-0.073(8)	0.123(6)	0.688(6)	1.3497
H(2)	0.161(9)	0.155(6)	0.636(6)	1.3497
H(3)	0.308(9)	-0.046(7)	0.535(6)	1.9767
H(4)	0.181(10)	-0.116(8)	0.746(7)	3.0732
H(5)	0.06(1)	-0.308(8)	0.564(7)	2.9816
H(6)	-0.160(7)	-0.186(5)	0.627(5)	0.4715

Bond lengths in MnOX-1

atom	atom	distance (Å)	atom	atom	distance (Å)
Mn(1)	O(1)	2.224(2)	N(1)	C(4)	1.492(5)
Mn(1)	O(2)	2.225(2)	N(1)	C(5)	1.497(5)
Mn(1)	O(3)	2.216(2)	N(1)	H(1)	0.92(5)
Mn(1)	O(3)	2.220(2)	N(1)	H(2)	0.80(5)
Mn(1)	O(4)	2.347(3)	C(1)	C(1)	1.554(6)
Mn(1)	O(5)	2.269(3)	C(2)	C(2)	1.561(6)
Mn(1)	O(6)	2.248(3)	C(3)	C(3)	1.547(6)
O(1)	C(1)	1.233(4)	C(4)	C(5)	1.511(5)
O(2)	C(1)	1.272(4)	C(4)	H(3)	1.08(5)
O(3)	C(2)	1.276(4)	C(4)	H(4)	1.08(6)
O(4)	C(2)	1.233(4)	C(5)	H(5)	1.03(6)
O(5)	C(3)	1.260(4)	C(5)	H(6)	0.96(4)
O(6)	C(3)	1.243(4)			

Bond angles in MnOX-1

atom	atom	atom	angle (°)	atom	atom	atom	angle (°)
O(1)	Mn(1)	O(2)	74.03(8)	Mn(1)	O(1)	C(1)	116.1(2)
O(1)	Mn(1)	O(3)	87.99(9)	Mn(1)	O(2)	C(1)	116.4(2)
O(1)	Mn(1)	O(3)	81.82(9)	Mn(1)	O(3)	Mn(1)	105.72(9)
O(1)	Mn(1)	O(4)	87.76(9)	Mn(1)	O(3)	C(2)	117.3(2)
O(1)	Mn(1)	O(5)	121.36(9)	Mn(1)	O(3)	C(2)	135.9(2)
O(1)	Mn(1)	O(6)	164.9(1)	Mn(1)	O(4)	C(2)	112.0(2)
O(2)	Mn(1)	O(3)	144.28(8)	Mn(1)	O(5)	C(3)	117.3(2)
O(2)	Mn(1)	O(3)	130.92(9)	Mn(1)	O(6)	C(3)	117.3(2)
O(2)	Mn(1)	O(4)	76.63(9)	C(4)	N(1)	C(5)	111.5(3)
O(2)	Mn(1)	O(5)	75.27(9)	O(1)	C(1)	O(2)	126.6(3)
O(2)	Mn(1)	O(6)	105.96(9)	O(1)	C(1)	C(1)	118.2(3)
O(3)	Mn(1)	O(3)	74.28(9)	O(2)	C(1)	C(1)	115.1(3)
O(3)	Mn(1)	O(4)	71.97(8)	O(3)	C(2)	O(4)	126.8(3)
O(3)	Mn(1)	O(5)	139.36(9)	O(3)	C(2)	C(2)	114.5(3)
O(3)	Mn(1)	O(6)	83.73(9)	O(4)	C(2)	C(2)	118.7(3)
O(3)	Mn(1)	O(4)	144.94(9)	O(5)	C(3)	O(6)	126.9(3)
O(3)	Mn(1)	O(5)	82.33(9)	O(5)	C(3)	C(3)	115.3(3)
O(3)	Mn(1)	O(6)	107.84(9)	O(6)	C(3)	C(3)	117.8(3)
O(4)	Mn(1)	O(5)	130.71(9)	N(1)	C(4)	C(5)	110.0(3)
O(4)	Mn(1)	O(6)	77.71(9)	N(1)	C(5)	C(4)	110.3(3)
O(5)	Mn(1)	O(6)	72.29(9)				

Hydrogen Bonds in MnOX-1

A	H	B	A-H (Å)	H...B (Å)	A...B (Å)	A-H...B (°)
N(1)	H(1)	O(5)	0.92(5)	1.80(5)	2.716(4)	176(5)
N(1)	H(2)	O(2)	0.80(5)	2.02(5)	2.771(4)	156(5)
N(1)	H(1)	O(4)	0.92(5)	2.82(5)	3.050(4)	151(2)

APPENDIX 9 - GdOX-1

$[Gd(C_2O_4)_2(H_2O)](CH_3NH_2CH_3)(H_2O)_3$

Atomic co-ordinates and temperature factors in GdOX-1

atom	x	y	z	B(eq)
Gd(1)	0.2860(1)	0.01485(8)	0.16866(9)	1.48(2)
O(1)	0.187(2)	-0.103(1)	0.299(1)	2.4(5)
O(2)	0.362(2)	-0.181(1)	0.170(1)	1.7(4)
O(3)	0.142(2)	-0.285(1)	0.344(1)	2.5(5)
O(4)	0.308(2)	-0.361(1)	0.204(1)	2.2(5)
O(5)	0.453(1)	0.021(1)	0.3470(9)	2.3(3)
O(6)	0.321(1)	0.012(1)	-0.0213(8)	2.2(3)
O(7)	0.465(1)	-0.011(1)	-0.1446(8)	1.7(3)
O(8)	0.086(2)	0.119(1)	0.067(1)	1.9(4)
O(9)	-0.101(2)	0.110(1)	-0.067(2)	2.6(5)
O(10)	0.170(2)	-0.009(2)	-0.496(1)	6.0(5)
O(11)	0.085(2)	-0.339(1)	-0.036(1)	4.5(5)
O(12)	0.420(2)	-0.283(1)	-0.031(1)	5.8(6)
N(1)	0.270(2)	-0.132(2)	-0.304(1)	3.6(5)
C(1)	0.201(3)	-0.208(2)	0.293(2)	1.7(7)
C(2)	0.302(3)	-0.252(2)	0.216(2)	2.0(7)
C(3)	0.431(2)	-0.001(2)	-0.049(1)	1.9(4)
C(4)	-0.006(4)	0.063(1)	-0.002(3)	1.9(4)
C(5)	0.154(3)	-0.126(2)	-0.247(2)	5.5(8)
C(6)	0.310(3)	-0.247(2)	-0.335(3)	7.1(9)
H(1)	0.47(2)	0.08(2)	0.41(1)	3.0064
H(2)	0.47(2)	-0.06(2)	0.37(1)	3.0064
H(3)	0.134	-0.0477	-0.2326	6.6275
H(4)	0.0736	-0.1595	-0.2897	6.6275
H(5)	0.1748	-0.1653	-0.178	6.6275
H(6)	0.3484	-0.0989	-0.2578	4.2653
H(7)	0.2476	-0.0889	-0.3694	4.2653
H(8)	0.3361	-0.2903	-0.2685	8.4942
H(9)	0.3876	-0.2407	-0.3723	8.4942
H(10)	0.2332	-0.2813	-0.3791	8.4942

Bond lengths in GdOX-1

atom	atom	distance (Å)	atom	atom	distance (Å)
Gd(1)	O(1)	2.42(2)	O(7)	C(3)	1.27(2)
Gd(1)	O(2)	2.40(1)	O(8)	C(4)	1.30(4)
Gd(1)	O(3)	2.45(1)	O(9)	C(4)	1.24(4)
Gd(1)	O(4)	2.41(2)	N(1)	C(5)	1.42(3)
Gd(1)	O(5)	2.50(1)	N(1)	C(6)	1.46(3)
Gd(1)	O(6)	2.41(1)	N(1)	H(6)	0.955
Gd(1)	O(7)	2.47(1)	N(1)	H(7)	0.943
Gd(1)	O(8)	2.44(2)	C(1)	C(2)	1.54(2)
Gd(1)	O(9)	2.48(2)	C(3)	C(3)	1.64(3)
O(1)	C(1)	1.24(2)	C(4)	C(4)	1.49(4)
O(2)	C(2)	1.21(3)	C(5)	H(3)	0.951
O(3)	C(1)	1.28(3)	C(5)	H(4)	0.949
O(4)	C(2)	1.29(2)	C(5)	H(5)	0.954
O(5)	H(1)	1.0(2)	C(6)	H(8)	0.962
O(5)	H(2)	0.9(2)	C(6)	H(9)	0.936
O(6)	C(3)	1.17(2)	C(6)	H(10)	0.937

Bond angles in GdOX-1

atom	atom	atom	angle (°)	atom	atom	atom	angle (°)
O(1)	Gd(1)	O(2)	66.7(5)	O(5)	Gd(1)	O(9)	140.0(5)
O(1)	Gd(1)	O(3)	137.0(5)	O(6)	Gd(1)	O(7)	66.0(3)
O(1)	Gd(1)	O(4)	71.8(4)	O(6)	Gd(1)	O(8)	74.7(5)
O(1)	Gd(1)	O(5)	72.8(5)	O(6)	Gd(1)	O(9)	73.0(5)
O(1)	Gd(1)	O(6)	139.6(5)	O(7)	Gd(1)	O(8)	130.8(5)
O(1)	Gd(1)	O(7)	124.2(5)	O(7)	Gd(1)	O(9)	124.2(5)
O(1)	Gd(1)	O(8)	104.8(6)	O(8)	Gd(1)	O(9)	65.9(4)
O(1)	Gd(1)	O(9)	70.6(6)	Gd(1)	O(1)	C(1)	118(1)
O(2)	Gd(1)	O(3)	145.0(4)	Gd(1)	O(2)	C(2)	119(2)
O(2)	Gd(1)	O(4)	135.5(5)	Gd(1)	O(3)	C(1)	119(2)
O(2)	Gd(1)	O(5)	82.3(5)	Gd(1)	O(4)	C(2)	120(2)
O(2)	Gd(1)	O(6)	84.5(5)	Gd(1)	O(6)	C(3)	124(1)
O(2)	Gd(1)	O(7)	71.3(5)	Gd(1)	O(7)	C(3)	120.7(9)
O(2)	Gd(1)	O(8)	133.9(5)	Gd(1)	O(8)	C(4)	119(2)
O(2)	Gd(1)	O(9)	68.7(5)	Gd(1)	O(9)	C(4)	117(1)
O(3)	Gd(1)	O(4)	66.8(5)	C(5)	N(1)	C(6)	116(2)
O(3)	Gd(1)	O(5)	83.0(6)	O(1)	C(1)	O(3)	127(2)
O(3)	Gd(1)	O(6)	82.4(5)	O(1)	C(1)	C(2)	117(2)
O(3)	Gd(1)	O(7)	73.7(5)	O(3)	C(1)	C(2)	116(2)
O(3)	Gd(1)	O(8)	72.8(6)	O(2)	C(2)	O(4)	126(3)
O(3)	Gd(1)	O(9)	136.0(6)	O(2)	C(2)	C(1)	117(2)
O(4)	Gd(1)	O(5)	70.8(5)	O(4)	C(2)	C(1)	116(2)
O(4)	Gd(1)	O(6)	139.5(5)	O(6)	C(3)	O(7)	131(1)
O(4)	Gd(1)	O(7)	124.2(6)	O(6)	C(3)	C(3)	117(2)
O(4)	Gd(1)	O(8)	71.6(6)	O(7)	C(3)	C(3)	112(2)
O(4)	Gd(1)	O(9)	111.5(6)	O(8)	C(4)	O(9)	124(2)
O(5)	Gd(1)	O(6)	132.6(4)	O(8)	C(4)	C(4)	116(5)
O(5)	Gd(1)	O(7)	66.7(4)	O(9)	C(4)	C(4)	120(4)
O(5)	Gd(1)	O(8)	140.9(5)				

Hydrogen Bonds in GdOX-1

A	H	B	A-H (Å)	H...B (Å)	A...B (Å)	A-H...B (°)
O(5)	H(1)	O(11)	1.0(2)	2.0(2)	2.91(2)	152(15)
N(1)	H(6)	O(7)	0.96	1.94	2.87(2)	163
N(1)	H(7)	O(10)	0.94	1.86	2.79(3)	169
O(5)	H(1)	O(4)	1.0(2)	2.9(2)	2.84(2)	127(6)

APPENDIX 10 - $FePO_4$-1

$K_3[Fe_4O(OH)(PO_4)_4(H_2O)_2](H_2O)_2$

Atomic co-ordinates and temperature factors in $FePO_4$-1

atom	x	y	z	B(eq)
Fe(1)	0.39226(4)	0.54320(3)	-0.12856(3)	0.443(4)
Fe(2)	0.59242(4)	0.21234(3)	-0.17144(3)	0.462(4)
K(1)	0.5	0.5	-0.5	2.04(2)
K(2)	1.02401(9)	0.33998(9)	-0.1200(1)	2.40(2)
P(1)	0.28836(7)	0.31101(6)	-0.35786(6)	0.470(7)
P(2)	0.71445(7)	0.50820(6)	-0.15728(6)	0.476(8)
O(1)	0.4677(2)	0.0758(2)	-0.1022(2)	1.35(3)
O(2)	0.4427(2)	0.2606(2)	-0.3329(2)	0.86(2)
O(3)	0.2437(2)	0.3352(2)	-0.5137(2)	0.87(3)
O(4)	0.2798(2)	0.4474(2)	-0.2829(2)	0.90(2)
O(5)	0.3127(2)	0.7139(2)	-0.1984(2)	0.88(2)
O(6)	0.5057(2)	0.6387(2)	0.0507(2)	0.63(2)
O(7)	0.5684(2)	0.5752(2)	-0.2110(2)	0.78(2)
O(8)	0.7440(2)	0.5001(2)	0.0023(2)	0.77(2)
O(9)	0.8367(2)	0.5861(2)	-0.2023(2)	0.87(3)
O(10)	0.2842(2)	0.6357(2)	0.2162(2)	0.84(2)
O(11)	0.2371(4)	0.1825(3)	0.0148(3)	2.54(6)

Bond lengths in $FePO_4$-1

atom	atom	distance (Å)	atom	atom	distance (Å)
Fe(1)	O(4)	1.952(2)	Fe(2)	O(9)	1.971(2)
Fe(1)	O(5)	1.944(2)	Fe(2)	O(10)	2.017(2)
Fe(1)	O(6)	2.128(2)	P(1)	O(2)	1.536(2)
Fe(1)	O(6)	2.141(2)	P(1)	O(3)	1.537(2)
Fe(1)	O(7)	2.017(2)	P(1)	O(4)	1.559(2)
Fe(1)	O(8)	1.997(2)	P(1)	O(5)	1.538(2)
Fe(2)	O(1)	2.007(2)	P(2)	O(7)	1.554(2)
Fe(2)	O(2)	2.002(2)	P(2)	O(8)	1.548(2)
Fe(2)	O(3)	1.985(2)	P(2)	O(9)	1.532(2)
Fe(2)	O(6)	2.212(2)	P(2)	O(10)	1.552(2)

Bond angles in $FePO_4$-1

atom	atom	atom	angle (°)	atom	atom	atom	angle (°)
O(4)	Fe(1)	O(5)	91.57(8)	O(6)	Fe(2)	O(9)	173.33(7)
O(4)	Fe(1)	O(6)	175.29(8)	O(6)	Fe(2)	O(10)	85.88(7)
O(4)	Fe(1)	O(6)	90.94(7)	O(9)	Fe(2)	O(10)	93.84(8)
O(4)	Fe(1)	O(7)	98.63(8)	O(2)	P(1)	O(3)	107.7(1)
O(4)	Fe(1)	O(8)	92.73(8)	O(2)	P(1)	O(4)	109.8(1)
O(5)	Fe(1)	O(6)	90.58(7)	O(2)	P(1)	O(5)	112.3(1)
O(5)	Fe(1)	O(6)	176.01(8)	O(3)	P(1)	O(4)	107.8(1)
O(5)	Fe(1)	O(7)	91.21(8)	O(3)	P(1)	O(5)	112.0(1)
O(5)	Fe(1)	O(8)	98.79(8)	O(4)	P(1)	O(5)	107.1(1)
O(6)	Fe(1)	O(6)	87.15(7)	O(7)	P(2)	O(8)	111.2(1)
O(6)	Fe(1)	O(7)	85.52(7)	O(7)	P(2)	O(9)	111.5(1)
O(6)	Fe(1)	O(8)	82.80(7)	O(7)	P(2)	O(10)	109.7(1)
O(6)	Fe(1)	O(7)	85.34(7)	O(8)	P(2)	O(9)	107.9(1)
O(6)	Fe(1)	O(8)	84.19(7)	O(8)	P(2)	O(10)	108.6(1)
O(7)	Fe(1)	O(8)	164.67(7)	O(9)	P(2)	O(10)	107.9(1)
O(1)	Fe(2)	O(2)	92.80(8)	Fe(2)	O(2)	P(1)	137.6(1)
O(1)	Fe(2)	O(3)	88.03(8)	Fe(2)	O(3)	P(1)	141.2(1)
O(1)	Fe(2)	O(6)	86.78(9)	Fe(1)	O(4)	P(1)	136.9(1)
O(1)	Fe(2)	O(9)	93.88(9)	Fe(1)	O(5)	P(1)	131.2(1)
O(1)	Fe(2)	O(10)	171.78(9)	Fe(1)	O(6)	Fe(1)	92.85(7)
O(2)	Fe(2)	O(3)	178.91(8)	Fe(1)	O(6)	Fe(2)	123.01(8)
O(2)	Fe(2)	O(6)	87.29(7)	Fe(1)	O(6)	Fe(2)	126.07(8)
O(2)	Fe(2)	O(9)	86.05(8)	Fe(1)	O(7)	P(2)	123.8(1)
O(2)	Fe(2)	O(10)	90.53(8)	Fe(1)	O(8)	P(2)	128.2(1)
O(3)	Fe(2)	O(6)	93.46(7)	Fe(2)	O(9)	P(2)	150.5(1)
O(3)	Fe(2)	O(9)	93.19(8)	Fe(2)	O(10)	P(2)	125.0(1)
O(3)	Fe(2)	O(10)	88.73(8)				

APPENDIX 11 – PUBLICATIONS

The following publications have resulted from the work described in this thesis:

Mixed inorganic-organic anion frameworks: synthesis and characterisation of $[Mn_4(PO_4)_2(C_2O_4)(H_2O)_2]$ and $[H_3N(CH_2)_3NH_3][Mn_2(PO_4)_2(C_2O_4)(H_2O)_2]$
Zoe A. D. Lethbridge, Adrian D. Hillier, Robert Cywinski and Philip Lightfoot
J. Chem. Soc., Dalton Trans., 2000, 1595.

Synthesis, structural relationships and magnetic properties of new amine-templated manganese(II) phosphate oxalate framework materials
Zoe A. D. Lethbridge, Satish K. Tiwary, Andrew Harrison and Philip Lightfoot
J. Chem. Soc., Dalton Trans., 2001, 1904.